Cover Page

Universiteit Leiden

Corticosteroid receptor dynamics

analysis by advanced fluorescence microscopy

Femke Lokke Groeneweg

Corticosteroid receptor dynamics

analysis by advanced fluorescence microscopy

Proefschrift

ter verkrijging van
de graad van Doctor aan de Universiteit Leiden,
op gezag van Rector Magnificus prof. mr. C.J.J.M. Stolker,
volgens besluit van het College voor Promoties
te verdedigen op donderdag 6 november 2014
klokke 10:00 uur

door

Femke Lokke Groeneweg
geboren te Leiden
in 1982

Promotiecommissie

Promotor   Prof. Dr. E.R. de Kloet

Co-promotor   Dr. M.J.M. Schaaf

Overige leden   Prof. Dr. A.B. Houtsmuller (Erasmus MC, Rotterdam)
                  Prof. Dr. M. Joëls (UMC, Utrecht)
                  Dr. O.C. Meijer
                  Prof. Dr. T. Schmidt
                  Prof. Dr. H.P. Spaink
                  Prof. Dr. H. Tanke

List of Abbreviations

AF-1/-2	Activating Function domain (1 and 2)
AR	Androgen Receptor
BLA	Basolateral Amygdala
DBD	DNA Binding Domain
ER	Estrogen Receptor
FRAP	Fluorescence Recovery After Photobleaching
FCS	Fluorescence Correlation Spectroscopy
GFP	Green Fluorescent Protein
GR	Glucocorticoid Receptor
GRE	Glucocorticoid Response Element
HPA	Hypothalamic-Pituitary-Adrenal
LBD	Ligand Binding Domain
LBP	Ligand Binding Pocket
MR	Mineralocorticoid Receptor
PFC	Prefrontal Cortex
PICS	Particle Image Correlation spectroscopy
PR	Progesteron Receptor
PVN	Paraventricular Nucleus
SMM	Single-Molecule Microscopy
TIRF	Total Internal Reflection Fluorescence
YFP	Yellow Fluorescent Protein

Contents

General introduction

1.1 The stress response

Stress is broadly defined as a disruption of homeostasis, be it real or anticipated. The response to stress has two faces. On the one hand, it is a highly adaptive response to disturbances in homeostasis. On the other hand, if the stress response is dysregulated it is a potential risk factor for a large number of diseases, ranging from peripheral illnesses such as obesity and heart and cardiovascular problems to psychiatric disorders including major depression, schizophrenia, drug addiction and posttraumatic stress disorder (de Kloet et al., 2005; McEwen, 2008; Yehuda, 2009). Stress-related disorders can occur when the balance between the multiple players, phases and responsive tissues in the stress system is disturbed, so the adaptive stress response converts into a maladapted, detrimental chain of events (de Kloet et al., 1998; McEwen, 2001). Individual variations in this balance, due to genetic or environmental factors, determine whether an individual is resistant or sensitive to stress-related disorders (Kaffman and Meaney, 2007; Oitzl et al., 2010). Key to understanding what causes the balance to shift from adaptive towards detrimental effects of stress is a comprehensive understanding of the different players and phases involved in the stress response and their interactions with each other.

Two stress systems: the ANS- and HPA-axis

The body rapidly responds to a stressor by a combined activation of two stress systems in order to deal with the stressor and reinstate homeostasis as rapidly as possible. These two stress systems are the autonomic nervous system (ANS) and the hypothalamic-pituitary-adrenal (HPA) axis. The autonomous nervous system responds within seconds via sympathetic and parasympathetic innervations throughout the body. This system results in a rapid release of adrenaline and noradrenaline and a number of peripheral effects, such as an increase in blood pressure and heart rate, combined with a number of rapid effects in the brain. Together this results in an increased state of alertness, vigilance, fear or aggression also called the "fight-or-flight" response (de Kloet et al., 2005; Ulrich-Lai and Herman, 2009).

On a slightly slower time scale (minutes to hours) the HPA-axis is activated (see Box I). This hormonal response system culminates in the release of corticosteroid hormones in the blood stream. Cortisol is the main corticosteroid in humans, while rodents produce mainly corticosterone. Corticosteroids enable a long-term response to the stressor and affect tissues throughout the periphery as well as major response sites within the brain. Their most pronounced actions include the regulation of glucose, fat and protein metabolism, anti-inflammatory actions and effects on mood, memory and cognition (de Kloet et al., 2005; McEwen, 2008; Ulrich-Lai and Herman, 2009; Silverman and Sternberg, 2012; McGaugh, 2013). Throughout this thesis I will use the term corticosteroids in reference to the naturally occurring glucocorticoids: cortisol and corticosterone and their endogenous metabolites. Mineralocorticoids, such as aldosterone, are officially also part of the family of cor-

Box I The HPA-axis

The release of corticosteroids is regulated by the HPA-axis (Figure 1.1). Perception of a potentially threatening situation activates the paraventricular nucleus (PVN) of the hypothalamus. In the PVN, corticotrophin releasing hormone (CRH) and vasopressin-containing neurons are activated and stimulate the pituitary to release adrenocorticotropin hormone (ACTH). In turn, this hormone induces the release of corticosteroids from the adrenal glands. Corticosteroids circulate in the blood stream and thus reach every organ in the body, including the brain. Corticosteroids signal back to the HPA-axis at all levels to inhibit further release, thus giving a negative feedback and preventing overexposure (Figure 1.1). Activation of the HPA-axis is also affected by higher brain areas, most notably by the limbic system. Corticosteroids are released in hourly pulses that are highest in amplitude during the active period, thereby causing an overall circadian release pattern (Young et al., 2004). This pattern of pulsatility is essential to keep tissues responsive to stress-induced peaks in corticosteroid release (Lightman and Conway-Campbell, 2010; Sarabdjitsingh et al., 2012). Super-

Figure 1.1: The HPA-axis
Schematic overview of the HPA-axis. Secreted cortisol or corticosterone exerts a negative feedback on all levels to prevent overstimulation of the axis. Through limbic areas, corticosteroids exercise an additional level of feedforward and feedback regulation.

imposed on this ultradian and circadian rhythm is the response to a stressor, which (depending on the severity of the perceived stressor) results in high circulating corticosteroid levels for several hours.

ticosteroids, but are different in both their function and release regulation. I will always name these separately when including them in my discussions. (see Box II)

Two corticosteroid receptors: MR and GR

The actions of corticosteroids are mediated by two receptor types, the glucocorticoid receptor (GR) and the mineralocorticoid receptor (MR) (Reul and de Kloet, 1985). Both belong to the family of nuclear receptors, a family of hormone-activated transcription factors. The dual receptor system gives corticosteroids a versatile response pattern. The MR has a $\sim$10-fold higher affinity for the naturally occurring corticosteroids (corticosterone and cortisol) than the GR (MR: Kd of 0.5 nM and GR of 5 nM). This implies that both receptors are activated at different time points during a stress response: the MR is already activated to a large extent by basal corticosteroid levels, while the GR becomes gradually activated when corticosteroid

levels rise, for example after a stressful event, during the circadian rise in corticosteroids (Reul and de Kloet, 1985; Kitchener et al., 2004) or during the peak of ultradian pulses (Conway-Campbell et al., 2007). Of note, the membrane-associated subpopulation of the MR (to be discussed later in this introduction) has reduced corticosteroid affinity and requires higher hormone levels. The GR is expressed in virtually every cell of the body. Within the brain, the GR is expressed ubiquitously as well, both in glia cells and neurons, with highest levels in the PVN and in the hippocampus (Reul and de Kloet, 1985). The expression of the MR, on the other hand, is more restricted. High levels of MR are found in limbic areas, with moderate levels in the (prefrontal) cortex and the amygdala and high levels in the hippocampus (Reul and de Kloet, 1985). In addition, MR expression is found in circumventricular organs and the nucleus of the solitary tract (Geerling et al., 2006) and peripherally within the kidneys and throughout the cardiovascular system. But, in these latter tissues the MR acts as aldosterone receptor as corticosterone is metabolized into an inactive form in these tissues (see Box II).

The differences in affinity and expression pattern between the MR and GR are also reflected in their respective functions within the stress response. Due to its high affinity for corticosteroids, the MR plays a proactive role in maintaining homeostasis. Within the brain, low levels of corticosteroids, activating the MR, are required to maintain basal firing frequency and stability of limbic circuits (Joëls et al., 2008). Probably through input of higher brain regions to the PVN, the MR modulates HPA-axis activation (Reul et al., 2000). In cognition, the MR is involved in appraisal of novel situations, learning strategies, response selection and emotional reactivity (Oitzl and de Kloet, 1992; Schwabe et al., 2010; Zhou et al., 2010, 2011; Kruk et al., 2013; Souza et al., 2014). Part of these MR-mediated actions are likely due to non-genomic signaling (to be discussed further in *Chapter 2*). Conversely, the GR, which is only activated when corticosteroid levels rise, plays a reactive role in the stress response. For one, through the GR, corticosteroids inhibit their own release in order to prevent corticosteroid overexposure (de Kloet and Reul, 1987). Within the brain, GR activation generally suppresses transiently raised excitatory transmission for instance by enhancement of calcium dependent K+ afterhyperpolarization (Joëls and de Kloet, 1989) and by increasing serotonin dependent K+hyperpolarization (Joëls and de Kloet, 1990; Joëls et al., 1991). GR activation can also stimulate recruitment and mobility of AMPA receptors into the post-synaptic membrane (Groc et al., 2008; Popoli et al., 2011). As a result LTP, the cellular form of memory, is occluded by these GR-mediated effects (Alfarez et al., 2002; Kim and Diamond, 2002). One of the main function of the GR within cognition is to promote consolidation of stress-related information and to facilitate behavioral adaptation (Oitzl and de Kloet, 1992; de Kloet et al., 1999; de Quervain et al., 2009; Zhou et al., 2010). In addition, the GR exerts important functions within the periphery, for example regarding glucose metabolism and suppression of immune activation during stress (de Bosscher and Haegeman, 2009).

Box II The promiscuity of the mineralocorticoid receptor

The MR is an odd receptor in the sense that it binds multiple families of functionally different hormones. Thus, both the naturally occurring glucocorticoids (corticosterone or cortisol) and mineralocorticoids (aldosterone and deoxycorticosterone) bind the MR with similar affinity, and also progesterone is bound with high affinity (Joëls et al., 2008; Funder, 2010; Gomez-Sanchez, 2010). In the epithelial cells of the kidneys and distal colon, the MR acts as the prime receptor for aldosterone and is essential for the regulation of the body's salt and fluid balance (Gomez-Sanchez, 2011). However, the circulating plasma level of corticosterone/cortisol is 100 to 1000-fold higher than that of aldosterone, so how does the MR in the kidney retain its mineralocorticoid sensitivity? This enigma was solved with the discovery of the key enzyme 11β-hydroxysteroid dehydrogenase type 2 (11β-HSD2) (Edwards et al., 1988; Funder et al., 1988). This enzyme converts cortisol and corticosterone into inactive metabolites (see Figure 1.2) and thus strongly reduces the excess of these glucocorticoids in aldosterone-sensitive tissues. Indeed, 11β-HSD2 is highly expressed in aldosterone-sensitive tissues, such as the kidneys, skin and colon and is absent from classical glucocorticoid target tissues as the liver, brain and immune system (Wyrwoll et al., 2011). In the brain its expression is limited to some nuclei in the brainstem, most notably the nucleus of the solitary tract, an important nucleus in salt homeostasis regulation (Geerling et al., 2006). In addition to regulating the hormone accessibility of the MR, 11β-HSD2 also acts to protect tissues against glucocorticoids. For example, there is widespread expression of 11β-HSD2 throughout the placenta during gestation and the developing fetus shows 10–100 fold lover glucocorticoid levels as the mother (Wyrwoll et al., 2011). Deficiencies in 11β-HSD2 expression during late pregnancy generally decrease the birth weight and may be associated with cognitive and affective deficits later in life (most notably increased anxiety and a dysregulation of the HPA-axis) (Cottrell et al., 2014). In classical glucocorticoid target tissues such as the liver and the brain, another type of enzyme is expressed: 11β-HSD type 1 (Agarwal et al., 1989). The enzyme 11β-HSD1 has predominant reductase activity. It converts inactive cortisone and 11β-dehydrocorticosterone into the active 11β-hydroxy form (see Figure 1.2) and thus potentiates glucocorticoid effects (Jamieson et al., 1995).
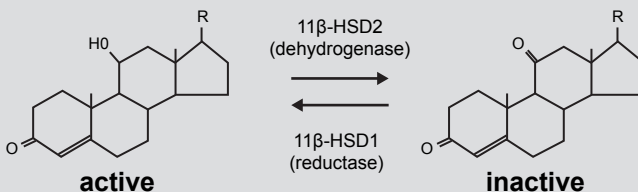
Figure 1.2: 11β-HSD1 and 2
The active corticosteroids, cortisol and corticosterone are metabolized into their inactive counterparts, cortisone and 11-dehydrogenated corticosterone by 11β-HSD2 and vice versa regenerated by 11β-HSD1.

Two modes of actions: genomic and non-genomic

Both MR and GR are ligand-driven transcription factors. They predominantly reside in the cytoplasm in their unbound state. Upon hormone binding, the receptor-ligand complex translocates to the nucleus and affects gene transcription (Beato and Sanchez-Pacheco, 1996). Although the MR and GR share almost identical DNA-binding domains, they do not regulate the same sets of genes. For example, the set of genes that are over- or under-expressed after MR versus GR activation show only limited (less than 30 %) overlap (Datson et al., 2001).

However, over the last decades an alternative mode of action was found for both receptors that does not involve gene transcription. Genomic effects are slow in onset and the first physiological responses are expected after a delay of at least 15 minutes, and often in the order of hours (Haller et al., 2008). This is in sharp contrast to the reality of some of the corticosteroid effects, of which the fastest have been observed within seconds to minutes. Thus, there must be an alternative mode of action of corticosteroids that does not involve the genomic MR and GR mediated pathways. Indeed, a small portion of the population of the MR and GR is localized at the plasma membrane where they interact with multiple kinase signaling pathways and exert rapid, non-genomic effects (Di et al., 2003, 2009; Johnson et al., 2005; Karst et al., 2005, 2010; Prager et al., 2009). As such, both the MR and GR affect neuronal excitability and behavior over a wide time range: from a few minutes after corticosteroid exposure until many hours thereafter (Joëls et al., 2012).

To understand the response of a tissue or an organism to stress it is important to understand what happens at the lower levels; i.e. at the cellular level. These cellular actions are the result of a complex interplay between the effects of corticosteroids and other stress hormones, and effects mediated by the two corticosteroid receptors (MR and GR). The existence of two corticosteroid responsive pathways (genomic and non-genomic) adds to the complexity. For the cellular basis of both modes of action much has already been discovered but more remains unknown. In the next two sections, I will introduce the state of knowledge for both the genomic and the non-genomic mode of action of corticosteroids.

1.2 Non-genomic corticosteroid signaling

For many years rapid actions of corticosteroids on neurotransmission and behavior were noted but their cellular basis remained ill understood. For one, corticosteroid application can inhibit neuroendocrine output of the brain within a few minutes (Evanson et al., 2010b). On the level of behavior, depending on the context, corticosterone application results rapidly in increased locomotion (Sandi et al., 1996a), aggression (Mikics et al., 2004; Kruk et al., 2013) or risk assessment (Mikics et al., 2005). Also in humans corticosteroids affect learning and emotional processing in a non-genomic manner (Henckens et al., 2012; van Ast et al., 2013).

The Tasker group (Di et al., 2003, 2005, 2009; Malcher-Lopes et al., 2006) performed a set of pioneering experiments that opened the field to understanding the cellular basis of these rapid effects. They demonstrated that a high dose of corticosterone (from 100 nM) irreversibly reduces the frequency of miniature excitatory postsynaptic currents (mEPSCs) within 5 minutes within the PVN of the hypothalamus. This effect did not require gene transcription or protein synthesis. The frequency of mEPSCs is a measure of the excitability of neurons, reflecting either the release probability of glutamate vesicles or the number of synaptic contacts. In subsequent years, the Joëls group (Karst et al., 2005, 2010; Pasricha et al., 2011) found rapid effects of corticosterone on mEPSC frequency in the hippocampus (both CA1 and DG) and the basolateral amygdala. They observed a rapid reduction of mEPSC frequency in the hippocampus, which is opposite to what was found in the PVN. Moreover, within the hippocampus, the rapid reduction was reversible and induced by lower doses of corticosterone (from 10 nM). Over recent years many more effects have been identified in stress responsive areas in the brain, I will summarize these in *Chapter 2*.

Membrane-associated MR and GR

A large part of the non-genomic actions of corticosteroids require the presence of the MR or GR. For instance, the enhanced mEPSC frequency in the hippocampus is absent in MR-/- mice and prevented by pretreatment with MR antagonists (Karst et al., 2005). Similarly, in the amygdala rapid GR-dependent effects were observed (Karst et al., 2010). Rapid behavioral effects have been shown to depend on the GR (Barsegyan et al., 2010) and MR (Khaksari et al., 2007) as well. Thus, the MR and GR appear to have an alternative function as mediators of non-genomic corticosteroid signaling. Intriguingly, in this role the MR and GR seem to be accessible at the outside of the plasma membrane. Rapid effects can still be induced with a membrane-impermeable conjugate of corticosterone (cort-BSA) (Karst et al., 2005, 2010; Groc et al., 2008; Roozendaal et al., 2010) and cannot be induced by intracellularly infused corticosterone (Liu et al., 2007; Olijslagers et al., 2008). Additionally, the presence of the MR and GR at the (synaptic) membrane was demonstrated in membrane extracts and synaptosomes (Komatsuzaki et al., 2005; Wang and Wang, 2009; Qiu et al., 2010) and with electron microscopy imaging (Johnson et al., 2005; Prager et al., 2009). Part of the downstream signaling cascades has also been unraveled. One of the most common signaling partners are the G-proteins, which bind to the receptors at the membrane. Inhibition of G-protein activation abolishes the rapid effects of corticosterone on a variety of neuronal functions (Zhu et al., 1998; Di et al., 2003, 2009; Olijslagers et al., 2008; Hu et al., 2010). More downstream, the cAMP-PKA and ERK1/2 pathways have been implicated in non-genomic corticosteroid actions (Liu et al., 2007; Olijslagers et al., 2008; Di et al., 2009; Barsegyan et al., 2010).

The regulation of membrane translocation for the MR and GR remains incompletely understood. For the related estrogen receptor α (ERα), presence within caveolae, association with caveolin-1 and palmitoylation have been established as vital steps in its membrane targeting (Levin, 2009). However, only association with caveolin-1 has been shown for the MR and GR (Matthews et al., 2008; Pojoga et al., 2010b). Moreover, the fraction of the receptors associated with the membrane, their local binding partners and the effect of ligand treatment on membrane trafficking and internalization have not yet been addressed.

1.3 Genomic corticosteroid signaling

As discussed, a small fraction of the MR and GR are anchored at the cell membrane, but the bulk of the receptor population is present within the cytoplasm. In the absence of ligand, these cytoplasmic receptors are kept in an inactive conformation by association with a large chaperone complex. Most chaperones are shared by all steroid receptors, these include heat shock proteins (HSP) 90, 40 and 70, p23, p70, and cochaperone proteins, such as the immunophilins FKBP51, FKBP52, and protein phosphatase 5 (PP5) (Picard, 2006). Association with chaperones also serves to keep the nuclear localization sequence hidden and prevents protein degradation (Faresse et al., 2010). Corticosteroids are lipophilic and as such easily pass the cell membrane and reach their receptors within the cytoplasm. Ligand binding to the ligand-binding pocket (LBP) results in a massive conformational shift that exposes the nuclear localization signal. Next, the ligand-receptor complex is actively transported into the nucleus by importins (primarily importin α (Tanaka et al., 2003)).

DNA binding

Through the two zinc fingers in their DBD (see Box III), the MR and GR bind directly to GREs on the DNA. Direct DNA-binding of the MR and GR to GREs is mostly associated with enhanced gene transcription or transactivation. The receptor binds the DNA as a dimer, forms a complex with coactivators and attracts the general transcription machinery to induce increased transcription of the related gene (Datson et al., 2008). A cofactor is defined as a protein that affects the interaction of a transcription factor with the DNA, but that does not act as a transcription factor itself. Cofactors have diverse functions and affect the stability of the transcriptional machinery, (de)acytelate histones or recruit other cofactors or transcription factors (Zalachoras et al., 2013). Cofactors are divided into coactivators and corepressors depending on their role in gene transcription. The GR also induces transrepression of genes. This can occur through direct binding to negative GREs, but it is mostly associated with indirect DNA-binding. For example, the GR has been well described to bind the transcription factors AP-1 and NFκB and inhibit transcription of their

Box III Functional domains of the GR and MR

All steroid receptors share a modular structure encompassing four functional domains. The N-terminal domain is least conserved between steroid receptors (around 15 % overlap) and contains the activating factor-1 (AF-1) domain. Adjacent is the highly conserved (90 % homology among steroid receptors) DNA-binding domain (DBD), which recognizes the hormone response elements in the DNA by its two zinc finger structures. Due to the almost perfect sequence homology between this region in the MR and GR they recognize and bind the same DNA sequences, dubbed glucocorticoid response elements (GREs) (Datson et al., 2008). C-terminally located is the ligand-binding domain (LBD). The sequence homology of the LBD is also generally quite high between steroid receptors (∼60 % between the MR and GR), but the structures lining the ligand-binding pocket show less overlap and determine ligand specificity (Bledsoe et al., 2002; Huyet et al., 2012). The conformation of the LBD is highly affected by ligand binding, it exposes chaperone binding sites in its unbound conformation, while ligand binding leads to exposure of the nuclear localization signal and AF-2 domain (Pascual-Le Tallec and Lombès, 2005). For most steroid receptors, helix-12 which contains the AF-2 domain refolds into an open conformation only when agonists are bound and not upon binding of antagonists (Fagart et al., 1998; Bledsoe et al., 2004). Both the AF-1 and AF-2 mediate cofactor binding and are affected by ligand-induced conformation changes. While the AF-2 domain is highly conserved, the AF-1 is very variable and determines receptor specific and cellular context-dependent cofactor binding patterns (Fuse et al., 2000; Simons and Kumar, 2013). In between the DBD and LBD is a small hinge region that enables folding and also contains a dimerization sequence and a nuclear localization signal.
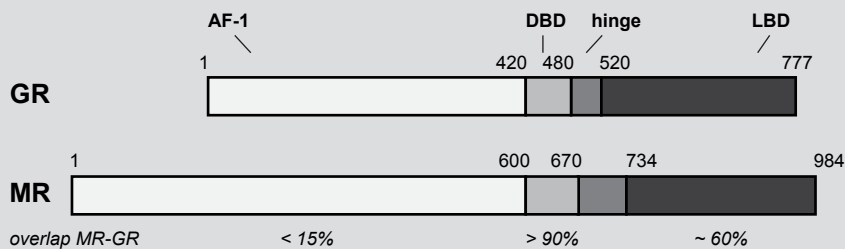
Figure 1.3: Functional domains of the GR and MR
Schematic overview of the modular structure of the GR and MR. Below the average sequence homology between the two receptors is given. Image adapted from Pippal and Fuller (2008).

target genes (Nixon et al., 2013). This is functionally important for GR's immunosuppressant actions. Indirect binding does not necessarily have to entail transrepression though. Co-binding of the GR and other transcription factors can also induce gene transcription (Kassel and Herrlich, 2007; Ratman et al., 2013).

The MR and GR show a large overlap in their DBD and activating function domains (see Figure 1.3) and as result their genomic actions overlap. In tissues where the MR and GR are coexpressed they also form heterodimers (Nishi et al., 2004) and DNA transactivation will thus occur through a mixture of GR-GR homodimers, MR-MR homodimers and GR-MR heterodimers. The extent of overlap between MR and GR regulated genes is still debated. Early gene expression profiling studies found only limited overlap in MR- and GR- responsive genes (Datson et al., 2001, 2008), while a recent study investigating direct DNA binding using chromatine immuno precipitation (ChiP) did find MR binding for all examined GR-target sequences (Polman et al., 2013). The MR and GR are known to share many cofactors (also with other steroid receptors), but each receptor uses a distinctive set as well (Yang and Young, 2009; Zalachoras et al., 2013). In regards to transrepression though indirect binding to the DNA, this has classically been associated with only the GR and not the MR. Indeed, the MR lacks immunosuppressant efficacy (Pippal and Fuller, 2008). However, *in vitro* transrepression of AP-1 activity by the MR have been shown by some (Africander et al., 2013), albeit with much reduced potency compared to the GR (Pearce and Yamamoto, 1993). This has not yet been validated *in vivo*. An overview of MRs and GRs cellular actions is represented in Figure 1.4.

Corticosteroids reach a multitude of tissues where they execute very variable functions, on a cellular level this means they require the capacity for tissue specific patterns of gene transcription. Indeed, Chip-Seq studies and microarray studies have both shown that there is only a moderate overlap in GR target genes and bound sequences between different cell types (Datson et al., 2008; Reddy et al., 2009; Yu et al., 2010; John et al., 2011; Polman et al., 2012, 2013). For example, the set of sequences bound by GR in a neuronal-like cell line overlapped for only 7 % with those found in an alveolar-derived cell line and for 11 % with an adipose-derived line (Polman et al., 2012). Differences in chromatin structure and cofactor availability are important determinants of this tissue specificity. The DNA sequence of the GR binding site (GBS) represents another level of complexity and regulation of GR's (and MR's) genomic output. Identified GR binding sites show a certain level of sequence homology and thus a consensus GBS (Strähle et al., 1987). However, there are also quite some variations to the consensus sequence possible. In an elegant study, the Yamamoto group showed that single nucleotide mutations to identified GBS's affected the conformation of the GR when bound and resulted in severe shifts in (*in vitro*) transactivation capacity (Meijsing et al., 2009). This effect was found to depend on cofactor recruitment. Within the brain an *in silico* search for preserved GR binding sequences resulted in the identification of a brain-specific consensus GBS (Datson et al., 2011) and also found considerable variation within this sequence and its flanking regions between different GR-regulated genes. The exact correlation between binding sequences and GR's conformation and capacity to induce gene transcription is still only partly understood but it is clear that this represents another important level of orchestrating GR's (and MR's) genomic actions.
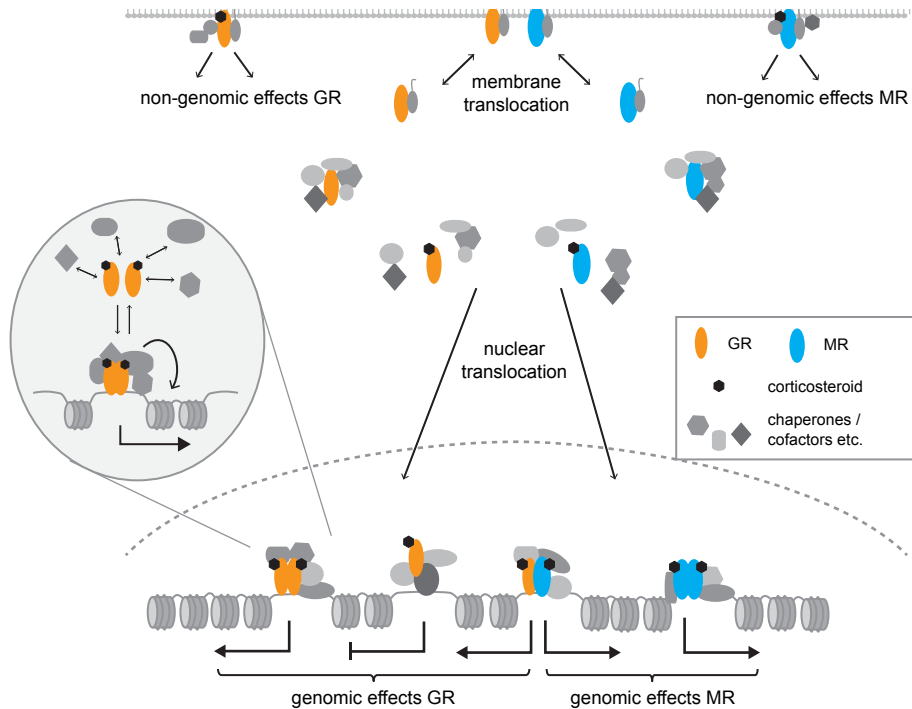
Figure 1.4: Cellular MR- and GR-mediated corticosteroid actions
A small fraction of MR and GR translocate (through unknown pathways) to the plasma membrane, where they associate with caveolin-1 and other binding partners and induce non-genomic corticosteroid effects. The largest fraction of both MR and GR resides within the cytoplasm while unbound and is bound here by chaperones. Hormone binding releases the chaperones and enables nuclear translocation. Within the nucleus both receptors bind the DNA in a dynamic fashion (see insert). The GR can bind its target genes through direct receptor-DNA interactions as dimer and indirectly through binding to / with other transcription factors as monomer. The first is predominantly associated with transactivation and the latter with transrepression, but both modes of DNA binding can lead to both stimulation and inhibition of gene transcription. Indirect DNA binding by the MR is less established and its genomic actions are thus mostly restricted to direct binding as dimer and transactivation. When coexpressed, the MR and GR also form heterodimers on the DNA.

Steroid receptors show highly dynamic DNA-binding

For many years the binding of steroid receptors (and other transcription factors) to their DNA-target sites was envisioned as a static event: the transcription factor binds, recruits cofactors and RNA polymerases and gene transcription is initiated (Perlmann et al., 1990). However, since the start of the new millennium all components of the transcriptional machinery have been found to be highly dynamic. In this new era many advanced (functional) imaging techniques have been developed, improved and used that enable the observation of protein dynamics on a seconds to even milliseconds timescale. I will discuss some of the most important advances in microscopy in the next section of the introduction. First the current view on steroid receptor DNA-binding dynamics will be discussed.

The first to study the dynamics of the GR at the DNA was the Hager group. They developed a tandem repeat of a naturalistic GR binding site, the mouse mammary tumor virus (MMTV) promoter, incorporated into the native DNA. This repeat consists of 800–1200 GR binding sites and as such binding of GFP-GR to this site can be visualized directly (Walker et al., 1999; McNally et al., 2000). With this model system, the Hager group used fluorescence recovery after photobleaching (FRAP) to show very rapid exchange of the GR at its binding site. The half maximum of recovery was obtained within 5 seconds at the site (McNally et al., 2000; Stavreva et al., 2004). A multitude of follow up studies on the GR and related steroid receptors (Stenoien et al., 2000; Schaaf and Cidlowski, 2003; Farla et al., 2004; Stavreva et al., 2004; Mueller et al., 2008; Stasevich et al., 2010b), irrevocably showed that activated steroid receptors remain very mobile within the nucleus. Similarly, a rapid exchange at the DNA was found for all transcription factors and also for cofactors and RNA polymerases (Dundr et al., 2002; Gorski et al., 2008; Johnson et al., 2008). Only a few structural chromatin components (core histone proteins) were found to be stably associated with the DNA (Kimura and Cook, 2001). An important observation was that mobility of steroid receptors is negatively correlated to their transcriptional activity (Schaaf and Cidlowski, 2003; Stavreva et al., 2004, 2009). This suggests that DNA-binding is either less frequent or shorter in duration for less potently activated receptors. In addition, a large fraction of the observed immobilizations are presumed to be due to nonspecific DNA binding (Mueller et al., 2013). Nonspecific DNA-binding likely aids a transcription factor in its search for specific binding sites, but the exact mechanisms remain debated. *In vitro* transcription factors show 1D sliding across the DNA (i.e. remains associated with the DNA), in addition to 3D hopping (rapid association and dissociation to the DNA), but whether this also occurs on nascent chromatin remains unclear (Gowers et al., 2005; Hager et al., 2009).

The highly dynamic behavior of steroid receptors at the second and millisecond level must further be integrated with additional levels of dynamics at longer time frames. For both the GR and the ERα spontaneous oscillations of receptor binding to responsive genes are observed within single cells in 20–40 minute cycles (Becker, 2002; Métivier et al., 2003). Id est: a responsive gene will cycle through 20–40 minute periods of high occupancy (by dynamically interchanging receptors) and similar periods with very low occupancy. These types of asynchronous oscillations are likely caused by local chromatin remodeling. Chromatin remodeling precedes recruitment of the GR to a DNA sequence and displacement of the chromatin remodeling complex is soon followed by GR displacement from the sequence (Nagaich et al., 2004). In addition to these oscillations, in the organism also the hormone secretion oscillates and also this induces oscillations in gene expression (Stavreva et al., 2009). Thus, oscillating pulses of corticosterone also result in oscillations of GR-DNA binding, RNA polymerase binding and mRNA transcript levels of endogenous GR-target genes in cells and even in an intact rat (Stavreva et al., 2009).

Taken together, these findings paint a picture of a highly dynamic transcriptional complex at gene promoters (and enhancers) with multiple components dynamically exchanging. This process has been dubbed the "hit-and-run" mode of transcription (Rigaud et al., 1991). This is a field still in development and theories about what types of DNA interactions occur and what their relevance to transcription is are still being developed (recent reviews on this topic include (Mueller et al., 2008; Biddie and Hager, 2009; Hager et al., 2009; Voss and Hager, 2014). More recently, the relevance of transcription factor dynamics for local chromatin remodeling and complex formation has received more attention and added another level of complexity to the view on transcription factor-DNA interplay (Voss and Hager, 2014). One of the largest challenges remains to accurately quantify the dynamics at sufficient spatial and temporal resolution and therefore the field is very dependent on the development of novel sophisticated imaging methods.

1.4 The analysis of protein dynamics using advanced fluorescence microscopy techniques

The use of fluorescently tagged receptors has revealed much about the dynamics of the MR and GR within the cell and within the nucleus. Over the last fifteen years a number of live imaging and advanced microscopy techniques have been developed to enable the tracking of fluorescent proteins within living cells. In the next sections I will introduce the three mostly used techniques and discuss their advantages and disadvantages. I will also briefly discuss some imaging approaches directed towards specific subcellular regions.

Fluorescence Recovery After Photobleaching

All fluorescent proteins experience photobleaching, i.e. the irreversible loss of fluorescent capacity due to (prolonged) excitation. This phenomenon can be utilized to measure protein dynamics with FRAP (van Royen et al., 2009a). In FRAP a target area is exposed to a high intensity laser pulse to effectively bleach all fluorescent molecules within that area. Subsequently, the recovery of fluorescence within that area is monitored. As photobleaching is a permanent state, any recovery of fluorescence is due to fluorescent proteins moving from unbleached areas into the target area and replacing the bleached molecules that are moving out of this area. Thus, the faster the recovery, the more mobile the fluorescent protein (Figure 1.5A). Advantages of FRAP are that it is relatively simple to implement and that it records protein dynamics over a large time range (from a few 100 milliseconds to several minutes; Table 1.1). Its main disadvantages are that it is not accurate in tracking fast diffusion (< 100 milliseconds) and that there is no consensus on how to quantify the FRAP recovery curves. A review of all quantitative FRAP studies showed that

	FRAP	**FCS**	**SMM**
Spatial resolution (in XY)	diffraction limited	diffraction limited	20 nm
Time domain	$\sim$100 ms – 10^2 sec	µs – 10^1 sec	$\sim$5 ms – 10^0 sec
Population modeling	yes	yes	yes/no
Tracking of fast diffusing proteins	poor	good	good
Assessment DNA-binding times	yes	no	yes/no*

Table 1.1: Comparison of advanced imaging techniques
* attenuations to the illumination schedule enable a quantification of DNA-binding times for SMM (Gebhardt et al., 2013).

differences in modeling parameters and a failure to correct for laser irregularities severely affected the acquired parameters (Mueller et al., 2008).

Fluorescence Correlation Spectroscopy

Fluorescence Correlation Spectroscopy (FCS) is a fluorescence imaging technique that can be used for accurate assessment of the mobility of fast diffusing proteins (Chen et al., 1999; Ries and Schwille, 2012). In FCS, the fluorescent signal in a relatively small ($\sim$200 nm diameter) area is monitored over time (Figure 1.5B). This measured fluorescence fluctuates as fluorescent proteins move in and out of the volume. The faster a protein diffuses, the shorter it will reside within this measuring volume. Therefore, the correlation of fluorescence over increasing time frames is recorded and the rate of change of the correlation curve over time is a measure of the diffusion rate of the protein. The main advantage of FCS is that it can reliably quantify relatively rapid diffusion. Its main disadvantages are that FCS can only be applied for a limited time domain (microseconds to several seconds) and that the size of the imaging volume is restricted by diffraction of light and can thus not become smaller than $\sim$200 nm in XY (depending on the objective and laser wavelength) (Table 1.1).

Single-Molecule Microscopy

In single-Molecule Microscopy (SMM), a wide-field fluorescence microscopy setup is used. Fast, ultra-sensitive imaging of samples with very low levels of fluorescence enables the visualization of single fluorescent molecules (Figure 1.5C). The fluorescent signal can be fitted with a Gaussian curve, of which the center represents the location of the fluorescent molecule. This approach results in a positional accuracy of 20–40 nanometer. The positional accuracy depends only on the signal-to-noise ratio and can therefore be a lot smaller than the diffraction-limited resolution of conventional fluorescence microscopy. A further advantage of SMM is its high temporal resolution (several milliseconds). Quantification of SMM data has been achieved by two methods: single-molecule tracking (SMT) or Particle Image Corre-
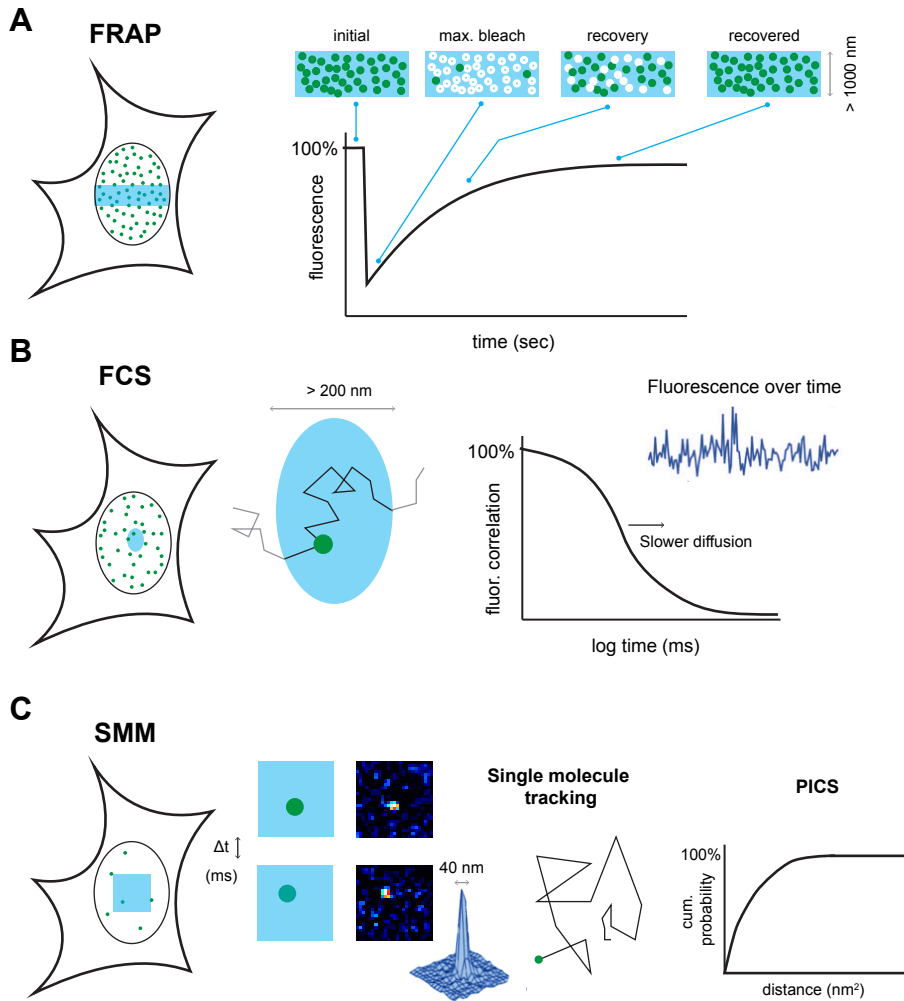
Figure 1.5: Functional imaging approaches
A schematic overview of the three main functional fluorescence imaging methods. (A) FRAP. In FRAP a > 1000 nm diameter area is bleached by a high-energy laser pulse and subsequently the recovery of fluorescence within this area is observed. Quantification of protein dynamics is obtained from modeling of the recovery curve. (B) FCS. In FCS a > 200 nm diameter area is observed and fluorescence within this area is observed. Quantification of protein dynamics is obtained by autocorrelation of the fluorescence over time. (C) SMM. In SMM a region of interest (ROI) is chosen within a lightly fluorescent cell. Within this ROI, single fluorescent molecules are observed and as their fluorescence is fitted with a Gaussian curve a positional accuracy of ∼40 nm is obtained. Quantification of protein dynamics occurs either through tracking of single molecules or by PICS where for each time lag all distances of molecules between the two images is fitted. FRAP: Fluorescence Recovery After Photobleaching, FCS: Fluorescence Correlation Spectroscopy, SMM: Single-Molecule Microscopy.

lation Spectroscopy (PICS). In SMT, a very low density of fluorescent molecules is required and the trajectories of single molecules are constructed over several frames (Persson et al., 2013). The length of these trajectories is restricted by blinking and

photo-inactivation (bleaching) of the used fluorophore. Population data can be extracted by population modeling or non-averaged data can be analyzed (Elf et al., 2007). In PICS, higher densities of fluorophores are allowed and blinking is less of a problem (Semrau and Schmidt, 2007). PICS measures the correlation of distances of each single fluorescent molecule to all existing fluorescent molecules in a subsequent time frame. From the overall data the uncorrelated distances are subtracted and the remaining correlated distances are fitted with population models. The main disadvantage of SMM is that it is not easily applied to long time ranges (Table 1.1). SMT is hampered by the stability of fluorophores over longer time delays and both SMT and PICS become less accurate over long time delays due to escaping of the faster diffusing molecules from the imaging volume (van Royen et al., 2014). Labelling of proteins with gold particles or quantum dots enables long-term imaging and is very promising, but has so far been applied in only a few occasions due to labeling issues (Cognet et al., 2014).

Total internal reflection fluorescence (TIRF) microscopy

Total internal reflection fluorescence (TIRF) microscopy provides a means to selectively excite fluorophores in a thin layer close to the glass-medium interface (Axelrod et al., 1983; Axelrod, 2008; Toomre, 2012; Martin-Fernandez et al., 2013). In short, in TIRF the excitation laser is redirected so that it exits the objective at a large angle relative to the optical axis. Once a critically large angle is achieved, the excitation light is totally internally reflected at the glass-medium interface. As a result a low energy electromagnetic field is generated from this interface, which is dubbed the evanescent wave field. The evanescent wave field is capable of exciting fluorophores, but its energy decreases exponentially, which results in an excitation field of 60–100 nm in depth. The biggest advantage of TIRF microscopy is that it produces wide-field images with very low background fluorescence from out-of-focus planes and thus a very high signal-to-noise ratio. TIRF microscopy can be combined with advanced imaging techniques as FCS, FRAP and SMM. Especially, the combination of SMM and TIRF has been used in a wide variety of studies to study the kinetics of membrane-bound proteins, near membrane structures and docking vesicles (Axelrod, 2008). In a variation of TIRF, entitled highly inclined and laminated optical sheet (HILO) microscopy, a thin sheet of excitation light penetrates the sample at an angle, thus exciting a thin section, but within the cell. HILO can thus be used to image within the cytoplasm or nucleus, with improved signal-to-noise ratio (Tokunaga et al., 2008). Similarly, reflected light sheet microscopy (RLSM) also enables imaging of a thin section within the cell and thus reducing out of focus light. RLSM has been successfully combined with single-molecule tracking (Ritter et al., 2010; Gebhardt et al., 2013).

1.5 Objective and outline

As the stress system is such a tightly regulated system, it is of vital importance to understand the finesses of the underlying molecular pathways, which ultimately determine the responses on the tissue and organism levels. Within a target cell corticosteroids can bind both the MR and GR and through these receptors it will activate both non-genomic and genomic pathways. Although much has been learned regarding the mode of action of both receptors, many questions still remain. In this thesis I will explore further finesses of the cellular actions of corticosteroids mediated by MR and GR in both their membrane-associated and nuclear subpopulations. I have three specific aims:

1. To investigate the multitude of non-genomic effects of corticosteroids in different brain areas and explore how these fit within the coordinated (rapid phase of the) stress response (*Chapter 2*).

2. To set up *in vitro* models to show the presence of a distinct membrane-associated population of the MR and further characterize its function, structure-function relationship and dynamics (*Chapter 3 and 4*).

3. To quantify the chromatin binding dynamics of the MR and GR within the nucleus and explore the effect of mutations within the receptors and different ligands on their DNA-binding dynamics (*Chapter 5 and 6*).

Thesis outline and approach

To investigate these three aims I will use a number of different experimental approaches.

In **Chapter 2** we will investigate available knowledge concerning the multitude of rapid non-genomic corticosteroid actions within different brain areas. We focus on the timing of the effects in each brain area, their interaction with delayed genomic effects and explore what this implies for the known behavioral and hormonal effects known to be associated with these brain areas.

Corticosteroids inhibit potassium A-type currents in a rapid, non-genomic and membrane-MR dependent fashion in hippocampal neurons. In **Chapter 3**, we will explore the potential of using neuronal-like cell lines, NS-1 and N1E-115 cells, as an *in vitro* setting to study a similar rapid potentiation of potassium currents by corticosterone in cells with or without MR protein expression. We show that the potassium A-type currents in NS-1 cells are inhibited by corticosterone in a membrane-initiated and MR-dependent fashion. The slow-inactivating potassium currents in N1E-115 cells are not affected by corticosterone. We further describe an instability of MR protein in *in vitro* settings.

Next, in **Chapter 4** we describe a novel approach to deduce whether a subpopulation of the MR is associated with the cell membrane. In these experiments we

use TIRF microscopy to specifically image fluorescently tagged MR at the cell membrane. Furthermore, we analyze the dynamics of this membrane-associated MR subpopulation with single-molecule analysis. Using these approaches, we find that near the membrane a distinct MR subpopulation is present, with dynamics substantially different from the cytoplasmic MR population.

In **Chapter 5** we use SMM and combine this with FRAP to derive a comprehensive characterization of the dynamics of nuclear GR. With this combined approach we obtain a reproducible quantification of the DNA-binding behavior of activated GR. When bound to potent agonists, GR molecules undergo frequent but transient immobilization due to DNA binding. Both the frequency and duration of DNA-binding are reduced when GR is bound by antagonists or, more surprisingly, by less potent agonists. We find evidence for specific ligand-receptor interactions to underlie differences in the GR's affinity for DNA. Furthermore, we study the effect of deletions of functional domains of the GR to show that receptors devoid of (direct) DNA-binding capacity indeed show reduced DNA binding.

In **Chapter 6** we build upon the approach and findings from **Chapter 5** and study the dynamics of nuclear MR with the same combination of SMM and FRAP. As for the GR, we find that also the MR shows more and longer DNA-binding when activated by its most potent agonists and reduced frequency and duration of these interactions when bound by antagonists or less potent agonists.

Finally, all results are discussed in a broader context in **Chapter 7**.

Rapid non-genomic effects of corticosteroids through the membrane-associated MR and GR and their role in the central stress response

Femke L Groeneweg[1], Henk Karst[2], E Ron de Kloet[1], Marian Joëls[2]

[1] Department of Medical Pharmacology, Leiden University / LUMC, Leiden, The Netherlands.
[2] Department of Neuroscience and Pharmacology, University Medical Center,
     Utrecht, The Netherlands

Corticosteroids affect brain functioning through both delayed, genomic and rapid, non-genomic mechanisms. The latter mode of action was long known but only in recent years the physiological basis in the brain is beginning to be unravelled. We now know that corticosteroids exert rapid, non-genomic effects on the excitability and activation of neurons in (amongst others) the hypothalamus, hippocampus, amygdala and prefrontal cortex. In addition, corticosteroids affect cognition, adaptive behaviour and neuroendocrine output within minutes. Knowledge on the identity of the receptors and secondary pathways mediating the non-genomic effects of corticosteroids on a cellular level is accumulating. Interestingly, in many cases an essential role for the 'classical' MR and GR in a novel membrane-associated mechanism is found.

Here, we systematically review the recent literature on non-genomic actions of corticosteroids on neuronal activity and functioning in selected limbic brain targets. We will discuss the relevance of these permissive effects for cognition and neuroendocrine control, and the integration of this novel mode of action into the complex balanced pattern of stress effects in the brain. Subsequently, we will review the knowledge regarding the underlying molecular pathways addressing the following questions: How do the MR and GR translocate to the membrane and what are their signalling partners?

Corticosteroids play a major role in the response of the brain to stress. For many years, they were believed to be only responsible for the delayed and prolonged effects of stress, as opposed to monoamines and neuropeptides which were thought to establish rapid effects (de Kloet et al., 2005). While this is generally true, the picture is actually more complex. For instance, corticosteroids influence a wide range of behaviors and endocrine outputs within minutes, a timeframe that is too rapid to be explained by genomic effects (de Kloet et al., 1999; Haller et al., 2008). In agreement, we and others recently established that corticosteroids rapidly alter neuronal activity and excitability in a number of brain areas, providing a physiological basis for the rapid effects on behavior (Tasker et al., 2006; de Kloet et al., 2008). Many rapid effects are still mediated by the classical corticosteroid receptors, the MR and the GR, but by a subpopulation of these receptors, anchored at the membrane (Karst et al., 2005, 2010). The existence of such a rapid mode of action raises many new questions. Where in the brain do these rapid effects take place? Which receptors and pathways are involved in these effects? What are the functional consequences for cognition and neuroendocrine control? How are these rapid corticosteroid actions integrated with other components of the stress response? Equally important are the remaining molecular questions. How strong is the evidence for a membrane-localization of the MR and GR and for other types of (novel) membrane receptors. Also, as steroid receptors do not have a transmembrane domain, how do MR and GR associate with the plasma membrane? And finally, are there common downstream pathways. In this chapter we discuss our current understanding of rapid actions of corticosterone, with emphasis on their function within the brain.

2.1 Rapid effects of corticosterone in the brain

The rapid effects of corticosterone on brain and cognition have been subject of several recent reviews (Dallman, 2005; Tasker et al., 2006; de Kloet et al., 2008; Haller et al., 2008; Prager and Johnson, 2009; Evanson et al., 2010a). However, over the last two years a number of new studies have emerged that extend and challenge the existing views on the function and nature of these rapid effects. Here, we focus on the integration of these new findings in the existing theories on rapid corticosteroid signalling. The findings are discussed per brain area; i.e. the hypothalamus, pituitary, hippocampus, amygdala and frontal cortical areas. In the following sections, the major findings in these four different brain areas are summarized (see for overview Table 2.1). In this review we restrict ourselves to the non-genomic roles of the MR and GR within neurons. Both receptors have vital functions in the periphery and also here many non-genomic actions have been observed. However, these are beyond the scope of this review and have been described elsewhere (Boldyreff and Wehling, 2003; Grossmann and Gekle, 2009; Funder, 2010).

Hypothalamus

The PVN is one of the core structures in the HPA-axis. PVN neurons express high levels of GR, but virtually no MR. Indeed, through GR activation in the PVN corticosterone negatively feeds back on the HPA-axis in a delayed, genomic fashion (de Kloet et al., 1998). However, corticosterone also regulates HPA-axis activity in a more rapid time frame, through non-genomic actions (Jones et al., 1972; Dallman, 2005). Importantly, a recent study showed that this rapid inhibition can be induced by local infusion of dexamethasone or a membrane-impermeable conjugate of dexamethasone with bovine serum albumine (dex-BSA) into the PVN (Evanson et al., 2010b). This effect can be prevented by co-administration of an antagonist of the cannabinoid receptor type 1 (CB1) (Evanson et al., 2010b). Thus, at the level of the PVN, corticosterone rapidly reduces HPA-axis activation in a non-genomic, membrane-associated manner, involving endocannabinoid signalling.

Insight in the neurobiological substrate of these fast effects was provided by Tasker and colleagues. This group was the first to carry out detailed studies on the frequency of miniature excitatory postsynaptic currents (mEPSCs) in the PVN and the nearby supraoptic nucleus (SON) (Di et al., 2003). An mEPSC reflects the postsynaptic current resulting from the spontaneous release of a single glutamatergic vesicle from a presynaptic terminal (Bekkers and Stevens, 1989). Importantly, the frequency of these events (particularly in the absence of changes in mEPSC amplitude) is considered to be determined by presynaptic properties, reflecting changes in either release probability of the vesicles or changes in the number of synaptic contacts. Tasker and colleagues established that a high dose of corticosterone (between 100 nM and 1 μM) or its synthetic analogue dexamethasone reduces the frequency of mEPSCs in PVN neurons (Di et al., 2003; Malcher-Lopes et al., 2006). This effect was detectable within 5 minutes and did not reverse when corticosterone was washed out. Effectively, the excitability of PVN neurons was reduced by application of corticosteroids in a rapid but prolonged manner. Rapid changes in mEPSC frequency induced by corticosterone could not be blocked by MR or GR antagonists (Di et al., 2003, 2009). In contrast, preliminary data shows that they are prevented by conditional knockout of the GR gene within the hypothalamus and thus will involve the (membrane-associated) GR (Haam et al., 2010; Tasker and Herman, 2011). How this new finding should be integrated with the lack of effect of antagonists remains unclear and awaits further clarification in a full study. The effects within the PVN were further shown to be non-genomic, membrane-initiated and to involve G-protein coupled signalling. Interestingly, rapid corticosteroid actions required retrograde endocannabinoid signalling and the CB1 receptor. The presumed cellular signalling pathway is visualized in Figure 2.1A. Since the CB1 receptor is also required for rapid inhibition of the HPA-axis (Evanson et al., 2010b), the rapid inhibition of mEPSC frequency (and thus excitability) of PVN neurons could provide the cellular substrate for this phenomenon.
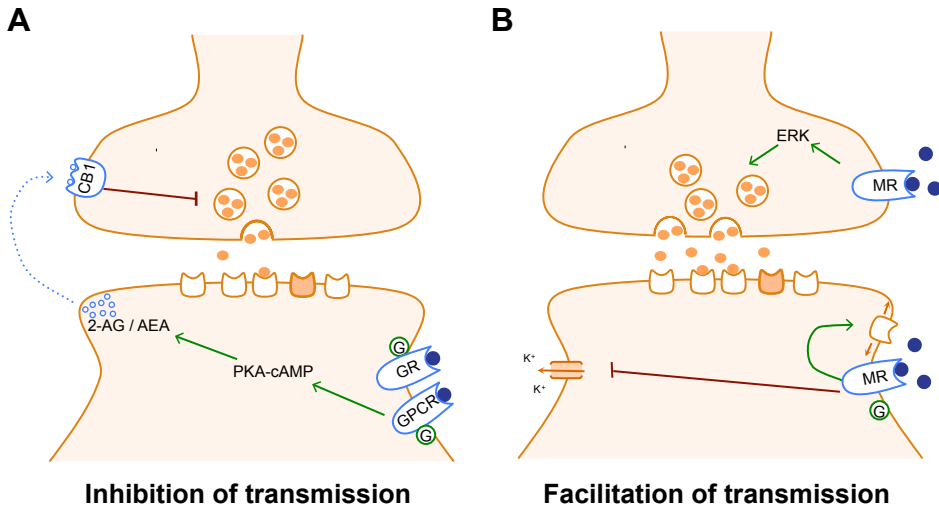
Figure 2.1: Schematic representation of the synaptic pathways of corticosterone-induced rapid effects on glutamatergic transmission
(A) Inhibition of glutamatergic transmission is initiated by postsynaptically located receptors; this can be either G-protein coupled receptors (hypothalamus) or membrane-localized GRs (amygdala). Activation of these receptors by corticosterone induces activation of G-proteins and the cAMP-protein kinase A (PKA) pathway, which eventually induces synthesis of the retrograde messengers anandamide (AEA) and 2-arachidonoylglycerol (2-AG). In a retrograde mode of action at the presynaptic terminal 2-AG and AEA activate the cannabinoid receptor type 1 (CB1), which in turn inhibits the release probability of glutamatergic vesicles. (B) Facilitation of glutamatergic transmission is initiated by both pre- and post-synaptically located membrane-MRs. Presynaptically, activation of the MR by corticosterone activates an extracellular signal-regulated kinase (ERK) pathway resulting in stimulation of the release probability of glutamate vesicles. At the same time, postsynaptic activation of a membrane-associated MR inhibits potassium I_A-currents, and stimulates membrane diffusion of AMPA receptors. All three effects together result in a facilitation of glutamatergic transmission.

However, rapid inhibitory effects of corticosterone in the PVN are not restricted to vasopressin- and CRH-containing parvocellular neurons, but they are seen in all neuronal populations (parvocellular and magnocellular) in the PVN (Di et al., 2003, 2005; Tasker et al., 2006). In the magnocellular neurons in the PVN and SON, a second effect was observed on the spontaneous release of *gamma-aminobutyric acid* (GABA), the main inhibitory neurotransmitter. The frequency of mIPSCs (miniature inhibitory postsynaptic currents) was rapidly increased by dexamethasone, but this required even higher concentrations (1 μM or more) (Di et al., 2005, 2009). Functionally, this suggests a more general coordinative role for the non-genomic effects of corticosterone in the hypothalamus, which requires further specification (Tasker et al., 2006).

Pituitary

Fast and delayed effects of corticosteroids have also been observed at the level of the anterior pituitary gland, where GR is abundantly expressed and MR levels are quite low (Reul et al., 1990). Already in the 1970's and 80's both rapid and delayed actions

of corticosteroids on pituitary ACTH release were reported (Jones et al., 1972; Widmaier and Dallman, 1984). Inhibition of ACTH release was seen as early as 1 minute and as late as 2 hours after corticosteroid administration. The latter is a genomic action mediated by GR-driven gene transcription, while the former action was insensitive to protein synthesis inhibitors and thus mediated by non-genomic pathways (Keller-Wood and Dallman, 1984). Interestingly, the rapid inhibition of ACTH release was only seen when corticosterone levels were rapidly rising and not when they were already high, suggesting that this feedback is rate-sensitive (Jones et al., 1972; Kaneko and Hiroshige, 1978).

The cellular basis of the rapid effects is not well established and controversy remains about the receptor mediating the effects. On the one hand, pretreatment with a GR antagonist did not prevent the rapid effects of corticosterone on CRH-induced ACTH secretion *in vivo* (Hinz and Hirschelmann, 2000). Also, in a pituitary-derived cell line a membrane binding place for dexamethasone and corticosterone was identified that did not have any affinity for the GR-antagonist RU486 (Maier et al., 2005). However, another line of evidence does suggest a role for the classical GR in mediating rapid feedback at the pituitary. Thus, a rapid and non-genomic translocation of annexin-I by dexamethasone was prevented by GR-antagonist treatment in a pituitary derived cell line (Solito et al., 2003). This translocation of annexin-I was required for rapid inhibition of ACTH release (Buckingham et al., 2003; Tierney et al., 2003). Thus, corticosterone rapidly inhibits ACTH release from the pituitary, but whether this is due to a novel receptor or to the classical GR is still controversial. This rapid inhibition is also seen in control human subjects, while it is absent in depressed patients, suggesting that the rapid negative feedback is somehow associated with disease (Young et al., 1991).

Hippocampus

Adaptation to a stressful situation is a coordinated effort mediated by the limbic system —the hippocampus and amygdala— in coordination with the prefrontal cortex (see Figure 2.2). This, among other things, involves projections of these areas to and hence control over the PVN (Ulrich-Lai and Herman, 2009). Collectively, these areas also facilitate the formation of a memory trace of a stressful emotional event. Processing of contextual information depends predominantly on hippocampal function. The hippocampus expresses high levels of both MR and GR in all subfields (except its cornu ammonus-3 (CA3) region that mainly expresses MR) (Reul and de Kloet, 1985). Corticosterone exerts strong genomic effects on the activity and plasticity of all hippocampal subfields as well as on hippocampus-dependent memory (McEwen, 2001; Kim and Diamond, 2002; Mirescu and Gould, 2006; Joëls, 2008). Low levels of corticosterone, through MR activation, facilitate plasticity and hippocampus-dependent memory (Diamond et al., 1992). By contrast, absence or very high levels of corticosterone inhibit plasticity; the latter is mediated through the GR (Alfarez et al., 2002; Kim et al., 2004).
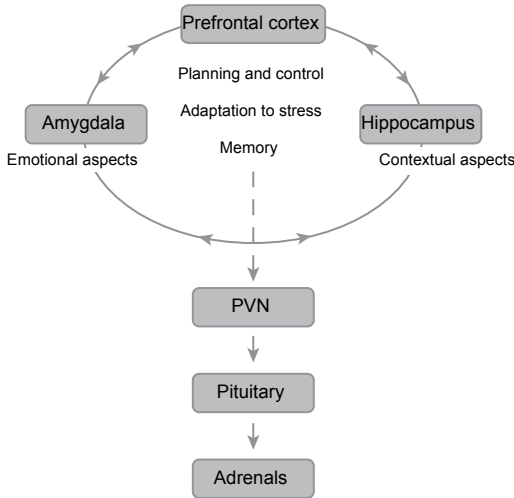
Figure 2.2: Brain circuitry of stress
The limbic system is implicated in adaptation, learning & memory processes, mood, and control of the HPA-axis. The hormones of the HPA-axis coordinate information processing and promote connectivity between amygdala, prefrontal cortex and hippocampus to facilitate behavioral adaptation. Projections from the limbic structures innervate the PVN network and regulate trans-synaptically the activity of the HPA-axis.

Similar to neurons in the hypothalamus, hippocampal neurons spontaneously show mEPSCs. In a first study (Karst et al., 2005), the effect of corticosterone was examined on mEPSC frequency in the CA1 region of the hippocampus. It appeared that within 5 minutes of corticosterone administration, the frequency of mEPSCs is significantly *enhanced*, i.e. changed in a direction opposite to that observed in the PVN. The amplitude was unaffected (Karst et al., 2005; Olijslagers et al., 2008) (see Figure 2.3A,B). This effect was recently reproduced by other investigators (Qiu et al., 2010) and granule neurons in the dentate gyrus respond similarly to corticosterone as CA1 neurons (Pasricha et al., 2011). Similar to the corticosteroid effect in the hypothalamus, the rapid effect in the hippocampus does not depend on gene transcription and involves a membrane-located receptor (Karst et al., 2005). However, further studies established profound differences between rapid responses to corticosterone in the hippocampus compared to the PVN. The increased mEPSC frequency in hippocampus rapidly reversed when corticosterone was washed out. Also, in the CA1 the effect occurred at a 10-fold lower dose of corticosterone (10 nM or higher) than in the hypothalamus. Importantly, corticosterone efficiently enhanced mEPSC frequency in the hippocampus of wild type and GR knockout mice, but the effects were completely abolished in MR knockout mice, supporting that rapid effects in the hippocampus are mediated by MRs (Karst et al., 2005). This was confirmed with specific MR and GR antagonists. Importantly, the membrane-located MR appears to have a lower affinity than the cytosolic form (Karst et al., 2005), so that it potentially could play an important role when corticosteroid levels rise, shortly after stress (Joëls et al., 2008). Follow-up studies suggested that rapid corticosteroid effects involve MRs inserted into the presynaptic membrane (Olijslagers et al., 2008) (see Figure 2.1B). This is backed up by preliminary evidence that shows localization of the MR in the plasma membrane of hippocampal neurons, co-localized with the presynaptic marker synapsin I (Qiu et al., 2010).
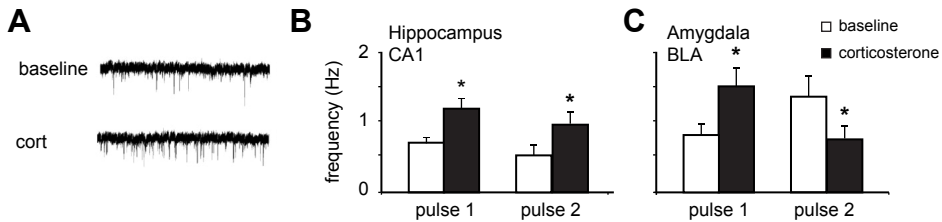
Figure 2.3: Effect of two pulses of corticosterone on mEPSC frequency in the CA1 region and the basolateral amygdala (BLA)
(A) Typical traces of mEPSC pulses recorded from hippocampal neurons before (white bars) and after (black bars) treatment with $100\,$nM corticosterone. (B) In hippocampal CA1 neurons exposure to two consecutive pulses of $100\,$nM corticosterone (1 hour apart) both induce a reversible increase in mEPSC frequency. (C) In amygdalar BLA neurons, the first pulse of corticosterone induces an increase in mEPSC frequency, this increase is not reversible. For the second pulse of corticosterone the basal mEPSC frequency is already elevated and the second pulse induces an irreversible decrease instead. mEPSC, miniature excitatory postsynaptic current. $*\,p < 0.05$ compared with baseline (paired t test). *Figure reprinted with permission from Karst et al. (2010).*

Corticosterone also affects two postsynaptic features of CA1 neurons through the MR. Firstly, corticosterone was found to inhibit postsynaptic I_A-currents, an effect that could be blocked with an MR-antagonist (Olijslagers et al., 2008). I_A-currents are potassium currents that are negative regulators of neuronal excitability and plasticity (Hoffman et al., 1997; Yuan et al., 2002). Consequently, the inhibition of these currents by corticosterone is expected to stimulate excitability and plasticity of hippocampal neurons. Secondly, corticosterone stimulated, within 5 minutes, lateral diffusion of *α-amino-3-hydroxyl-5-methyl-4-isoxazole-propionic acid* (AMPA) receptors in cultured hippocampal neurons (Groc et al., 2008). This effect also turned out to depend on membrane-localized MRs (Groc et al., 2008). Potentially, a more mobile pool of AMPA receptors facilitates the induction of synaptic plasticity. All of these studies support a membrane-localised form of the MR as main mediator of rapid corticosteroid signalling in the hippocampus. Overall, corticosterone seems to rapidly potentiate the excitability of hippocampal neurons via membrane-MRs located on both pre- and postsynaptic sites, thus priming the hippocampal circuit for subsequent stimulation by context-dependent factors.

However, not all rapid effects in the hippocampus involve the MR. First, a non-genomic increase in spine density of hippocampal neurons was found to depend on GRs rather than MRs (Komatsuzaki et al., 2005). Yet other rapid corticosterone effects occur independent of MR or GR and therefore could be mediated by a novel (so far not identified) membrane-localized receptor. This applies to rapid stimulatory corticosterone effects on inhibitory transmission (Hu et al., 2010), on levels of extracellular excitatory amino acid (Venero and Borrell, 1999), long-term potentiation (LTP) induction (Wiegert et al., 2006) and *N-methyl-D-aspartatic acid* (NMDA)-dependent neurotoxicity (Xiao et al., 2010). Some studies also reported inhibitory actions of corticosterone on NMDA signalling (Sato et al., 2004; Liu et al., 2007). Apparently, corticosterone affects hippocampal signalling in multiple ways, involving membrane-located MRs, GRs and other, still unknown receptors.

Amygdala

Stressful events invariably activate the amygdala, the brain's principal emotional centre (Roozendaal et al., 2009). The amygdala expresses both MR and GR in its various subnuclei (Reul and de Kloet, 1985) and amygdala-dependent memory, such as cued learning and emotional memory is very sensitive to stress and corticosteroids (Roozendaal et al., 2009). Interestingly, genomic effects of corticosterone on the amygdala are generally opposite to those seen in the hippocampus, with enhanced activity in the former (Duvarci and Pare, 2007; Mitra and Sapolsky, 2008) and reduced activity and plasticity in the latter (Alfarez et al., 2002, 2009; Kim et al., 2004). In addition, the amygdala is one of the main targets of the adrenergic system. Many corticosteroid effects on amygdala functioning in fact require adrenergic signalling (Roozendaal et al., 2009). This interaction might in part be mediated by non-genomic effects of corticosteroids. For instance, a systemic injection of corticosterone directly after a learning task rapidly (within 15 minutes) increased the levels of noradrenaline in the basolateral amygdala (BLA) and this was correlated to the later facilitation of fear memory by corticosterone (McReynolds et al., 2010).

An important finding that raised interest in non-genomic actions of corticosterone in the amygdala was the demonstration of MR and GR at the plasma membrane in amygdalar neurons. Johnson et al. used detailed electron microscopic analyses to study the subcellular distribution of the GR (Johnson et al., 2005) and MR (Prager et al., 2010) in the lateral amygdala. The GR was identified at the plasma membrane as well as in the nucleus and cytoplasm. GRs turned out to be present at both post-synaptic dendrites and presynaptic sites (Johnson et al., 2005). More recently the same was shown for the MR (Prager et al., 2010).

The functional consequences of corticosterone on mEPSC frequency in the BLA and the central nucleus of the amygdala (CeA) were recently revealed (Karst et al., 2010). In the CeA, corticosterone had no effect on either frequency or amplitude of the mEPSCs. However, in the BLA, corticosterone induced a significant increase in mEPSC frequency, comparable to the effects found in hippocampus albeit slightly slower in onset (Karst et al., 2010) (Figure 2.3c). Comparable to the hippocampus, this enhanced mEPSC frequency after corticosterone treatment was MR-dependent and non-genomic in nature (Karst et al., 2010). However, in contrast to the hippocampus, the effect in the amygdala was not only slower in onset, but also persistent after washout of the hormone. One hour after a pulse of corticosterone mEPSC frequency was still high. This lasting phase of the response was found to depend on protein synthesis and required the presence of both MR and GR (Karst et al., 2010).

The long-lasting effects of corticosterone were shown to also determine the responses of BLA neurons to subsequent pulses of the hormone. When BLA cells were exposed to a second pulse of corticosterone, mEPSC frequency was *reduced* (Karst et al., 2010) (see Figure 2.3c). Reduction in mEPSC frequency also occurred in tissue prepared from animals exposed to restraint stress prior to slice preparation. Interestingly, this rapid and non-genomic effect to renewed corticosteroid expo-

sure depended on the GR rather than the MR. Similar to the hypothalamus (but in contrast to the hippocampus), it was shown to involve a postsynaptically localized GR and subsequent retrograde endocannabinoid signalling (see Figure 2.1A). Thus, in a non-stressed animal corticosterone seems to have a stimulatory effect in the (basolateral) amygdala. However, due to the long-lasting nature of these effects, a second exposure to corticosterone induces opposite effects, suggesting metaplasticity of corticosteroid responses. These data suggests that the amygdala will respond differently to a stressor depending on the recent stress history of the organism.

Prefrontal cortex

The prefrontal cortex (PFC) is critically involved in complex behavioural control, such as behavioural inhibition, decision-making and working memory. It is extensively connected to the amygdala and receives afferents originating in the hippocampus (Arnsten, 2009). Despite its important function, the PFC is underrepresented concerning studies on the effects of corticosteroids and stress. A number of studies have examined the effect of chronic stress or corticosterone exposure on the PFC. Under these conditions, LTP, dendritic complexity and PFC-dependent working memory were reduced in a genomic fashion (Arnsten, 2009; Holmes and Wellman, 2009). On the contrary, exposure to acute stress or corticosterone increased glutamatergic transmission and improved working memory performance (Yuen et al., 2009, 2010). These effects occurred with a delay of several hours and were shown to require gene transcription (Yuen et al., 2010). Thus acute and chronic stress affect PFC plasticity and functionality in an opposite manner.

The only studies so far in the PFC that focused on rapid, non-genomic effects were performed in synaptosomes. In this preparation, corticosterone induced a rapid enhancement of glutamate uptake and of calcium-dependent calmodulin stabilization (Sze and Iqbal, 1994; Zhu et al., 1998). Unfortunately, the receptors or pathways involved were not examined. In a recent study, Roozendaal and colleagues reported a putative membrane-GR mediated effect of corticosterone in the insular cortex that is involved in memory acquisition. In this elegant study, administration of either corticosterone or cort-BSA directly into the insular cortex facilitated the acquisition of object recognition memory (Roozendaal et al., 2010). Although there are some concerns about the stability of cort-BSA *in vivo*, this is still indicative of a membrane-initiated effect. The effect was prevented by co-administration of a GR antagonist. The authors further proved that the facilitation of memory by membrane-GR activation was established through protein kinase A (PKA), cAMP response element-binding (CREB) and histone acetylation (Roozendaal et al., 2010). Taken together, rapid non-genomic actions of corticosterone are found in (some) prefrontal areas; so far they seem to be mostly excitatory (as are the sub-acute genomic effects) and could have implications for higher-order learning in complex tasks. However, the data is still very sparse.

2.2 Functional implications of rapid corticosteroid effects in the brain

Taking all results into account, we can distinguish some interesting general features of the rapid effects of corticosteroids in the brain.

i) It is important to notice that all non-genomic effects are permissive or conditional effects. In none of the studies corticosteroids induced any activity on their own, instead they facilitate or inhibit signalling of ion channels, receptors and neurotransmitters. In short, they increase or decrease the threshold for activation of these neurons by context-dependent factors. Therefore, it will depend on the context which effects (in which brain areas) will be most pronounced during a stressful encounter.

ii) We see a distinctive pattern with a general increase in excitability for some areas (hippocampus, amygdala and potentially the prefrontal cortex) and a decrease in others (the hypothalamus).

iii) While some responses are transient (mostly in the hippocampus), other effects are prolonged (hypothalamus, pituitary and amygdala). The brain circuitry activated by stress will thus be different depending on the delay after the stressor.

iv) In general, the inhibitory effects on hypothalamic functioning seem to require a higher dose of corticosterone than most effects in other brain areas. If so, the set of responses seen after a mild stressor may be different from that of a more severe stressor, the latter having an additional negative effect on PVN-related responses (Prager and Johnson, 2009).

v) Finally, a number of rapid corticosteroid effects require the presence of classical MR and GR inserted in or attached to the plasma membrane, while other effects are mediated through yet unknown (G-protein coupled) receptors. In general, MR-mediated effects tend to stimulate excitation, while GR-mediated effects can also be inhibitory (see Figure 2.1).

We will refer to these five general points when we next consider the potential functional consequences of rapid corticosteroid actions in the brain for HPA-axis regulation and cognition, also taking the ultradian release pattern into consideration. Finally we will address the integration of these rapid effects with the rest of the brain's response to stress.

Regulation of the HPA-axis

Corticosteroids exert rapid, as well as delayed, inhibitory feedback at the core structures of the HPA-axis; the PVN of the hypothalamus (Evanson et al., 2010b) and the pituitary gland (Jones et al., 1972; Hinz and Hirschelmann, 2000). In the pituitary this seems to be caused by both GR-dependent (Buckingham et al., 2003) and GR-independent (Hinz and Hirschelmann, 2000) rapid signalling pathways. In the PVN, the rapid suppression of glutamatergic transmission by corticosterone could well underlie (amongst others) fast suppression of the HPA-axis in a GR-independent

manner (Tasker, 2006). As mentioned earlier, this hypothesis is backed up by the effectiveness of intra-PVN infusions of dexamethasone or dex-BSA on HPA-axis activity in a rapid time frame (Evanson et al., 2010b).

In addition, extra-hypothalamic structures also control the activity of the HPA-axis. For instance, the hippocampus and prefrontal cortex exert negative feedback on the HPA-axis through (indirect) projections to the PVN, while the amygdala has a stimulatory influence on the PVN and thus HPA-axis (Ulrich-Lai and Herman, 2009). Rapid non-genomic corticosteroid actions in these areas may affect this limbic control over the HPA-axis. This also enables a role for the MR, absent from the hypothalamus, in the regulation of HPA-axis activation. Indeed, MRs in the hippocampus are important to determine the threshold of the stress response (Reul et al., 2000; Joëls et al., 2008). In agreement, treatment of rats with MR agonists induced a rapid suppression of both ACTH and corticosterone release (Atkinson et al., 2008). Thus, not only can corticosterone inhibit HPA-axis activation directly through its genomic and non-genomic effects at core structures of the axis, it also provides a second layer of control at limbic areas that enables a subtler and context-dependent rapid trans-synaptic regulation of the HPA-axis.

Adaptation of behaviour and cognition

In addition to regulation of the HPA-axis through (trans-synaptic) connections to the PVN, the limbic circuitry is vital for adaptation to stressful events and the formation of memory of these events (Figure 2.2). Many actions of corticosteroids, for example facilitation of memory consolidation, are dependent on gene transcription, through activation of the genomic GR (and MR) (Oitzl et al., 2001). However, corticosteroids also affect behaviour and memory in a rapid and presumably non-genomic manner. Thus, rapid effects of corticosteroids have been described for a number of adaptive behaviours, including rapid facilitation of novelty-induced locomotion (Sandi et al., 1996a,b), context-dependent aggression (Mikics et al., 2004) and risk assessment behaviour (Mikics et al., 2005). These effects were all observed within 7 minutes and the latter two were proven to be independent of gene transcription, see also Table 2.1. In all cases, an injection with corticosterone rapidly increased a specific type of behaviour that is seen as adaptive in that context (i.e. aggression towards an intruder, or locomotion and risk assessment in a novel environment). Interestingly, the MR has been repeatedly reported to be involved in these types of behaviour, involving novelty reactivity, coping strategies and aggression (Oitzl and de Kloet, 1992; Sandi and Rose, 1994; Berger et al., 2006; Joëls et al., 2008; Brinks et al., 2009; Kruk et al., 2013). As these behavioural effects are rapidly induced and by stress-doses of corticosterone, they always seemed incompatible with the constitutively active genomic MR. The lower affinity membrane-MR could prove to be the logical substrate for these effects. Unfortunately, this role of the membrane-MR has not been studied directly yet. There is circumstantial evidence for involvement of MRs in novelty behaviour. This comes from a study using knock-

out mice for the limbic system-associated membrane protein (LSAMP). These mice showed increased novelty reactivity and impaired learning (Catania et al., 2008; Qiu et al., 2010), and associated with this, a reduction in non-genomic MR function in the hippocampus (Qiu et al., 2010).

In behavioural studies on the regulation of memory, the GR is reported to have a predominant function in memory consolidation, while the MR is mostly involved in memory retrieval and learning strategies (Oitzl and de Kloet, 1992; de Kloet et al., 1999). A similar convergence of functions is seen in the rapid domain. Firstly, a rapid facilitation of memory consolidation by corticosterone was shown to depend on the (presumably membrane localized) GR in the cortex (Roozendaal et al., 2010). Secondly, application of antagonists for endocannabinoid signalling in the amygdala was reported to block corticosterone-induced effects on memory consolidation (Campolongo et al., 2009). Together, this suggests that the membrane-GR mediated and endocannabinoid-dependent inhibition of neuronal excitability (see Figure 2.1A and Karst et al. (2010)) might be implicated in memory consolidation. In contrast, corticosterone effects on memory retrieval seem to be MR-mediated. Administration of corticosterone 30 minutes before a memory retrieval task impaired retrieval of information in a non-genomic, hippocampal-dependent and MR-mediated manner (Khaksari et al., 2007; Sajadi et al., 2007). Finally, acute stress or cort-BSA infusion into the hippocampus induced a shift in memory retrieval tested 5 or 15 minutes later, although this study did not investigate the receptor involved (Chauveau et al., 2010). Rapid —in addition to delayed— corticosteroid effects thus seem to be involved in all phases of the memory process, i.e. acquisition, consolidation and retrieval. In general, the GR seems to potentiate consolidation via both rapid and delayed (genomic) pathways. Conversely, the MR seems to have a specific (non-genomic) role during memory retrieval, possibly as a mechanism to focus attention to a new stressor. Taken together, in its role as rapid corticosteroid sensor, the MR facilitates adaptive behaviour in the context of the stressor while inhibiting behaviours that are no longer relevant.

Implication of ultradian pulses

Corticosteroids do not only reach the brain in high amounts during a stressful situation, but also during ultradian peaks (Droste et al., 2008). Rapid non-genomic corticosteroid actions might have an additional function in translating these pulses into ultradian alterations in brain function. Indeed, both rapid feedback on the HPA-axis (Windle et al., 1998), aggressive behaviour (Haller et al., 2000) and novelty reactivity (Sarabdjitsingh et al., 2010) depend on the phase of an ultradian pulse the animal is in. In a recent study by Sarabdjitsingh et al., ultradian pulses were manipulated experimentally. Exposure to noise stress induced a stronger ACTH release and higher behavioural reactivity when animals were stressed during the rising phase of an ultradian corticosterone pulse compared to animals exposed to the same stressor during the falling phase (Sarabdjitsingh et al., 2010).

Effect		Receptor	Conc	Area	Delay	Preparation	Signalling pathways	Reference
mEPSC freq	→	other or mGR	100 nM	PVN & SON	5 min	rat, ex vivo	Gαs, cAMP-PKA, ECB, CB1	[1–5]
mIPSC freq	↑	other	1 μM	PVN & SON	5 min	rat, ex vivo	Gβγ, NO release	[2,4]
eEPSC freq ↓ eIPSC amplitude	↑	unknown	1 μM	SON	7 min	rat, ex vivo		[4]
2-AG and AEA levels	↑	unknown	1 μM	hypoth	10 min	rat, ex vivo	PKA	[3–4]
Vasopressin release	→	mGR	100 nM	hypoth	20 min	rat, ex vivo	Ca²⁺, PLC	[6–7]
HPA-axis	→	unknown	10 ng local	PVN	15 min	rat, in vivo	CB1	[8]
mEPSC freq	↑	mMR	10 nM	CA1 & DG	5 min	mouse, ex vivo	ERK1/2	[9–12]
I_A current	→	MR	100 nM	CA1	5 min	mouse, ex vivo	G-proteins	[10]
AMPAR mobility	↑	mMR	50 nM	CA1	2 min	rat, culture		[13]
mIPSC freq	↑	MR	30 nM	Ventral CA1	not known	rat, ex vivo		[14]
MR at membrane		mMR		hippoc		mouse, culture		[11]
spine density	↑	mGR	100 nM	CA1	60 min	rat, ex vivo		[15]
GR at membrane		mGR		hippoc		mouse, ex vivo		[15]
aspartate and glutamate levels	↑	other	600 ng/ml local	hippoc	20 min	rat, in vivo		[16]
NMDA-dependent neurotoxicity	↑	other	10 nM	hippoc	15 min (+24 h)	rat, culture	ERK1/2, NR2A	[17]
LTP induction	↑	other	100 nM	CA1	10 min	mouse, ex vivo	G-proteins, NO	[18]
sIPSC freq	↑	other	25 nM	CA1	5 min	rat, ex vivo	G-proteins, PKC	[19]
JNK & p38 phosphorylation	↑	other	1 nM	hippo	5 min	rat, culture	cAMP-PKA	[20]
NMDA-dependent current	→	not GR	100 nM	hippoc	seconds	rat, culture		[21]
NMDA-dependent current prolonged		not GR	1 μM	hippoc	seconds	rat, culture		[22]
AEA levels	↑	unknown	3 mg/kg sc	hippoc	10 min	rat, in vivo		[23]
NMDA-dependent current	→	unknown	400 nM	CA1	seconds	mouse, ex vivo		[24]
Ca²⁺-currents	→	unknown	10 pM	CA1	4 min	guinea pig, ex vivo	G-proteins, PKC	[25]
Memory retrieval altered		unknown	0.3 nmol local	dorsal hippoc	10 min	mouse, in vivo		[26]

Chapter 2

	Receptor		Dose	Region	Mechanism	Species/prep	Ref
GR in membrane	mGR			BLA		mouse	[27]
MR in membrane	mMR			BLA		mouse	[28]
mEPSC freq	mMR	↑	100 nM	BLA		mouse, *ex vivo*	[29]
mEPSC freq	mGR	↓	100 nM	BLA	CB1	mouse, *ex vivo*	[29]
AEA levels	unknown	↑	3 mg/kg sc	amygdala		rat, *in vivo*	[23]
glutamate uptake	unknown	↑	10 nM	frontal cortex	G-proteins	rat, synaptosomes	[30]
calmodulin dynamics	unknown	↑	30 nM	cortex		rat, synaptosomes	[31]
Memory consolidation	mGR	↑	3 ng local	insular cortex / mPFC	βAC, cAMP, PKA, CREB	rat, *in vivo*	[32–33]
Working memory	mGR	↓	3 ng local	mPFC	βAC, cAMP, PKA	rat, *in vivo*	[33]
ATP-induced currents	GR	↓	10 nM	DRG	PKA	rat, culture	[34]
memory retrieval	MR	↓	1 mg/kg		opioids	rat, *in vivo*	[35–36]
risk assessment	unknown	↑	0.5 mg/kg			rat, *in vivo*	[37]
aggressive behaviour	unknown	↑	0.5 mg/kg			rat, *in vivo*	[38]
locomotion	other	↑	2.5 mg/kg		NO	rat, *in vivo*	[39–40]

Table 2.1: Rapid effects of corticosterone on neuronal functioning in the hypothalamus, hippocampus, amygdala and prefrontal cortex 'unknown' receptor was not examined, 'other' not the MR or GR, **DRG** dorsal root ganglion, **eIPSC/EPSC** evoked IPSC/EPSC, **AEA** anandimide, **2-AG** 2-arachidonoylglycerol, **sIPSC** spontaneous IPSC, **mMR/mGR** membrane-associated MR/GR, **sc** subcutaneous, **ECB** endocannabinoids, **CB1** cannabinoid receptor type 1, **NO** nitric oxide, **NR2A** NMDA receptor 2A subunit, **PKC** protein kinase C, **βAC** β-adrenoceptor, **WB** western blot, **IFM** immunofluorescent microscopy, **EM** electron microscopy.

[1] (Di et al., 2003), [2] (Di et al., 2005), [3] (Malcher-Lopes et al., 2006), [4] (Di et al., 2009), [5] (Haam et al., 2010), [6] (Liu et al., 1995), [7] (Liu and Chen, 1995), [8] (Evanson et al., 2010b), [9] (Karst et al., 2005), [10] (Olijslagers et al., 2008), [11] (Qiu et al., 2010), [12] (Pasricha et al., 2011), [13] (Groc et al., 2008), [14] (Maggio and Segal, 2009), [15] (Komatsuzaki et al., 2005), [16] (Venero and Borrell, 1999), [17] (Xiao et al., 2010), [18] (Wiegert et al., 2006), [19] (Hu et al., 2010), [20] (Qi et al., 2005), [21] (Liu et al., 2007), [22] (Takahashi et al., 2002), [23] (Hill et al., 2010), [24] (Sato et al., 2004), [25] (Ffrench-Mullen, 1995), [26] (Chauveau et al., 2010), [27] (Johnson et al., 2005), [28] (Prager et al., 2010), [29] (Karst et al., 2010), [30] (Zhu et al., 1998), [31] (Sze and Iqbal, 1994), [32] (Roozendaal et al., 2010), [33] (Barsegyan et al., 2010), [34] (Liu et al., 2008), [35] (Khaksari et al., 2007), [36] (Sajadi et al., 2007), [37] (Mikics et al., 2005), [38] (Mikics et al., 2004), [39] (Sandi et al., 1996b), [40] (Sandi et al., 1996a)

These responses were seen within minutes, so that non-genomic mechanisms must have been involved. In the brain, these effects were associated with *in*creased activity of the amygdala and *de*creased activity of the PVN (recorded by c-fos expression) during the rising compared to the falling phase (Sarabdjitsingh et al., 2010), reminiscent of the corticosteroid effects seen for mEPSC frequency in PVN and amygdala. Hypothetically, during the rising phase of an ultradian pulse, non-genomic pathways are activated in limbic areas, which in turn could affect stress-related behaviour.

Integration of non-genomic and genomic effects

In several cases, rapid non-genomic corticosteroid actions were shown to transgress into more lasting effects, integrating two temporal domains (rapid and delayed) which up till recently were each linked to different classes of stress hormones, i.e. monoamines (and to some extent neuropeptides) on the one hand and corticosteroids on the other hand. For example, rapid effects in the hypothalamus are long lasting (Di et al., 2003) and thus HPA-axis feedback will be inhibited over a long period of time. Indeed, dexamethasone infusions in the PVN exert both rapid and delayed negative feedback actions on the HPA-axis activity (Dallman et al., 1994; Dallman, 2005). Similarly, the increased excitability in the BLA starts as a non-genomic MR-dependent phenomenon and eventually evolves into a genomic phenomenon that also requires the GR (Karst et al., 2010). At a cognitive level, the facilitation of memory consolidation by cort-BSA injections in the insular cortex is evoked by a membrane-associated effect that evolves into a genomic effect through activation of the transcription factor CREB (Roozendaal et al., 2010). Finally, rapid corticosterone effects on aggressive and risk assessment behaviour are independent of gene transcription immediately after corticosterone injection but develop into transcription-dependent effects later on (Mikics et al., 2004, 2005). Thus, many non-genomic effects of corticosterone are tightly linked to later genomic actions. At least in one case (Karst et al., 2010), the initial non-genomic action is required for the subsequent genomic phase, suggesting that both phases work in coordination.

However, non-genomic and genomic actions can also be integrated if they occur independent from each other. In the hippocampus, the initial enhanced mEPSC frequency is quickly reversed: when corticosteroid levels drop, the effects are immediately lost (Karst et al., 2005). Supposedly, a brief period of enhanced excitability is followed by a refractory period with an increased threshold for the induction of new signals, the latter depends on genomic GR signalling (Alfarez et al., 2002, 2009; Krugers et al., 2010). A similar dichotomy was seen with respect to LTP induction in the hippocampus. Corticosterone given immediately before LTP induction stimulated LTP induction (Wiegert et al., 2006), while corticosterone applied hours earlier inhibited the induction of the same type of LTP (Diamond et al., 1992; Pavlides et al., 1993). The initial rapid facilitation of signalling might help the organism to

appraise the novel situation; gradually the genomic phase will take over and restore the activity of the circuits to regain homeostasis (Joëls et al., 2006).

Overall, this implies that the temporal pattern of activation by corticosterone is different for the various areas. As summarized in Figure 2.2, both the hippocampus and amygdala, are more sensitive for incoming signals during stress or corticosterone exposure, while activity in the PVN is rapidly inhibited. In a delayed fashion, the hippocampus will switch to a state where the threshold for activation is elevated, while activation thresholds in the amygdala and hypothalamus do not differ between the two time-domains. Hypothetically, this can have consequences for the cognitive functions associated with these brain areas. For example, as the amygdala is involved in emotional memory formation, the prolonged activation in this area might support efficient encoding of emotional aspects of a stressful event, which could explain the preferential memory of emotional over neutral, hippocampal-dependent information (Buchanan and Lovallo, 2001; Karst et al., 2010). Finally, it seems that a second exposure of corticosterone switches amygdalar excitability back to its pre-stress state (Karst et al., 2010). This mechanism could protect the amygdala from inappropriately prolonged activation (McEwen, 2001; Karst et al., 2010). For the PFC, the limited data so far, suggest that its sensitivity is elevated by corticosterone in both an acute and more prolonged manner. However, as the data for the PFC is still sparse, we have not included it in Figure 2.2.

2.3 Molecular aspects of non-genomic corticosterone actions

The quest for a better understanding of the role of non-genomic corticosteroid signalling is paralleled by another quest: that for a better understanding of the cellular basis of these non-genomic effects. Here we will summarize the current state of understanding of the membrane localization, and translocation, of the MR and GR as well as that of their downstream signalling partners. We will, again, focus mostly on corticosteroid signalling in neural tissues but we will also use knowledge from the periphery and of related steroids and their receptors where necessary.

Presence of MR and GR at the plasma membrane, critical evaluation of the evidence

For many years the membrane localization of the MR and GR has been controversial, however, over the last years evidence of their membrane presence has culminated. (i) Intracellular applied corticosterone cannot induce rapid non-genomic effects; therefore it is unlikely that the receptors are located inside the cells. (ii) Membrane impermeable corticosterone-BSA (cort-BSA) and dex-BSA conjugates induce the same rapid effects as free corticosterone or dexamethasone. Moreover, they do so with equal (Xiao et al., 2010) to slightly reduced (Karst et al., 2005; Qi et al., 2005)

Hippocampus
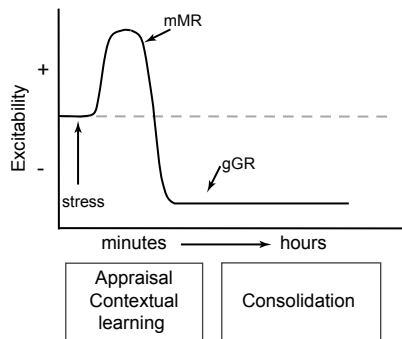
Amygdala (BLA)
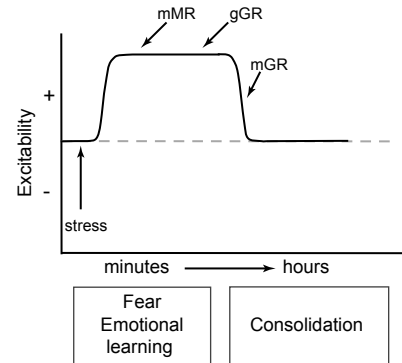
Hypothalamus
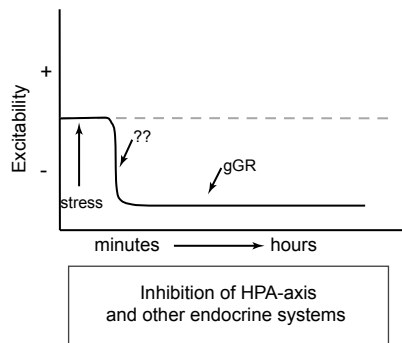
Figure 2.4: A putative model of the temporal dynamics of excitability in the hippocampus, amygdala and hypothalamus

A stressor or corticosterone injection induces a temporal diverse set of responses in the three different brain areas. Denoted are the receptors that are (mainly) responsible for the effects in the different areas. Importantly, the temporal pattern of excitability in hippocampus, amygdala and hypothalamus determines the actions of stress and corticosterone on neuroendocrine regulation, behaviour and cognition. mMR/mGR (membrane-associated MR/GR), gGR (genomic GR), ?? (receptor unclear).

efficacy. (iii) Most convincingly, the presence of MR and GR has been shown in synaptosome extracts (Komatsuzaki et al., 2005; Wang and Wang, 2009; Qiu et al., 2010) and at neuronal membranes using electron microscopy (Johnson et al., 2005; Prager et al., 2010). (iv) Finally, the MR and GR are by no means unique in their association with the plasma membrane. Membrane localization has been shown for most, if not all, steroid receptors including the ER α and β, AR and PR (Hammes and Levin, 2007).

Not all rapid corticosteroid effects can be attributed to the MR or GR though. Multiple non-genomic actions of corticosteroids on neurotransmission (Wiegert et al., 2006; Di et al., 2009), HPA-axis regulation (Evanson et al., 2010b) and behaviour (Sandi et al., 1996b) remain in the presence of MR and GR antagonists and are thus postulated to require a novel membrane-associated receptor. However, the identity of this receptor has proved very difficult to resolve; as yet, none have been cloned. The most likely candidates are G-protein coupled receptors (GPCR), because inhibitors of G-proteins can prevent many —though not all (Orchinik et al., 1997)— MR/GR independent corticosteroid effects (Di et al., 2003, 2005). Multiple non-MR/GR corticosteroid binding sites have been identified in the membrane of

neuronal substrates in a number of species (Orchinik et al., 1991, 1992, 1997, 2000; Guo et al., 1995; Maier et al., 2005; Breuner and Orchinik, 2009; Schmidt et al., 2010). However, the affinity and selectivity of these binding sites is very variable, making it unlikely that they all stem from a single type of evolutionary conserved receptor.

The association of steroid receptors at the plasma membrane

How is the membrane association of receptors mediating rapid corticosteroid actions accomplished and how is this process regulated? Unfortunately, there is little known about this subject regarding MR and GR. However, much more results have been obtained on the membrane translocation of ERα. Since ERα and corticosteroid receptors may share some of the pathways involved in membrane localization, we will first evaluate the available insights in the ERα and next compare this with what is presently known about corticosteroid receptors.

The estrogen receptors ERα and ERβ can both be targeted to the cell membrane (Gorosito et al., 2008; Micevych and Dominguez, 2009) where they primarily exist in caveolae (Razandi et al., 2002). Caveolae are invaginations of the plasma membrane formed by caveolins, scaffolding proteins that bind and bring together a large number of signalling molecules including GPCRs, G-proteins, c-Src and other kinases; this facilitates rapid signal transduction (Anderson, 1998; Cohen et al., 2004). The most ubiquitously expressed caveolin is caveolin-1. Ablation of caveolin-1 severely diminished ERα membrane localization (Sud et al., 2010). Moreover, mutation of a single amino acid (S522A) in the ligand binding domain of the ERα resulted in a 60 % reduction of caveolin-1 binding, membrane localization and rapid signalling of ERα (Razandi et al., 2003). Caveolin-1 binding is also required for membrane translocation of the ERβ, AR and PR (Lu et al., 2001; Salatino et al., 2006; Gilad and Schwartz, 2007). Mutation of another amino acid, cysteine477 (C477A), resulted in an almost complete reduction of ERα membrane localization, while its genomic functions were left undisturbed (Acconcia et al., 2005). This mutation was shown to be essential for palmitoylation of the receptor. Palmitoylation is a post-translational modification where a lipid tail is attached to the receptor, thus enabling insertion into the plasma membrane. ERα palmitoylation is essential for caveolin-1 binding, membrane translocation and rapid signalling (Acconcia et al., 2005; Pedram et al., 2007). A final component of the ERα membrane translocation pathway was identified recently: disruption of heat shock protein (HSP) 27 prevented palmitoylation, caveolin-1 binding, membrane localization and rapid signalling of ERα (Razandi et al., 2010). Together this leads to a model where ERα associates with HSP27, this interaction enables ERα to get palmitoylated, and due to the palmitoylation the receptor can bind caveolin-1 which facilitates transport to the plasma membrane (see Figure 2.5A).

Importantly, this membrane translocation process seems to be a common pathway for all steroid receptors. The group of Levin (Pedram et al., 2007) identified a conserved sequence surrounding the palmitoylation site of ERα and this same
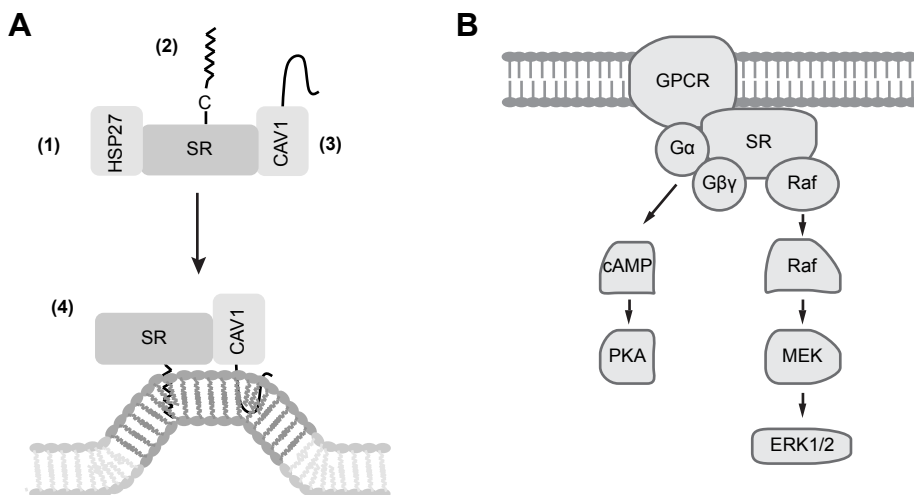
Figure 2.5: Steroid receptor membrane association and downstream signalling
(A) The putative common pathway for membrane translocation of steroid receptors is shown with the ERα as example. Translocation of the ERα requires the association of heat shock protein 27 (HSP27) (step 1), subsequently the receptor is palmitoylated at cysteine 477 (step 2), this facilitates association of the adaptor protein caveolin-1 (CAV1) (step 3). Finally, the ERα is transported to the plasma membrane, where it is localized in caveolae (step 4). (B) Model of the downstream signalling pathways implied in non-genomic corticosteroid signalling in neurons.

sequence was identified in the AR, PR, ERβ and other receptors. Mutation of key amino acids in this sequence abolished membrane localization and rapid signalling for all steroid receptors tested (Pedram et al., 2007). Similarly, association of HSP27 is required for membrane translocation of ERα, PR and AR (Razandi et al., 2010). Thus, so far the data suggest that there is a common membrane translocation pathway for all (or most) steroid receptors involving caveolin-1, palmitoylation and HSP27.

Membrane translocation of MR and GR

Now the question remains whether the MR and GR are transported to the membrane in a similar way. For these receptors only a few studies have been reported and none in brain cells. In peripheral models an association between both MR and GR to caveolin-1 has been demonstrated. In epithelial cells, dexamethasone induced rapid binding of GR to c-Src and subsequent activation of the PI3K-Akt pathway (Matthews et al., 2008). Transfection of a double-negative form of caveolin-1 disrupted all aspects of this signalling cascade, as did disruption of caveolae. In addition, a direct interaction between the GR and caveolin-1 was seen with co-immunoprecipitation (Matthews et al., 2008). In contrast, in hepatic cells no colocalization of membrane-associated GR and caveolin-1 could be found with conventional confocal microscopy (Spies et al., 2006).

For MR, a similar association was studied in caveolin-1 knockout (cav1-/-) mice (Pojoga et al., 2010a,b). First of all, a direct association between the MR and caveolin-1 (but not caveolin-2) was shown with co-immunoprecipitation in heart homogenates from both rat and mouse as well as in cultured human endothelial cells (Pojoga et al., 2010a). As expected, this association was lost in cav1-/- mice. Secondly, these mice showed heightened vascular responses to treatment with the MR antagonist eplerenone (as compared to wild type mice) and a reduced sensitivity to aldosterone treatment on myocardial damage (Pojoga et al., 2010b). Thus, not only is the MR associated with caveolin-1 in vascular tissues, but a loss of caveolin-1 also alters the vascular responses to MR agonists and antagonists. The precise consequences of the loss of caveolin-1 for MR-associated functioning seem to depend strongly on the context of the response.

Additional supporting evidence for the membrane localization of the MR comes from the group of Grossmann and Gekle (2008, 2010). In an initial study, they showed that transfection of only the ligand binding domain of the MR was sufficient for aldosterone to rapidly activate the ERK1/2 pathway in Chinese hamster ovary cells (Grossmann et al., 2008). This is similar to the ERα, where the ligand binding domain suffices for membrane translocation and signalling (Razandi et al., 2002). More recently, they studied the colocalization between the MR and the EGF receptor. This colocalization was lost when lipid rafts (including caveolae) were disrupted (Grossmann et al., 2010). This strongly suggests that the MR is localized in caveolae, since the EGF receptor is known to be associated with caveolae.

Finally, regarding the conserved palmitoylation motif, an interesting picture emerges. The palmitoylation motif of the GR contains all essential groups and would be predicted to be a palmitoylation site (although the GR was not tested in the original study) (Pedram et al., 2007). The MR, by contrast, lacks the essential cysteine residue. As this cysteine provides the thiol group to which the palmitate tail is transferred, the MR cannot be palmitoylated at this sequence. The MR could be palmitoylated at another motif or could translocate to the membrane through an alternative pathway.

Regulation of membrane translocation and place in the membrane

Why does only part of the receptor population translocate to the membrane while the bulk remains in the cytoplasm and nucleus, and what determines the proportion of these pools? For the ERα, most studies estimate that approximately 5–10 % of the receptor population is localized at or in the membrane, which leaves 90–95 % of the population in the cytoplasm and nucleus (Chambliss et al., 2000). Caveolin-1 overexpression was found to elevate the proportion of membrane ERα (Sud et al., 2010), suggesting that this protein has a regulatory effect.

It is known that ligand binding affects membrane translocation. Most studies show that treatment with (high concentration of) ligands reduces palmitoylation, association with caveolin-1 and membrane expression (Razandi et al., 2002; Ac-

concia et al., 2005; Micevych and Dominguez, 2009). In contrast, other studies report an *increased* membrane translocation with steroid treatment (Razandi et al., 2002; Gorosito et al., 2008; Bondar et al., 2009). Clearly, the timing, concentration and duration of ligand exposure will influence these effects. GR expression in hippocampal synaptosomes was slightly decreased after 3 weeks of daily corticosterone injections and increased by adrenalectomy (which abolishes endogenous corticosterone) (Wang and Wang, 2009), suggesting that the GR also traffics from the membrane by ligand treatment. Interestingly though, in amygdalar neurons acute stress or corticosterone treatment abolished MR-mediated non-genomic signalling, while it actually allowed GR-mediated actions to take place (Karst et al., 2010).

It is still unclear how steroid receptors are integrated into the plasma membrane. The effectiveness of impermeable hormone conjugates (such as estradiol-BSA or cort-BSA) suggests that the receptors are accessible from the outside of the plasma membrane. In addition, biotinylation studies (for ERα) provide evidence for an extracellular recognition site of the receptors (Bondar et al., 2009). This would suggest that the receptors are integrated in the outer sheet of the membrane with their palmitate tail. However, this seems in contradiction with studies showing a direct interaction of steroid receptors with caveolin-1 (Razandi et al., 2002; Sud et al., 2010) and second messenger molecules such as c-Src and G-proteins (Sanchez et al., 2011), which suggest that receptors are inserted into the inner sheet of the membrane, where they are able to interact with the cytoplasmic molecules. Possibly the steroid receptor shuttles to the inside of the membrane upon activation, but at present this is mere speculation.

A general model of steroid downstream signalling

As a final point we will evaluate the secondary pathways of steroid receptors. Surprisingly, although the physiological functions of steroids are very diverse (ranging from sexual differentiation to electrolyte balance) the non-genomic signal pathways show a large overlap. We will discuss the very basics of steroid receptor downstream signalling in order to come to general characteristics.

As steroids are lipophilic and easily penetrate the plasma membrane, their receptors do not need to be located at the plasma membrane. More likely, membrane-association of steroid receptors is required for binding to signalling partners that are present only at the membrane. In fact, caveolae are well known signalosomes that bring receptors, adaptor molecules and kinases together (Anderson, 1998). Indeed, the ERα was shown to assemble a multi-protein complex consisting of other membrane-spanning receptors (most often growth factor receptors) and multiple small adaptor molecules like G-proteins (both Gα and Gβγ subtypes) (Kumar et al., 2007), c-Src (Sanchez et al., 2011) and PI3K (Simoncini et al., 2000). Through this signalosome a variety of kinase pathways are activated (Hammes and Levin, 2007; Vasudevan and Pfaff, 2007; Micevych and Dominguez, 2009). Most commonly, activation of the phospholipase C - protein kinase C (PLC-PKC), cAMP-PKA (protein

kinase A), PI3K-Akt and Ras-ERK pathways have been found (Figure 2.1). Importantly, activation of components of these three general pathways has been reported for the ERα, ERβ, AR, PR, MR and GR. For example, ERK1/2 phosphorylation can be seen within minutes of stimulation with aldosterone, corticosterone, estradiol, androgens or vitamin D (Qiu et al., 2001; Pedram et al., 2007; Grossmann et al., 2008) and reviewed in Hammes and Levin (2007) and Grossmann et al. (2010).

The initial event, i.e. the composition of the signalosome, seems to determine which downstream pathway is recruited. For example, in hippocampal neurons estradiol can activate two distinctive pathways in a single cell; on the one hand activation of ERK1/2 leads to subsequent genomic effects through activation of the transcription factor cAMP response element binding (CREB), on the other hand inhibition of PKA induces a decrease in Ca^{2+}-currents (Boulware et al., 2005). These two effects originate from two separate pathways; one involves ERα bound to caveolin-1 and attracts the metabotrophic glutamate receptor GluR1A and G_q resulting in the activation of ERK1/2 and CREB, while the other effect originates from an ERα/β heterodimer bound to caveolin-3, GluR2/3 and G_{io}, this pathway results in the inhibition of PKA and Ca^{2+}-currents (Boulware et al., 2007). Also interesting in this regard is the role of the coreceptors in the signalosomes; multiple studies showed that inhibition of growth factor signalling prevented the non-genomic effects of steroids. For example, phosphorylation of ERK1/2 by either aldosterone (Grossmann et al., 2005) or estrogen (Razandi et al., 2003) could be prevented by inhibitors of the EGF receptor. Direct interactions between the MR (Grossmann et al., 2010) and ERα (Song et al., 2010) with growth factor receptors were also shown. In fact, some people opt for a GPCR hypothesis for rapid steroid signalling; the activation of a membrane steroid receptor activates a growth factor receptor and this enables further signalling (see Micevych and Dominguez, 2009). Whether this is just *one* mechanism of action or *the* mechanism of action remains to be determined.

Ultimately, activation of the cellular pathways affects the physiology of cells and tissues. Depending on the precise composition of the signalosome and the cellular context a wide variety of effects are obtained. These are too diverse to discuss in full here, but we will give a few examples for rapid aldosterone signalling in the periphery. In kidney cells, aldosterone rapidly enhances sodium transport through an ERK pathway, this results in a rapid effect on sodium absorption in these cells which eventually also regulates blood pressure (Gekle et al., 2001). In the vascular system, activation of the enzyme nitric oxide (NO) synthase by aldosterone (through a PI3K-Akt pathway) results in an increased release of NO which attracts immune cells and affects constriction of vascular smooth muscle cells (Hafezi-Moghadam et al., 2002; Mutoh et al., 2008).

The signal partners of central non-genomic corticosteroid signalling

The cellular pathways involved in neuronal non-genomic corticosteroid actions have not been studied in detail yet, however, many studies did examine the involve-

ment of some signal partners (see Table 2.1) and we can fit these within the general model of non-genomic steroid signalling. As for ERα and other steroid receptors, the most obvious effectors of the rapid effects are G-proteins. Inhibition of G-protein activation abolished the rapid effects of corticosterone on (i) inhibition of mEPSCs in the hypothalamus (Di et al., 2003), (ii) facilitation of mIPSCs in the hypothalamus (Di et al., 2005), (iii) facilitation of mEPSC's in the hippocampus (Olijslagers et al., 2008) (iv) inhibition of potassium currents in the hippocampus (Olijslagers et al., 2008), (v) inhibition of calcium currents in the hippocampus (Ffrench-Mullen, 1995) and (vi) activation of glutamate uptake in frontal neurons (Zhu et al., 1998) (see also Table 2.1). Interestingly, as for the estradiol effects in the hypothalamus, corticosterone can activate two different signalling pathways in single neurons in the hypothalamus. Through activation of Gαs, corticosterone induces the release of endocannabinoids and an inhibition of glutamate release, while Gβγ activation leads to the release of NO and the facilitation of GABA release in the same neuron (Di et al., 2009). It remains to be investigated whether different GPCRs or caveolin subtypes are also involved.

More downstream, corticosterone rapidly activates both the cAMP-PKA pathways and the ERK1/2 pathway in neurons. cAMP-PKA signalling is required in the hypothalamus (Malcher-Lopes et al., 2006) and for one effect in the hippocampus (Liu et al., 2007). Activation of the ERK1/2 pathway is seen after corticosteroid exposure in some cases (Xiao et al., 2005, 2010; Roozendaal et al., 2010) and is required for other effects (Olijslagers et al., 2008). Evidence for the involvement of the PI3K pathway has not yet been studied in the brain. Thus, although still very limited, non-genomic corticosteroid signalling in neurons follows similar kinase pathways as their peripheral counterparts and as that of other steroid receptors. Likely, the regional variation in the precise signalling cascades activated will prove to be crucial for understanding the more subtle difference between the actions in different neurons and under changing conditions. As examples from related fields show, this variation could well arise from the recruitment of different proximal adaptor molecules and interactions with signalling of other (neurotransmitter) receptors. In Figure 2.5B we show a very general model of the downstream signalling partners in central non-genomic corticosteroid signalling.

2.4   Concluding remarks

The existence of rapid effects of corticosterone has been known for over 50 years; however, it is only in the last 10 years that these effects have been studied in more detail. Yet, there are still many unanswered questions.

First, we cannot appreciate the consequences of non-genomic effects of corticosteroids when they are studied in isolation, instead we must view these effects in the context of the complete stress response. Exactly how rapid non-genomic and

genomic actions are integrated to collectively accomplish the behavioural response to stress awaits further investigation, as discussed in the previous section.

Secondly, through its non-genomic effects corticosterone acts in the same time-domain as other transmitters and hormones released after stress, e.g. catecholamines or CRH. This gives ample opportunities for cross-talk between the various stress hormones (Alfarez et al., 2009). For example, activation of the noradrenergic system in the amygdala is required for effects of corticosterone to take place (Roozendaal et al., 2002, 2006). However, at this time relatively little is known about the mechanism by which corticosteroids alter responsiveness to other stress factors and if non-genomic corticosteroid signalling is involved.

Thirdly, only a few signalling partners for rapid effects have been discovered. A comparison of the available data (see Table 2.1) suggests that many pathways are shared across brain areas. For example, multiple studies have proven involvement of G-proteins and the ERK-CREB pathway. Importantly, these same pathways are also activated by rapid signalling of other steroid receptors (Hammes and Levin, 2007; Vasudevan and Pfaff, 2007; Levin, 2008). Information gathered in these related fields could serve as an important guideline for investigation of the signalling partners of corticosteroids in the brain. For instance, both rapid corticosterone (Di et al., 2009) and estradiol signalling (Boulware et al., 2007) in neurons suggests that the specific type of G-protein that is engaged in the hormonal actions is an important determinant of the subsequent signalling cascade and the physiological outcome.

Fourthly, regulation of membrane translocation of the MR and GR in neurons is still undiscovered. Caveolin-1 is required for membrane translocation of all steroid receptors including the MR and GR (Matthews et al., 2008; Pojoga et al., 2010b). However, this has yet to be shown for the MR and GR in neurons. All three types of caveolins are expressed in the brain and they are known to be required for ERα and ERβ non-genomic signalling (Boulware et al., 2007). Interestingly, neurons do not have caveolae (Head and Insel, 2007), instead caveolins seem to be associated with synaptic markers and interact with multiple types of glutamate receptors. Thus, it is likely that caveolin association enables the enrichment of MR and GR at synaptic sites in the membrane (Johnson et al., 2005; Prager et al., 2010) and places the receptors well in reach to regulation of synaptic transmission.

Finally, the conserved palmitoylation motif found in many steroid receptors, including the ERα and the GR, is presumably ineffective in the MR. This motif is absolutely required for palmitoylation and membrane expression of ERα, ERβ, PR and AR (Pedram et al., 2007) and it thus remains unclear if and how the MR could be palmitoylated, possibly at another sequence. Consensus palmitoylation sequences were identified in the MR with the online CSS-Palm tool (Ren et al., 2008), however, this still needs conformation *in vivo*. Alternatively, the MR could use another pathway for translocation to the membrane.

Potassium currents in neuronal-like cell lines, models to study non-genomic Mineralocorticoid Receptor functionality

Femke L. Groeneweg[1], Henk Karst[2],
Roel de Rijk[1], E. Ron de Kloet[1], Marian Joëls[2]

[1] Department of Medical Pharmacology, Leiden University / LUMC, Leiden, The Netherlands.
[2] Department of Neuroscience and Pharmacology, University Medical Center Utrecht, Utrecht, The Netherlands.

Many rapid non-genomic actions of corticosterone in the brain act through the membrane-associated subpopulation of the MR, including a rapid reduction in fast-inactivated A-type potassium currents by corticosterone. Here we present two attempts to reproduce this membrane-associated role of the MR in neuronal-like cell lines. In differentiated NS-1 cells we obtain A-type potassium currents. Corticosterone did not affect these currents in empty-vector transfected cells. Importantly, upon transfection with the MR both corticosterone and cort-BSA did lead to a rapid reduction of A-type current amplitude ($> 25\%$). In contrast, the slowly-inactivated potassium currents in N1E-115 cells were not affected by corticosterone in the presence of the MR. The MR is thus sufficient for a rapid inhibition of fast-inactivated potassium channels by corticosterone and this effect is specific for certain subtypes of potassium channels. We further find that the MR is very instable in an *in vitro* setting and that successful DNA transfection and MR mRNA transcription does not necessarily lead to detectable MR protein levels.

3.1 Introduction

Corticosteroids play a major role in the response of the brain to stress. Within the brain, corticosteroids exert their actions through two receptors: the GR and MR. For many years, the MR and GR were purely associated with a genomic role as they act as transcription factors within the nucleus (de Kloet et al., 2005; Datson et al., 2008). While this is generally true, corticosteroids can also influence a wide range of behaviors and endocrine outputs within minutes, a time frame that is too rapid to be explained by genomic effects (Groeneweg et al., 2011). In agreement, we and others recently established that corticosteroids rapidly alter neuronal activity and excitability in a number of brain areas (Di et al., 2003; Karst et al., 2005, 2010; Tasker et al., 2006). Several of these rapid actions require the MR (and some also the GR) and seem to occur by corticosteroids binding to a molecule that is accessible from the outside of the cell membrane. In agreement, a subpopulation of the MR and GR have been shown to be present at the plasma membrane (Johnson et al., 2005; Prager et al., 2010). Despite considerable knowledge regarding the functional significance of membrane-initiated corticosteroid signaling, the molecular pathways underlying these actions are just beginning to be unraveled in neurons (see also *Chapter 2*).

In vitro cell lines have been very valuable to examine the effects of aldosterone or corticosterone through the MR on cell signaling. The identification of many signaling partners of membrane-associated MR signaling has been accomplished in cell lines, including cAMP, ERK1/2, G-proteins, caveolin-1, PKC and PI3K (Grossmann and Gekle, 2009; Dooley et al., 2012). Additionally, structure-function relationships can be delineated. Thus far, it has been established that transfection of the ligand binding domain of the MR is sufficient for aldosterone to rapidly activate the ERK1/2 pathway (Grossmann et al., 2008). For other steroid receptors mutations of single amino acids have aided the understanding of the membrane translocation pathways of these receptors (Levin, 2009). However, the genomic actions of corticosteroids are greatly affected by cell-context (John et al., 2011) and remarkably low overlap in corticosteroid regulated gene patterns were found between neuronal and non-neuronal cells types (Polman et al., 2012, 2013). Whether non-genomic corticosteroid actions are also different between neuronal and non-neuronal settings remains to be addressed. In addition, numerous single nucleotide polymorphisms (SNPs) in the MR gene, including the promoter region, have found to be associated with variability in neuroendocrine and autonomic activity (Martinez et al., 2009; DeRijk et al., 2011; van Leeuwen et al., 2010a,b) and the occurrence of psychiatric symptoms (Kuningas et al., 2007; Klok et al., 2011). Functional *in vitro* models would be valuable to investigate whether altered brain function associated with MR SNPs is purely explained by MRs genomic actions and expression levels or whether they also depend on the non-genomic membrane-associated functions of the MR.

Earlier, potassium currents of hippocampal cells were reported to be rapidly affected by MRs. The amplitude of fast-inactivating (A-type) potassium currents in CA1 neurons reduced rapidly after corticosterone application (Olijslagers et al.,

Chapter 3

2008). This effect was prevented by pretreatment with an MR antagonist. A-type channels are important for determining firing frequencies and to reduce the amplitude of back-propagating action potentials in dendrites (Hoffman et al., 1997). As such they are important for plasticity and excitability. For example, deletion of A-type channels potentiates the induction of LTP (Chen et al., 2006). A decrease in A-type current amplitude after corticosterone application would thus enhance plasticity and excitability in neurons.

Potassium currents can be induced in multiple neuronal-like cell lines. The widely used PC12 cell line expresses multiple types of voltage-dependent potassium channels (Hoshi and Aldrich, 1988; Castillo et al., 2001), including fast-inactivating A-type currents. In addition, a number of neuroblastoma cell lines show expression of multiple subtypes of potassium and other ion channels. Of these, the mouse neuroblastoma cell line N1E-115 shows induction of large amplitude potassium currents with both inactivating and non-inactivating components (Hirsh and Quandt, 1996; Lima et al., 2008).

Here, we tested the feasibility of using *in vitro* neuronal-like cell lines to mimic non-genomic effects of corticosterone on potassium currents, with the ultimate aim of unraveling the underlying mechanism. As both these cell lines are devoid of endogenous MR, we can further test whether MR expression is sufficient for rapid corticosterone actions to occur.

3.2   Methods

Compounds
Corticosterone was obtained from Sigma and first diluted in EtOH to a concentration of 15 mM and next to the final concentration in PBS or recording medium. The same concentration of EtOH was used as vehicle. Corticosterone-BSA (cort-BSA) was dissolved to a concentration of 12.5 µM in 0.9 % NaCl, 0.25 % carboxymethyl cellulose and 0.2 % Tween (solvent A). There are 23 molecules of corticosterone bound to one BSA-molecule, therefore 4.4 nM cort-BSA matches 100 nM of free corticosterone.

Cell culturing procedures and plasmids
In addition to PC12-Neurocreen-1 (NS-1) and N1E-115 cells, in some experiments COS-1 or CHO cells were used. COS-1 cells are maintained in high glucose DMEM and CHO cells in F-12 medium (both GIBCO), both supplemented with 10 % fetal bovine serum (FBS) and 1 % penicillin and streptomycin. The pRSV-MR plasmid that was used contains the human MR gene under a Lac promotor (kind gift of R. Evans (The Salk Institute for Biological Studies, La Jolla, CA)). pEYFP-hMR was generated by cloning the MR gene from the pRSV plasmid into the pEYFP-C1 plasmid (described in more detail in *Chapter 6*), generating an N-terminally YFP-tagged MR. pEYFP-C1 was from Addgene.
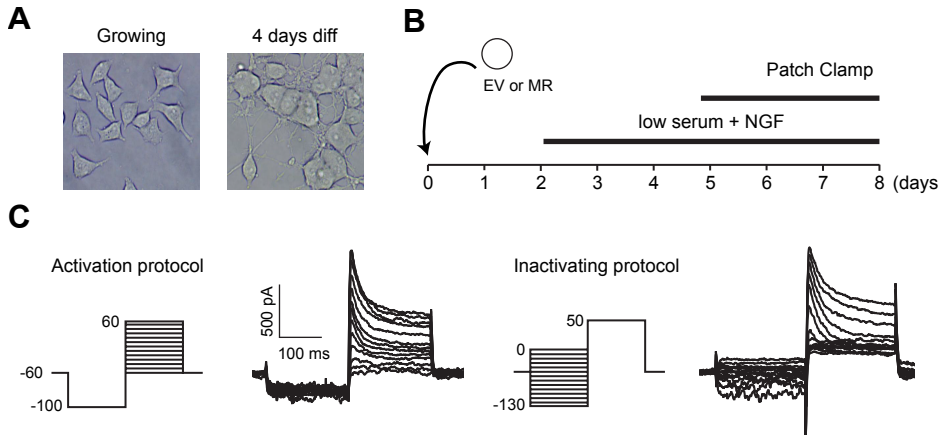
Figure 3.1: Patch protocols for NS-1 cells
(A) 3 days of NGF application leads to a neuronal-like phenotype in NS-1 cells. (B) The general experimental outline of single-cell patch clamp experiments in NS-1 cells. (C) Voltage dependency of the potassium currents are obtained with the activation (left) and inactivation protocols (right). Example currents are shown next to the corresponding protocols.

NS-1 cells

NS-1 cells were maintained in RMPI 1640, supplemented with 10 % horse serum (HS), 5 % FBS and 1 % penicillin and streptomycin. Throughout culturing, all plates and coverslips were pre-coated with collagen (60 μg / 10 cm^2, overnight at RT) to enable better cell attachment. DNA transfection was performed with an electroporation method, using the Amaxa Nucleofection apparatus (Lonza). In short, NS-1 cells were trypsinated and divided in 1 mln aliquots and spun down. Cell pellets were dissolved in 100 μl prewarmed nucleofector-solution, carefully mixed with 5 μg DNA and transferred to a certified cuvette for electroporation (program U29). Immediately after, cells were remixed with growth medium and plated onto collagen coated ø 13 mm coverslips, allowing differentiation 24 h later. For NS-1 cells, differentiation into a neuronal-like phenotype is acquired with a combination of serum starvation and nerve growth factor (NGF) treatment. At 24 h after transfection, culture medium was replaced for low serum medium (RMPI 1640 supplemented with 3.4 % HS and 1.6 % FBS). After 24 h this was replaced for fresh low serum medium with 0.05 % NGF. Cells were kept in NGF-containing low serum medium for 3–5 days and medium was replaced every 2 days. NS-1 cells can differentiate into an adrenocortical-like phenotype with glucocorticoids, therefore all sera used in the low serum medium were 2× charcoal-stripped to bind and wash away all reminiscent endogenous hormones. Cells were used for electrophysiology after 3–5 days of NGF treatment (the timeline of all procedures is summarized in Figure 3.1B).

N1E-115 cells

N1E-115 cells were maintained in low glucose DMEM, supplemented with 10 % FBS and 1 % penicillin and streptomycin. N1E-115 cells differentiate into a neuronal-like cell type with serum starvation and 2 % DMSO. Thus, cells were plated onto ø 13 mm coverslips coated with poly-l-lysin (100 μg/10 cm^2, 2 h at RT). 24 h after plating, normal growth medium was replaced for differentiation medium (low glucose DMEM, supplemented with 2 % FBS and

51

2 % sterile DMSO; medium replaced every 2 days). N1E-115 cells were transfected with lipo-fectamine (Life Technologies) during differentiation. In short, cells were washed with PBS and transfected in empty DMEM according to normal protocol (lipofectamine:DNA = 3:1, 1 µg DNA / 100 000 cells). Cells were incubated with the lipofectamine-DNA mixture for 4 h and thereafter replenished with differentiation medium. Cells were used for electrophysiol-ogy 2–3 days after transfection, thus after 6–7 days of differentiation (for the time line see Figure 3.6B). 24 h before patch clamping, normal differentiation medium was replaced for media containing charcoal-stripped sera to prevent effects of endogenous hormones.

Western blot

For Western blot analysis of MR and control proteins, cells were transfected with the required plasmids, harvested 48 h after transfection and prepared for western blot. Protein lysates, SDS-polyacrylamide gel electrophoresis and Western blotting were performed as described previously (Vreugdenhil et al., 2007). For each experiment, equivalent amount of samples (10–15 µg) were used. The blots were incubated with 1:500–2500 MR 1D5 or 2B7 antibodies (both are generous gifts of Gomez-Sanchez (Gomez-Sanchez et al., 2006)) and co-assessed for α-tubulin (1:5000; Sigma-Aldrich) in combination with 1:5000 goat-anti-mouse IgG HRP. All antibodies were diluted in TBST with 0.5 % milk powder. Primary antibody incubation was done for 1 hour at RT or for 16 hours at 4 °C. Detection was performed with the ECL detection system (GE Healthcare).

Immonufluorescence staining

For immunofluorescence stainings cells were plated on collagen-coated coverslips (diameter 12 mm) and used for experiments 48 h after transfection. If required, cells were treated with hormones or vehicle for 2 h before fixation. Fixation was performed with 4 % paraformalde-hyde (PFA) for 30 min at RT. Subsequently, cells were permeabilized with 0.5 % Triton-100 in PBS, incubated with primary antibody (1:1000 MR 1D5 antibody (Gomez-Sanchez et al., 2006)) in PBST (0.1 % Triton-100 in PBS), supplemented with 1 % BSA for 60 min. Next, cells were incubated for 60 min with 1:1000 goat-anti-mouse AlaxaFluor488 (or 594) in PBST with 1 % BSA and finally for 10 min with 1:5000 with Hoechst 33342 (Life Technologies) for nuclear counterstaining (all in the dark). Between all steps, cells were washed for 3×5 min with PBST. Cells were mounted with Aqua Poly/Mount (Polysciences) and imaged on a conventional flu-orescence microscope (Leica DM6000). For YFP-MR, fixation, permeabilization and Hoechst staining and mounting were performed according to the same protocol, but no antibodies were applied.

qPCR

For RT-qPCR, NS-1, N1E-115 and COS-1 cells were either left untransfected or transfected with 5 µg EV, 1, 5, or 10 µg MR / mln cells (with their respective transfection methods) and har-vested by TRIZol method 48 h later. Reminiscent DNA was removed by DNAse treatment (Life Technologies, 1 µl DNAse for 1 µg DNA). Subsequently, cDNA was synthesized using the iScript kit (Bio-Rad). A set of 20 bp primers was designed to span a 220 bp region in exon 2–3 of the MR. RT-qPCR was conducted using the capillary-based LightCycler® thermocycler and fast start DNA masterPLUS SYBR Green I kit (Roche) according to the manufacturers'

instructions and described in more detail in (Polman et al., 2012). All samples were run twice and relative expression levels were calculated with a generated standard curve.

Luciferase essay

For the luciferase essay, cells were transfected with a combination of $500\,ng/10\,cm^2$ YFP, YFP-MR or MR together with $100\,ng/10\,cm^2$ TAT3-Luciferase (tyrosine amino transferase triple hormone response element) and $2\,ng/10\,cm^2$ pCMV-Renilla (Promega). 24 h after transfection cells were treated with 10 nM corticosterone, 10 nM aldosterone or 0.001 % EtOH in culture medium supplemented with charcoal stripped FBS. After 20 h, cells were lysed with passive lysis buffer and firefly and renilla luciferase luminescence was determined according to the general prescription of the dual label reporter essay (Promega) on a luminometer (CENTRO XS3 LB960, Berthold). For analysis, the ratio of the two luminescent signals were used to control for differences in transfection efficiency and cell density.

Electrophysiology

Differentiated NS-1 or N1E-115 cells plated on ø 13 mm coverslips were submerged in recording solution in a custom made recording chamber. For NS-1, recording medium contained 130 mM NaCl, 5 mM KCl, 2 mM CaCl$_2$, 1 mM MgCl$_2$, 10 mM HEPES and 5 mM glucose, supplemented with 10 mM tetraethylammonium (TEA) to block sustained potassium currents, pH 7.3 adjusted with NaOH (all from Sigma-Aldrich). For N1E-115 cells, no TEA was added and molarity was compensated by using 15 mM glucose. Throughout the recordings the recording solution was continuously refreshed and kept at 32 °C. For both cell lines, the recording pipette contained: 140 mM KCl, 10 mM HEPES, 5 mM EGTA, 2 mM MgCl$_2$, 0.1 mM CaCl$_2$, 2 mM MgATP and 0.4 mM Na$_2$GTP (pH 7.3 adjusted with KOH; all from Sigma-Aldrich). Cells were imaged with an upright microscope (Axioskop 2 FS plus, Zeiss), equipped with differential interference contrast and wide field fluorescence. Healthy and well differentiated cells were identified manually and patched using 4–6 MΩ borosilicate glass electrodes (0.86/1.5 mm inner/outer diameter, Harvard Apparatus). For some experiments, GFP or YFP-MR fluorescence was checked with wide field fluorescence and moderately fluorescent cells were chosen for patch clamping. To prevent phototoxicity, fluorescence exposure duration was kept at a minimum and low intensity fluorescence was used. Whole cell voltage clamp recordings were made with an Axopath 200B amplifier (Axon instruments) interfaced to a computer via a Digidata (type 1322A; Axon Instruments). After reaching a gigaseal, the membrane patch was ruptured and the cell was kept at a holding potential of $-60\,mV$ (NS-1) or $-70\,mV$ (N1E-115). Series resistance was compensated for 60 %. To test voltage dependency of A-type current activation and inactivation, two types of protocols were used. Protocol 1 tested activation properties by changing the activation step from $-60\,mV$ to $+60\,mV$ in 10 mV steps. Protocol 2 tested voltage dependency of inactivation by changing a prepulse from 0 mV to $-130\,mV$ in 10 mV steps. Duration of the voltage steps differed for NS-1 and N1E-115 cells, all protocols are shows in Figure 3.1C and 3.6C.

Data analysis was performed with ClampFit (Molecular Devices). Data was corrected for leak current and baseline and maximum current amplitudes were recorded and plotted against voltage steps. Half maximal values were calculated as the first voltage step where the half maximum amplitude was achieved.

Statistics and data representation

Rapid effects of compounds on potassium currents were tested with two-tailed paired samples t-tests on the original, uncorrected data. Due to large differences in basal amplitudes between cells, the A-type current data is represented as % of maximum amplitude during baseline recordings in all figures. All between-subject comparisons were performed with two-tailed independent sample T-tests for comparisons of 2 groups or one-way ANOVAs for < 2 groups.

3.3   Results

A-type currents in Neuroscreen-1 cells

PC12 cells are a well-known neuronal-like cell line that shows large potassium currents upon differentiation (Hoshi and Aldrich, 1988; Castillo et al., 2001). Neuroscreen-1 (NS-1 cells are a subclone of PC12 cells with a higher responsiveness to NGF (Dijkmans et al., 2008). Upon stimulation with NGF, NS-1 cells show neuritogenesis within a day and develop a network of extensive neurites within 2–5 days upon NGF-induced differentiation (Dijkmans et al., 2008). We recorded single well-differentiated NS-1 cells in the voltage-clamp mode after 3–5 days of differentiation. Comparable to their parent strain, differentiated NS-1 cells showed large potassium currents with a large non-inactivating (delayed rectifier) and a smaller fast-inactivating (A-type) component. The delayed rectifying component was effectively blocked by $10\,\text{mM}$ TEA, thus revealing clear rapidly inactivating A-type currents (Figure 3.1C). The maximum A-type current amplitude (at $+60\,\text{mV}$) showed large cell-to-cell variation, ranging from 145 to $5600\,\text{pA}$, with an average of $1491 \pm 155\,\text{pA}$ ($n = 59$). A-type currents are most efficiently activated with a hyperpolarizing prepulse preceding the depolarizing step, relieving the voltage-dependent inactivation of the channels. Indeed, we found that a prepulse of $-130\,\text{mV}$ increases the potassium current to a subsequent depolarization by 2.5 ± 0.4 fold (compared to stepping directly from a holding potential of $-60\,\text{mV}$). NS-1 A-type currents were half maximally activated with a depolarization to $20.2 \pm 1.3\,\text{mV}$ and the half maximal value for inactivation was $-71.6 \pm 2.8\,\text{mV}$. Further characterization of the currents is presented in Figures 3.1 and 3.2.

Corticosterone and cort-BSA reduce A-current amplitude only after MR transfection

In the mouse hippocampus, corticosterone application led to a reduction in A-type current amplitude and a shift in activation properties so that larger depolarizations were required for the induction of similar A-type currents (Olijslagers et al., 2008). These effects were shown to require the MR. PC12 cells do not express endogenous MR (Lai et al., 2005).

First, we tested whether corticosterone could similarly affect A-type current amplitudes in NS-1 cells transfected with an empty vector (EV). In EV-transfected NS-1 cells, we observed a small, but statistically significant, decrease in maximal A-type current amplitudes ($-12.4 \pm 0.5\,\%$ compared to baseline; Figure 3.2A,B), presumably due to run down of cells during the patch procedure.

Next, we electroporated NS-1 cells with a plasmid containing human MR and induced differentiation the next day. The transfection efficiency of this method was assessed with transfection with (untagged) GFP. We found that the transfection efficiency was very high: $24\,h$ and $48\,h$ after transfection $89.4 \pm 1.1\,\%$ and $90.1 \pm 1.4\,\%$ of cells respectively was GFP positive ($n = 12$ wells). Due to differentiation cells do not divide and transfection efficiency is thus not expected to drop significantly over time, although this was not verified directly. We observed a rapid action of corticosterone on A-type currents in MR transfected cells. Within 5 to 10 minutes after application of $100\,nM$ corticosterone, A-type current amplitudes were strongly reduced (Figure 3.2A and C, top panel). This effect was most apparent with high depolarization steps. No effect was seen on activation or inactivation properties. Thus, the maximum A-type current amplitude was reduced to $64.7 \pm 0.1\,\%$ of baseline levels, but the voltage dependency of the channels was unaffected (Figure 3.2C–E, ½ max of $15.7 \pm 2.2\,mV$). This reduction of maximal A-type current amplitudes was significantly greater than in EV-transfected cells. In its non-genomic role, corticosterone has been reliably show to act at the cell membrane (Groeneweg et al., 2012). We therefore tested the effect of BSA-conjugated corticosterone (cort-BSA), a membrane-impermeable conjugate of corticosterone. Comparable to corticosterone, also cort-BSA application led to a reduction of the maximal A-type current amplitude (to $72.6 \pm 6.2\,\%$ of baseline levels), but did not affect voltage dependencies of the channels (Figure 3.2C, middle panel). Finally, vehicle treatment led to a much smaller reduction of A-type amplitudes in MR-transfected NS-1 cells (to $84.6 \pm 4.4\,\%$ of baseline levels, Figure 3.2C, bottom panel).

To conclude, we show that we can reproduce —in cell lines *in vitro*— the rapid, membrane-initiated reduction of A-type current amplitudes earlier observed in hippocampus slices. Moreover, here we show that expression of the MR is not only required for these effects, but MR expression is sufficient to obtain non-genomic corticosterone-induced effects.

Instability of MR protein in NS-1 cells leads to failure to reproduce results

We transfected NS-1 cells with a method known to give high transfection efficiency and with an MR plasmid (pRSV-MR) known to induce robust MR protein expression in other cell lines (Klok et al., 2011). However, when we assessed MR expression by Western blot $48\,h$ after electroporation we failed to find any MR protein (Figure 3.3A). As a control we also transfected COS-1 cells with the same pRSV-MR plasmid and here we found a clear MR positive band of the expected size ($107\,kDa$)
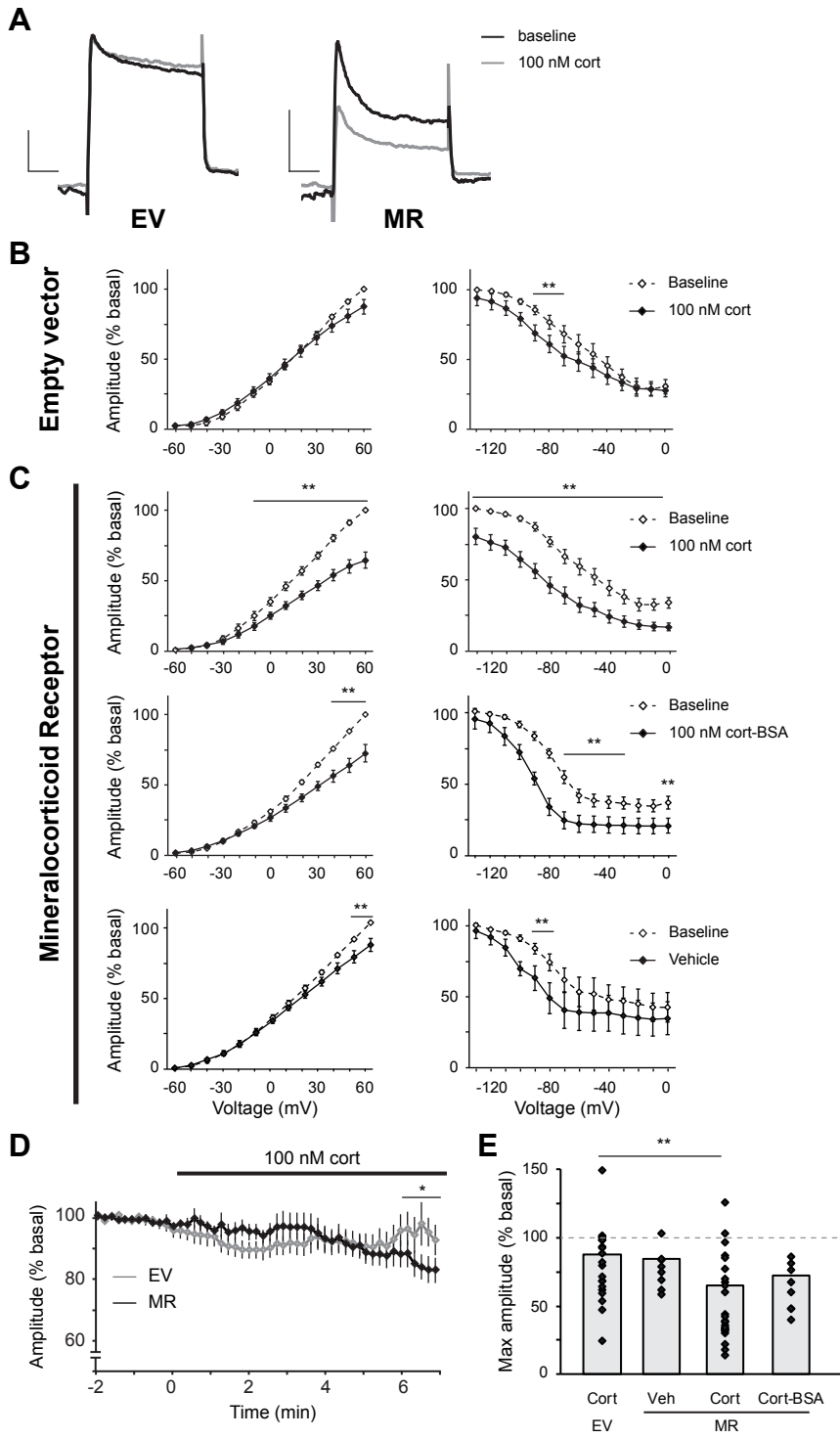
in transfected cells. Similarly, prolonged exposure, different transfection procedures or a different MR antibody (N2B7 (Gomez-Sanchez et al., 2006)) all failed to show MR expression in transfected NS-1 cells (data not shown). The MR is known to be a very unstable protein and can be lysed during lysate preparations leading to fragments of incorrect size (Gomez-Sanchez et al., 2011). However, even though we did observe fragments of incorrect size on the Western blot (Figure 3.3A), these were seen in both transfected and untransfected NS-1 cells and are likely to be due to aspecific interactions of the antibody.

Next we initiated a number of different biochemical approaches to test for presence of MR protein. First, we showed that MR immunofluorescence is indistinguishable between NS-1 cells transfected (according to normal procedure) with the MR or EV with immunofluorescence staining (Figure 3.3B). Again, COS-1 cells transfected with MR showed clear MR immunofluorescence and in the expected pattern of enhanced nuclear localization. Secondly, we obtained YFP-tagged MR and assessed YFP fluorescence in YFP-MR transfected NS-1 cells after treatment with vehicle or $100\,$nM corticosterone for $2\,$h. Also here, we failed to find a higher fluorescence in transfected cells compared to untransfected cells (Figure 3.3C); neither was there an indication of nuclear translocation of the YFP signal to the nucleus (data not shown). Transfection of YFP or GFP alone did lead to clear fluorescence throughout the cell (Figure 3.3C). As a final attempt, we assessed MR function with a transactivation essay. We cotransfected NS-1 or COS-1 cells with MR, EV or YFP-MR with Firefly luciferase under an MR-dependent TAT3 promotor (van Leeuwen et al., 2010a; Klok et al., 2011), and Renilla luciferase under a control (CMV) promotor. In COS-1 cells, we observed an increase in Firefly-to-Renilla luminescence ratio after transfection with either the MR or YFP-MR (Figure 3.3D). As expected, treatment with either corticosterone or aldosterone ($10\,$nM for $16\,$h) resulted in a 6 and 7 fold increased Firefly luciferase production respectively. In contrast, in NS-1 cells there was no increase in Firefly-luciferase induction in MR or YFP-MR transfected cells. We did

Figure 3.2 *(preceding page)*: **A-type currents are reduced by corticosterone only in MR-expressing NS-1 cells**

(A) Example of A-type currents from NS-1 cells transfected with an empty vector (EV) (left panel) or the MR (right panel). Corticosterone induces a reduction in A-type current amplitude for MR-transfected, but not for EV-transfected NS-1 cells. Currents elicited with $-100\,$mV priming and $60\,$mV depolarization step, scale bars: $500\,$pA (vertical) and $50\,$ms (horizontal). (B-C) A-type currents are measured before and 10 to 15 minutes after hormone treatment with the activation (left) and inactivation (right) protocols. (B) In NS-1 cells transfected with an empty vector (EV), corticosterone only marginally affects the amplitude of A-type currents. (C) NS-1 cells transfected with pRSV-MR. In MR-expressing cells, both $100\,$nM corticosterone (top) and $100\,$nM cort-BSA (middle) treatment results in decreased A-type current amplitudes. Vehicle treatment has little effect (bottom). (D) The effect of corticosterone on A-type current amplitude is rapid in onset, as a significantly reduced current amplitude is already observed after 6 minutes. No significant reduction is observed for EV-transfected cells. (E) The decrease in maximum A-type current amplitude ($+60\,$mV step) is significantly larger in the MR-cort versus the EV-cort group. *Statistics. (A-C) Paired samples t-test. Significant effects with $p < 0.01$ are shown. (D) Repeated measures (against baseline). (E) One-way ANOVA with post hoc multiple comparison (Tukey). Group sizes: EV+cort $n = 20$, MR+veh $n = 8$, MR+cort $n = 23$, MR+cort-BSA $n = 8$ (cells). $** = p < 0.01$.*
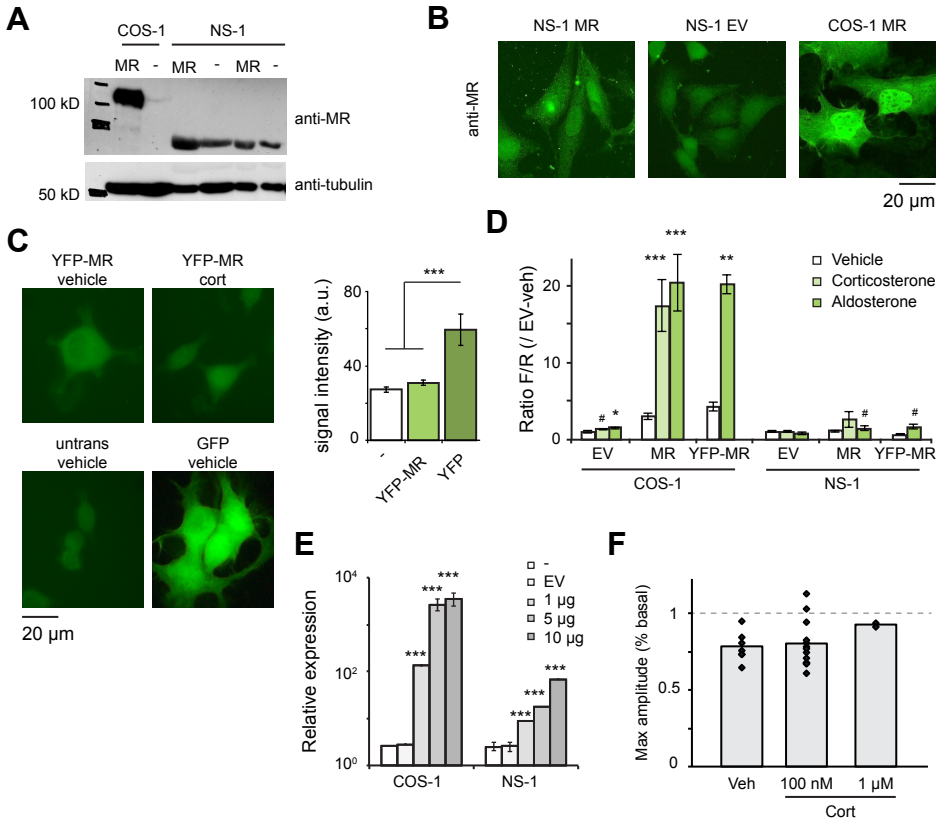
Figure 3.3: MR mRNA is present, but MR protein absent from MR-transfected NS-1 cells
NS-1 cells do not show detectable MR protein expression after pRSV-MR transfection in NS-1 cells. (A-D) (A) Representative western blot of MR expression after MR transfection in COS-1 and NS-1 cells. There is no appreciable MR protein expression 48 h after transfection in NS-1 cells, while MR protein is clearly seen in transfected COS-1 cells. Expected size of MR: 107 kDa. α-tubulin is coassessed as loading control. (B) Representative IF images for MR do not show quantitative difference in fluorescence between MR and EV-transfected NS-1 cells. In COS-1 cells, clear MR IF signal is seen with, as expected a high nuclear localization. (C) Transfection with YFP-MR does not lead to detectable YFP fluorescence 48 h after transfection, nor is there an accumulation of fluorescence in the nucleus after corticosterone treatment. Transfection of YFP alone does show clear YFP fluorescence in NS-1 cells. Quantification of average IF levels is shown on the right. (D) Transactivation essay. COS-1 and NS-1 cells are transfected with MR, YFP-MR or EV and the ratio between MR-driven Firefly and control-driven Renilla luminescence is assessed 48 h after transfections. In COS-1 cells, both aldosterone and corticosterone (10 nM, 16 h) induce an increased Firefly/Renilla ratio. In NS-1 cells, however, corticosterone does not affect the Firefly/Renilla ratio and aldosterone does so only marginally. (E) MR mRNA levels assessed with RT-qPCR. In contrast to the lack of detectable MR protein and function, there is clear MR mRNA expression 48 h after pRSV-MR transfection in NS-1 cells, albeit in a > 100 fold lower amount as in COS-1 cells. (F) The corticosterone-induced decrease in A-type current amplitude is not reproduced in a new set of MR-transfected NS-1 cells. Both 100 nM and 1 μM corticosterone fail to induce a decrease of maximum A-type current amplitude ($n = 13/2$). *Statistics. Independent-samples t-test against untransfected condition in C and E and against corresponding vehicle conditions in D.* $\# = p < 0.1, * = p < 0.05, ** = p < 0.01, *** = p < 0.001$
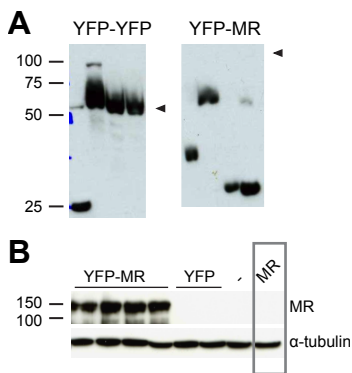
Figure 3.4: Stable MR cell lines show selection against MR expression

(A) Clones of CHO cells stably transfected with YFP-YFP (52 kDa; left panel) or YFP-MR (137 kDa; right panel) and stained for YFP (1:1000). For YFP-YFP clones, 3 out of 4 show a primary band at the expected size. However, none of the 4 putative YFP-MR clones show a band at the correct size (indicated by triangle), but instead a selection of low weight protein bands suggestive of YFP with a small portion of the MR attached. (B) Western blot for an assortment of CHO cells. Band to the right is of clone A09 previously described to be stably expressing the MR (Grossmann et al., 2005). No MR band is seen for this sample, while clear bands are seen in cells transiently transfected with YFP-MR (left). MR: 1D5 antibody 1:1000.

observe a small, but statistically significant, increase in Firefly-to-Renilla ratio after aldosterone treatment, i.e. 1.4 to 2.4 fold in MR and YFP-MR transfected cells respectively which was not seen in EV-transfected cells (Figure 3.3D). Possibly, this indicates a very low expression of the MR.

A failure to induce MR protein expression after transfection could be due to a low transfection efficiency or due to autolysis of the expressed protein within the cells. We showed clear expression of GFP and YFP (both under a CMV promotor) after electroporation in NS-1 cells, but failed to find expression of pRSV-MR (Lac promotor) or YFP-MR (CMV promotor), thus it is unlikely that the lack of protein expression was due to problems with transfection efficiency or transcription of the transfected plasmids. Still, to verify that MR DNA was expressed and transcribed in transfected NS-1 cells, we measured MR mRNA levels. As shown in Figure 3.3E, we found clear expression of MR mRNA in both COS-1 and NS-1 cells after transfection with increasing levels of the MR plasmid. Thus, transfection with $1\,\mu g$, $5\,\mu g$ and $10\,\mu g$ (/mln cells) MR resulted in 4-, 8- and 15-fold higher mRNA levels respectively. MR mRNA levels in NS-1 cells were > 100 fold lower than what is seen in COS-1 cells after transfection with similar doses of MR plasmid (Figure 3.3E). Also in differentiated cells, 7 days after transfection, there was still clear MR mRNA expression, although this was approximately 4-fold lower compared to that found 48 h after transfection (data not shown).

In an additional set of experiments, we attempted to create stable expression of YFP-tagged MR in CHO cells. However, while the procedure led to successful expression of another YFP construct (YFP-YFP) in 3 out of 4 clones, for YFP-MR all YFP positive clones only had fragments of the MR attached (Figure 3.4A). Similarly, the group of Claudia Grossmann and Michael Gekle had successfully created stable expression of the MR plasmid in CHO cells (Krug et al., 2002; Grossmann et al., 2005). However, they observed decreasing levels of MR within these cells even under antibiotic selection and correspondingly, we found no indication of MR protein expression within these cells by Western blot (Figure 3.4B; personal communication with C. Grossmann).

Chapter 3

In the first set of electrophysiological experiments we observed a reduction in potassium A-type currents specifically after MR transfection (Figure 3.2). This seems irreconcilable with the lack of MR protein expression observed. However, there was large variation between cells and no decrease in amplitudes was observed in about 25 % of cells (Figure 3.2E). Moreover, a new experiment where we electrophysiologically measured the effect of either vehicle, 100 nM corticosterone or 1 μM corticosterone in a new group of MR-transfected NS-1 cells failed to reproduce these earlier obtained results (Figure 3.3F).

Taken together, the MR protein seems to be highly instable in NS-1 cells. MR mRNA was observed after transfection of NS-1 cells with an MR plasmid. But, whereas the same plasmids resulted in clear and reproducible MR protein expression in COS-1 cells, we found no indications for MR protein expression after successful transfection in NS-1 cells. The MR is thus either not translated or immediately degraded in NS-1 cells, for reasons unknown to us. We have noted problems with MR expression on other occasions as well. Consequently, these expression issues make the NS-1 cell line unsuitable for reliable and reproducible electrophysiological experiments.

Potent MR protein expression in a second neuronal-like cell line: N1E-115 cells

A number of neuroblastoma-generated cell lines also show large potassium currents. Of these, the N1E-115 cells, a mouse neuroblastoma cell line, is known to express large amplitude potassium currents, consisting of a (slow-) inactivating and a non-inactivating component (Hirsh and Quandt, 1996; Lima et al., 2008; Vicente et al., 2010). It is unclear whether the inhibitory effect of corticosterone on fast-inactivating potassium currents seen in CA1 hippocampal cells (Olijslagers et al., 2008) is specific for a subtype of potassium channels or a more broad effect on (inactivating) potassium channels. Thus, we tested the effect of corticosterone on potassium currents in N1E-115 cells after transfection with MR.

We first employed a number of biochemical approaches to verify that MR protein was expressed and functional after transfection in N1E-115 cells. Indeed, on Western blots we found proteins of the correct size 48 h after transfection (Figure 3.5A). In addition, YFP-MR transfection showed clear YFP fluorescence in N1E-115 cells and nuclear translocation of YFP-MR after corticosterone treatment as expected (Figure 3.5B). Moreover, all MR plasmids (pRSV-MR, pcDNA3-MR and YFP-MR) led to the expression of a functional MR protein as shown by robust transactivational capacity (Figure 3.5C). Without additional hormone treatment, TAT3-Firefly luciferase was already produced at higher levels as compared to EV transfected cells. Treatment with 10 nM corticosterone for 16 h led to a strong induction of Firefly production when cotransfected with any of the three MR plasmids. The pRSV-MR plasmid (which was used in NS-1 cells) showed the lowest, but still apparent, transactivational capacity (Figure 3.5C). Finally, we also found clear MR
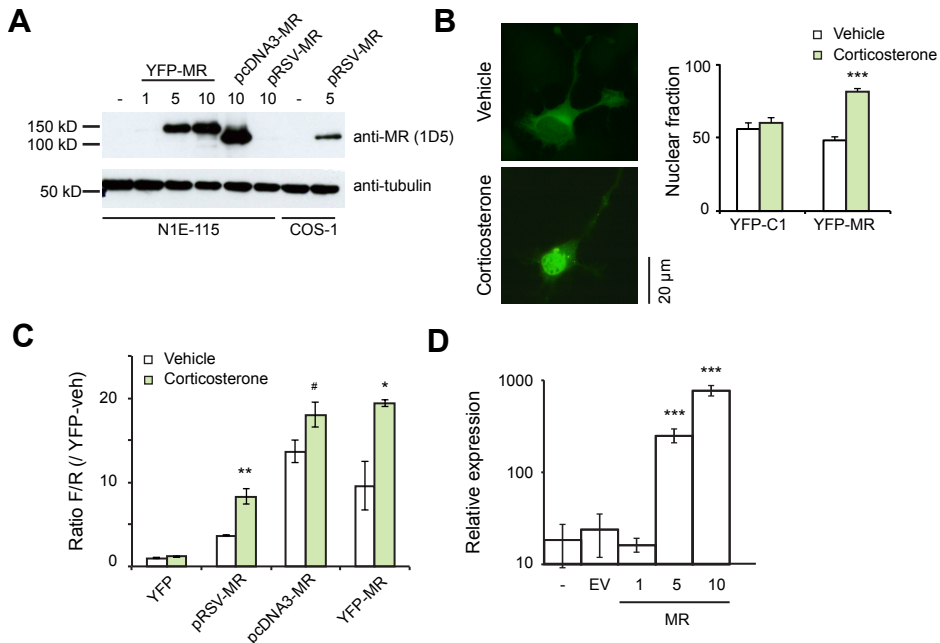
Figure 3.5: YFP-MR is robustly expressed in N1E-115 neuroblastoma cells
(A) Representative western blot assessed for MR. Transfection of increasing amounts of YFP-MR shows robust expression of YFP-MR protein (125 kDa). Similarly transfection with two different MR constructs results in expression of MR protein (107 kDa), with low levels after pRSV-MR transfection. α-tubulin is coassessed as loading control. (B) IF imaging shows clear YFP-MR fluorescence in transfected N1E-115 cells and nuclear translocation after corticosterone (10 nM, 4 h) treatment. (C) Transactivation essay. In MR-transfected N1E-115 cells the ratio between MR-driven Firefly and control-Renilla luminescence is increased as compared to EV-transfected cells. Additionally, the ratio is further increased after application of corticosterone (10 nM, 16 h) in cells transfected with MR plasmids and not with EV. (D) RT-qPCR on N1E-115 cells shows increasing amount of MR mRNA after transfection with 1, 5 and 10 μg of pRSV-MR. *Statistics. Independent-samples t-test against corresponding vehicle conditions in B and C and against untransfected condition in D.* $\# = p < 0.1, * = p < 0.05, ** = p < 0.01, *** = p < 0.001$

mRNA expression with increasing levels of MR transfection in N1E-115 cells 48 h after transfection (Figure 3.5D) and still detectable mRNA expression (2–3 fold lower compared to 48 h) after 5 days of differentiation (data not shown).

Corticosterone does not affect potassium currents in N1E-115 cells

Subsequently, we assessed if we obtained currents with the expected properties in differentiated N1E-115 cells. After 5 days of serum starvation and DMSO application we observed a neuronal-like phenotype in the cells with strong neuritogenesis (Figure 3.6A). We patch clamped N1E-115 cells after 4–6 days of differentiation and maintained the cells in voltage clamp mode to measure ion currents. Similar to what was reported before (Hirsh and Quandt, 1996; Lima et al., 2008), we found large outward currents, that showed both a slow-inactivating and a non-inactivating component (Figure 3.6C). Maximal amplitudes ranged from 820 to 7200 pA, with an average
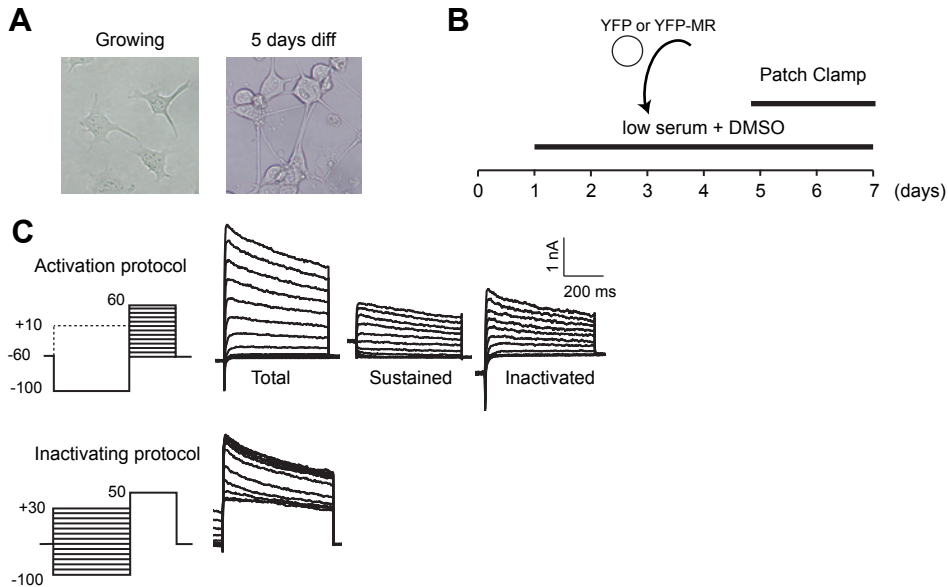
Figure 3.6: Patch protocols for N1E-115 cells
(A) N1E-115 cells develop a neuronal-like phenotype within 5 days of serum deprivation and DMSO treatment. (B) The general experimental outline of single-cell patch clamp experiments. (C) Voltage dependency of the potassium currents are obtained with the activation (top) and inactivation protocols (bottom). A combination of a sustained and an inactivating current is seen in N1E-115 cells. A prepulse of $+10$ mV generates only the sustained component, subtracting this from the total current generated the inactivating component. Typical traces are shown next to the corresponding protocols.

of 2366 ± 317 pA ($n = 19$). As expected (Lima et al., 2008), both current components were sensitive to TEA and 4-AP. Thus, at a dose of 1 mM, both TEA and 4-AP reduced the currents roughly by half, while an even stronger reduction was seen when both inhibitors were given simultaneously (Figure 3.7A). This is in sharp contrast to the A-type currents in NS-1 cells, which were recorded with 10 mM TEA in the recording medium. Finally, a hyperpolarized prepulse did not potentiate the potassium currents in N1E-115 cells. Thus, maximal potassium currents were already induced at resting potential, while the currents were partially inactivated by a preceding depolarization as expected (half maximum inactivation at -28.9 ± 3.8 mV, Figure 3.7B). In NS-1 cells hyperpolarizations did lead to larger A-type currents (½ max of -71.6 ± 2.8 mV). Finally, as compared to NS-1 cell A-type currents, in N1E-115 cells the voltage dependency of the currents was shifted marginally to the right (half maximal activation at $+23.7 \pm 3.8$ mV; Figure 3.7B). Thus, we found an overall potassium current in N1E-115 cells which is seemingly the combination of slow-inactivating and non-inactivating channels as was previously reported (Hirsh and Quandt, 1996; Lima et al., 2008).

We then chose to transfect YFP-MR instead of untagged MR to be absolutely sure that we only recorded from MR (protein) expressing cells. Thus, prior to patching we identified YFP-MR fluorescence and patched only fluorescent cells (we con-
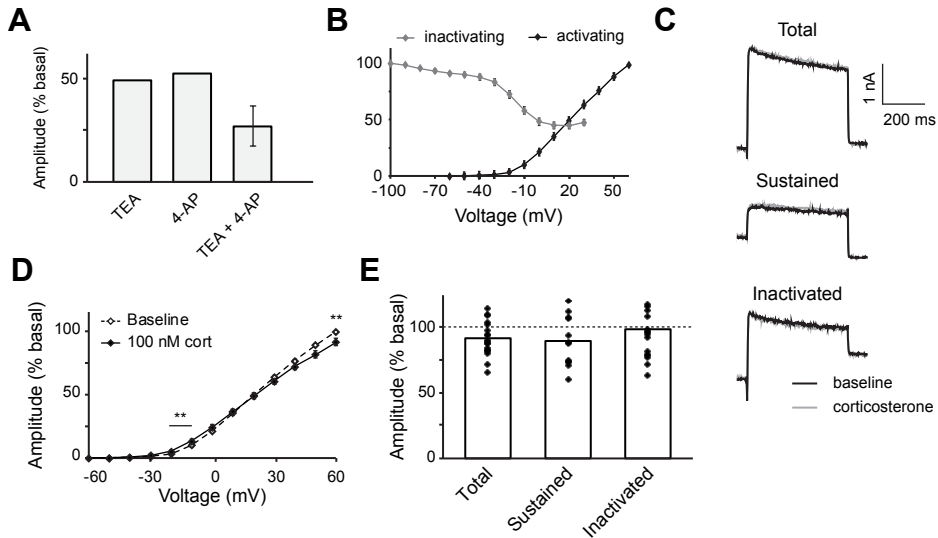
Figure 3.7: Potassium A-type currents show different kinetics in N1E-115 cells and are unresponsive to corticosterone
Differentiated N1E-115 cells are transfected with YFP-MR and YFP-expressing cells are identified and patched. (A) The potassium currents in N1E-115 cells are sensitive to both TEA (1 mM) and 4-AP (1 mM). The two compounds also have an additive effect. (B) The voltage dependency of the N1E-115 potassium currents is obtained with the activation and inactivation protocols. The potassium current in N1E-115 cells is not potentiated by a hyperpolarized prepulse. (C) Typical potassium currents elicited with a -100 mV prepulse (total), a $+10$ mV prepulse (sustained) and by subtracting the two (activated) shows in baseline and 5–10 min after 100 nM corticosterone (all $+60$ mV depolarization step). (D) Total potassium currents are assessed with the activation protocols before and 10–15 minutes after treatment with 100 nM corticosterone. Corticosterone does not affect the amplitude or voltage dependency of potassium currents in YFP-MR expressing N1E-115 cells ($n = 19$ cells). (E) Maximal amplitudes (at $+60$ mV) of either the total current, the sustained current or the inactivated current are only marginally lower than baseline values after corticosterone treatment. *Statistics. (D) Paired sample t-test ($n = 19$). Significance with $p < 0.01$ is shown. $** = p < 0.01$*

stricted ourselves to cells with moderate levels of YFP). As before, we measured the activating and inactivation characteristics of the potassium currents in baseline condition and within 5–10 minutes of corticosterone treatment; the results are presented in Figure 3.7C-E. The data shows that corticosterone application did not affect the overall potassium current in N1E-115 cells. Neither activation, nor inactivation voltage dependency were affected by corticosterone treatment. There was a marginal decrease in maximal amplitude ($8.4 \pm 3.0\%$), but this was more indicative of some run down of the currents than of a corticosterone-specific effect. As the potassium current in N1E-115 cells is comprised of two components we also tested the effect of corticosterone treatment on each component separately. To do so, we inactivated the transient component with a depolarizing prepulse ($+10$ mV) and thus obtained only the sustained component. The inactivating component was then obtained by subtraction of the sustained components from the total current (Figure 3.6C). However, neither the sustained current nor the inactivated current

were affected by corticosterone treatment (maximal amplitudes of $89.7 \pm 5.5\%$ and $98.2 \pm 5.3\%$ of baseline levels respectively, Figure 3.7E).

3.4 Discussion

Rapid, non-genomic actions of corticosterone are increasingly accepted as functionally important action of corticosteroids. Within minutes after a stressful event or an otherwise achieved surge in corticosteroids a shift in neuronal excitability is induced in multiple brain areas (Karst et al., 2005, 2010; Tasker et al., 2006), potentially resulting in increased learning and behavioral reactivity (Khaksari et al., 2007; Groeneweg et al., 2011). The MR is required for many of these effects and involves a membrane-associated receptor, but the downstream signaling pathways and structure-function relationship remain ill understood.

We here sought to mimic a functional non-genomic action of corticosterone on neuronal excitability in a cell line, affording the possibility to alter the MR structure and signaling through transfection. Initially, in NS-1 cells we found the amplitude of rapidly-inactivating potassium currents to be strongly and significantly reduced by 100 nM corticosterone in a rapid, membrane-initiated and MR-dependent fashion (Figure 3.2). A lack of a corticosterone-induced effect in empty vector transfected NS-1 cells further suggests that the presence of the MR is sufficient to render (neuronal-like) cells responsive to non-genomic corticosterone actions. We did not observe the shift in voltage dependencies of the channels which was shown in CA1 neurons (Olijslagers et al., 2008). In N1E-115 cells, the sustained and slowly-inactivating potassium currents were not affected by corticosterone (Figure 3.7), suggesting that corticosterone only affects the kinetics of a specific subset of potassium channels.

Instability of the MR in cell lines

Much care must be taken in interpreting our current results as we were unable to reliably show the presence of the MR protein in MR-transfected NS-1 cells. Moreover, whereas we found a clear MR-specific effect of corticosterone in an initial large set of experiments ($n = 23$), we were unable to replicate these results in a further smaller subset of recordings ($n = 13$). We assessed potential MR protein expression by numerous methods, including Western blot, immunofluorescence staining, YFP-tagged MR transcripts and transactivation essays. Interestingly, while MR expression and functionality was found on all occasions in both COS-1 and N1E-115 cells, none of the methods showed expression in transfected NS-1 cells. Only aldosterone did show some transactivational potency in MR and YFP-MR transfected NS-1 cells, while this was absent in EV-transfected NS-1 cells. This finding could indicate a small, hard to detect presence of the MR in some of these cells.

The failure to detect a protein while mRNA is expressed could be caused by either an inhibition of mRNA translation or by protein degradation. Silencing of mRNA by microRNAs is recognized as an endogenous mechanism to inhibit translation (Lee et al., 1993; Bartel, 2004). The 3′ UTR region of the MR contains several microRNA recognition sites (de Kloet et al., 2009; Sõber et al., 2010) but their effect on MR expression has not been investigated. Moreover, the 3′ UTR region was not included in the plasmid DNA, making mRNA silencing through this route unlikely. As all steroid receptors, unliganded MR forms a multimer with several chaperones and heat shock proteins that keep it in its inactive conformation and that also protect against degradation (Yang and Fuller, 2012). Indeed, inhibition of HSP90, one of the main chaperones, leads to increased ubiquitylation and degradation of the MR (Faresse et al., 2010). Insufficient amounts of HSP90 might thus explain rapid degradation of transfected MR. However, HSP90 is endogenously expressed in PC12 cells. Moreover, steroid receptors share most, if not all, chaperones. To our knowledge there are no indications for an enhanced degradation of the MR and one study even found the opposite (Lightman et al., 2008). However, we and others have noted that the MR is a peculiar protein in *in vitro* settings. I will discuss the apparent instability of the MR *in vitro* in more detail in the general discussion (*Chapter 7*).

The lack of reliable MR protein expression is a likely explanation for the failure to reproduce the functional effects of corticosterone through the MR observed in the first series of experiments. We never assessed MR protein expression directly on cells that were also used for electrophysiology, thus, it remains possible that in this first series there was sufficient MR protein expression during recordings to induce the functional effects. Indeed, either mRNA silencing or efficient protein degradation are likely strongly affected by the cell context and could thus result in small fractions of viable MR protein depending on subtle differences in culturing conditions. Regardless, the lack of MR stability in NS-1 cells make this cell line unsuitable for further experiments.

Potassium channel subtypes and their responsiveness to corticosterone

While corticosterone —at least in the first series of recordings— affected the rapidly inactivating potassium currents in NS-1 cells, it had no effect on the potassium currents in N1E-115 cells. This suggests that the corticosterone-induced effects are specific for certain potassium channel subtypes. Potassium channels are the most diverse group of ion channels. Functionally, potassium currents can be grouped into transient or "A-type" channels and two subtypes of delayed rectifying channels; the slow-inactivating "D-type" and non-inactivating "M-type" channels. The potassium pore is formed by homo- or hetero-tetramers of α-subunits, encoded by one of the Kv families (Chandy et al., 1990; Vacher et al., 2008). Each type of current can be generated by a variety of channels. For example, A-type currents are generated by Kv1.4, Kv3.3, Kv3.4, Kv4.1, Kv4.2 or Kv4.3 channels (Vacher et al., 2008).

To build onto the complexity, heterotetramers form channels with intermediate kinetics and auxiliary (β) subunits affect the kinetics of the channels (Rettig et al., 1994). Neurons generally express multiple Kv subtypes, resulting in a summed cellular potassium current of intermediate kinetics. Olijslagers et al. (2008), found a reduction in A-type potassium currents by corticosterone in CA1 neurons. Within these neurons, A-type channels Kv1.4 and Kv4.2 are most abundantly expressed (Coetzee et al., 1999; Chen et al., 2006). The reduction in potassium amplitudes further required G-proteins and likely MAPK/ERK activation (Olijslagers et al., 2008). Kv4.2 is widely recognized as direct target of ERK1/2 (Schrader et al., 2006; Adams et al., 2008). ERK activation results in reduced surface expression, inhibition of current amplitude and a right-shift in activation kinetics of Kv4.2 (Yuan et al., 2002, 2006), making this subtype a prime candidate for corticosterone-induced regulation of potassium currents. However, ERK1/2 potentially affects other Kv subtypes as well (Yuan et al., 2006).

In PC12 cells, at least 4 different voltage-dependent potassium currents have been identified (Hoshi and Aldrich, 1988; Conforti and Millhorn, 2000). These include sustained, slow-inactivating and fast-inactivating currents. Of note, multiple studies reported transient A-type currents in only a small subset of differentiated PC12 cells (Hoshi and Aldrich, 1988; Conforti and Millhorn, 2000; Castillo et al., 2001), while others found them more frequently (Pannaccione et al., 2005, 2007). Although we did not quantify it here, we found clear A-type currents in the majority of NS-1 cells. It is possible that NS-1 cells represent a subclone of PC12 cells associated with larger (transient) potassium currents. Which Kv channels underlie the observed currents in PC12 cells remains a matter of debate; expression of many Kv subtypes, including the Kv1.2/1.3/1.4, Kv2.1, Kv3.1/3.2/3.3/3.4 and Kv4.2/4.3 channels, was found in PC12 cells (Conforti and Millhorn, 2000; McCrossan et al., 2003; Pannaccione et al., 2007). Highest expression of A-type channels was observed for the Kv3.4 and Kv4.2 channels. In NS-1 cells we recorded high amplitude A-type currents in the presence of 10 mM TEA. Whereas Kv3 channels are sensitive to TEA (Pannaccione et al., 2005), Kv4 subtypes are highly resistant (Coetzee et al., 1999). We thus presume that we recorded mainly from Kv4.2 mediated A-type channels. It thus seems likely that the reduction in A-type current amplitude found in CA1 neurons (Olijslagers et al., 2008) and here in NS-1 cells by corticosterone (albeit only in the first series) both involve actions on Kv4.2 channels. However, in CA1 neurons a decrease in maximal A-type current amplitude was seen in concert with a shift in the activation kinetics towards higher depolarizations (Olijslagers et al., 2008). In NS-1 cells we found no indications for a shift in kinetics. Whether this is due to different signaling cascades, different auxiliary subunits or a different Kv subunit composition remains to be established.

N1E-115 cells show two main potassium currents, a sustained current and a slowly-inactivating current (Quandt, 1988; Lima et al., 2008). Also for N1E-115 cells the channel subunits underlying the observed currents have not yet been deter-

mined in detail. One study, however, associated a reduction in Kv3.1 mRNA with a reduction in the slow-inactivating current (Hirsh and Quandt, 1996). Moreover, the inactivating current in N1E-115 cells is highly TEA sensitive, is not potentiated by a hyperpolarized prepulse and has slow inactivation kinetics, which all fit with Kv3.1 or Kv3.2 channels (Coetzee et al., 1999). Thus, we presume that the inactivating component of the N1E-115 potassium current is generated through a Kv3 channel (most likely Kv3.1) and this current is insensitive to corticosterone. Altogether, the data indicates that the suppressive effect of corticosterone on inactivating potassium currents is specific for some Kv channel subtypes and is not seen for slowly-inactivating Kv3.1 channels. Expression of specific Kv subtypes in isolation in non-neuronal cells could narrow down which Kv subtypes are responsive to rapid corticosterone actions.

In conclusion, the current experiments show that neuronal-like cell models can be used to reproduce a functional non-genomic effect of corticosterone on neuronal excitability. With the combination of NS-1 and N1E-115 cells we show that the reduction in potassium current amplitudes is Kv subtype specific. However, the stability of the MR in cell lines (at least the two we recorded from) is a limiting factor and must always be carefully monitored. Better understanding of MRs dynamics and half-life after transfection in cell lines would be very valuable to improve future models.

Chapter 3

A combination of wide-field and TIRF single-molecule microscopy as method to visualize the membrane-associated population of the Mineralocorticoid Receptor

Femke L. Groeneweg[1], Martijn Sierksma[1,2], E. Ron de Kloet[1],
John van Noort[3], Thomas Schmidt[3], Marcel J.M. Schaaf[2]

[1] Department of Medical Pharmacology, Leiden University / LUMC, Leiden, The Netherlands.
[2] Molecular Cell Biology, Institute of Biology, Leiden University, Leiden, The Netherlands.
[3] Physics of Life Processes, Institute of Physics, Leiden University, Leiden, The Netherlands.

THE mineralocorticoid receptor (MR) mediates both genomic and non-genomic actions of its ligands. It is known to be localized in the cytoplasm and in the nucleus. However, over the previous decade, evidence has accumulated showing that the MR also has a smaller membrane-associated population that is involved in rapid non-genomic actions of its ligands. This membrane localization has been confirmed by electron microscopy, but the relative size of the membrane population, its regulation and its dynamics remain unknown. Total Internal Reflection Fluorescence (TIRF) microscopy is a well-established technique to image membrane proteins, since the background signal from cytoplasmic proteins is very low. Here, we utilize the combination of wide-field and TIRF single-molecule microscopy to study the dynamics of the MR near the membrane and compare this to the dynamics of the cytoplasmic population. We find that, in two different cell lines, YFP-tagged MR shows two diffusing populations, with a 30–100 fold difference in diffusion coefficients. In TIRF, a larger fraction of the imaged molecules show slow diffusion (35–51 % versus 11–30 % in wide-field microscopy). Our data suggest that this is not due to a loss of fast moving molecules in TIRF and thus represents an enriched fraction of slow-moving MRs at or near the membrane. Short-term treatment with corticosterone or membrane-impermeable corticosterone did not affect the dynamics of the MR near the membrane. In conclusion, the combination of TIRF and wide-field SMM provides a suggestion for the existence of a membrane-associated MR fraction.

4.1 Introduction

The MR is a member of the family of steroid receptors. This family encompasses a group of structurally related receptors that exert their main action within the nucleus where they bind DNA and act as transcription factors. As such they are dubbed nuclear receptors. Without hormone bound, most MRs are located in the cytoplasm while hormone binding induces nuclear translocation (Nishi et al., 2001; Sarabdjitsingh et al., 2009). In addition to its well-known nuclear function, the MR has more recently been found to mediate rapid actions of its hormones (corticosteroids and mineralocorticoids) (Grossmann et al., 2005; Karst et al., 2005, 2010; Mihailidou and Funder, 2005; Olijslagers et al., 2008; Qiu et al., 2010). These effects do not involve *de novo* transcription or protein synthesis and are therefore called non-genomic effects. Non-genomic actions are not restricted to the MR but have been found for most, if not all, steroid receptors (Hammes and Levin, 2007). Intriguingly, non-genomic effects can be induced by membrane-impermeable conjugates of the hormones and the receptors have thus been suggested to be present at the plasma membrane (Hammes and Levin, 2007; *Chapter 2*). Immunohistochemical staining with new antibodies (Gomez-Sanchez et al., 2011), cell fractionation studies (Qiu et al., 2010) and electron microscopy (Prager et al., 2010) indeed found indications for membrane localization of the MR. However, this membrane-associated fraction is postulated to be very small and does not show up with conventional microscopy. The size of this fraction, its submembrane localization and its regulation all remain unknown.

TIRF microscopy is a well-established technique for imaging of fluorescently labeled membrane-associated molecules. In TIRF microscopy, the laser is redirected so that it hits the glass-water interface between the coverglass and the specimen at a large angle relative to the optical axis. As a result, the beam is totally internally reflected, which generates an electromagnetic field, termed the evanescent field that penetrates into the specimen perpendicular to the interface. This evanescent field, is capable of exciting fluorophores present in a thin plane of 60–100 nm above the coverglass (Axelrod et al., 1983; Axelrod, 2001; Martin-Fernandez et al., 2013). TIRF microscopy thus provides images of cultured cells plated on a coverglass with a very strong enrichment for membrane-associated molecules, although membrane-associated fluorescent proteins are not exclusively excited. This technique is therefore widely used to study membrane-associated receptors, membrane-association of vesicles and near-membrane cytoskeletal dynamics (Vale et al., 1996; Sako et al., 2000; Lommerse et al., 2006; Toonen et al., 2006). In the current study, we have combined TIRF with single-molecule microscopy (SMM). In SMM, a highly sensitive CCD camera enables the imaging of single fluorophores. Time lapse imaging of single fluorophores enables an analysis of protein dynamics with very high spatial and temporal resolution (Schmidt et al., 1996; Lord et al., 2010; Persson et al., 2013). SMM can be applied using both TIRF and wide-field microscopy.

Chapter 4

In the present study we have tested the feasibility of using TIRF microscopy to acquire images that are enriched for the membrane-associated subpopulation of (fluorescently-tagged) MR and thereby distinguish it from the cytoplasmic subpopulation. Membrane-associated molecules generally show much slower kinetics than free cytoplasmic molecules (Murase et al., 2004; Owen et al., 2009). Thus, if a sufficiently big fraction of MR exists at the membrane this should display slower protein dynamics in TIRF versus wide-field single-molecule microscopy. Indeed, we observed a larger slowly diffusing fraction of YFP-tagged MR molecules in TIRF as compared to wide-field recordings, suggesting the presence of a membrane-associated population of MR molecules. Surprisingly, short-term treatment with either corticosterone or BSA-conjugated corticosterone did not affect the kinetics of YFP-MR molecules as recorded using TIRF single-molecule microscopy.

4.2 Methods

Cell culture and DNA constructs

Generation of the expression plasmid pcDNA3.1-YFP-C10H-Ras has been described previously (Lommerse et al., 2004; Schaaf et al., 2009). YFP-MR contains the human MR gene cloned in frame into the pEFYP-C1 vector (Invitrogen), which generates an N-terminally tagged YFP-MR (described in detail in *Chapter 6*). In all experiments, either CHO (Chinese Hamster Ovary) or COS-1 cells were used. CHO cells were grown in F12 medium (GIBCO), supplemented with $10\,\%$ FBS, $0.5\,\%$ streptomycin and penicillin. COS-1 cells were grown in high glucose D-MEM (GIBCO), supplemented with $10\,\%$ FBS, $0.5\,\%$ streptomycin and penicillin. All cells were maintained at $37\,°C$ and $5\,\%$ CO_2. One day before transfection, the cells were plated on glass coverslips (ø $13\,mm$) in 6-well plates, at a density of $300\,000$ cells per well. Glass cover slips were cleaned by sonication and $1\,\%$ RBS50 treatment and bleached by a UV-lamp to minimize (fluorescing) contaminations. The next day the cells were transfected with TransIT-CHO kit or TransIT-COS-1 kit (both Mirus) according to the manufacturer's instructions. YFP-C10H-Ras and YFP-MR were transfected at a concentration of $5\,\mu g$ / $10\,cm^2$. Cells were incubated with the transfection mixture overnight, then washed once with PBS and placed on growth medium. $24\,h$ before measuring, medium was replaced with serum-free medium (F-12 or D-MEM).

TIRF microscopy

For TIRF recordings we used a homebuilt microscopy setup (previously described in Koopmans et al., 2007), equipped with a 100× oil-immersion TIRF objective (NA 1.45, Nikon, Tokyo, Japan). A 100 by 100 pixel region of interest was defined at a pixel size of $213\,nm$. Excitation was performed using a $514\,nm$ Arg+ laser (Coherent, Santa Clara, CA), illuminating an area of $\sim\!600\,mm^2$ with a power of $1.7\,\mu W$ for $12\,ms$. The beam was circularly polarized and displaced parallel to the optical axis of the objective, so an evanescent wave was generated by total internal reflection at the glass-water interface (Figure 4.1A). The critical angle for TIRF was checked manually (Snaar-Jagalska et al., 2013). Fluorescence light was filtered using a custom made dual-color bandpass filter (Chroma) and a long-pass filter (OG530, Schott). The

A Wide-field   TIRF

Fluorophore   Excited fluorophore

Evanescent wavefield

↕ ~ 100 nm

2200

-100

B

0   50   100   150   ms

C Vehicle   Corticosterone   **D** Vehicle   Corticosterone

Chapter 4
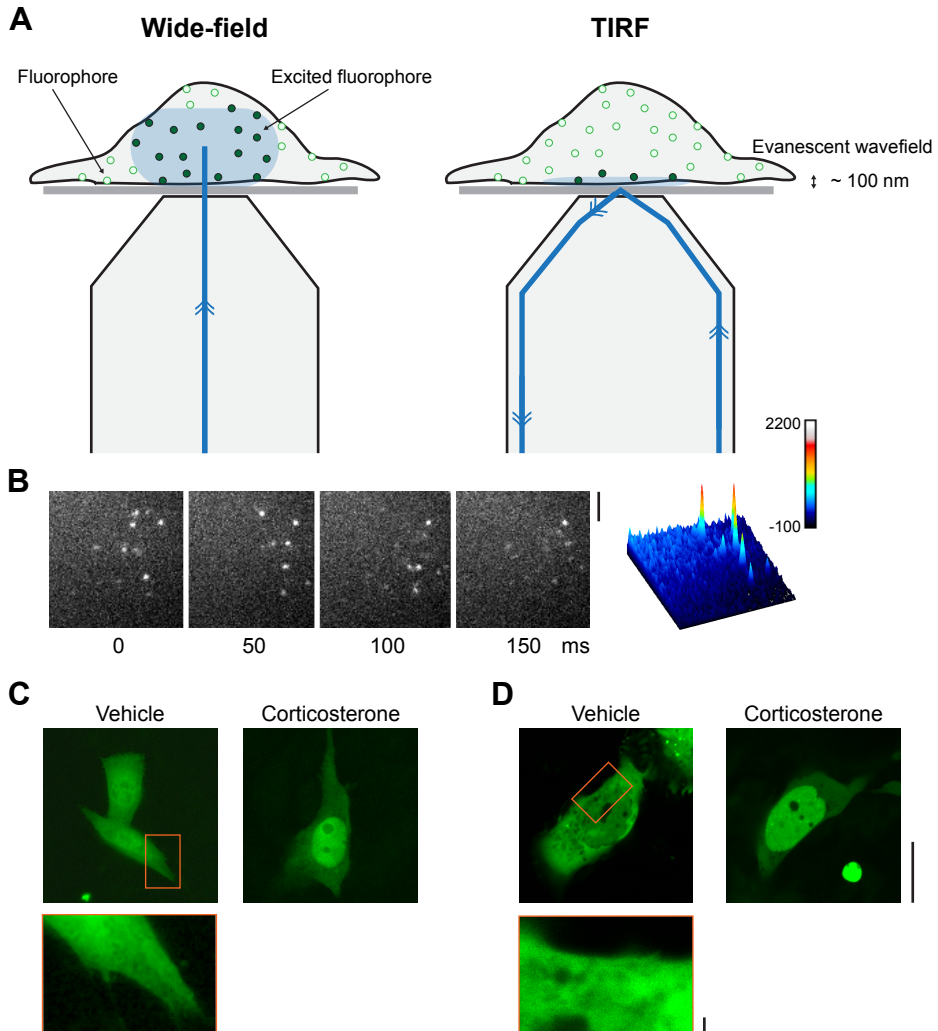
Figure 4.1: Microscopy setup
(A) Schematic diagram showing the principles of TIRF microscopy. In wide-field fluorescence microscopy the excitation light beam is directed perpendicular to the coverglass and excites fluorophores in a thick section (~1 μm). In TIRF, the excitation beam is redirected to the periphery of the objective lens and reaches the sample at a large angle relative to the optical axis. When this angle is critically large, the laser light is totally internally reflected at the glass-water interface. As a result an evanescent wave field is generated that excites fluorophores in a thin section of 60–100 nm above the coverglass. (B) Single fluorescence intensity peaks attributed to single YFP-C10H-Ras molecules are clearly discernable from the background in TIRF mode. To obtain kinetics, data sequences of 2000 images with an interval of 50 ms are obtained. (C-D) Confocal images of YFP-MR in both CHO (C) and COS-1 (D) cells. YFP-MR is seen mostly in the cytoplasm without hormone and the putative membrane-associated subpopulation is not distinguishable from the surrounding cytoplasm. After treatment with 100 nM corticosterone (16 h), YFP-MR translocates to the nucleus. *Scale bars:* 5 μm.

images were recorded by a multiplication-gain CCD camera (Cascade 512B, Roper Scientific, Trenton, NJ).

Wide-field microscopy

For wide-field recordings a customized wide-field setup (Axiovert 100TV, Zeiss) was used, equipped with a 100× / 1.4NA oil-immersion objective (Zeiss). A region-of-interest (ROI) of 50 × 50 pixels (pixel size of 220 nm) was selected. The sample was illuminated by a 514 nm argon laser at an intensity of 2 kW/cm^2 (measured at the sample). The pulse length is controlled by an acousto-optical tunable filter (AA optoelectronics, France). The YFP fluorescence signal was detected through a combination of filters (DCLP530, HQ570/80 (Chroma Technology, Brattleboro, VT) and OG530-3 (Schott, Mainz, Germany)), by a liquid-nitrogen cooled CCD camera (Princeton Instruments, Trenton, NJ). Camera read out and AOTF timing were tightly controlled.

Single-molecule imaging

For both TIRF and wide-field imaging the general procedures were identical. Transfected cells were used 2 or 3 days post transfection. For a recording, a coverslip with cells was mounted on a custom made sample-holder, the cells were washed with PBS and kept in 1 ml PBS at room temperature. Cells with moderate fluorescence intensity were selected. Cells were photobleached until single diffraction-limited spots could be distinguished. These fluorescence intensity profiles of these spots were fitted by a 3D-gaussian peak, and the center of this peak was defined as the location of the fluorescent molecule. We used a signal-to-noise ratio of > 5 and a maximal peak width of ∼600 nm as exclusion parameters.

Analysis of protein dynamics

For each cell, an image sequence of 2000 frames was recorded with a time lag of 50 ms (Figure 4.1B). We used the Particle Image Correlation Spectroscopy (PICS) method to determine the molecular mobility pattern. In PICS, the correlation between peak positions at two different time points (for example $t = 0$ ms and $t = 50$ ms) is calculated. The cumulative distribution of all distances (C_{cum}) for each time lag can be described by:

$$C_{\text{cum}}(l, \Delta t) = \frac{\left(\sum_{i=1}^{m_a} m_b(r_{ai}l) \right) \Delta t}{m_a} \tag{4.1}$$

Where r_{ai} is the position of a molecule in image A and m_a/m_b is the number of molecules in images A and B (see for further details Semrau and Schmidt, 2007). C_{cum} includes both contributions from diffusing molecules as well as distances due to random proximity to other molecules. We can then rewrite the equation as:

$$C_{\text{cum}}(l, \Delta t) = P_{\text{cum}}(l, \Delta t) + c\pi l^2 \tag{4.2}$$

In which $P_{\text{cum}}(l, \Delta t)$ is the cumulative probability function of displacement steps over the time lag, and c is the peak density. As proximity to unrelated molecules is independent of distance and solely dependent on peak density, we can fit this fraction with a straight line with offset $P_{\text{cum}}(\text{max})$ and slope of $c\pi$ and subtract it from the raw data to obtain P_{cum}. P_{cum} then includes only distances due to molecular diffusion. Population modeling is used to calculate

the diffusion pattern of the molecules. Given that the population of molecules is homogeneous, a single population of displacing molecules is determined by:

$$P_{\text{cum}}(l, \Delta t) = 1 - \exp\left(-\frac{l^2}{\text{MSD}_0(\Delta t)}\right) \tag{4.3}$$

Here MSD_0 is the mean squared displacement of one population of molecules over the time lag. However, this one fraction model did not fit the experimental data. Therefore a second fraction was introduced and the resulting equation reads as follows:

$$P_{\text{cum}}(l, \Delta t) = 1 - \left[\alpha \cdot \exp\left(-\frac{l^2}{\text{MSD}_1(\Delta t)}\right) + (1 - \alpha) \cdot \exp\left(-\frac{l^2}{\text{MSD}_2(\Delta t)}\right)\right] \tag{4.4}$$

Where MSD_1 and MSD_2 denote the mean squared displacement of the first (fast) and the second (slow) fractions respectively, and α is the fraction size of the first (fast) fraction. PICS analysis was repeated for each time lag and α, MSD_1 and MSD_2 were plotted as a function of time (Δt). The data from each experimental day (on average 6.8 ± 0.7 cells/day) was pooled and analyzed together. Data is always presented as mean $\pm$ SEM. Fitting of the MSD plots was performed with SEMs as a weighting factor, and diffusion coefficients (D_{fast} and D_{slow}) were calculated using the following equation:

$$\text{MSD}(\Delta t) = 4 \cdot D \cdot \Delta t \tag{4.5}$$

Hormone treatments

For the hormone treatments, corticosterone was prediluted to a concentration of 0.1 mM in 100% EtOH and further diluted in PBS to its final concentration of 1 mM. Corticosterone-BSA (cort-BSA) was dissolved in 0.9% NaCl, 0.25% carboxymethyl cellulose and 0.2% Tween (solvent A) to 12.5 mM (1 mg/ml) and further diluted in PBS to its final concentration of 43.6 nM. There are 23 molecules of corticosterone bound to a BSA molecule, therefore the concentration of corticosterone molecules equals that of 1 μM free corticosterone. Each recorded cell was measured first without hormone (baseline) in 900 l PBS. Hereafter, the appropriate hormone (diluted in 100 ml PBS at room temperature) was added. Five minutes after the hormone was added, cells were measured again. As vehicle both 1% EtOH and 0.4% solvent A were used, but as the kinetics of YFP-C10H-Ras or YFP-MR was not different between the two types of vehicle solutions, they were combined for further analysis.

Statistics

In order to test for statistical significance between imaging methods we determined diffusion patterns of YFP-MR for each day of recording separately and tested significance (n = number of recording days). Significance was tested with repeated measures tests, with cell type, microscopy setup or hormone treatment as between-subject factors. Statistical analysis for the peak characteristics was performed with one-way ANOVAs, with post-hoc tests according to Fisher's LSD (least significant difference) method. Statistical significance was accepted at $p < 0.05$.

4.3   Results

Single-molecule imaging using TIRF microscopy

First, as a proof-of-principle the combination of single-molecule imaging and TIRF microscopy was performed using a membrane-associated protein. For this purpose we used YFP C-terminally tagged to the membrane anchor of H-Ras, YFP-C10H-Ras. The mobility pattern of YFP-C10H-Ras has been described in previous studies (Lommerse et al., 2004; Schaaf et al., 2009). CHO cells were transiently transfected with YFP-C10H-Ras and imaged on the TIRF setup 2 to 3 days after transfection. Very low background fluorescence levels were found as well as single diffraction-limited spots(Figure 4.1B). The fluorescence intensity profiles of these spots were fitted by a 3D-gaussian peak, and peaks that could be attributed to single YFP molecules were selected using criteria based on previous studies (Harms et al., 2001).

To verify the validity of our approach, we compared the average background intensity, peak intensity, peak width and number of recorded peaks for cells transfected with YFP-C10H-Ras or YFP-tagged MR to untransfected cells. As can be seen in Figure 4.3A 8–20 fold more peaks were identified in YFP transfected cells as compared to untransfected cells. This indicates that the vast majority of selected peaks can be attributed to individual YFP molecules. In addition, higher peak intensity and peak width was obtained from peaks identified in cells transfected with either of our YFP fusion proteins (Figure 4.3B–C). We also found a larger peak width for YFP-MR transfected versus YFP-C10H-Ras transfected cells (Figure 4.3C). This larger peak width could be due to faster protein diffusion (displacement during the camera opening time) or due to a larger distance of the peak to the focus point of the objective. Both explanations could be valid, since YFP-MR generally shows faster diffusion than YFP-C10H-Ras (Table 4.1) and its partial cytoplasmic localization will also result in a larger distance to the focus point. Furthermore, more peaks per image were found for YFP-C1-H-Ras compared to YFP-MR cells. This is due to a higher percentage of molecules within the focal plane for the purely membrane localized YFP-C10H-Ras.

Series of 2000 subsequent images of these cells were obtained with time lags of 50 ms to investigate the dynamics of YFP-C10H-Ras. The mobility pattern of YFP-C10H-Ras was analyzed by PICS (Semrau and Schmidt, 2007). In this method, for each identified peak, the distances to all peaks in the subsequent image are recorded. This includes distances from two sources: random proximity of unrelated molecules and molecular displacements. The cumulative distribution of all distances (C_{cum}) was determined for each time lag (light grey line, Figure 4.3A). As proximity to other molecules is not dependent on distance, its contribution to C_{cum} will show a linear increase over distance (fine dotted line, Figure 4.3CA). The intercept of the fit of this linear curve represents the size of the fraction due to molecular displacements. Subtraction of this fit leaves only the distances resulting from molec-
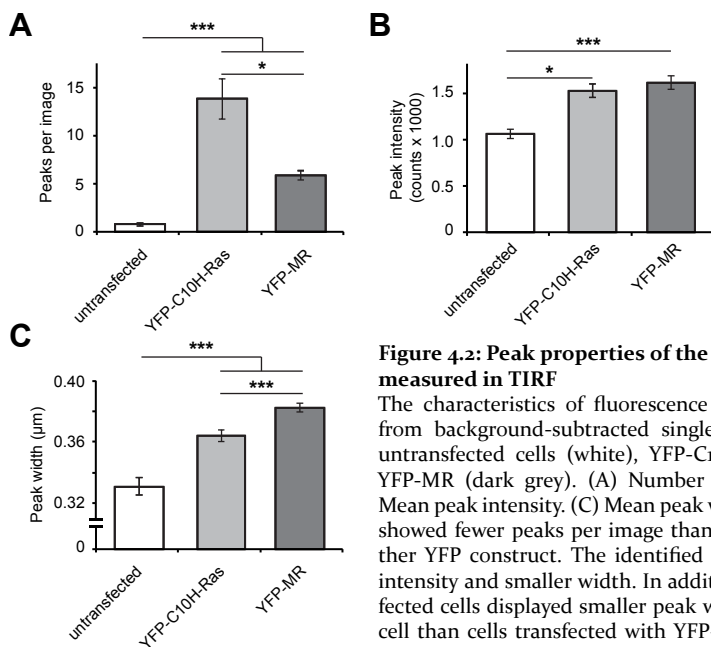
Figure 4.2: Peak properties of the fluorophores measured in TIRF

The characteristics of fluorescence intensity peaks selected from background-subtracted single-molecule recordings of untransfected cells (white), YFP-C10H-Ras (light grey) and YFP-MR (dark grey). (A) Number of peaks per image. (B) Mean peak intensity. (C) Mean peak width. Untransfected cells showed fewer peaks per image than cells transfected with either YFP construct. The identified peaks also showed lower intensity and smaller width. In addition, YFP-C10H-Ras transfected cells displayed smaller peak width and more peaks per cell than cells transfected with YFP-MR. Our imaging conditions thus result in primarily YFP peaks and include only a small, negligible contribution of autofluorescence. Untransfected $n = 7$, YFP-C10H-Ras $n = 15$ and YFP-MR $n = 37$. $* p < 0.05$; $** p < 0.01$; $*** p < 0.001$.

ular displacements (P_{cum}). For YFP-C10H-Ras, the size of the diffusing fraction is 27 %, 21 % and 18 % over increasing time lags (50, 100 and 150 ms respectively).

The resulting cumulative plot of molecular displacements (P_{cum}, dark grey line, Figure 4.3A) can be fitted with multiple population models. A one-population model failed to fit the curves well, while a two-population model did give an accurate fit (coarse dotted line, Figure 4.3A). Introduction of a third population hardly improved the fit and gave inconsistent results over different time lags (data not shown). We found that the mobility of membrane-associated YFP could be best described by two fractions each moving with a different speed: a large 'fast' fraction of 83 ± 2 % (Figure 4.3B), and a small 'slow' fraction of 17 ± 2 %. Subsequently, the mean squared displacements (MSDs) determined for both the fast and the slow fraction for each time lag were plotted as a function of the time lag (Figure 4.3C). For the fast fraction this resulted in a linear curve, indicating free diffusion of this fraction of molecules. Based on the slope of this curve a diffusion coefficient (D_{fast}) of 0.23 ± 0.01 mm^2/s was determined. The slow fraction, on the other hand showed displacements around our positional accuracy (0.0068 μm^2; indicated by triangle in Figure 4.3C). In previous studies, the mobility of the slow fraction of YFP-C10H-Ras was best described by confined diffusion, in which the molecules diffuse freely within a domain with impermeable borders (Lommerse et al., 2004; Schaaf et al., 2009). Different cell types showed large differences in the size of these restricted mem-
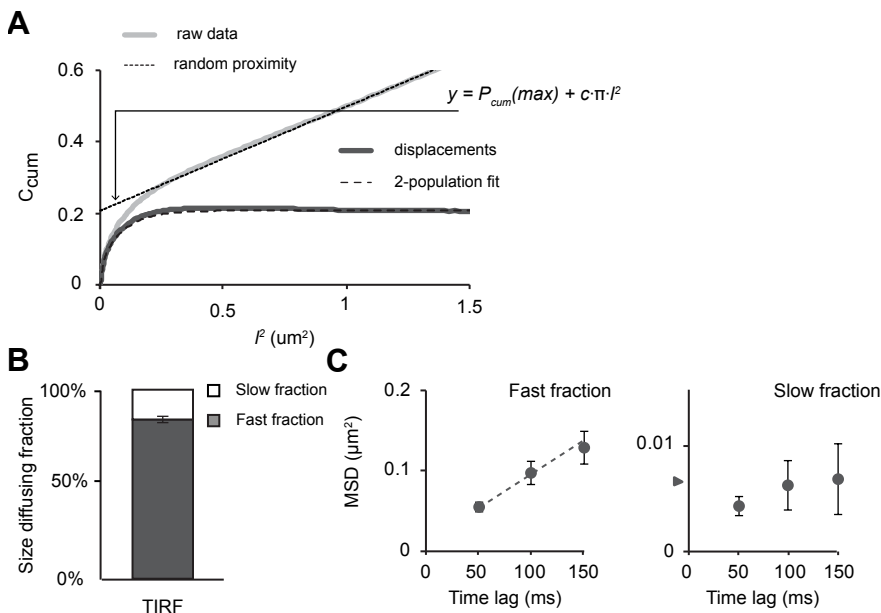
Figure 4.3: Proof of principle of TIRF microscopy using YFP-C10H-Ras
(A) PICS analysis. Shown is the cumulative plot of distances (l^2) for YFP-C10H-Ras with a time lag of 100 ms. The raw data (light grey line) contains contributions from both random proximity and molecule displacements. The contribution of distances due to random proximity can be fitted with a straight line (fine dotted line) and subtraction of these from the raw data leaves only the distances due to molecular displacement (dark grey line). The cumulative displacements are well fitted with a 2-population model of two moving fractions (coarse dotted line). (B-C) Quantification of diffusion of YFP-C10H-Ras. For YFP-C10H-Ras, 84 % of all molecules belong to the fast, freely diffusing fraction (B: grey bar, C: left panel). The remaining 16 % shows negligible displacement steps (B: white bar, C: right panel, positional accuracy indicated by the triangle) and are considered immobile. Data is shown as mean of recording days. $n = 3/17$ (days/cells).

		% slow	D_{slow} (μm^2/s)	% fast	D_{fast} (μm^2/s)
YFP-C10H-Ras	TIRF	16 ± 2	n.a.	84 ± 2	0.23 ± 0.01
YFP-MR (CHO)	TIRF	51 ± 7	0.005 ± 0.001	49 ± 7	1.06 ± 0.48
	Wide-field	30 ± 2	0.031 ± 0.002	70 ± 2	1.45 ± 0.05
YFP-MR (COS-1)	TIRF	35 ± 6	0.015 ± 0.003	65 ± 6	0.36 ± 0.07
	Wide-field	11 ± 11	0.039 ± 0.018	89 ± 11	0.85 ± 0.17

Table 4.1: Comparison of single-molecule kinetics of YFP-C10H-Ras, YFP-YFP and YFP-MR between TIRFM and wide-field microscopy
% diffusing is the fraction of distances due to molecule displacements obtained from PICS analysis of the shortest time lag (50 ms).

brane domains. In the current study YFP-C10H-Ras does not show displacements larger than the spatial resolution, which suggest that in CHO cells this fraction represents either immobile molecules or molecules restricted to very small membrane domains (< 40 nm).

		Fraction of molecular displacements		
		50 ms	100 ms	150 ms
YFP-C₁₀H-Ras	TIRF	27 %	21 %	18 %
YFP-MR (CHO)	TIRF	18 %	13 %	12 %
	Wide-field	12 %	12 %	13 %
YFP-MR (COS-1)	TIRF	14 %	13 %	12 %
	Wide-field	13 %	11 %	9 %

Table 4.2: Fraction of distances due to molecule displacement

Lower mobility of YFP-MR in TIRF than in wide-field microscopy suggestive for the existence of a membrane-associated population of YFP-MRs

Next, YFP-tagged human MR was examined. We chose to perform our experiments in CHO cells, since Grossmann et al. (2005, 2008) showed non-genomic, membrane-initiated signaling through the MR in these cells. In CHO cells, YFP-MR is seen throughout the cytoplasm in the absence of hormone and translocates to the nucleus upon stimulation with corticosterone (Figure 4.1c). When analyzed with conventional confocal microscopy, no obvious enrichment of YFP-MR at the membrane can be discerned (Figure 4.1c, insert).

We next imaged single-molecules of YFP-MR in CHO cells in TIRF and wide-field microscopy. In both TIRF and wide-field modus clear single YFP-MR molecules were observed. The molecular dynamics were analyzed using PICS, and the cumulative plot of observed peak distances was generated (C_{cum}; Figure 4.4A). We found that the fraction of measured distances as a result of molecular displacements of YFP-MR is larger in TIRF than in wide-field (for 50 ms: 18 % in TIRF and 12 % in wide-field; see also Table 4.2). Next, we fitted P_{cum} with a 2-population method and determined fraction sizes and MSDs of both fractions. In wide-field, a small fraction (30 ± 2 %) of YFP-MR showed small displacement steps. Plotting MSDs against the time lag resulted in a curve that could be fitted with a straight line, indicating free diffusion of this slow fraction. The diffusion coefficient (D_{slow}) was $0.031 \pm 0.002\,\mu\text{m}^2/\text{s}$. The remaining 70 ± 2 % also showed free diffusion, but with ~50 fold larger displacements and a diffusion coefficient D_{fast} of $1.45 \pm 0.05\,\mu\text{m}^2/\text{s}$ (Figure 4.4B,C). Interestingly, when imaged in TIRF, the size of the slow fraction was larger: 51 ± 7 % (Figure 4.4B). At the same time, the displacements of both fractions were smaller (Figure 4.4C; $D_{\text{slow}} = 0.005 \pm 0.001\,\mu\text{m}^2/\text{s}$; D_{fast} of $1.06 \pm 0.48\,\mu\text{m}^2/\text{s}$).

To examine whether the observed difference in mobility patterns for YFP-MR between wide-field and TIRF imaging was specific for the cell line used, we repeated the same procedure in a second cell line, COS-1 cells. Also in COS-1 cells, conventional confocal microscopy failed to show an obvious enrichment of YFP-MR at the membrane (Figure 4.1D insert). Subsequently, YFP-MR expressing COS-1 cells were imaged using TIRF and wide-field single-molecule microscopy. The size of the

Chapter 4

A **CHO cells**

B

C

D **COS-1 cells**

E

F
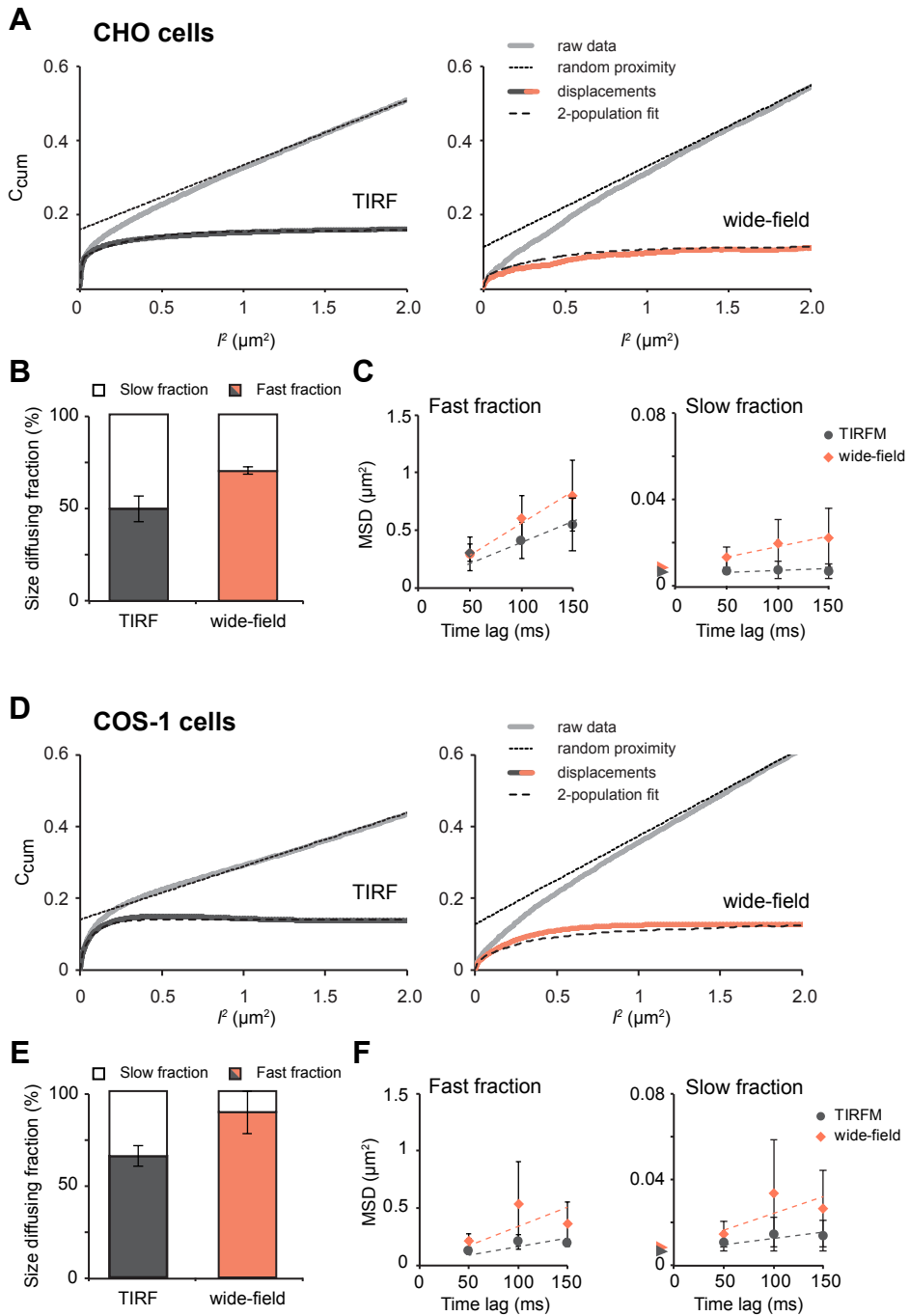
fraction of measured distances due to molecular displacements was highly similar between TIRF (14 %) and wide-field (13 %), see also Table 4.2. We found a larger slowly diffusing fraction in TIRF modus, highly comparable to what we observed in CHO cells. Only 11 ± 11 % of molecules showed slow diffusion in wide-field recordings, and in TIRF this fraction was increased to 35 ± 6 % (Figure 4.4E). In COS-1 cells, the measured diffusion coefficients of both the slow and the fast fraction were slightly decreased in TIRF (D_{fast} of 0.36 ± 0.07 μm^2/s versus 0.85 ± 0.17 μm^2/s in wide-field and D_{slow} of 0.015 ± 0.003 μm^2/s versus 0.039 ± 0.018 μm^2/s in wide-field; Figure 4.4F). In order to test for statistical significance we analyzed the diffusion patterns of YFP-MR separately for each recording day and tested significance for the full data set (CHO and COS-1 cells combined; $n =$ recording days). We found a significant difference between TIRF and wide-field recordings for the displacements of the slow fraction ($p = 0.04$) and for the size of the slow fraction ($p = 0.01$). No significant differences were seen between the two cell lines.

Corticosterone and BSA-bound corticosterone do not affect the mobility pattern of YFP-MR

In order to determine whether hormone treatment affects the kinetics of the receptor, a set of experiments was designed in which the receptor was exposed to its ligand. Ligand binding is known to alter the conformation of the receptor (at least in the cytoplasm) and to induce protein-protein interactions of membrane-associated steroid receptors (Levin, 2008). CHO cells were exposed to 1 μM corticosterone which is known to saturate MR binding (Karst et al., 2005), or to a similar concentration of BSA-conjugated corticosterone (cort-BSA). Cort-BSA is membrane-impermeable and any alteration in the kinetics of YFP-MR induced by this ligand will be the result of changes in the mobility of a membrane-associated YFP-MR. We assessed the mobility of YFP-MR by SMM before treatment and at 5 minutes after hormone treatment. The imaging took approximately 2 minutes, so diffusion was measured from 5–7 minutes post hormone treatment. We restricted ourselves to this short term treatment as it is known that membrane-associated receptors can become internalized by prolonged hormone treatment (Razandi et al., 2002; Wang and Wang, 2009; Karst et al., 2010). As a control, we tested the effects of the different hormone treatments on the kinetics of YFP-C10H-Ras.

Figure 4.4 *(preceding page)*: A smaller diffusing fraction of YFP-MR near the membrane in CHO and COS-1 cells
The diffusion behavior of YFP-MR recorded in TIRF and wide-field modes in both CHO (A-C) and COS-1 (D-F) cells. (A & D) Cumulative distances plots. (B & E) Fraction distributions. For both cell lines, the fraction of molecules that shows slow diffusion (white bars) is larger in TIRF than in wide-field. (C & F) MSD plots for both fractions (left panels: fast fractions, right panels: slow fractions). For CHO cells, the displacements of the slowly diffusing fraction are smaller in TIRF. Data is shown as mean of recording days. CHO: TIRF, $n = 5/45$; wide-field, $n = 4/43$; COS-1: TIRF, $n = 3/32$; wide-field, $n = 2/26$ (days/cells).
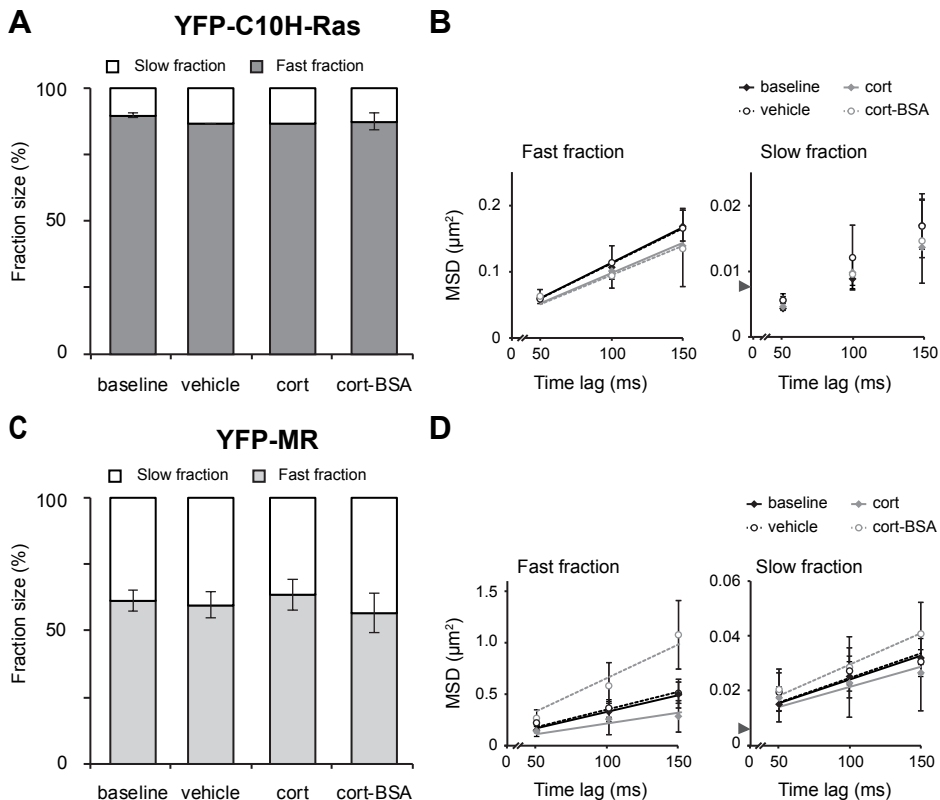
Figure 4.5: Corticosterone and cort-BSA do not affect diffusion behavior of YFP-C10H-Ras or YFP-MR

The effect of short-term treatment (5–7 min) with 100 nM corticosterone (cort) or BSA-conjugated corticosterone (cort-BSA) on fraction distribution was examined for both YFP-C10H-Ras (A-B) and YFP-MR (C-D). (A-B) Neither cort, cort-BSA, or vehicle treatment affected the fraction distribution (A) or the MSDs (B) of YFP-C10H-Ras, an inert membrane-associated molecule. (C-D) Hormone administration did not affect the fraction distribution (C) or the MSDs (D) of YFP-MR either. Data is shown as mean of recording days. YFP-C10H-Ras: baseline, $n = 4/18$; vehicle, $n = 3/7$; cort, $n = 2/5$; cort-BSA, $n = 2/6$. YFP-MR: baseline, $n = 6/64$; vehicle, $n = 5/18$; cort, $n = 4/21$; cort-BSA, $n = 4/25$ (days/cells).

		% slow	D_{slow} ($\mu m^2/s$)	% fast	D_{fast} ($\mu m^2/s$)
YFP-C10H-Ras	Baseline	10 ± 1	n.a.	90 ± 1	0.28 ± 0.01
	Vehicle	13 ± 0	n.a.	87 ± 0	0.27 ± 0.00
	Cort	13	n.a.	87	0.23
	Cort-BSA	13 ± 3	n.a.	87 ± 3	0.29 ± 0.01
YFP-MR	Baseline	39 ± 4	0.04 ± 0.00	61 ± 4	0.77 ± 0.03
	Vehicle	40 ± 5	0.05 ± 0.01	60 ± 5	1.00 ± 0.07
	Cort	36 ± 6	0.04 ± 0.01	64 ± 6	0.58 ± 0.07
	Cort-BSA	43 ± 8	0.06 ± 0.00	57 ± 8	1.46 ± 0.14

Table 4.3: Effect of hormone treatments on protein kinetics of YFP-C10H-Ras and YFP-MR in CHO cells

Treatment with vehicle, corticosterone or cort-BSA did not change the displacements nor the relative fraction sizes of YFP-C10H-Ras (Figure 4.5A–B; Table 4.3). Next, we subjected the same treatments to YFP-MR-transfected CHO cells. However, no effects were seen with either treatment. Thus, the slowly diffusing fraction of YFP-MR (measured using TIRF microscopy) remains around 40 % with either treatment (Figure 4.5C). MSDs and diffusion coefficients were not affected by hormone treatment either (Figure 4.5D; Table 4.3).

4.4 Discussion

In the present study we have investigated YFP-tagged MR using single-molecule microscopy in TIRF and wide-field mode. The results are summarized in Tables 4.1 till 4.3. TIRF is a well-established method that provides images that are strongly enriched for near-membrane molecules (Axelrod, 2008). Thus, if a membrane-associated subpopulation of YFP-MR was present in the investigated cell lines, it would have been be strongly enriched for in TIRF. We analyzed the protein dynamics of YFP-MR with SMM in wide-field and TIRF in two cell lines, and observed a larger slow fraction of YFP-MR molecules in TIRF versus wide-field modes in both cell lines (51 % versus 30 % and 35 % versus 11 %, see Table 4.1). In one cell line (CHO), the slow fraction also showed slower diffusion in TIRF as compared to wide-field microscopy.

In general, membrane-associated proteins are less mobile than cytoplasmic proteins (Owen et al., 2009; Sanderson, 2012), mainly due to the higher viscosity of the membrane. Diffusion of membrane-anchored proteins ranges from 0.01 to $1.0\,\mu\text{m}^2/\text{s}$ (Owen et al., 2009). The diffusion of the observed slow fraction of YFP-MR (D_slow of 0.012 and 0.015 $\mu\text{m}^2/\text{s}$ in CHO and COS-1 cells respectively) fits within this expected range for membrane-anchored proteins. Cytoplasmic MR, in contrast, is expected to diffuse much faster. The diffusion of steroid receptors has never been analyzed within the cytoplasm, but has extensively been measured in the nucleus. We found that both the MR and GR diffuse with a diffusion coefficient of 2–3 $\mu\text{m}^2/\text{s}$ (*Chapters 5 and 6*) within the nucleus, and similar diffusion would be expected for the cytoplasmic fraction. Here, we obtained a fast diffusing fraction with D_fast of 1.4 and 0.9 $\mu\text{m}^2/\text{s}$ (in CHO and COS-1 cells respectively), which is slightly lower than expected for freely diffusing cytoplasmic MR. The MR is bound by a large chaperone complex within the cytoplasm (Picard, 2006), which could underlie this slower diffusion. Taken together, the slow fraction shows diffusion that fits to what is known for membrane-associated proteins and the fast fraction diffuses slightly slower than what is expected for cytoplasmic steroid receptors.

Of note, we did find a slowly diffusing fraction of 11–30 % in wide-field recordings where we expect a negligible contribution of the membrane-associated population. This suggests that also cytoplasmic MR encompasses a slowly diffusing frac-

tion (potentially due to protein complex formation) and we thus do not presume that the entire slow fraction will represent membrane-associated MR. The larger size of the slowly diffusing fraction measured using TIRF microscopy fits very well with the notion of a mixed cytoplasmic (both fast and slow diffusing populations) and membrane-associated (purely slow diffusing) population of the MR in TIRF.

There is one large difference between TIRF and wide-field recordings that could influence the obtained protein diffusion: the thickness of the optical slice (or Z-depth). By default, the Z-depth of TIRF is very small and estimated to be around 60–100 nm thick. In contrast, our wide-field recordings will have a Z-depth of 0.5–1 µm (van Royen et al., 2014). As proteins diffuse in 3D, they will 'escape' from the field of view during the time lag. This effect will be larger when a smaller Z-depth is used (as in TIRF) and will occur most readily for fast diffusing molecules (van Royen et al., 2014). Thus, a smaller Z-depth will enrich for slowly moving molecules and the larger size of the slow fraction observed using TIRF could therefore represent an artifact of the imaging conditions. However, the results from our PICS analysis show that in TIRF mode fewer molecules 'escape' than in wide-field mode. With PICS analysis we could directly calculate the fraction of recorded distances that are due to molecule displacements from the C_{cum} graphs (Figure 4.3c). When this fraction is large, many molecules are imaged in two consecutive images, so only few molecules leave the z-plane during the interval between the images. We found that a similar or even larger fraction of molecules can be imaged in two consecutive images in TIRF mode (Table 4.2). In CHO cells, for example, 18 % of molecules can be imaged in two consecutive images, while this drops to 12 % in wide-field recordings. Thus, even though the z-depth is a lot smaller in TIRF mode, more molecules are imaged in two consecutive images, indicating that fewer molecules 'escape' from the z-slice. We therefore conclude that there is a true enrichment for slowly diffusing YFP-MRs near the membrane in TIRF mode, and that the increased size of the slow fraction observed in TIRF recordings of YFP-MR is not an artifact of the imaging conditions.

Conclusively, we find a larger fraction of slowly diffusing molecules for YFP-MR in TIRF as compared to wide-field microscopy, and this difference cannot be accounted for by technical artifacts. The most likely explanation for the increased size of this fraction in TIRF would be the enrichment for membrane-associated proteins in TIRF that show slower diffusion. Alternatively, the slower diffusion near the membrane may not result from association with the membrane, but may be due to steric hindrance or a higher concentration of signaling partners in the cytoplasmic region near the membrane.

Manipulation of the membrane-associated fraction

In the current study we applied corticosterone or its membrane-impermeable conjugate cort-BSA to YFP-MR expressing cells. Unfortunately, we did not find any effect of either hormone on the dynamics of YFP-MR in TIRF (Table 4.3), indicating

that the mobility of a putatively membrane-associated MR population is not altered upon ligand binding. It has been reported for many membrane receptors that ligand activation affects protein mobility within our time range. For example, treatment with insulin led to rapid (within 5 minute) recruitment of H-Ras to smaller microdomains (Lommerse et al., 2005). In another study, the chemotactic receptor cAR1 was activated by its ligand cAMP. This resulted, within a minute, into a larger diffusing fraction (Keijzer et al., 2008). On the other hand, ligand treatment does not necessarily affect protein dynamics. The available literature suggests that a membrane-associated MR will bind adaptor proteins upon activation, but is also bound to other proteins (such as caveolin-1) before activation (Grossmann et al., 2010; Pojoga et al., 2010b), which could result in no net change in diffusional characteristics after activation.

Other options remain to specifically alter the dynamics of the membrane-associated MR population. Disruption of lipid rafts, caveolae or actin compartmentalization are all known to affect the kinetics of membrane-associated proteins (Lajoie et al., 2007; Ganguly et al., 2008). Moreover, as the MR is presumably also localized in caveolae (Pojoga et al., 2010b) and is known to associate with lipid rafts (Grossmann et al., 2010), disruption of these structures would likely affect the membrane-association of the MR as well. Future studies that specifically disrupt the membrane-associated fraction of the MR would provide the final proof that TIRF can enrich for this population in a sufficient manner to distinguish it from the cytoplasmic background.

Chapter 4

85

Quantitation of Glucocorticoid Receptor DNA-binding dynamics by Single-Molecule Microscopy and FRAP

Femke L. Groeneweg[1], Martin E. van Royen[2], Suzanne Fenz[3,4],
Jurrien Prins[1,5], Bart Geverts[2], E. Ron de Kloet[1],
Adriaan B. Houtsmuller[2], Thomas S. Schmidt[3], Marcel J.M. Schaaf[5]

[1] Department of Medical Pharmacology, Leiden University / LUMC, Leiden, The Netherlands.
[2] Department of Pathology, Erasmus MC, Rotterdam, The Netherlands.
[3] Physics of Life Processes, Institute of Physics, Leiden University, Leiden, The Netherlands.
[4] Cell & Developmental Biology, Biocenter, Würzburg University, Würzburg, Germany.
[5] Molecular Cell Biology, Institute of Biology, Leiden University, Leiden, The Netherlands.

RECENT advances in live cell imaging have provided a wealth of data on the dynamics of transcription factors. However, a consistent quantitative description of these dynamics, explaining how transcription factors find their target sequences in the vast amount of DNA inside the nucleus, is still lacking. In the present study, we have combined two quantitative imaging methods, single-molecule microscopy and fluorescence recovery after photobleaching, to determine the mobility pattern of the GR, a ligand-activated transcription factor. For dexamethasone-activated GR, both techniques showed that approximately half of the population is freely diffusing, while the remaining population is bound to DNA. Of this DNA-bound population about half the GRs appeared to be bound for short periods of time ($\sim 0.7\,\text{s}$) and the other half for longer time periods ($\sim 2.3\,\text{s}$). Inactive receptors (mutant or antagonist-bound receptors) show a decreased DNA binding frequency and duration, but also a higher mobility for the diffusing population. Likely, very brief ($\sim 1\,\text{ms}$) interactions with DNA induced by the agonists underlie this difference in diffusion behavior. Surprisingly, different agonists also induce different mobilities of both receptors, presumably due to differences in ligand-induced conformational changes and receptor complex formation. In summary, our data provide a consistent quantitative model of the dynamics of the GR, indicating three types of interactions with DNA, which fit into a model in which frequent low-affinity DNA binding facilitates the search for high-affinity target sequences.

5.1 Introduction

In the past decade, imaging studies of fluorescently tagged proteins inside living cells have enormously increased our understanding of transcription factor dynamics (Stenoien et al., 2001; Schaaf and Cidlowski, 2003; Stavreva et al., 2004; Schaaf et al., 2005, 2006; Hager et al., 2009; van Royen et al., 2009a, 2012; Mueller et al., 2010). These studies have shown that transcription factors display a remarkably high mobility in the nucleus. Even in its most activated state a typical transcription factor appears to be able to diffuse through the entire nucleus, and to be immobilized only transiently (Gorski et al., 2006; Biddie and Hager, 2009; Hager et al., 2009). One often-studied transcription factor is the GR. This cytoplasmically localized receptor translocates to the nucleus upon binding of naturally occurring glucocorticoids (corticosterone and cortisol) or their synthetic analogs. In the nucleus the steroid-GR complexes can bind either directly or indirectly (through interactions with other transcription factors) to DNA and alter transcription rates of responsive genes (Beato and Sanchez-Pacheco, 1996; Heitzer et al., 2007; Datson et al., 2008). Like other transcription factors, ligand-activated GRs display a high mobility within the nucleus in FRAP studies (McNally et al., 2000; Schaaf and Cidlowski, 2003; Stavreva et al., 2004; Schaaf et al., 2005; Mueller et al., 2008). Using GR mutants with reduced DNA-binding capacity or antagonist-bound GR, a negative correlation was shown between GR mobility and the capacity to initiate transcription (Schaaf and Cidlowski, 2003; Elbi et al., 2004; Stavreva et al., 2004).

In the last decade many new imaging techniques have become available that open possibilities for more detailed quantifications of protein dynamics (Stasevich et al., 2010b; Li and Xie, 2011; Mazza et al., 2012; Gebhardt et al., 2013). One such approach is single-molecule microscopy (SMM). In SMM, conventional wide-field fluorescence microscopy is combined with a fast, ultra-sensitive CCD camera to enable the visualization of single fluorescent molecules with high temporal ($\sim$6 ms) and spatial (positional accuracy of $\sim$40 nm) resolution (Lord et al., 2010; Li and Xie, 2011). Initially, SMM was used to study the mobility patterns of membrane proteins (Lommerse et al., 2004; Suzuki et al., 2005; Schaaf et al., 2009; Kasai et al., 2011; Serge et al., 2011), and it has now been adapted for studies of nuclear proteins (Yang et al., 2004; Yang and Musser, 2006) and transcription factors (Elf et al., 2007; Li and Elf, 2009; Mazza et al., 2012), including a recent study on the GR (Gebhardt et al., 2013). Importantly, the analysis of single-molecule displacement patterns gives a very direct and unbiased picture of protein dynamics (Schutz et al., 1997; Semrau and Schmidt, 2007). For the more conventional population-based approaches, the correct control for confounding factors such as laser irregularities and the requirement of many *a priori* assumptions and independent variables introduce bias in the outcomes and have been a major challenge for the field (Mueller et al., 2008, 2010; van Royen et al., 2009a,b). To control for any confounding factors that might still exist in the SMM analysis, we combine SMM analysis with an established Monte Carlo quantification approach of FRAP imaging (Farla et al., 2004; van Royen et al.,

2009b). The combination with FRAP not only gives independent cross-validation of the SMM predictions, but also enables a quantification of protein kinetics over a longer time frame than SMM.

Our data show that this combination of techniques provides a very consistent quantitative analysis of GR dynamics. Based on our data, we can distinguish three states of agonist-activated GR molecules; one diffusing state and two DNA-bound states, one with short (< 1 sec) and one with a longer (2–4 sec) binding duration. Transcriptionally inactive GR variants show a reduction in the frequency and in the duration of both DNA binding events, and an increase in the diffusion rate of the diffusing population. This suggests that within this diffusing population an additional very brief DNA-binding event is hidden, resulting in a lower effective diffusion rate.

5.2   Methods

Cell culture and plasmids

In most experiments, COS-1 cells were used, grown in high-glucose D-MEM (Invitrogen) supplemented with 10 % FBS and 1 % penicillin/streptomycin (both GIBCO). 24 h prior to transfection, cells were plated on sterile coverglasses (25 mm diameter). Cells were transfected with the TransIT-COS kit (Mirus) according to the manufacturer's instructions at a concentration of 500 ng DNA / 10 cm². Transfected cells were used in experiments 2–5 days after transfection. For one experiment, Hep3B cells were used, stably transfected with the pEYFP-hGR expression vector (Schaaf and Cidlowski, 2003). These cells were grown in α-MEM (Cambrex), supplemented with 5 % FBS, 2 mM L-glutamine, 1 % Penicillin/Streptomycin and 600 µg/ml G418 (Invitrogen). The generation of the pEYFP-GR plasmid, the three deletion mutants of this vector (pEYFP-GR Δ9–385, pEYFP-GR Δ428–490, and pEYFP-GR Δ551–777, and the point mutant (pEYFP-GR F623A) have been described previously (Schaaf and Cidlowski, 2003; Schaaf et al., 2005).

Compounds

The following ligands were used in these studies: dexamethasone, corticosterone, cortisol, Δ-fludrocortisone (*1,4-pregnadien-9α-fluoro-11β,17,21-triol-3,20-dione*), prednisolone (*1,4-pregnadien-11β,17,21-triol-3,20-dione*) and RU486 (*4,9-estradien-17α-propynyl, 11β-[4-dimethylaminophenyl]-17β-ol-3-one*). All steroids were purchased from Sigma-Aldrich and diluted in 100 % EtOH to a concentration of 1 mM. All steroids were used at a final concentration of 1 µM in the medium.

Single molecule microscopy

For all SMM experiments, COS-1 cells were grown on coverslips and transiently transfected with the corresponding plasmid (500 ng / 10 cm²) 3–5 days prior to analysis. Before SMM recordings, cells were exposed to 1 µM of corresponding hormones for 3–6 h. For SMM measurements, this medium was replaced by serum- and phenol red-free D-MEM medium (Invitrogen), which is also supplemented with 1 µM of the corresponding hormone. Subsequently, cells were transferred to the SMM setup and imaged for up to 90 min at 35 °C. A wide-field

fluorescence microscope (Axiovert 100TV, Zeiss) was used, equipped with a 100× / 1.4NA oil-immersion objective (Zeiss). A region-of-interest (ROI) of 50 × 50 pixels (pixel size of 220 nm) was selected. The sample was illuminated by an 514 nm argon laser at an intensity of 2 kW/cm^2. The pulse length of 3 ms was controlled by an acusto-optical tunable filter (AA optoelectronics, France). The EYFP fluorescence signal was detected through a combination of filters (DCLP530, HQ570/80 (Chroma Technology, Brattleboro, VT) and OG530-3 (Schott, Mainz, Germany)), by a liquid-nitrogen cooled CCD camera (Princeton Instruments, Trenton, NJ), camera read out and AOTF timing were tightly controlled. Healthy and moderately fluorescent nuclei were selected and then photobleached until single fluorescence intensity peaks could be distinguished. The position of each individual molecule was fitted with the intensity profile of a 2D Gaussian model of EYFP peaks (Harms et al., 2001). Our peaks were identified with a signal to noise ratio of ∼8 (peak fluorescence intensity divided by the variation of the background), which resulted in a positional accuracy of ∼40 nm in the X- and Y-direction (determined by the quotient of the full-width-at-half-maximum of the Gaussian fit and the square root of the number of photons detected (Bobroff, 1986)). On average, each picture contained ∼1.5 peaks. Image sequences were recorded in series of 8 subsequent images with a time lag of either 6.25 ms or 12.5 ms (Figure 5.1C). Data on molecular dynamics were obtained for multiple step sizes. We used all time lags from 6.25 to 37.5 ms in our analysis. From each cell 180 series of 8 images were taken and data from 20 independent cells (imaged on at least 3 different days) was combined for the analysis.

PICS analysis of single-molecule kinetics

We used the Particle Image Correlation Spectroscopy (PICS) method to determine peak displacement over time (Semrau and Schmidt, 2007). In PICS, the cross-correlation between peak positions at two different time lags (for example $t = 0$ ms and $t = 6.25$ ms) is calculated. This yields the cumulative probability distribution (C_{cum}) of all 'diffusion steps' detected within 6.25 ms. C_{cum} includes both contributions from diffusing molecules as well as random correlations between unrelated molecules in the two frames. The latter follows a linear relation in the cumulative plot and was subtracted prior to further analysis. From the remaining cumulative probability function (P_{cum}) of diffusion steps l, we use population modeling to calculate diffusion characteristics of the nuclear population of YFP-GR (Figure 5.1D). Given that the population of molecules is homogeneous, a single population of displacing molecules is determined with

$$P_{cum}(l, \Delta t) = 1 - \exp\left(-\frac{l^2}{\mathrm{MSD}_0(\Delta t)}\right) \tag{5.1}$$

Here MSD$_0$ is the mean square displacement of one population of molecules over the time lag. However, this one fraction model could not explain the experimental data (Figure 5.1D). Therefore a second fraction was introduced and the equation reads as follows:

$$P_{cum}(l, \Delta t) = 1 - \left[\alpha \cdot \exp\left(-\frac{l^2}{\mathrm{MSD}_1(\Delta t)}\right)(1-\alpha) \cdot \exp\left(-\frac{l^2}{\mathrm{MSD}_2(\Delta t)}\right)\right] \tag{5.2}$$

Where MSD$_1$ and MSD$_2$ denote the mean square displacement of the first (fast) and the second (slow) fractions respectively, and α is the fraction size of the first (fast) fraction. A two-population model fitted the experimental data with high accuracy (Figure 5.1D). Although diffusion happens in 3D, we measure only the 2D projection, and to prevent distortion of the
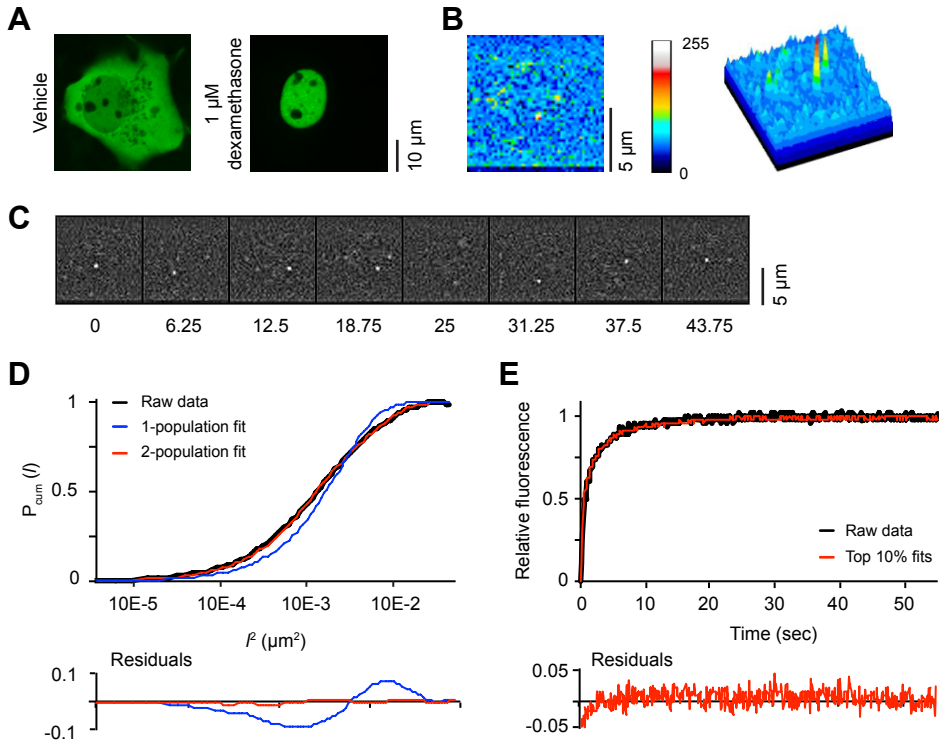
Figure 5.1: SMM and FRAP procedures
(A) Representative confocal images show complete nuclear translocation of YFP-GR after 3 hours of $1\,\mu\text{M}$ dexamethasone treatment. (B) A representative CCD image of single molecules of YFP-GR after background subtraction shows two discernible Gaussian peaks of YFP fluorescence. (C) Regime for single molecule kinetics; images are taken with a time lag of $6.25\,\text{ms}$ or $12.5\,\text{ms}$ in 300 series of 8 per cell. In background-subtracted images, single molecules of YFP fluorescence are easily discernible. (D). PICS analysis of single molecule displacements, shown for dexamethasone-bound YFP-GR at time delay of $6.25\,\text{ms}$. The cumulative probability distribution as a function of the squared distance l (black line) is best fitted with a 2-population model (red line), while a 1-population model gives a suboptimal fit (blue line) ($n = 20$ cells). (E) FRAP procedure of dexamethasone-bound YFP-GR. At $t = 0$ a $100\,\text{ms}$ bleach pulse is applied to a strip spanning the nucleus. Subsequently, FRAP recovery curves of 30 cells are recorded, combined and adjusted to baseline fluorescence (black line). Subsequently, Monte Carlo simulations are generated using a 3-population model and fitted to the combined FRAP curve. The top 10 fits are combined (red line) and show a good fit of the experimental data with small residuals.

data due to molecules 'escaping' in 3D space, we restrict ourselves to only small time lags (up to $42.5\,\text{ms}$). In simulation experiments, we have demonstrated that within this time from the effects of 'escaping' molecules can be neglected (data not shown). The analysis was repeated for each time lag and α, MSD_1 and MSD_2 were plotted against time (Δt). The displacements over time were best described using a free diffusion model in 2D, from which the diffusion coefficients (D_{fast} and D_{slow}) were calculated using the following equation:

$$\text{MSD}_i(\Delta t) = 4 \cdot D_i \cdot \Delta t \tag{5.3}$$

OriginPro software was used to obtain weighted, linear fits, to calculate D_{fast} and D_{slow}. The fraction size α decreased slightly (on average $-0.18 \pm 0.03\,\%/\text{ms}$) over increasing time lags in

all groups. Due to this effect, we always report the fraction distribution of the smallest time step (6.25 ms) as a representative of the overall fraction distribution. All analyses were first performed on all data from each treatment group pooled together ($n = 20$). Subsequently, all analyses were run again in 3 fractions ($n = 6/7$) and these 3 separate analyses are used to generate standard errors of the mean.

FRAP

For FRAP recordings, COS-1 cells were grown on coverslips and transiently transfected with $500 \text{ ng} / 10 \text{ cm}^2$ of the corresponding plasmid and used 2–3 days after transfection. Before FRAP recordings, cells were exposed to $1 \mu\text{M}$ of the appropriate ligand for 3–6 hours in normal growth medium. For each experiment, a coverglass with transfected COS-1 cells was placed in a preheated ring and medium was replaced for empty D-MEM without phenol red, supplemented with $1 \mu\text{M}$ of the corresponding ligand. Cells were used for no longer than 90 minutes and kept at $37\,°\text{C}$ and $5\,\%$ CO_2. We used a Zeiss LSM510 META confocal laser scanning microscope equipped with a 40× / 1.3NA oil-immersion objective, an argon laser (30 mW) and an AOTF. For FRAP analysis a narrow strip spanning the entire width of the nucleus was scanned at 514 nm excitation with short intervals (100 ms) at low laser power (0.2 %). Fluorescence intensity was recorded using a 560 nm longpass filter. After 40 scans, a high intensity (100 % laser power), 100 ms-bleach pulse at 514 nm was applied over the whole strip. Subsequently, the recovery of the fluorescence intensity in the strip was followed for another 55 seconds at 100 ms intervals. For each treatment group 30 cells were measured by FRAP on two separate days. All curves were normalized to baseline fluorescence intensity and combined.

Monte Carlo quantification of FRAP curves

The FRAP data was quantitatively analyzed by comparing the experimental data to curves generated using Monte Carlo modeling (van Royen et al., 2009b). The Monte Carlo computer simulations used to generate FRAP curves for the fit were based on a model that simulates diffusion of molecules in three dimensions and binding to immobile elements in an ellipsoidal volume. In short, simulated FRAP curves were generated with a 3-population model, containing a diffusing fraction and two bound (immobile) fractions. We take the D_{fast} obtained from SMM analysis as a fixed parameter in these simulation, leaving 4 parameters as variables: short bound fraction, long bound fraction (both ranging from 0–90 %), and time spent in short and long bound state (ranging from 0.1 s to 1 s and from 1 s to 300 s respectively). The laser bleach pulse was simulated based on experimentally derived three-dimensional laser intensity profiles, which were used to determine the probability for each molecule to get bleached considering their 3D position. The simulation of the FRAP curve was run using discrete time steps corresponding to the experimental scan interval of 21 ms. Diffusion was simulated at each new time step $t + \Delta t$ by deriving the new positions $(x_{t+\Delta t}, y_{t+\Delta t}, z_{t+\Delta t})$ of all mobile molecules from their current positions (x_t, y_t, z_t) by $x_{t+\Delta t} = x_t + G(r_1)$, $y_{t+\Delta t} = y_t + G(r_2)$, and $z_{t+\Delta t} = z_t + G(r_3)$, where r_i is a random number ($0 \leq r_i \leq 1$) chosen from a uniform distribution, and $G(r_i)$ is the inverse of a cumulative Gaussian function with $\mu = 0$ and $\sigma^2 = 2D\Delta t$, where D is the diffusion coefficient (obtained from SMM analysis). Immobilization was derived from simple binding kinetics described by:

$$\frac{k_{\text{on}}}{k_{\text{off}}} = \frac{F_{\text{imm}}}{F_{\text{mob}}} \tag{5.4}$$

where F_{imm} is the relative number of immobile molecules and $F_{mob} = 1 - F_{imm}$. The probability for each particle to become immobilized (representing chromatin-binding) is defined as:

$$P_{immobilized} = k_{on} = \frac{F_{imm}}{T_{imm} \cdot F_{mob}} \tag{5.5}$$

where T_{imm} is the characteristic time spent in the immobile state. The probability to be released is given by:

$$P_{mobilized} = k_{off} = \frac{1}{T_{imm}} \tag{5.6}$$

As our model includes two bound fractions with different immobilization times, two immobilization/mobilization probabilities were evaluated for each unit time step. In all simulations, the size of the ellipsoid was based on the average size of measured nuclei, and the FRAP region used in the measurements determined the size of the simulated bleach region. The laser intensity profile using the simulation of the bleaching step was previously derived from confocal image stacks of chemically fixed nuclei containing GFP that were exposed to a stationary laser beam at various intensities and varying exposure times. The unit time step (Δt) corresponded to the experimental sample rate of $21\,ms$. The number of molecules in the simulations was 10^6, which was empirically determined by producing curves that closely approximate the data with comparable fluctuations. The parameters of the top 10 best fitting Monte Carlo curves (by ordinary least squares) were averaged to represent the properties of the fractions in the experimental data.

5.3 Results

We first investigated the nuclear dynamics of the GR by SMM. We used COS-1 cells, transiently transfected with EYFP-tagged human GR (YFP-GR). This YFP-GR fusion protein was previously shown to retain a good transcriptional activity (Schaaf and Cidlowski, 2003). Before analysis, cells were exposed for 3 to 6 hours to a saturating dose ($1\,\mu M$) of the high affinity GR agonist dexamethasone, which induces nuclear translocation of YFP-GR (Figure 5.1A). Nuclei were photobleached until single diffraction-limited fluorescence intensity peaks could be distinguished (Figure 5.1B). These peaks are attributed to single YFP-GR molecules as they had comparable width and intensity as fluorescence intensity peaks derived from single EYFP molecules previously observed using the same setup (Harms et al., 2001). In our current approach, EYFP molecules were identified with a positional accuracy of $\sim 40\,nm$ in one dimension (x or y). Next, GR mobility was analyzed by assessing molecule displacements over image sequences with short time lags ($6.25\,ms$ and $12.5\,ms$; Figure 5.1C), using the PICS analysis method (Semrau and Schmidt, 2007). We use PICS analysis instead of single particle tracking, as PICS is less affected by blinking of YFP or overlapping trajectories of multiple molecules (Schutz et al., 1997; Semrau and Schmidt, 2007). PICS analysis calculates the cumulative probability distribution for each displacement, which is subsequently fitted with multiple-population models (Figure 5.1D, see material and methods). We use a

model with only fractions of moving molecules instead of a model encompassing a bound (immobile) fraction, because this is the more general model without *a priori* assumptions. DNA-bound and thus immobile molecules should show negligible displacement steps in this model. For YFP-GR, a one-population model was unable to describe the experimental data (Figure 5.1D), while a three-population model did not give consistent results over different time lags or resulted in two fractions with similar displacements. A two-population model fitted the observed displacements consistently, and with high accuracy, and was chosen for all analyses. Thus, we obtained the relative size and mean squared displacement (MSD) of two fractions of YFP-GR molecules that differed in their relative displacements over time.

We plotted the MSDs of the two identified fractions versus the time lag and calculated the diffusion coefficients (D_{fast} and D_{slow}; Figure 5.3B). The displacements of the "slow" fraction never exceeded our detection limit ($0.009\,\mu m^2$) by more than 2-fold and only increased marginally over time: D_{slow} of $0.03 \pm 0.01\,\mu m^2/s$. This is very similar to the slow restricted movement of chromatin (Blainey et al., 2006; Elf et al., 2007), indicating that this "slow" fraction describes DNA-bound molecules. In contrast, the remaining fraction showed > 40-fold higher displacements and a D_{fast} of $1.31 \pm 0.13\,\mu m^2/s$, representing YFP-GR molecules diffusing through the nucleus. The nuclear GR population is approximately evenly distributed over the two fractions; $55.1 \pm 2.0\,\%$ belongs to the diffusing fraction, which leaves $44.9 \pm 2.0\,\%$ as bound fraction (Figure 5.3A).

FRAP analysis of dexamethasone-bound YFP-GR

Subsequently, we employed a quantitative FRAP approach on similarly treated YFP-GR expressing COS-1 cells. In selected nuclei a small strip, spanning the width of the nucleus, was bleached with a $100\,ms$ pulse of maximal laser power. This effectively bleached most fluorescence within this area. The subsequent recovery of the fluorescence in this strip was recorded (with $100\,ms$ intervals) for 55 seconds (Figure 5.1E). Comparable to previous results (Schaaf and Cidlowski, 2003; Schaaf et al., 2005), a complete recovery of YFP-GR fluorescence was seen well within 30 seconds (Figure 5.1E). The obtained recovery curves were quantitatively analyzed by fitting them to FRAP curves generated using Monte Carlo simulations (van Royen et al., 2009a,b). Our data was best fitted with a model in which freely diffusing molecules (diffusion rates as obtained by SMM were used) show transient binding with two different durations ('short' and 'long'; Figure 5.1E). Quantitative FRAP analysis of dexamethasone-treated GR identified a diffusing fraction of $44 \pm 2\,\%$, a 'short' bound fraction of $33 \pm 2\,\%$ (average binding of $0.7 \pm 0.1\,s$) and a 'long' bound fraction of $23 \pm 2\,\%$ (average binding of $2.3 \pm 0.3\,s$) (Figure 5.3C,D). As both bound fractions in FRAP remain bound for much longer time periods than the time range used in SMM (less than $50\,ms$), these two fractions could be distinguished using FRAP, but not by SMM. Indeed, the size of the single bound fraction in SMM, is similar to the combined size of the two bound fractions identified in FRAP (com-

Chapter 5

A

B

D_{fast} = 1.31 ± 0.13 μm²/s
D_{slow} = 0.03 ± 0.01 μm²/s
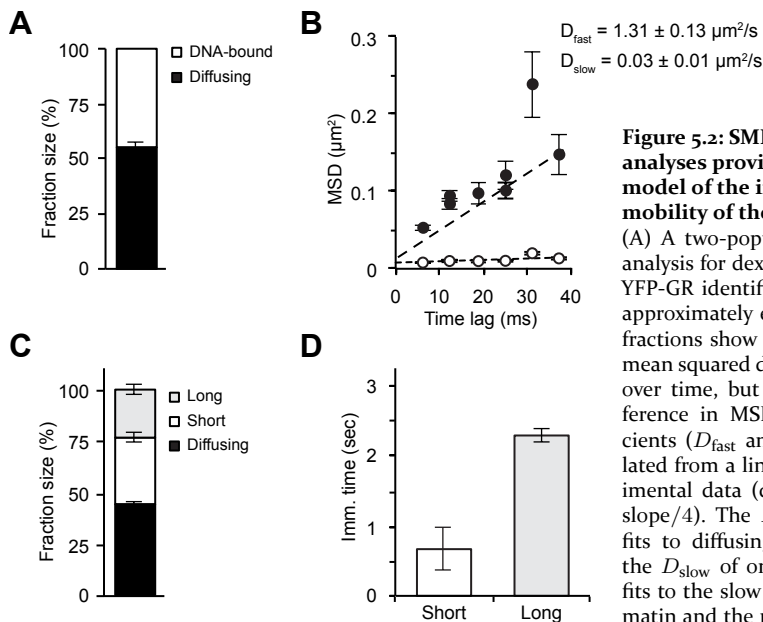
Figure 5.2: SMM and FRAP analyses provide a consistent model of the intranuclear mobility of the GR
(A) A two-population fit of SMM analysis for dexamethasone-bound YFP-GR identifies two fractions of approximately equal size. (B) Both fractions show a linear increase in mean squared displacement (MSD) over time, but with a 40-fold difference in MSD. Diffusion coefficients (D_{fast} and D_{slow}) are calculated from a linear fit of the experimental data (dashed lines; D = slope/4). The D_{fast} of $1.31\,\mu m^2/s$ fits to diffusing molecules, while the D_{slow} of only $0.03\,\mu m^2/s$ best fits to the slow movement of chromatin and the molecules bound to it. (C) Monte Carlo simulation of

C

D

dexamethasone-bound YFP-GR with a 3-population model identifies 3 fractions of dexamethasone-bound YFP-GR; almost half of the nuclear population is diffusing, while the remainder is subdivided into two bound fractions that differ in their immobilization times. The fraction size of the diffusing fraction is similar in size as that obtained from SMM analysis. (D) Both bound fractions are only transiently immobilized, with a 3-fold difference in duration. (A and B) Data represented as best fit ± SEM (of 3 separate PICS analyses). (C and D) Data represented as average of top 10 % best fits ± SEM.

pare Figure 5.3A and 5.3C). Therefore, the mobility patterns assessed by SMM at the millisecond range are confirmed with realistic accuracy using an independent FRAP approach.

YFP-GR mobility is dependent on ligand structure

Next we used our combined SMM and FRAP approach to investigate how binding of different ligands affects GR-DNA binding dynamics. We have previously shown by FRAP that the structure of the ligand is an important determinant of GR affinity, with important roles for the 17-hydroxyl and 9-fluoro groups on the steroids, which induce a decrease in GR mobility (Schaaf and Cidlowski, 2003; Schaaf et al., 2005). In the present study, this was studied in more detail in order to investigate which of the mobility parameters were affected. Therefore, we tested a panel of GR agonists that enabled us to study the effects of the 17-hydroxyl, 9-fluoro, and 16-methyl groups and the 1,4-pregnadien structure of the A ring. We used dexamethasone (which contains all four structural elements), Δ-fludrocortisone (same structure as dexamethasone, but lacking the 16-methyl group), prednisolone (same structure as Δ-fludrocortisone, but lacking the 9-fluoro group), cortisol (same structure as prednisolone, but having a 4-pregnen instead of a 1,4-pregnadien structure),

and corticosterone (same structure as cortisol, but lacking the 17-hydroxyl group). In addition to this panel of agonists, the GR antagonist RU486 was used. Importantly, all hormones were administered at a saturating concentration (1 μM), thus the fraction of bound receptor should be similar for all ligands (Rupprecht et al., 1993; Hellal-Levy et al., 1999; Grossmann et al., 2004; Schaaf et al., 2005).

Again, the two independent experimental approaches gave a consistent pattern of fraction sizes for all 6 ligands tested. On average the size of the diffusing fractions identified with SMM and FRAP differed by only $7.8 \pm 2.6\%$ (Table 5.1). The data show that the 16-methyl group does not affect GR mobility, but the other structural elements decrease the mobility of the receptor, indicating increased DNA binding (Figure 5.3A–C). Interestingly, this decreased mobility was reflected in all parameters measured. Both the size of the bound fractions and their respective binding time were affected, so both on- and off-rates of DNA binding were altered. In addition, the diffusion coefficient of the diffusing fraction was decreased suggesting that DNA binding results in slower diffusion of the receptor (Figure 5.3A and Table 5.1). Binding of the antagonist RU486 induces a very mobile nuclear YFP-GR (Figure 5.3A–C).

It is known that the 9-fluoro group (present on Δ-fludrocortisone and dexamethasone) creates a strong hydrogen bond with phenylalanine at position 623 of GR's ligand binding pocket (Bledsoe et al., 2002), suggesting that this amino acid is crucial in conferring the effects of the 9-fluoro-group. To test this association in our setup, phenylalanine 623 was mutated to an alanine (F623A). We tested the mobility of F623A with SMM in presence of prednisolone and Δ-fludrocortisone, which are identical except that Δ-fludrocortisone contains a 9-fluoro group and prednisolone does not. In presence of either steroid the F623A mutant translocates fully to the nuclear compartment (Figure 5.3D). Within the nucleus, no difference in F623A mobility was observed between Δ-fludrocortisone and prednisolone (Figure 5.3E). Therefore we conclude that the effect of the 9-fluoro group on mobility is indeed mediated by phenylalanine 623.

Specific receptor domains determine YFP-GR mobility

In order to elucidate the role of the different domains of GR on DNA-binding dynamics, we tested three different GR deletion mutants, each lacking one of its three functional domains. Thus, we obtained YFP-GR ΔAF-1 (lacking the N-terminal domain containing the AF-1 (amino acids 9–385)), YFP-GR ΔDBD (lacking the DNA-binding domain (amino acids 428–490)) and YFP-GR ΔLBD (lacking the ligand-binding domain (amino acids 551–777)), see Figure 5.4A. We investigated the mobility of the three deletion mutants of YFP-GR by SMM and FRAP in the presence of dexamethasone or corticosterone. All results are shown in Figure 5.4 and Table 5.1. Deletion of the AF-1 showed the smallest effect on receptor mobility. Dexamethasone binding to the ΔAF-1 mutant induces a large DNA-bound fraction and long binding times, and a slow diffusing fraction. In contrast, corticosterone binding,
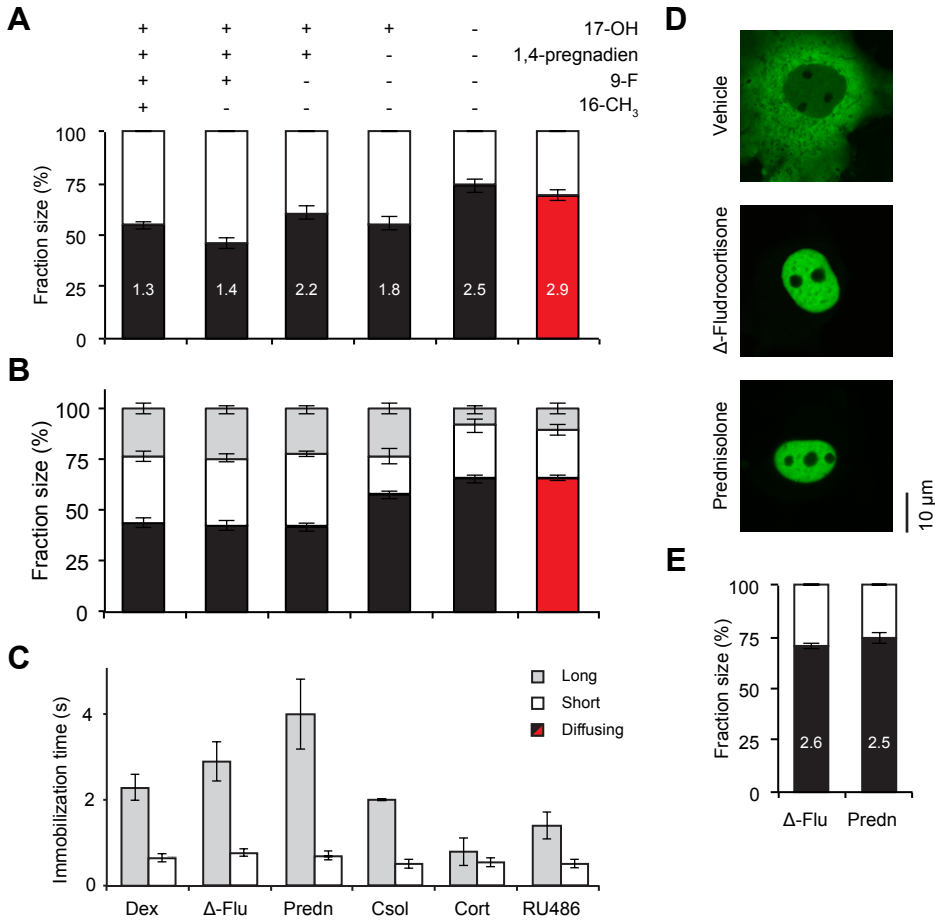
Figure 5.3: Ligand structure determines the nuclear mobility of the GR

A range of natural and synthetic agonists (black bars) and an antagonists (red bar) were tested for their effect on the intranuclear mobility of the GR by both SMM (A) and FRAP (B, C) analysis. Multiple structural elements of the steroids are associated with a reduced mobility of the receptor, with the strongest effects observed for the 9-fluoro (9-F) and the 17-hydroxyl (17-OH) groups. Altered mobility is generally reflected in all aspects of mobility: a larger bound fraction (SMM; white bars and FRAP; white and light grey bars combined), a lower diffusion coefficient (in $\mu m^2/s$, written in its corresponding bar in A) and longer immobilization times (C). (D and E) A mutation of phenylalanine 623 to alanine (F623A) prevents interactions of the 9-fluoro group of steroids within the ligand binding pocket of the GR. (D) F623A YFP-GR still translocates completely to the nucleus after 3 hours of 1 μM prednisolone or Δ-fludrocortisone treatment (E). SMM analyses of nuclear F623A YFP-GR shows that the mobility of F623A YFP-GR is highly similar after either Δ-fludrocortisone or prednisolone treatment (black bars for the diffusing fraction, with their corresponding diffusion coefficient (in $\mu m^2/s$) written within their corresponding bar). SMM: $n = 20$, FRAP: $n = 30$. Data represented as total fit ± SEM (of 3 separate PICS analyses) for SMM and as average of top 10 % fits ± SEM for FRAP. Δ-flu; Δ-fludrocortisone, dex; dexamethasone, predn; prednisolone, csol; cortisol, cort; corticosterone. The data for GR-dexamethasone is the same as in Figure 5.3.
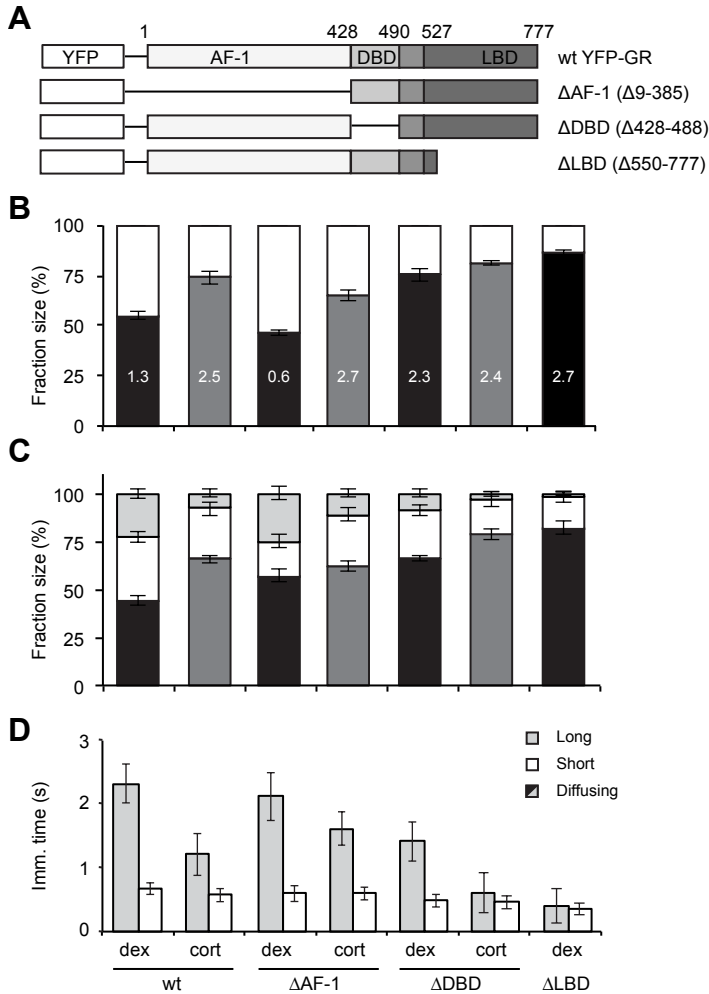
Figure 5.4: Loss of either the DNA-binding or the ligand-binding domain results in a high GR mobility
(A) Schematic representation of three functional YFP-GR deletion mutants tested. (B and C) Fraction distributions as analyzed by SMM (B) and FRAP (C). Diffusion coefficients are written within the corresponding bars in B (in μm^2/s). (D) Immobilization times of the short and long bound fractions. While loss of the AF-1 domain hardly affects GR's nuclear mobility, deletion of the DBD and especially the LBD leads to a very mobile receptor with reduced frequency and average duration of DNA-binding and a higher diffusion coefficient. SMM: $n = 20$, FRAP: $n = 30$. Data represented as total fit $\pm$ SEM (of 3 separate PICS analyses) for B and as average of top 10% fits $\pm$ SEM for C and D. The data for wild type GR is the same as in Figure 5.3.

results in a much faster receptor with less stable DNA-binding (Figure 5.4). Thus, without its N-terminal domain, the GR's intranuclear mobility is still differently affected by high and low affinity agonists and its mobility is similar to the wild type receptor.
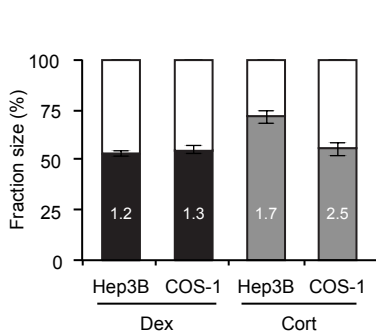
Figure 5.5: A similar pattern of YFP-GR's nuclear mobility in stably transfected Hep3B cells
SMM analysis of YFP-GR's nuclear mobility after treatment (3–6 h with 1 μM) with either dexamethasone or corticosterone was performed in Hep3B cells stably transfected with YFP-GR. These experiments were performed to check for effects of differences in cellular context and a lower level of YFP-GR expression on the mobility patterns. Both the size of the diffusing fraction (filled bars) and the diffusion coefficients (written in their corresponding bars in $\mu m/s^2$) were highly similar between COS-1 and Hep3B cells. COS-1 data is the same as in Figure 5.3. All groups: $n = 20$. Data is represented as total fit $\pm$ SEM (of 3 separate PICS analyses).

As expected, deletion of the DBD did affect the receptor's mobility (Figure 5.4). For corticosterone-bound GR, deletion of the DBD slightly increased the size of the diffusing fraction and completely prevents the longer binding events, resulting in two bound fractions with almost equal immobilization times: $0.5 \pm 0.1\,s$ ($18 \pm 3.9\,\%$) and $0.6 \pm 0.3\,s$ ($3 \pm 1.5\,\%$, Figure 5.4D). For dexamethasone-bound ΔDBD not all stable DNA-binding is lost; here $25 \pm 2.7\,\%$ remains bound for $0.5 \pm 0.1\,s$ and even $9 \pm 2.3\,\%$ remains bound for $1.4 \pm 0.3\,s$. Dexamethasone-bound YFP-GR ΔDBD does show a large increase of the size of the diffusing fraction (from 44–$55\,\%$ (wild type) to 76–$66\,\%$ (ΔDBD)), and a ∼2-fold higher diffusion coefficient (Figure 5.4). Thus, deletion of the DBD induces less frequent and shorter DNA-binding for both dexamethasone and corticosterone bound GR, but a fraction of longer bound YFP-GR ΔDBD remains when bound to dexamethasone. Deletion of the DBD abolishes all direct binding of the GR to the DNA but leaves some of its indirect binding to DNA intact, which has been shown to occur through (direct or indirect) interactions with other transcription factors (Reichardt et al., 1998; Kassel and Herrlich, 2007). Therefore, the DNA-bound fraction of ΔDBD probably reflects indirect DNA-binding.

Deletion of the LBD prevents the ligand-induced conformational change that is required for any type of stable interaction with DNA. As expected, YFP-GR ΔLBD was the most mobile receptor variant, it had the smallest DNA-bound fraction ($13.5\,\%$ to $18\,\%$ in SMM and FRAP respectively) with a single (short) binding state of $0.4 \pm 0.1\,s$ and a high diffusion coefficient ($2.71 \pm 0.08\,\mu m^2/s$; Figure 5.4). Most importantly, this DNA-binding deficient mutant indeed did not show any stably-bound fraction.

YFP-GR mobility is stable across cell lines and expression levels

In order to test whether overexpression or transient transfection had produced artifacts in our experiments, we stably transfected Hep3B cells with the same YFP-GR expression vector. The resulting cell line showed a much lower expression level of YFP-GR than that observed in the transiently transfected COS-1 cells. The DNA-binding dynamics were studied of corticosterone- and dexamethasone-bound YFP-GR in this cell line with SMM. Dexamethasone induced a diffusing fraction

			SMM		FRAP	
			Fraction size (%)	D ($\mu m^2/s$)	Fraction size (%)	Imm. time (s)
GR wt	Δ-Flu	Diffusing	46.3 ± 2.6	1.38 ± 0.11	43.0 ± 2.6	-
		Short	53.7 ± 2.6	0.050 ± 0.004	33.0 ± 2.1	0.8 ± 0.1
		Long			24.0 ± 2.2	2.9 ± 0.5
	Dexamethasone	Diffusing	55.1 ± 2.0	1.31 ± 0.13	44.0 ± 2.2	-
		Short	44.9 ± 2.0	0.030 ± 0.009	33.0 ± 2.6	0.7 ± 0.1
		Long			23.0 ± 2.6	2.3 ± 0.3
	Prednisolone	Diffusing	60.7 ± 3.1	2.20 ± 0.11	42.0 ± 2.5	-
		Short	39.3 ± 3.1	0.090 ± 0.008	36.0 ± 1.6	0.7 ± 0.1
		Long			22.0 ± 2.5	4.0 ± 0.8
	Cortisol	Diffusing	55.6 ± 3.5	1.77 ± 0.10	58.0 ± 2.0	-
		Short	44.4 ± 3.5	0.040 ± 0.003	19.0 ± 3.8	0.5 ± 0.1
		Long			23.0 ± 2.6	2.0 ± 0.0
	Corticosterone	Diffusing	74.1 ± 3.3	2.49 ± 0.24	66.0 ± 2.2	-
		Short	25.9 ± 3.3	0.080 ± 0.024	26.0 ± 3.7	0.6 ± 0.1
		Long			8.0 ± 2.5	1.2 ± 0.3
	RU486	Diffusing	69.1 ± 2.4	2.86 ± 0.11	66.0 ± 1.6	-
		Short	30.9 ± 2.4	0.140 ± 0.018	24.0 ± 3.1	0.5 ± 0.1
		Long			10.0 ± 2.6	1.4 ± 0.3
GR ΔAF-1	Dexamethasone	Diffusing	46.5 ± 1.9	0.61 ± 0.08	57.0 ± 3.0	-
		Short	53.5 ± 1.9	0.000 ± 0.006	18.0 ± 3.6	0.6 ± 0.1
		Long			25.0 ± 3.4	2.1 ± 0.4
	Corticosterone	Diffusing	64.7 ± 2.8	2.69 ± 0.08	62.0 ± 2.5	-
		Short	35.3 ± 2.8	0.050 ± 0.012	27.0 ± 4.0	0.6 ± 0.1
		Long			11.0 ± 2.3	1.6 ± 0.3
GR ΔDBD	Dexamethasone	Diffusing	75.6 ± 3.4	2.27 ± 0.15	66.0 ± 1.6	-
		Short	24.4 ± 3.4	0.010 ± 0.006	25.0 ± 2.7	0.5 ± 0.1
		Long			9.0 ± 2.3	1.4 ± 0.3
	Corticosterone	Diffusing	81.3 ± 1.0	2.37 ± 0.19	79.0 ± 3.1	-
		Short	18.7 ± 1.0	0.060 ± 0.004	18.0 ± 3.9	0.5 ± 0.1
		Long			3.0 ± 1.5	0.6 ± 0.3
GR ΔLBD	Dexamethasone	Diffusing	86.5 ± 1.9	2.71 ± 0.08	82.0 ± 3.3	-
		Short	13.5 ± 1.9	0.030 ± 0.010	16.0 ± 3.1	0.4 ± 0.1
		Long			2.0 ± 1.3	0.4 ± 0.3

Table 5.1: SMM and FRAP analyses of all YFP-GR and deletion mutants
Short, 'short' bound fraction; long, 'long' bound fraction; imm. time, average immobilization time; Δ-Flu, Δ-Fludrocortisone; Results are represented as best fit ± SEM (of three separate fits) for SMM and as average ± SEM of top 10 % fits for FRAP.

of $52.9 ± 1.6\%$ and a diffusion coefficient of $1.16 ± 0.08\,\mu m^2/s$ in Hep3B cells (Figure 5.5). As expected, corticosterone treatment induced a more mobile YFP-GR, with a diffusing fraction of $71.6 ± 3.4\%$ and a D_{fast} of $1.70 ± 0.16\,\mu m^2/s$ (Figure 5.5). These results were very similar to those obtained in COS-1 cells, indicating that our

results are not cell-type specific or affected by expression levels obtained by transient transfection.

5.4 Discussion

Here we report on a combination of SMM and quantitative FRAP analysis to characterize the intranuclear dynamics of the GR. In our SMM experiments, we find that single molecules of nuclear YFP-GR can be detected with high spatial and temporal resolution and that by subsequent data analysis two fractions of GR molecules are detected; a diffusing and a (DNA-)bound fraction. For all 11 treatment groups studied, this two-population model consistently fitted the experimental data with high accuracy. For dexamethasone-bound GR, 55% of nuclear GR molecules are diffusing with a diffusion coefficient of $1.31 \pm 0.13 \, \mu m^2/s$. The remaining 45% show a > 40-fold lower diffusion coefficient, which fits the low, restricted mobility of DNA-bound molecules (Blainey et al., 2006; Elf et al., 2007; Li and Xie, 2011). To enable cross-validation with an established technique, we combined our SMM analysis with a second technique, FRAP. We analyzed the FRAP curves using established Monte Carlo simulations (Farla et al., 2004; van Royen et al., 2009b). To best describe the FRAP recovery curves we required two bound fractions (for most receptors), which differed 2–4 fold in their binding duration. The binding times of both bound fractions are orders of magnitude longer than the time scale used in our SMM experiments and these fractions combined represent the single bound fraction detected in SMM, providing two independent estimates of the size of this (combined) fraction. Within our 11 experimental conditions, the sizes of the combined bound fractions determined by SMM and FRAP showed an average difference of only $6.9 \pm 1.6\%$. This high level of consistency between the two independent techniques shows that a combination of techniques generates a reliable quantitative description of protein dynamics.

Combinations of FRAP and FCS have been reported earlier (Stasevich et al., 2010b; Mazza et al., 2012). Here, FSC and FRAP generally gave comparable estimates, although large discrepancies were found for binding times, due to laser irregularities. Recently, Mazza and colleagues reported on a similar combinational approach with FRAP and single-molecule microscopy, in their case also combined with FCS (Mazza et al., 2012). In this study the mobility of p53, a well-known transcription factor was assessed and single-molecule tracking was used to guide the choices in models used for FRAP and FCS quantitation. Wild type p53 showed a much smaller DNA-bound fraction ($\sim20\%$) than agonist-activated GR does in our study, but in both studies mutations in the DNA-binding domains give a large reduction in size and residence time of the DNA-bound fractions (Mazza et al., 2012). In a recent study, Gebhardt et al. applied SMM on the GR as well, using reflected light sheet microscopy (Gebhardt et al., 2013). In this study unbound and dexamethasone-bound

GR and the ΔDBD mutant were analyzed. Their data are well in line with ours, especially the obtained values for the sizes of the diffusing and bound fractions and of binding times (Gebhardt et al., 2013). Discrepancies exist in the analysis of the diffusing fraction. Gebhardt et al. found two diffusing fractions, whereas we only detect one. As shown by Mazza et al., it is likely that any diffusion coefficient is a simple representation of the more complex nature of the continual scale of true transcription factor diffusion (Mazza et al., 2012).

Ligand structure affects the DNA-binding profile of nuclear GR

We observed profound differences in the nuclear dynamics of the GR depending on the ligand it was bound to (Figure 5.3), even among agonists. For example, the synthetic GR agonists dexamethasone and Δ-fludrocortisone induce a larger DNA-bound fraction with longer residence times than the naturally occurring agonists cortisol and corticosterone. Structure-function studies showed that the 17-hydroxyl, and 9-fluoro groups and the 1,4-pregnadien structure of the A ring of these steroids were involved in the increased DNA binding of GR. We further showed that the effect of the 9-fluoro group depends on the presence of phenylalanine at position 623 of the GR LBD, the amino acid it is known to interact with (Bledsoe et al., 2002). This phenylalanine residue, like the glutamine residue at position 642, which interacts with 17-hydroxyl group, is located in a region of the LBD that has been shown to be involved in receptor dimerization (Bledsoe et al., 2002). It may therefore be suggested that these specific interactions shape the receptor into a conformation that favors receptor dimerization, and that these dimers have higher DNA binding affinity. We have previously suggested a similar model for AR dimerization and DNA binding (van Royen et al., 2012).

   Many of these structural elements also affect the affinity of the ligand and it could therefore be argued that the affinity of the ligand determines the receptor mobility. However, affinity and mobility are not always correlated. In a previous study we have shown that the 16-hydroxy group of triamcinolone dramatically decreases the binding affinity for GR, but leaves GR mobility unaffected (Schaaf and Cidlowski, 2003; Schaaf et al., 2005). Furthermore, mechanistically it is unlikely that ligand affinity is a determinant of receptor mobility since all ligands are administered at above saturating concentrations (Schaaf and Cidlowski, 2003). Finally, ligand dissociation rates are in the order of minutes (corticosterone) to hours (dexamethasone) (Munck and Foley, 1976; Meijsing et al., 2007), whereas the immobilizations of the receptor observed in this study are in the order of seconds.

A model of GR-DNA interactions

Interestingly, our data shows a strong correlation between different components of the mobility pattern. Immobilization times correlate to the size of the bound fractions, but more surprisingly, we also found that a low frequency and duration of

binding events correlated with a higher diffusion coefficient throughout our different experiments. Thus, where antagonist-bound or low-affinity agonist bound GR, and the ΔDBD and ΔLBD mutants were all associated with a low frequency of DNA-binding, these same receptors all showed a high diffusion coefficient (1.5 to 2-fold higher than that of highest-potency agonist bound GR, see Table 5.1). This suggests that all components of the mobility pattern are associated with each other and presumably are representations of a same biological phenomenon, i.e. DNA-binding. A plausible explanation could be that changes in the diffusion coefficient are due to DNA-binding events shorter than the temporal resolution of our SMM experiments ($\sim$6 ms), which result in a decreased effective diffusion coefficient as long as the system is in equilibrium. Alternatively, reduced diffusion coefficients can be caused by an increased size of the diffusing protein complex (e.g. through increased co-factor binding affinity).

Thus, for agonist-bound GR we identified three possible DNA-binding events: frequently in a very transient manner (< 6 ms), intermitted with transient binding ($\sim$0.5 s) and occasionally more stable interactions (> 1 s). This fits well with the idea that steroid receptors and other transcription factors search the DNA by different forms of low affinity DNA interactions and are only occasionally bound for longer time periods at their high-affinity target sites. Indeed, steroid receptors do not show competition for high-affinity binding sites, and in fact seem to do the opposite (assisted loading), suggesting that high-affinity DNA-binding cannot make up a large population (Voss et al., 2011). Multiple *in vitro* studies and theoretical modeling approaches have suggested that frequent low-affinity interactions with DNA increase the efficiency of transcription factor target finding, because it keeps the transcription factor in close proximity of open DNA (Gowers et al., 2005; Elf et al., 2007; van den Broek et al., 2008). We suggest that the more transient interactions identified in our quantitative analysis represent non-specific DNA binding and that the longest DNA-binding events represent specific DNA binding.

Quantitative analysis of the nuclear dynamics of the Mineralocorticoid Receptor reveals ligand-specific modulation of chromatin binding

Femke L. Groeneweg[1], Martin E. van Royen[2], Rudie Weij[1],
Suzanne Fenz[3,4], E. Ron de Kloet[1], Adriaan B. Houtsmuller[2],
Thomas S. Schmidt[3], Marcel J.M. Schaaf[5]

[1] Department of Medical Pharmacology, Leiden University / LUMC, Leiden, The Netherlands.
[2] Department of Pathology, Erasmus MC, Rotterdam, The Netherlands.
[3] Physics of Life Processes, Institute of Physics, Leiden University, Leiden, The Netherlands.
[4] Cell & Developmental Biology, Biocenter, Würzburg University, Würzburg, Germany.
[5] Molecular Cell Biology, Institute of Biology, Leiden University, Leiden, The Netherlands.

Steroid receptors are remarkably dynamic within the nucleus where they exert a combination of free diffusion and frequent transient DNA binding events. The frequency and duration of DNA binding is positively correlated to transcriptional potency. Previously we showed that specific interactions between agonist side groups and amino acids within the ligand-binding pocket determine the DNA-binding dynamics of the GR and AR. Here, we study the closely related MR by a combination of single-molecule microscopy and FRAP. This is the first detailed study of the DNA-binding dynamics of the MR. We determined that, when bound to a potent natural agonist, the receptor is bound to chromatin for roughly 50% of the time in either short (~0.6 sec, $\sim30\%$) or prolonged (2–3 sec, $\sim20\%$) binding events. This mobility pattern is shifted towards less frequent and shorter DNA-binding events for antagonist-bound MR and, to a lesser extent, when bound to the weak synthetic agonist dexamethasone. We also compared the chromatin binding dynamics of the MR when bound to natural glucocorticoids or mineralocorticoids. Our results show that the two classes of endogenous MR-ligands do not induce different MR-DNA binding dynamics. However, the receptor was less often DNA-bound when activated by the weaker mineralocorticoid DOC, which suggest that specific ligand-receptor interactions do affect the receptors affinity for DNA.

6.1 Introduction

The family of steroid receptors encompasses a large group of related receptors that are present in the nucleus, or translocate to the nucleus upon ligand binding, and act as ligand-induced transcription factors (Fuller, 1991). All family members share key features, but differ largely in ligand specificity, ligand-binding dynamics and in their choice of co-factors, which enables the enormous variety of biological functions that steroid receptors have. In the past decade, imaging studies of fluorescently tagged proteins inside living cells showed that steroid receptors, and transcription factors in general, display a remarkably high mobility in the nucleus (Stenoien et al., 2000, 2001; Stavreva et al., 2004; Schaaf et al., 2005, 2006; Hager et al., 2009; van Royen et al., 2009b, 2014; Mueller et al., 2010). This high mobility is characterized by free diffusion intermitted by frequent, but transient, DNA binding (Gorski et al., 2006; Biddie and Hager, 2009).

We have previously employed a combination of imaging techniques to study the nuclear dynamics of two steroid receptors, the GR and the AR (van Royen et al., 2014). In these studies, we combined SMM and FRAP and, for the AR, also FCS. SMM enables an unbiased quantification of protein dynamics with high temporal and spatial resolution (Semrau and Schmidt, 2007; Lord et al., 2010; Li and Xie, 2011). The combination with FRAP allows cross-validation with an independent analysis method and greatly extends the time line (from $50\,\text{ms}$ for SMM to a minute with FRAP), thus enabling quantification of DNA-binding times (Farla et al., 2004; van Royen et al., 2009a). We found that this combination of techniques gave a consistent pattern of both AR and GR nuclear dynamics and identified 3 fractions for each steroid receptor; one diffusing fraction, and two transiently bound fractions, with DNA-binding times of half a second to several seconds (van Royen et al., 2014).

In the current study, we utilize the same combinational approach of SMM supplemented with FRAP to study the nuclear dynamics of a third steroid receptor: the MR. The chromatin binding dynamics of the MR have not been studied extensively (Tirard et al., 2007; Nishi et al., 2011). The receptor shares a high sequence analogy with both the GR and AR (Fagart et al., 1998). It is activated by the naturally occurring glucocorticoids (cortisol or corticosterone) and by mineralocorticoids (aldosterone and DOC) (Arriza et al., 1987; Joëls et al., 2008; Funder, 2010). As such the MR shares part of its endogenous ligands with the GR, but with different affinities. Cortisol and corticosterone have a much higher affinity for the MR than for the GR (Reul and de Kloet, 1985), whereas many synthetic glucocorticoids, such as prednisolone and dexamethasone, have a very high affinity for the GR but only little affinity for the MR (Arriza et al., 1987; Grossmann et al., 2004). Interestingly, for the GR we found that agonist properties determine the receptor's DNA-binding properties in a manner unrelated to receptor-ligand binding dynamics (*Chapter 5*). We propose that ligand-induced effects are due to their specific binding profile within the receptors ligand-binding groove, which ultimately affects the receptor's affinity for DNA (*Chapter 5*). Although the MR and GR share $\sim 55\,\%$ sequence homology

within their LBD, they differ much more in their ligand-binding pocket architecture (Fagart et al., 1998; Li et al., 2005) and a different set of interactions occur between the steroids and the receptor's ligand-binding pocket (Bledsoe et al., 2002, 2005; Huyet et al., 2012). Thus, we expect different steroid side groups to affect binding strength to the MR and thus likely to affect its nuclear mobility.

Here, we report that agonist-bound MR shows three functionally distinct states within the nucleus. MRs spend approximately 50 % of the time diffusing through the nucleus, the remaining time the receptor is transiently bound to chromatin for either short ($\sim$30 %: 0.5–0.8 sec) or longer ($\sim$20 %: 2–3 sec) binding events. When bound to an antagonist, the MR spends more time diffusing ($\sim$70 %), with a moderately higher diffusion coefficient and loses most of its capacity for longer DNA-binding; short DNA-binding is hardly affected. Finally, we find that agonist properties affect MR's nuclear mobility, with a role for the 11-hydroxyl group. No overall difference in MR's nuclear dynamics was found when bound to endogenous gluco-corticoids or mineralocorticoids.

6.2   Methods

Cell culture and transfection

For all experiments transiently transfected COS-1 cells were used. Cultures were maintained in high glucose D-MEM, supplemented with 10 % FBS and 1 % Pennicillin/Streptomycin (all Invitrogen). Transfections were performed with the TransIT-COS kit (Mirus), according to the manufacturer's instructions (500 ng DNA / 10 cm^2). Transfected cells were used in experiments 2–5 days after transfection. pEYFP-hMR was generated by PCR amplification (Phusion HF polymerase, Finnzymes) of the human MR gene from a pRSV human MR template (kindly provided by Dr. R. Evans and described in Arriza et al. (1987)). A set of primers was designed to generate BglII and SmaI sites at the 5′ and 3′ end of the MR coding sequence. Subsequently, the PCR fragment was digested with BglII and SmaI, purified and cloned into the pEYFP-C1 vector, resulting in a vector with an in-frame fusion of hMR with EYFP, separated by 17, mostly nonpolar, amino acids. Plasmid integrity was checked by sequencing. YFP-YFP is a fusion product of EYFP with a second non-fluorescent YFP in the original pEYFP-C1 construct.

Confocal microscopy, western blot and luciferase assays

For confocal analysis, COS-1 cells were grown on coverslips and transfected with YFP-MR (500 ng / 10 cm^2). 48 h after transfection cells were fixated with 4 % PFA for 15 minutes and nuclei were stained with 1 µg/ml Hoechst 33258 (Invitrogen) in 0.1 % PBST for 10 minutes and mounted with Aqua Poly/Mount (Polysciences Europe). Confocal images were obtained with a Nikon TE-2000 E confocal microscope equipped with a 60× oil-immersion objective. eYFP expression was analyzed using the 488 excitation laser and emission collected at 510–530 nm. Exposure and gain settings were adjusted as to prevent over or underexposure. Image analysis was performed with ImageJ.

For western blot, COS-1 cells transfected with the required plasmids ($500\,ng$ / $10\,cm^2$) were harvested $48\,h$ after transfection and prepared for western blot. Protein lysates, SDS-polyacrylamide gel electrophoresis and western blotting were performed as described previously (Vreugdenhil et al., 2007). MR protein was detected with 1:1000 MR 1D5 (generous gift of Gomez-Sanchez (Gomez-Sanchez et al., 2006)) and all samples were co-assessed for α-tubulin (1:5000; Sigma-Aldrich) in combination with 1:5000 goat-anti-mouse IgG HRP. All antibodies were diluted in TBST with $0.5\,\%$ milk powder. Detection was performed with the ECL detection system (GE Healthcare).

For the luciferase assay, COS-1 cells were transfected with a combination of $500\,ng$ / $10\,cm^2$ YFP-YFP, YFP-MR or MR together with $100\,ng$ / $10\,cm^2$ TAT3-Luciferase (tyrosine amino transferase triple hormone response element) and $2\,ng$ / $10\,cm^2$ pCMV-Renilla (Promega). $24\,h$ after transfection cells were treated with $10\,nM$ corticosterone, $10\,nM$ aldosterone or $0.001\,\%$ EtOH in culture medium supplemented with charcoal stripped FBS. After $20\,h$, cells were lysed with passive lysis buffer and firefly and renilla luciferase luminescence was determined according to the general prescription of the dual label reporter essay (Promega) on a luminometer (CENTRO XS3 LB960, Berthold).

Compounds

The following hormones were used in these studies: aldosterone, corticosterone, cortisol, deoxycorticosterone (*21-hydroxy-4-pregnene-3,20-dione, 4-pregnen-21-ol-3,20-dione*), spironolactone (*4-pregnen-21-oic acid-17α-ol-3-one-7α-thiol γ-lactone 7-acetate, 7α-(acetylthio)-17α-hydroxy-3-oxopregn-4-ene-21-carboxylic acid γ-lactone*), eplerenone (*pregn-4-ene-7,21-dicarboxylic acid, 9,11-epoxy-17-hydroxy-3-oxo-, γ-lactone, methyl ester*) and dexamethasone. All steroids were purchased from Sigma-Aldrich and diluted in $100\,\%$ EtOH to a concentration of $1\,mM$, except for eplerenone, which was diluted in DMSO. Steroids were further diluted to their required concentrations in the respective media.

Single-molecule microscopy

For all SMM experiments, COS-1 cells were grown on coverslips and transiently transfected with YFP-MR ($500\,ng$ / $10\,cm^2$) 3–5 days prior to analysis. Before SMM recordings, cells were exposed to $1\,\mu M$ of corresponding hormones for 3–6 h. For SMM measurements, this medium was replaced by serum- and phenol red-free D-MEM medium (Invitrogen), which is also supplemented with $1\,\mu M$ of the corresponding hormone. Subsequently, cells were transferred to the SMM setup and imaged for up to $90\,min$ at $35\,°C$. A wide-field fluorescence microscope (Axiovert 100TV, Zeiss) was used, equipped with a 100× / 1.4NA oil-immersion objective (Zeiss). A region-of-interest (ROI) of 50 × 50 pixels (pixel size of $220\,nm$) was selected. The sample was illuminated by an $514\,nm$ argon laser at an intensity of $2\,kW/cm^2$. The pulse length of $3\,ms$ was controlled by an acusto-optical tunable filter (AA optoelectronics, France). The EYFP fluorescence signal was detected through a combination of filters (DCLP530, HQ570/80 (Chroma Technology, Brattleboro, VT) and OG530-3 (Schott, Mainz, Germany)), by a liquid-nitrogen cooled CCD camera (Princeton Instruments, Trenton, NJ), camera read out and AOTF timing were tightly controlled. Moderately fluorescent nuclei were selected and photobleached until single fluorescence intensity peaks could be distinguished. The position of each individual molecule was fitted with the intensity profile of a 2D Gaussian model of EYFP peaks (Harms et al., 2001). Our peaks were identified with a signal to noise ratio of ∼8 (peak fluorescent intensity divided by the variation of the background),

which resulted in a positional accuracy of $\sim 40\,$nm in the X- and Y-direction (determined by the quotient of the full-width-at-half-maximum of the Gaussian fit and the square root of the number of photons detected (Bobroff, 1986)). On average, each picture contained ~ 1.5 peaks. Image sequences were recorded in series of 8 subsequent images with a time lag of either $6.25\,$ms or $12.5\,$ms (Figure 6.1B). Data on molecular dynamics were obtained for multiple step sizes. We used all time lags from 6.25 to $37.5\,$ms in our analysis. From each cell 180 series of 8 images were taken and data from 20 independent cells (imaged on at least 3 different days) was combined for the analysis.

PICS analysis of single-molecule kinetics

We used the Particle Image Correlation Spectroscopy (PICS) method to determine peak displacement over time (Semrau and Schmidt, 2007). PICS procedures are described in detail in *Chapters 4 and 5*. In short, random correlations between unrelated molecules are subtracted from the cumulative cross-correlation between peak positions at two different time lags. This gives a cumulative probability function (P_{cum}) of diffusion steps l. We use population modeling to calculate diffusion characteristics of the nuclear population of YFP-MR molecules and found that a two-population model best describes YFP-MR's dynamics (Figure 6.1c). The two populations are determined with Given that the population of molecules is homogeneous, a single population of displacing molecules is determined with.

$$P_{cum}(l, \Delta t) = 1 - \left[\alpha \cdot \exp\left(-\frac{l^2}{\mathrm{MSD}_1(\Delta t)} \right) (1 - \alpha) \cdot \exp\left(-\frac{l^2}{\mathrm{MSD}_2(\Delta t)} \right) \right] \qquad (6.1)$$

Where MSD_1 and MSD_2 denote the mean square displacement of the first (fast) and the second (slow) fractions respectively, and α is the fraction size of the first (fast) fraction. The analysis was repeated for each time lag and α, MSD_1 and MSD_2 were plotted against time (Δt). The displacements over time were best described using a free diffusion model in 2D, from which the diffusion coefficients (D_{fast} and D_{slow}) were calculated using the following equation:

$$\mathrm{MSD}_i(\Delta t) = 4 \cdot D_i \cdot \Delta t \qquad (6.2)$$

OriginPro software was used to obtain weighted, linear fits, to calculate D_{fast} and D_{slow}. The fraction size α decreased slightly (on average $-0.27 \pm 0.07\,\%$/ms) over increasing time lags in all groups. Due to this effect, we always report the fraction distribution of the smallest time step ($6.25\,$ms) as a representative of the overall fraction distribution. All analyses were first performed on all data from each treatment group pooled together ($n = 20$). Subsequently, all analyses were run again in 3 fractions ($n = 6/7$) and these 3 separate analyses are used to generate standard errors of the mean.

FRAP

For FRAP recordings, COS-1 cells were grown on coverslips and transiently transfected with $500\,$ng / $10\,$cm^2 YFP-MR and used 2–3 days after transfection. Before FRAP recordings, cells were exposed to $1\,\mu$M of the appropriate ligand for 3–6 hours in normal growth medium. For each experiment, a coverglass with transfected COS-1 cells was placed in a preheated ring and medium was replaced for empty D-MEM without phenol red, supplemented with $1\,\mu$M of the corresponding ligand. Cells were used for no longer than 90 minutes and kept at $37\,°$C and $5\,\%\,CO_2$. We used a Zeiss LSM510 META confocal laser scanning microscope equipped with a
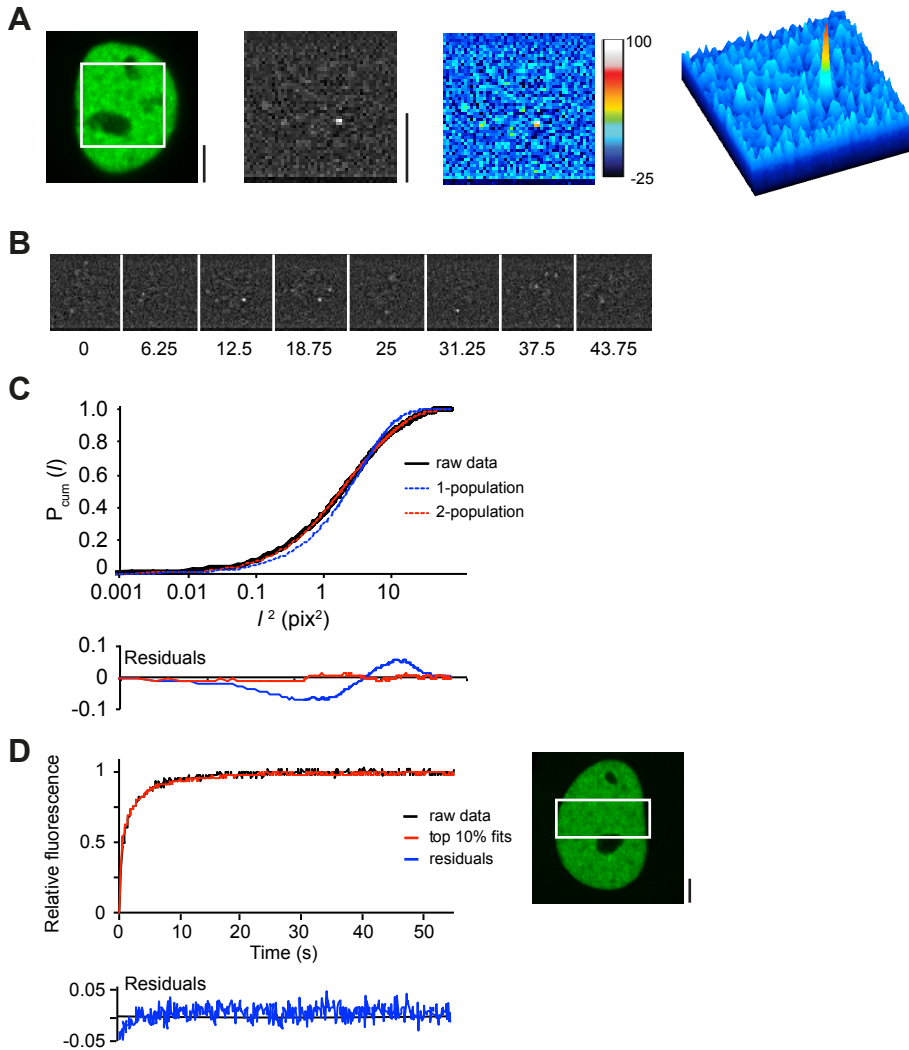
Figure 6.1: SMM and FRAP procedures

(A) A $11\,\mu\mathrm{m} \times 11\,\mu\mathrm{m}$ area within a nucleus is bleached to obtain single fluorescent peaks representing single YFP molecules. A representative CCD image of single molecules of YFP-MR after background subtraction shows single discernible Gaussian peaks of YFP fluorescence. (B) Regime for single molecule kinetics; images were taken with a time lag of $6.25\,\mathrm{ms}$ or $12.5\,\mathrm{ms}$ in 300 series of 8 per cell. In background-subtracted images, single molecules of YFP fluorescence are easily discernible. (C) PICS analysis of single molecule displacements, shown for corticosterone-bound YFP-MR at time delay of $6.25\,\mathrm{ms}$. The cumulative probability distribution as a function of the squared distance l^2 (black line) was best fitted with a 2-population model (red line), while a 1-population model gives a suboptimal fit (blue line) ($n = 20$ cells). (D) FRAP procedure of corticosterone-bound YFP-MR. At $t = 0\,\mathrm{s}$ a $100\,\mathrm{ms}$ bleach pulse was applied to a strip spanning the nucleus. Subsequently, FRAP recovery curves of 30 cells were recorded, combined and adjusted to baseline fluorescence (black line). Subsequently, Monte Carlo simulations were generated using a 3-population model and fitted to the combined FRAP curve. The top 10 fits were combined (red line) and showed a good fit of the experimental data with small residuals (blue line).

40× / 1.3NA oil-immersion objective, an argon laser (30 mW) and an AOTF. For FRAP analysis a narrow strip spanning the entire width of the nucleus was scanned at 514 nm excitation with short intervals (100 ms) at low laser power (0.2 %). Fluorescence intensity was recorded using a 560 nm longpass filter. After 40 scans, a high intensity (100 % laser power), 100 ms-bleach pulse at 514 nm was applied over the whole strip. Subsequently, the recovery of the fluorescence intensity in the strip was followed for another 55 seconds at 100 ms intervals. For each treatment group 30 cells were measured by FRAP on two separate days. All curves were normalized to baseline fluorescence intensity and combined.

Monte Carlo quantification of FRAP curves

The FRAP data was quantitatively analyzed by comparing the experimental data to curves generated using Monte Carlo modeling (van Royen et al., 2009b). The Monte Carlo simulation is described in detail in *Chapter* 5. In short, simulated FRAP curves were generated with a 3-population model, containing a diffusing fraction and two bound (immobile) fractions. We take the D_{fast} obtained from SMM analysis as a fixed parameter in these simulation, leaving 4 parameters as variables: short bound fraction, long bound fraction (both ranging from 0–90 %), and time spent in short and long bound state (ranging from 0.1 s to 1 s and from 1 s to 300 s respectively). A description of the calculation for all parameters can be found in *Chapter* 5. The laser bleach pulse was simulated based on experimentally derived three-dimensional laser intensity profiles, which were used to determine the probability for each molecule to get bleached considering their 3D position. In all simulations, the size of the ellipsoid was based on the average size of measured nuclei, and the FRAP region used in the measurements determined the size of the simulated bleach region. The laser intensity profile using the simulation of the bleaching step was previously derived from confocal image stacks of chemically fixed nuclei containing GFP that were exposed to a stationary laser beam at various intensities and varying exposure times. The unit time step (Δt) corresponded to the experimental sample rate of 21 ms. The number of molecules in the simulations was 10^{6}, which was empirically determined by producing curves that closely approximate the data with comparable fluctuations. The parameters of the top 10 best fitting Monte Carlo curves (by ordinary least squares) were averaged to represent the properties of the fractions in the experimental data.

6.3   Results

Characterization of YFP-tagged MR

A fusion of the human MR gene, N-terminally tagged with enhanced YFP, was generated. We assessed if the YFP-tag does not affect the function of the MR. First, we showed that YFP-MR is present throughout the cytoplasm and nucleus when unbound and translocates to the nucleus upon application of a high concentration of ligand (Figure 6.2A). Next, we showed that the YFP-MR fusion protein retains its predicted size by Western blot (27 kDa larger than the untagged MR; Figure 6.2B). No

A

Vehicle Aldosterone Corticosterone Cortisol DOC

Dexamethasone Spironolactone Eplerenone

10 μm

B

C
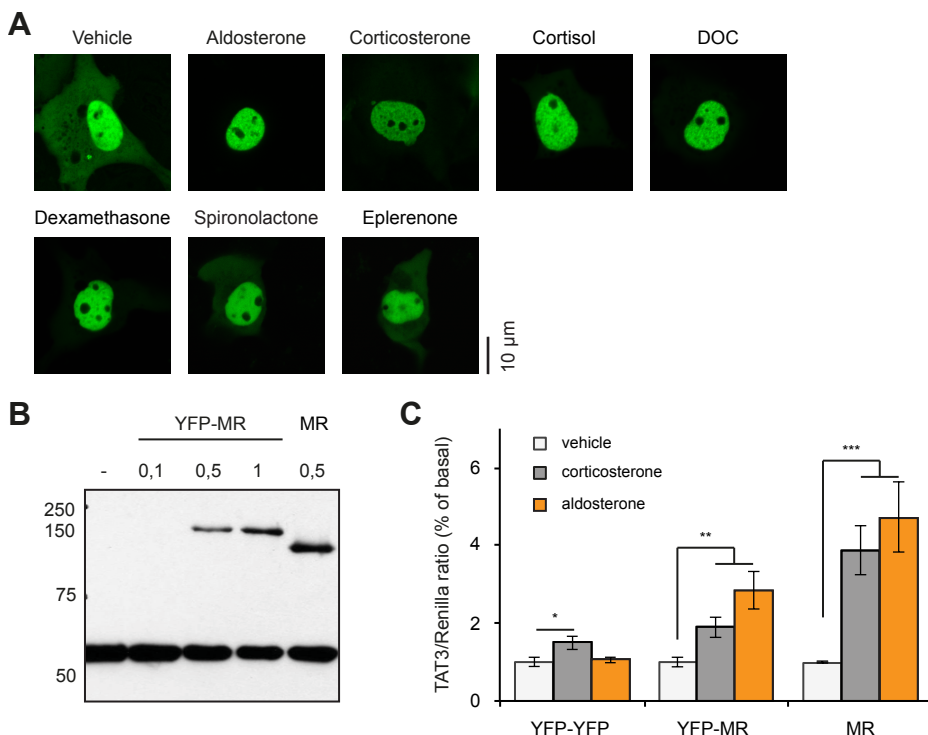
Figure 6.2: Characterization of YFP-MR
(A) Representative confocal images of YFP-MR transfected COS-1 neurons after 3 h treatment with vehicle (0.1 % EtOH) or 1 μM of hormone. YFP fluorescence was distributed over both cytoplasm and nucleus in the vehicle condition and translocated fully to the nucleus for all tested hormones. (B) COS-1 cells transfected with YFP-MR or untagged MR were analyzed on western blot and stained for MR and α-tubulin. A 60 kDa α-tubulin band was observed for all samples. MR transfected cells showed an addition band at the expected size of MR (107 kDa), while YFP-MR transfection gave a slightly larger MR band, representing the fused MR-YFP protein (134 kDa). (C) Transactivation assay. COS-1 cells were transfected with YFP-YFP, YFP-MR or untagged MR in combination with TAT3-Firefly and CMV-renilla luciferases and analyzed for firefly and renilla luciferase luminescence. Corticosterone or aldosterone treatment (10 nM for 20 h) led to a significant increase in TAT3-luciferase luminescence in both the MR and YFP-MR transfected cells, while only corticosterone had a small effect in YFP-YFP transfected cells. Thus, YFP-MR has transactivational capacity, although to a lesser extent as untagged MR. $n = 8, * = p < 0.05, ** = p < 0.01, *** = p < 0.001$, unpaired t-test. Scale bars: 5 μm.

detectable MR expression was seen in untransfected COS-1 cells. The YFP tag does lead to slightly reduced expression levels of MR. Finally, we assessed the transcriptional activities by cotransfection with a luciferase gene under control of a triple-GRE (TAT3-luciferase) (van Leeuwen et al., 2011). Both YFP-MR and MR lead to a clear induction of luciferase activity with 10 nM corticosterone or aldosterone (Figure 6.2C). Control transfected cells (with YFP-YFP) showed only a small induction after corticosterone treatment, probably due to endogenous GR expression in these cells. However, the induction of TAT3-luciferase by YFP-MR was ∼2-fold less efficacious than that with MR alone (Figure 6.2C). Concluding, we see that YFP-MR is

Chapter 6

fully functional, although its relative expression levels and transcriptional activity are slightly reduced.

SMM analysis of agonist-activated YFP-MR

The combination of SMM and FRAP analysis has been successfully applied to study the nuclear mobility patterns of YFP-AR and YFP-GR (van Royen et al., 2014). For both steroid receptors, three distinctive fractions were identified; a single diffusing fraction and two immobilized fraction (which differed in their respective immobilization times). However, it is not to say that a similar model would best fit the nuclear dynamics of YFP-MR also. Thus, we first applied a full, unbiased analysis of the nuclear dynamics of corticosterone-bound YFP-MR. We prepared YFP-MR transfected COS-1 cells for SMM analysis 3 to 5 days after transfection. For SMM, cells are exposed to a saturating dose (1 µM) of corticosterone for 3 to 6 hours, which leads to complete nuclear translocation of YFP-MR (Figure 6.2A). Selected nuclei were photobleached until single fluorescent peaks could be distinguished (Figure 6.1A). These peaks were attributed to single YFP-MR molecules as they had comparable width and intensity as fluorescence intensity peaks derived from single EYFP molecules previously observed using the same setup (Harms et al., 2001). In our current approach, EYFP molecules were identified with a positional accuracy of ~ 40 nm in one dimension (x or y). Next, MR mobility was analyzed by analyzing image sequences with 6.25 ms and 12.5 ms time lags (Figure 6.1B) by the Particle Image Correlation Spectroscopy (PICS) analysis method (Semrau and Schmidt, 2007). PICS detects the average mean square displacement (MSD) of YFP-MR molecules for each time lag. These displacements are subsequently fitted with multiple population models. We found that, comparable to the AR and GR, the mobility of YFP-MR could best be described with a two-population model. A one-population model gave a less accurate fit (Figure 6.1C), while a three population model did not improve the fit substantially and gave inconsistent fractions over different time lags. We thus determined the relative fraction sized and mean squared displacements (MSD) of two separate fractions of YFP-MR, a 'fast' and a 'slow' fraction.

In Figure 6.3A, the size of the 'fast' fraction is plotted against the time lag. For corticosterone-bound YFP-MR the fast fraction makes up about $\sim 50\,\%$ of all nuclear molecules. This percentage decreases slightly with increasing time delays. This has been reported earlier as an experimental artifact (due to fast moving molecules 'escaping' in the Z-direction) and the population distribution of the shortest time lag was shown to be a good approximation of the real distribution (van Royen et al., 2014). Using this approach, we found a 'fast' fraction of $50.7 \pm 1.4\,\%$ and a 'slow' fraction of $49.3 \pm 1.4\,\%$ (Figure 6.3A). Next we plotted the MSD over time for both fractions of MR molecules (Figure 6.3B). The displacement of molecules from the 'slow' fraction did not exceed our detection limit (of $0.009\,\mu m^2$) by more than 2 fold and only increases slightly over time (D_{slow} of $0.080 \pm 0.005\,\mu m^2/s$). This type of diffusion befits the slow restricted movement of chromatin-bound molecules (Blainey
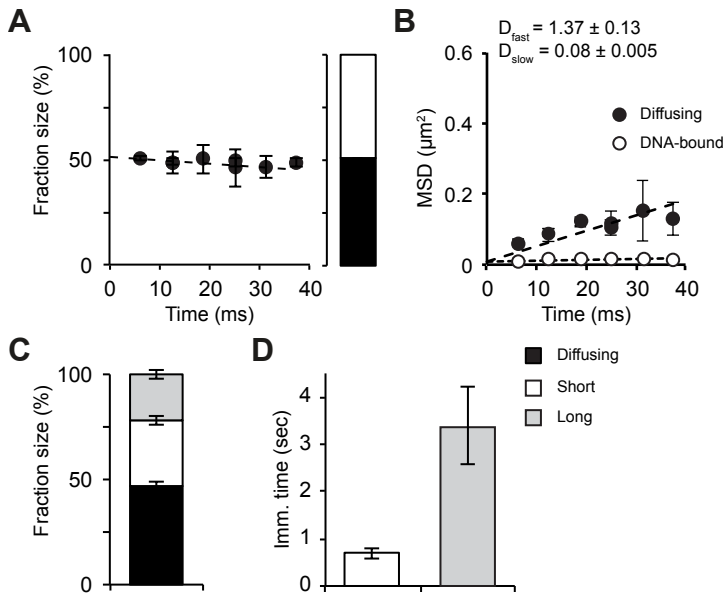
Figure 6.3: SMM and FRAP analyses provide a consistent model of the DNA-binding dynamics of agonist-bound MR
The nuclear dynamics of YFP-MR bound with corticosterone ($1\,\mu\text{M}$) was analyzed by SMM (A and B) and FRAP (C and D). (A) Fraction distribution obtained with SMM. All time lags were analyzed with a two-population fit and consistently found a diffusing fraction of $\sim$50%. To represent the overall fraction size the smallest time lag ($6.25\,\text{ms}$) was used. Bar graph: diffusing fraction (black bar) and DNA-bound fraction (white bar). (B) Mean squared displacements (MSD) of both fractions in SMM. Both fractions show a linear increase in MSD over time, but with a 50-fold difference in MSD. Diffusion coefficients (D_{fast} and D_{slow}) were calculated from a linear fit of the experimental data (dashed lines; $D = \text{slope}/4$). The D_{fast} of $1.37\,\mu\text{m}^2/\text{s}$ fits to diffusing molecules, while the D_{slow} of only $0.08\,\mu\text{m}^2/\text{s}$ best fits to the slow movement of chromatin and thus DNA-bound molecules. (C) Fraction distribution obtained with FRAP. Monte Carlo simulation of corticosterone-bound MR with a 3-population model identified 3 fractions; almost half of the nuclear population is diffusing (black bar), while the remainder is subdivided into two DNA-bound fractions that differ in their immobilization times (white bar is transient bound fraction, light grey bar is more stably bound fraction). The fraction size of the diffusing fraction is similar in size as that obtained from SMM analysis. (D) Both bound fractions in FRAP are transiently immobilized, but with a 4-fold difference in duration. (A and B) Data represented as best fit $\pm$ SEM (of 3 separate PICS analyses). (C and D) Data represented as average of top 10% best fits $\pm$ SEM.

et al., 2006; Elf et al., 2007; van Royen et al., 2014). We presume this fraction thus contains DNA-bound YFP-MR. For the 'fast' moving fraction, we saw a substantial and linear increase in displacements over time (D_{fast} of $1.37 \pm 0.13\,\mu\text{m}^2/\text{s}$), representing YFP-MR molecules diffusing freely throughout the nucleus.

Quantitative FRAP analysis of agonist-activated YFP-MR

Next, we analyzed the longer term dynamics of corticosterone-bound MR with quantitative FRAP analysis. We previously established that this technique, which uses an independent approach to quantify mobility patterns, reproduces the relative fraction sizes (of immobile and diffusing molecules) with very high accuracy

(*Chapter 5*; van Royen et al., 2014). In addition, FRAP analyzes the mobility pattern of fluorescent molecules over time frames from $100\,\text{ms}$ up to a minute and can therefore distinguish immobilization times. As with SMM, YFP-MR transfected COS-1 cells were treated for 3–6 hours with $1\,\mu\text{M}$ corticosterone. Moderately fluorescent nuclei were identified and a small strip spanning the entire nucleus was bleached with a short pulse of full laser power (Figure 6.1D). We observed that all fluorescence recovered within 30 seconds, suggesting that YFP-MR is completely mobile within this time frame (Figure 6.1D). The obtained recovery curves were quantitatively analyzed by fitting them to FRAP curves generated using Monte Carlo simulations (van Royen et al., 2009a, 2014). Diffusion rates as obtained by SMM were used as a fixed parameter in the simulations. Our data was best fitted with a model in which freely diffusing molecules show transient binding with two different durations ('short' and 'long'; Figure 6.1D).

First, we established that FRAP analysis gives a comparable fraction distribution as observed in the SMM analysis. Indeed, where SMM analysis found that $50.7 \pm 1.4\,\%$ of all corticosterone-bound YFP-MR molecules were diffusing, FRAP analysis gave a $47 \pm 2.1\,\%$ diffusing fraction (Figure 6.3C). Additionally, within this longer time frame, we can subdivide the immobile fraction into two immobile fractions, which differ in their immobilization time. The $53\,\%$ of immobilized molecules were further subdivided into a fraction of $31 \pm 2.3\,\%$ with an immobilization time of $0.8 \pm 0.1\,\text{s}$ and a second fraction of $22 \pm 2.5\,\%$ with a longer immobilization time of $3.4 \pm 0.8\,\text{s}$ (Figure 6.3D).

Taken together, we show that the combination of FRAP and SMM gives a reliable quantitative picture of YFP-MR intranuclear mobility patterns. The combination of techniques shows that upon activation by corticosterone, MR spends approximately half of the time diffusing throughout the nucleus and the other half being immobilized for short periods (0.1 to 3 seconds).

Combined SMM and FRAP analysis of antagonist-bound YFP-MR

To investigate the effect of different types of ligands on MR's nuclear mobility we first analyzed its nuclear mobility pattern when bound to an antagonist. We treated YFP-MR expressing COS-1 cells with $1\,\mu\text{M}$ of two MR antagonists, spironolactone and eplerenone, and analyzed the receptor mobility by SMM and FRAP. This high dose was sufficient to induce complete nuclear translocation of the MR with both antagonists (Figure 6.2A). YFP-MR bound to either spironolactone or eplerenone remained highly mobile within the nucleus. A larger fraction of nuclear YFP-MR was diffusing: for spironolactone $78.8 \pm 2.3\,\%$ to $71 \pm 3.5\,\%$ and for eplerenone $68.2 \pm 6.6\,\%$ to $66 \pm 1.6\,\%$ and (obtained with SMM and FRAP analysis respectively; Figure 6.4A,C), which is approximately $1.5 \times$ higher as what was observed for corticosterone-bound MR. This diffusing fraction also diffused approximately twice as fast as compared to corticosterone-bound MR (D_{fast} of 2.71 ± 0.05 and $2.49 \pm 0.12\,\mu\text{m}^2/\text{s}$ for spironolactone and eplerenone respectively; Figure 6.4B).
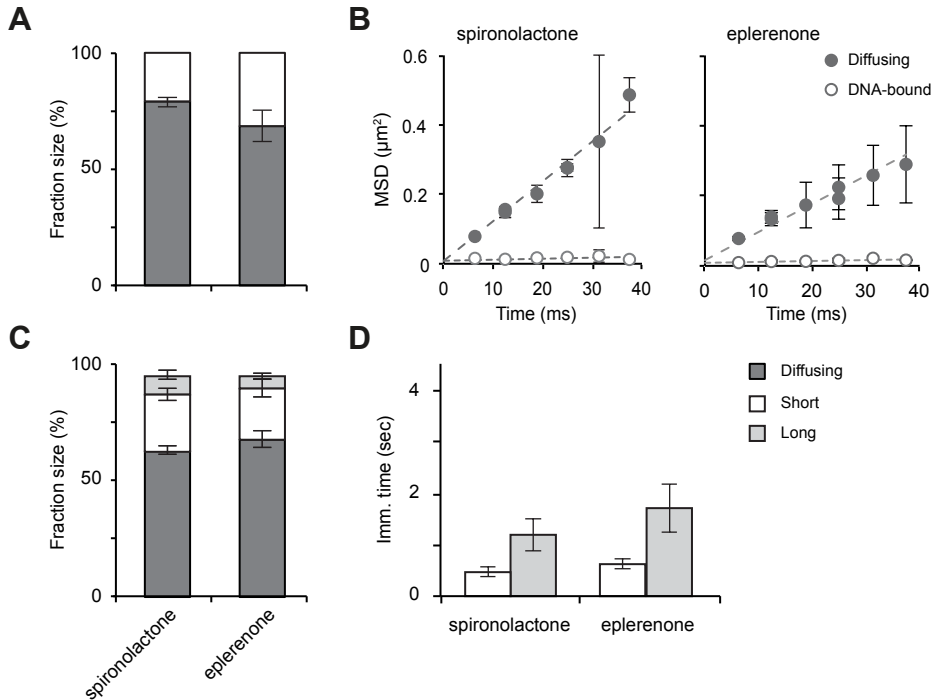
Figure 6.4: Antagonist-bound MR shows a shift towards shorter and less frequent DNA-binding
The nuclear dynamics of YFP-MR bound to its antagonists: spironolactone and eplerenone (both 1 μM)
was analyzed by SMM (A and B) and FRAP (C and D). (A) Fraction distribution obtained with SMM. For
all time lags a large diffusing fraction was found for both antagonists. Diffusing fraction (grey bar) and
DNA-bound fraction (white bar). (B) Mean squared displacements (MSD) of both fractions in SMM. The
diffusing fraction shows large displacements over time, while the DNA-bound fraction shows the small
displacements expected from chromatin bound molecules. (C) Fraction distribution obtained with FRAP.
Monte Carlo simulations with a 3-population model identified 3 fractions; a large diffusing fraction (grey
bar), a transiently bound fraction (white bar) and a very small longer-bound fraction (light grey bar).
The fraction size of the diffusing fraction is similar in size as that obtained from SMM analysis. (D) Both
bound fractions are only transiently immobilized, with a 2–3 fold difference in immobilization times. (A
and B) Data represented as best fit ± SEM (of 3 separate PICS analyses). (C and D) Data represented as
average of top 10 % best fits ± SEM.

Finally, especially the fraction of longer DNA-binding events was much reduced for
antagonist-bound MR. Spironolactone-bound MR induces a 23 ± 3.7 % fraction that
is transiently immobilized (0.5 ± 0.1 sec), but has a negligible fraction of 6 ± 1.6 %
that shows longer immobilizations (of 1.2 ± 0.3 sec). A similar pattern was observed
for eplerenone: 25 ± 2.7 % immobilized for 0.6 ± 0.1 seconds and only 9 ± 2.3 % im-
mobilized for 1.7 ± 0.5 seconds (Figure 6.4D). Thus, the entire population of nuclear
MR is shifted towards a more mobile state with longer stretches of 'free' diffusion,
a higher diffusion coefficient and fewer and shorter immobilizations.

A general pattern of intranuclear mobility after activation by different agonists

For the GR we established that a faster intranuclear mobility was seen not only for antagonist-bound receptors but also when bound to lower efficacy agonists (*Chapter* 5; Schaaf and Cidlowski, 2003). This effect was associated with multiple functional side-groups of the agonists and their interactions with specific amino acids within the ligand-binding groove of the receptor. The GR and MR share a number of (natural) agonists, but with very different relative affinities and associated differ in a number of the amino acids lining their ligand binding groove (Fagart et al., 1998; Bledsoe et al., 2005; Li et al., 2005). To assess the relationship between ligand side-groups and MR's intranuclear mobility, we tested an array of different agonists (natural and synthetic) on the mobility pattern of YFP-MR. A panel was tested that enabled us to study the effects of the P18-keto, and 11- and 17-hydroxyl groups on naturally occurring mineralocorticoid receptor agonists. We used aldosterone (which contains an 18-keto and 11-hydroxyl group), corticosterone (same structure as aldosterone, but lacking the 18-keto group), cortisol (same structure as corticosterone, but containing an additional 17-hydroxyl group), and deoxycorticosterone (DOC; same structure as corticosterone, but lacking the 11-hydroxyl group) (see Figure 6.5A). We also added the GR agonist dexamethasone, which is a weak MR agonist (Arriza et al., 1987; Hellal-Levy et al., 1999).

All ligands used induced complete nuclear translocation of YFP-MR at the high dose used (1 μM; Figure 6.2A). As compared to corticosterone, aldosterone and cortisol induced a similar mobility of the MR, which indicates that the 18-keto and 17-hydroxyl groups are not involved in determining MR's mobility (Figure 6.5 and Table 6.1). In contrast, DOC induced a higher mobility, with a 57 ± 1.5 to $60.5\pm3.6\,\%$ diffusing fraction and smaller DNA-bound fractions (but no effect on immobilization times). This suggests that the presence of the 11-hydroxyl group results in less frequent DNA-binding. As expected, the GR agonist dexamethasone induced a very mobile receptor, intermediate between agonist- and antagonist-bound MR (Figure 6.5).

6.4 Discussion

Here we utilized a combination of SMM and FRAP to quantify the nuclear dynamics of the MR. With SMM we reliably identified two fractions of MR molecules: one that shows diffusion and one that is DNA-bound (Table 6.1). These two populations of nuclear MR molecules were found for both agonist and antagonist bound MR, but with a decrease of the fraction size of the DNA-bound molecules for antagonists. We complemented SMM with a quantitative FRAP approach, and found two bound fractions and a single diffusing fraction. The binding times of both bound fractions are orders of magnitude longer than the time scale used in our SMM experiments

		SMM		FRAP	
		Fraction size (%)	D (μm^2/s)	Fraction size (%)	Imm. time (s)
Aldosterone	Diffusing	54.1 ± 3.4	1.43 ± 0.04	45.0 ± 1.7	-
	Short	45.9 ± 3.4	0.050 ± 0.002	32.0 ± 2.0	0.8 ± 0.1
	Long			23.0 ± 2.1	2.9 ± 0.5
Corticosterone	Diffusing	50.7 ± 1.4	1.37 ± 0.13	47.0 ± 2.1	-
	Short	49.3 ± 1.4	0.080 ± 0.005	31.0 ± 2.3	0.7 ± 0.1
	Long			22.0 ± 2.5	3.4 ± 0.8
Cortisol	Diffusing	51.5 ± 0.8	1.96 ± 0.19	44.0 ± 2.2	-
	Short	48.5 ± 0.8	0.050 ± 0.002	32.0 ± 2.9	0.6 ± 0.1
	Long			24.0 ± 2.7	2.3 ± 0.3
DOC	Diffusing	60.5 ± 3.6	1.60 ± 0.13	57.0 ± 1.5	-
	Short	39.5 ± 3.6	0.060 ± 0.003	23.0 ± 3.0	0.6 ± 0.1
	Long			20.0 ± 3.1	2.3 ± 0.3
Dexamethasone	Diffusing	64.3 ± 6.0	1.74 ± 0.20	67.0 ± 2.1	-
	Short	35.7 ± 6.0	0.040 ± 0.003	22.0 ± 4.4	0.7 ± 0.1
	Long			11.0 ± 3.1	1.7 ± 0.5
Eplerenone	Diffusing	68.2 ± 6.6	2.49 ± 0.12	66.0 ± 1.6	-
	Short	31.8 ± 6.6	0.060 ± 0.004	25.0 ± 2.7	0.6 ± 0.1
	Long			9.0 ± 2.3	1.7 ± 0.5
Spironolactone	Diffusing	78.8 ± 2.3	2.71 ± 0.05	71.0 ± 3.5	-
	Short	21.2 ± 2.3	0.060 ± 0.018	23.0 ± 3.7	0.5 ± 0.1
	Long			6.0 ± 1.6	1.2 ± 0.3

Table 6.1: SMM and FRAP analyses of all MR ligands
Short, 'short' bound fraction; long, 'long' bound fraction; imm. time, average immobilization time. Results are represented as best fit ± SEM (of three separate fits) for SMM and as average ± SEM of top 10 % fits for FRAP.

and these fractions combined represent the single bound fraction detected in SMM, providing two independent estimates of the size of this (combined) fraction. Within our 7 different treatment groups, the sizes of the combined bound fractions determined by SMM and FRAP showed an average difference of only 5.2 ± 1.1 %. This high level of consistency between the two independent techniques shows that a combination of techniques generates a reliable quantitative description of protein dynamics. We have previously shown that this combination of techniques reliably assessed chromatin-binding dynamics of the GR (*Chapter 5*) and the AR (van Royen et al., 2014) as well.

We assessed the nuclear dynamics of the MR when bound to a number of natural agonists, a weak synthetic agonist and two antagonists. In general, we found that the three most potent natural agonists (aldosterone, corticosterone, and cortisol) induce a very similar pattern of nuclear MR dynamics (see Table 6.1). When bound to either of these agonists, approximately $\sim$50 % of all MR molecules are diffusing (with a diffusion coefficient of $\sim$1.5 μm^2/s) while the remaining half is DNA-bound at any time. DNA binding times range from $\sim$0.6 seconds (30 % of MR population)
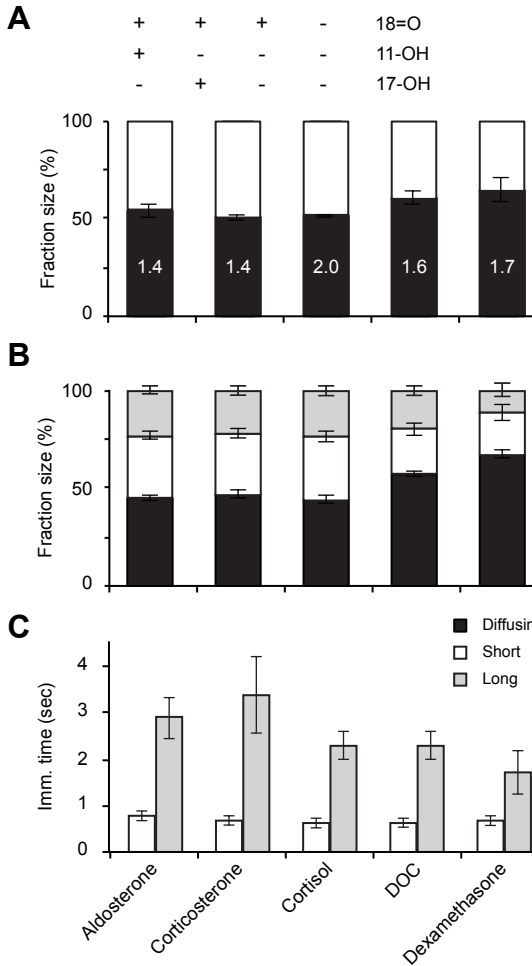
Figure 6.5: A panel of agonists identifies a structural determinant MR's DNA-binding dynamics
A range of natural agonists and one synthetic agonist were tested for their effect on the intranuclear mobility of the MR by both SMM (A) and FRAP (B-C) analysis. (A-B) Black bars represent the diffusing fraction with the diffusion coefficient written within its corresponding bar in A (in $\mu m^2/s$). White and light grey bars represent the DNA-bound fractions. (C) Immobilization times of the short-bound (white bars) and long-bound (light grey bars) fractions. With the combination of 5 agonists tested, we could examine the effect of 3 structural steroid side groups. Only for the 11-hydroxyl group (11-hydroxyl) an association with MR's DNA-binding pattern was found: DOC that lacks this group shows a lower frequency of (short) DNA-binding events. The poor MR agonist dexamethasone induced a very mobile MR with a low frequency and duration of DNA-binding events. SMM: $n = 20$, FRAP: $n = 30$. Data represented as total fit $\pm$ SEM (of 3 separate PICS analyses) for SMM and as average of top 10 % fits $\pm$ SEM for FRAP. aldo: aldosterone, cort: corticosterone, csol: cortisol, dex: dexamethasone. The data for corticosterone-bound MR is the same as in Figure 6.1.

to 2–3 seconds (20 % of MRs). When bound to an antagonist (spironolactone or eplerenone), the same three fractions still exist, but the entire population is shifted towards a more mobile and less stably (DNA-)bound MR. Under these conditions, only ∼30 % of all nuclear MR molecules are associated with DNA. In addition we also measured MR's DNA-binding dynamics when bound to dexamethasone, a high affinity GR agonist. Dexamethasone is known to bind with moderate affinity to the MR but has little potency for MR activation in cells (Arriza et al., 1987; Hellal-Levy et al., 1999). Associated, dexamethasone-bound MR shows high nuclear mobility, and takes up an intermediate position between the natural (highly potent) agonists and the two antagonists (Table 6.1). In most cases, the entire pattern of nuclear mobility was affected: reduced DNA-bound fractions, immobilization times and a higher effective diffusion coefficient (Table 6.1). A similar relationship between diffusion coefficients and DNA-binding frequency and duration was also seen for the

GR (*Chapter 5*). This correlation suggests that the same process, i.e. decreased DNA-binding affinity, underlies these effects. A lower effective diffusion coefficient could be obtained if very transient (< 6 ms) DNA-binding events are 'hidden' in the diffusion coefficient and the frequency of these transient events is affected by ligand properties.

The MR has long remained an understudied receptor. Few studies have assessed its nuclear dynamics (Tirard et al., 2007; Nishi et al., 2011), and none has compared different ligands. Here, we show that the MR has a similar rapid dynamics within the nucleus as seen for other steroid receptors: a combination of free diffusion and transient DNA-interactions (Stenoien et al., 2000; Rayasam et al., 2005; van Royen et al., 2014). Within the family of steroid receptors, the MR is most closely related to the GR with a high sequence homology, shared ligands and even the possibility to form MR-GR heterodimers on the DNA (Trapp et al., 1994; Liu et al., 1995; de Kloet et al., 1998). Therefore, we expected the MR to also support similar DNA-binding dynamics as the GR. Indeed, when compared to the GR and AR that were studied with the same combination of imaging techniques (van Royen et al., 2014), we find that the MR and GR display highly similar characteristics. For example, agonist-bound AR shows much longer stable DNA-binding ($\sim$8 s) than agonist-bound MR and GR (both: 2–3 s).

Mineralocorticoids and glucocorticoids do not differentially affect MR's nuclear dynamics

The MR can be bound by two functionally distinct groups of ligands, mineralocorticoids (aldosterone and DOC) and the naturally occurring glucocorticoids (cortisol and corticosterone) (Joëls et al., 2008). Brain MR binds these steroids equally well, but in the kidney MR is shielded from glucocorticoids because of enzymatic breakdown, rendering the kidney MR selective for mineralocorticoid only (Edwards et al., 1988; Funder et al., 1988). Aldosterone-bound MR is known to bind to a different set of genes (Sato and Funder, 1996; Wilson et al., 2009; Fuller et al., 2012) and was recently found to also bind to different cofactors as MR bound to endogenous glucocorticoids (Fuller et al., 2012). However, despite these differences we found no major differences in DNA-binding frequency or stability between aldosterone-bound or cortisol/corticosterone-bound MR. Thus, the subtle differences in the set of genes targeted by aldosterone-bound MR and cortisol/corticosterone-bound MR appear not to affect its overall binding profile to DNA. In addition, aldosterone has 3–4 fold slower dissociation from the MR than cortisol or corticosterone (Hellal-Levy et al., 1999, 2000), suggesting that ligand dissociation dynamics do not affect the DNA-binding dynamics of the receptor in our experiments either.

Chapter 6

Structure-function relationship of agonist binding

For the GR, we have previously established a relationship between specific steroid side groups and the duration and frequency of DNA binding of the receptor. Most notably steroids containing the 17-hydroxyl and / or the 9-fluoro groups were shown to lead to longer and more frequent DNA-binding of the GR (*Chapter 5*). A similar relationship could be expected for the MR as well. However, as the ligand-binding pockets of the GR and MR differ in a number of key features (Fagart et al., 1998; Li et al., 2005) different functional side groups of the agonists are known to affect binding strength of the ligands to the MR (Huyet et al., 2012). Here, we tested the effects of the 18-keto (=O) and 11- and 17-hydroxyl (–OH) groups. The only side group we found to affect MR's DNA-binding dynamics was the 11-hydroxyl group. When bound to DOC, that lacks this side group, the MR shows reduced DNA-binding as compared to corticosterone, cortisol and aldosterone (all of which have the 11-hydroxyl group; Figure 6.5 & Table 6.1). Interestingly, the strongest effect was seen on the frequency of short, and not of longer, binding events. *In vitro* DOC is a selective activator of the MR, with transactivational activities that are within the same range as those of aldosterone, corticosterone and cortisol (Hellal-Levy et al., 1999; Bledsoe et al., 2002; Quinkler et al., 2002). *In vivo*, however, its potency is debated as it shows near-aldosterone potency on some MR actions (e.g. on sodium retention), but retains only limited potency on other MR actions (e.g. potassium excretion) (Vinson, 2011). That the 11-hydroxyl group is important is clearly illustrated by the fact that oxidation of this group renders cortisol and corticosterone inactive (Edwards et al., 1988; Funder et al., 1988). But, how the 11-hydroxyl group affects the ligand-receptor binding is unclear. It has not been found to undergo specific interactions within the LBP directly (Fagart et al., 1998; Auzou et al., 2000; Bledsoe et al., 2005). Another difference between binding of DOC and aldosterone/corticosterone has been found for the strength of binding to Asparagine 770 (Asn770), a key amino acid that aids in the folding of helix 12 and thereby enables exposure of the AF-2 domain (Fagart et al., 1998; Bledsoe et al., 2005). Asn770 makes two hydrogen bonds with agonist side groups for both corticosterone and aldosterone, only one with DOC and none with any of the known antagonists (Bledsoe et al., 2005; Huyet et al., 2012). Mutation of Asn770 results in an almost complete inhibition of transactivation efficacy for all agonists (Fagart et al., 1998; Bledsoe et al., 2005). Mutational studies should be undertaken to show which of the LBP amino acids are involved in the differential effect of DOC and the other steroids tested on MRs DNA-binding pattern. Thus, also for the MR a difference in its DNA-binding dynamics is correlated to a specific steroid side group, but the relationship with the interactions of ligand side-groups to the receptor seems more complicated than what we observed for the GR and its ligands.

General Discussion

Chapter 7

7.1 Summary of main conclusions

Despite considerable knowledge regarding the molecular basis of corticosteroid actions within target cells, much still remains poorly understood. The molecular and cellular effects of corticosteroids ultimately determine their actions at the tissue and organism levels and a detailed understanding is required to understand how corticosteroids promote adaptation to stress. In this thesis I aimed to explore further finesses in the cellular dynamics of the MR and GR in both their membrane-associated and their nuclear subpopulations. I specified three aims.

1. To investigate the non-genomic effects of corticosteroids in different brain areas and to explore how these effects fit within the onset of the stress response.

2. To set up *in vitro* models to show the presence and function of a distinct membrane-associated population of the MR.

3. To characterize the chromatin binding dynamics of the MR and GR and to explore the effect of mutations within the receptors and of different ligands on their nuclear dynamics.

In *Chapter 2* I evaluated the current state of knowledge regarding the non-genomic actions of corticosteroids through membrane-associated receptors and their relevance for brain functioning. One of the most striking conclusions was that rapidly after stress, corticosteroids affect the excitability of multiple limbic brain areas, but in different response patterns over various time domains. These patterns include rapid non-genomic and slower genomic actions of the hormones that are mediated in a complementary manner by MR and GR. In addition, I discussed the rapid, non-genomic effects of corticosteroids on endocrine output and behavior and found that these effects correlate well with the observed patterns of neuronal excitability changes. Finally, I addressed the current state of knowledge regarding the underlying signaling cascades of these steroid effects and listed the main caveats in the current knowledge. For example, the regulation of MR and GR translocation to the membrane is still elusive, as is the proportion of the membrane population involved and its potential localization in specialized membrane compartments.

In *Chapters 3 and 4* we developed *in vitro* models to study the molecular pathways underlying the non-genomic effects of corticosteroids. In *Chapter 3* we showed that NS-1 cells have potassium A-type currents upon NGF-induced differentiation. These A-type currents are inhibited by corticosterone and cort-BSA within minutes, but only when the MR was present. We thus showed that the MR is required and sufficient for this rapid corticosteroid action. Moreover, this effect is specific for some subtypes of potassium channels. In N1E-115 cells, another type of potassium currents were observed: Kv3-generated slowly-inactivated currents. These currents were not affected by corticosterone. We also observed a remarkable instability of MR protein in our in vitro models. In *Chapter 4* we used TIRF in combination with

SMM to explore whether this combination of imaging techniques is a valid method to show and explore the membrane localization of YFP-tagged MR. One of our main findings here was that the MR shows a larger slow diffusing fraction near the membrane in two cell lines; CHO and COS-1 cells. As membrane-associated proteins are known to diffuse much slower than cytoplasmic proteins, this is a strong indication for the existence of a membrane-associated subpopulation of the MR. The mobility of the membrane-associated population was not affected by hormones.

In *Chapters 5 and 6* I explored the nuclear subpopulation of both GR (*Chapter 5*) and MR (*Chapter 6*) with a combination of SMM and FRAP. Here I found that the combination of both imaging techniques gave a detailed and reproducible quantification of the intranuclear dynamics of both receptors. Both GR and MR showed free diffusion within the nucleus interspersed with short (presumptively nonspecific) and long (presumptively specific) DNA-binding events. GR deletion mutants devoid of (most) DNA-binding showed a stark reduction of these DNA-binding events. The mobility pattern of the MR and GR were highly similar when bound to a high affinity agonist. When bound to an antagonist, both receptors showed less frequent nonspecific binding and less frequent and shorter specific DNA-binding events. Interestingly, intermediate patterns were seen for the GR and MR bound to less potent agonists, and this was correlated with steroid structure. Due to differences in their ligand-binding pocket, different steroid side-groups affected the DNA-binding of the MR and GR. This suggests that specific ligand-receptor interactions strongly affect the affinity for DNA binding in a receptor specific manner.

In conclusion, in this thesis I described a set of experiments that focuses on the function and the dynamics of the two phases of the (cellular) stress response: membrane-initiated / non-genomic and nuclear / genomic actions. The main results are graphically illustrated in Figure 7.1. In the next sections I will discuss a number of interesting observations we made in more detail.

7.2   The presence of the MR at the plasma membrane

In *Chapters 3 and 4* we set up two different *in vitro* models to study the role of the membrane-associated subpopulation of the MR in the rapid non-genomic actions of corticosterone. First, in *Chapter 3* we found that in differentiated NS-1 cells MR-transfection is required for a rapid reduction in potassium A-type current amplitudes by corticosterone. Importantly, we found here that a similar reduction in A-type amplitude is obtained with an equivalent dose of cort-BSA, which is membrane impermeable. These results thus strongly suggest that the MR is present at the cell membrane. In *Chapter 4* we studied the mobility of YFP-tagged MR in COS-1 and CHO cells with a combination of imaging techniques. Here we found that a larger fraction of YFP-MR molecules shows very slow diffusion when imaged near the membrane (with TIRF microscopy) than when imaged in the cytoplasm (with

Chapter 7
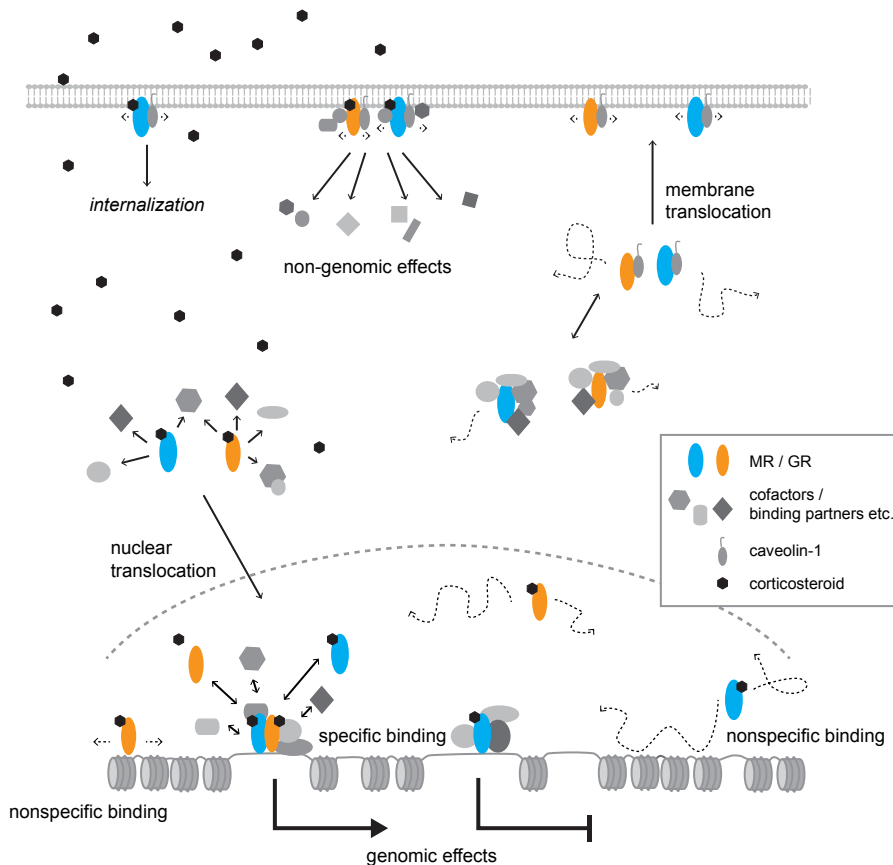
Figure 7.1: Cellular corticosteroid effects through the MR and GR
Without hormone, the bulk of the population of the MR and GR is present within the cytoplasm where it is bound to chaperones. Presumably, a small fraction of cytoplasmic receptors associate with caveolin-1, which induces membrane translocation. As discussed in *Chapters 2, 3, and 4*, at the membrane, hormone binding to the receptors attracts new binding partners and results in the activation of non-genomic signaling pathways. Putatively, ligand association also leads to receptor internalization. Ligand also reaches the cytoplasm where it results in the release of the receptors chaperones and nuclear translocation. Within the nucleus, the receptors interact with chromatin in either ultrashort, short or longer binding events. The first two likely represent nonspecific receptor-DNA interactions and aid in the search for specific binding sites. Also at specific binding sites the receptors interact only transiently with the DNA, as do all cofactors. Specific DNA-binding can occur as either homodimers (not shown), heterodimers or monomers. Ultimately, both MR and GR induce the transactivation and transrepression of a large set of responsive genes; i.e. genomic effects. The experiments presented in *Chapters 4, 5 and 6* suggest that the MR shows mostly very slow diffusion at the membrane, a mixture of slow and fast diffusion within the cytoplasm and both MR and GR show a mixture of fast diffusion and numerous immobilization due to chromatin binding within the nucleus. This is indicated by the dotted lines in the figure.

wide-field microscopy). Membrane-bound proteins generally show a much lower mobility than cytoplasmic proteins (Owen et al., 2009), thus also these findings support the notion of a membrane-bound subpopulation of the MR.

Our findings are in line with the available literature. Numerous studies have shown that cort-BSA was effective and intracellular corticosterone ineffective in mimicking rapid MR-dependent corticosterone effects on glutamate transmission in the brain (Karst et al., 2005; Olijslagers et al., 2008). The presence of a membrane-associated MR has also been convincingly demonstrated using synaptosome extracts and at neuronal membranes using electron microscopy (Prager et al., 2009; Qiu et al., 2010). Within neurons, the MR appeared to be enriched at the presynaptic and postsynaptic membranes. However, the how and why of membrane-association of the MR remain largely unknown. Regulation of membrane translocation of the ERα has been studied in considerable detail. At the membrane, ERα has been found primarily in caveolae, and binding to HSP27, palmitoylation and association with caveolin-1 were all shown to be essential for translocation to the plasma membrane (Razandi et al., 2002, 2010; Acconcia et al., 2005). The MR also binds caveolin-1 directly and seems to associate with lipid rafts (potentially caveolae) (Grossmann et al., 2010; Pojoga et al., 2010b). This suggests that the MR is transported towards caveolae by caveolin-1 association as well, but direct evidence is still lacking. The motif required for palmitoylation of the ERα is conserved among many steroid receptors and was shown to be required for membrane translocation of the AR, PR and ERβ (Pedram et al., 2007). However, the MR lacks the essential cysteine and can therefore not be palmitoylated at this sequence. Consensus palmitoylation sequences are found elsewhere in the MR (Ren et al., 2008), but the MR was never shown to be palmitoylated. Alternatively, the MR could use another pathway for translocation to the membrane.

A characterization of the essential steps in MR membrane association is thus still pending. Moreover, many questions exist regarding the signal partners the MR may associate with at the membrane and it is still incompletely understood whether the MR (and other steroid receptors) is located in the outer or the inner leaflet of the membrane (see *Chapter 2* for further discussion on these issues). Finally, for the ERα it is predicted that 5–10 % of the population exists at the membrane (Chambliss et al., 2000). A similar or smaller percentage is expected for the MR, but remains to be established and will probably depend on ligand binding and cell context as well (Wang and Wang, 2009; Karst et al., 2010). With the combination of TIRF and SMM we were already able to see a distinct diffusion of the MR near the membrane. In future studies, these experiments could be supplemented with disruptions of caveolin-1, palmitoylation or membrane compartments (lipid rafts). This would shine further light on the membrane translocation pathway of the MR.

7.3 *In vitro* MR expression

In *Chapter 3* we came across some important issues regarding the stability of the MR in *in vitro* settings.

Chapter 7

i) First, we used MR transfection in the (non MR-expressing) cell line NS-1. Strikingly, despite successful DNA transfection, we could not detect MR protein in this cell line. MR mRNA was expressed in NS-1 cells after transfection but this did not result in detectable MR protein levels, as assessed by numerous biochemical approaches: Western blot, immunofluorescence staining, detection of YFP-tagged MR and transactivational assays. Functionally, we did observe an MR-specific effect of corticosterone on potassium A-type currents in a large, well-controlled data set at first, but failed to reproduce these effects in a second smaller data set. This discrepancy we cannot explain. In *Chapters 3, 4 and 6* we used a number of other non MR-expressing cell lines: COS-1, CHO and N1E-115. In these three cell lines expression of the MR or YFP-MR was detected after transfections. The lack of MR protein expression thus appears cell line specific.

ii) Secondly, we encountered problems with MR expression during stable transfection in another cell line: CHO cells. We attempted to induce stable expression of YFP-tagged MR in CHO cells. While the procedure led to successful protein expression in a control experiment (transfection of YFP-YFP) in 3 out of 4 clones, for YFP-MR all YFP-positive clones only had fragments of the MR attached to the YFP. This strongly suggests that MR expression is selected against in these cells.

iii) Thirdly, we tested MR protein expression in a cell line that had been stably transfected with MR by the Grossmann-Gekle group (Krug et al., 2002; Grossmann et al., 2005). However, we could not detect MR protein within these cells and also the original investigators had noted a regression of MR levels in these cells even while grown in selection media (personal communication with C. Grossmann), again suggestive of selection against MR expression during cell division.

iv) In line with our observations, unexpected instability of the MR has been published by the Gomez-Sanchez group as well (Gomez-Sanchez et al., 2006). While testing an array of new MR-antibodies, this group found that the MR is easily degraded during *in vitro* handling. Thawing tissue samples (under protection of protease inhibitors and while kept cold) resulted in partially degraded MR, while such procedures kept other steroid receptors intact. Together, these and our observations suggest a remarkable instability of the MR protein and a selection against MR expression within (dividing) cell lines. One could expect that these types of observations have been made by others as well and more publicity on this issue would be valuable for the field. Our current studies were not directed towards this question and at present we can therefore merely speculate about underlying biochemical or functional mechanisms.

Regarding the lack of (detectable) MR protein expression in NS-1 cells in the light of detectable mRNA expression, a biochemical explanation remains elusive. The failure to detect a protein while mRNA is expressed could be caused by either an inhibition of mRNA translation or by protein degradation. First, microRNA induced inhibition of MR mRNA seems unlikely as most microRNA recognition sites for

the MR are found on its 3′ UTR (de Kloet et al., 2009; Sõber et al., 2010), which is not included in the MR plasmids used. Evidence for putative enhanced protein degradation of the MR is lacking as well. Steroid receptors are normally protected from degradation by chaperones, and therefore enhanced MR degradation is seen when the key chaperone HSP90 is inhibited (Faresse et al., 2010). However, HSP90 is expressed in NS-1 cells and the chaperone complex is highly homogenous between steroid receptors. Thus a lack of (common) chaperones is not expected in NS-1 cells in the light of functional expression of the GR, PR and ERs in these cells (MacLusky et al., 2003; Morsink et al., 2006).

Regarding the selection against MR expression during the generation and maintenance of stable cell lines, some speculations can be made. Functionally, MR is found to be protective and anti-apoptotic rather than detrimental, at least in neurons (Gass et al., 2000; Gomez-Sanchez and Gomez-Sanchez, 2012; Munier et al., 2012). However, MR expression is generally restricted to well-differentiated tissues and associated with cellular differentiation (Le Menuet et al., 2012). In line with this, within dividing cell lines endogenous expression of the MR is rare and mostly restricted to a small number of renal derived cell lines (Faresse et al., 2012; Hori et al., 2012). Of note, this is in contrast to other steroid receptors which do show widespread expression in commonly used cell lines (see for example Horwitz et al., 1975; Kao et al., 2009; Polman et al., 2012). Hypothetically, MR expression could be incompatible with undifferentiated, fast dividing cells and therefore selected against in (some) cell lines.

7.4 Advanced imaging methods to examine protein function and localization

In *Chapter 4* I presented a novel approach to test for membrane presence of the MR by a combination of SMM and TIRF microscopy. TIRF microscopy is an adaptation to wide field fluorescence microscopy. In TIRF, the excitation laser is redirected to exit the objective at a large angle relative to the optical axis and is totally internally reflected at the glass-medium interface. As a result an evanescent wave field is created that excites fluorophores in a very small (60–100 nm) section above the glass-medium interface (Axelrod et al., 1983; Axelrod, 2001; Martin-Fernandez et al., 2013). As such, TIRF is the method of choice to image membrane-associated molecules in the scope of unwanted cytoplasmic background. TIRF has been successfully combined with FRAP, FCS and especially SMM (see for an overview Axelrod, 2008). We were the first to utilize a combination of TIRF / wide field microscopy and SMM to distinguish between membrane-associated and cytoplasmic proteins. With this combination of techniques we found that a larger fraction of YFP-MR molecules shows slow diffusion when imaged in TIRF (imaging both membrane-associated and cytoplasmic MRs) than when imaged in wide field (negligible contribution of

membrane-associated MR). Importantly, we found that the shift in population distribution was not due to the smaller Z-depth in TIRF mode. This is strongly suggestive of the existence of a membrane-associated subpopulation. However, we found that short-term hormone treatment did not affect the dynamics of the MR when imaged in TIRF, indicating that ligand activation of the putative membrane-associated population of MRs does not change its mobility. However, our pioneering study does show great potential of combining imaging techniques to deduce protein localization and function.

In *Chapters 5 and 6* we used SMM in combination with quantitative modeling of FRAP with Monte Carlo simulations to quantify the DNA-binding dynamics of the GR (*Chapter 5*) and the MR (*Chapter 6*). More than a decade ago FRAP studies first demonstrated the high dynamics of steroid receptors and other transcription factors within the nucleus (McNally et al., 2000; Stenoien et al., 2000; Schaaf and Cidlowski, 2003; Farla et al., 2004). However, quantification of this dynamic behavior has been a major challenge. Quantitative analysis of FRAP is possible, but requires *a priori* predictions, careful control for laser properties and complicated mathematical models (van Royen et al., 2009b; Mueller et al., 2010, 2013). In addition, FRAP is not very accurate at predicting fast protein diffusion. SMM has an important advantage over FRAP and associated techniques in that the quantitative analysis requires fewer *a priori* assumptions. In addition, SMM has a very high temporal and spatial resolution and is therefore more accurate in describing the dynamics of fast diffusing proteins. A disadvantage of SMM is its shorter maximal time length (up to several hundred milliseconds maximally), which makes the combination with FRAP even more valuable (see for a comparison of imaging techniques: Table 1.1, *Chapter 1*). A combination of two or more independent imaging techniques is widely recognized as the most powerful approach to overcome modeling errors (Mueller et al., 2013; Voss and Hager, 2014). We found that the combination of these two independent quantitative models gave a very extensive and, most importantly, consistent quantification of the DNA-binding dynamics of both receptors. Throughout our studies we tested 18 experimental groups (including the MR and GR bound by a variety of ligands and multiple GR (deletion) mutants). For these 18 groups the quantification of the (combined) DNA-bound fraction was performed independently by SMM and FRAP and we found that the two approaches were on average within $6.5 \pm 1.1\%$ accuracy of each other. In addition, the combination of SMM and FRAP is valuable as it gave us a very complete overview of the dynamics of the MR and GR within the nucleus, from the millisecond to the minute time range. SMM has the temporal and spatial resolution to accurately predict diffusion coefficients of the freely diffusing fraction, while FRAP provides information over an extended time range to predict average DNA-binding times. In another study (van Royen et al., 2014), the accuracy of SMM to predict diffusion coefficients was compared to FCS. FCS is very sensitive for fast diffusing proteins and FCS analysis replicated the diffusion coefficient of the diffusing subfraction with high accuracy for the AR (aver-

age difference of $0.4 \pm 0.04 \,\mu m^2/s$, vanRoyenea2014). In addition to our current work a number of recent studies have been published that used combinations of FRAP with SMM and/or FCS (Stasevich et al., 2010a; Mazza et al., 2012; van Royen et al., 2014). For example, Mazza et al. (2012) used SMM to guide the choice of modeling parameters for FCS and FRAP and thereby restrict the degrees of freedom that made the analysis of these imaging approaches so variable in the past.

In conclusion, advanced fluorescence microscopy techniques have shown their merits for the study of many classes of proteins, including membrane-bound or nuclear proteins. New approaches such as SMM enable more precise quantifications of protein dynamics with a high temporal and spatial resolution. As each analysis method has its biases, a combination of multiple functional imaging approaches limits these biases to skew the outcome and should be common procedure in quantitative studies on protein dynamics.

7.5 Towards a unifying model of steroid receptor DNA-binding dynamics

In *Chapter 5* we used a combination of SMM and FRAP to quantify the intranuclear dynamics of the GR, and in *Chapter 6* we used the same experimental approach to study the dynamics of the MR. Here, we found that the diffusion behavior of both receptors in their ligand-activated state was best described by the existence of a single freely diffusing and multiple DNA-bound states. For example, GR bound to a potent agonist (such as Δ-fludrocortisone or dexamethasone), spends ∼50 % of the time diffusing freely through the nucleus, intermitted by DNA binding for either ∼0.5 second (∼30 %) or 2 to 3 seconds (∼20 %). A highly similar pattern of DNA-binding events was identified for the MR bound to corticosterone, cortisol or aldosterone.

Nonspecific and specific DNA-binding

As expected, GR mutants deficient for DNA-binding (the ΔDBD and ΔLBD mutants) had much reduced frequency and duration of the DNA-binding events, but in addition they also showed a higher effective diffusion rate. Whenever we observed a less mobile receptor (GR and MR bound by less potent agonists, antagonists or deletion mutants), this was always accompanied by both less frequent and shorter DNA-binding events and a higher diffusion coefficient. These observations led us to postulate that a further DNA-binding event was hidden in the diffusing fraction of the receptor: ultra-short DNA-binding for < 6.25 ms (our imaging time interval). Such ultra-short (millisecond) interactions with the DNA have been recognized for other transcription factors as well (Elf et al., 2007; Hammar et al., 2012). We thus presume that the dynamics of the MR and GR within the nucleus is characterized

Chapter 7

by (1) free diffusion, (2) ultra-short DNA interactions (< 6 milliseconds), (3) short DNA interactions (∼0.5 second) and (4) long DNA interactions (2–3 seconds).

There is still active debate regarding the proportion of specific and nonspecific DNA binding events for transcription factors (extensively discussed in Mueller et al., 2013). There are several indications to suggest that the two shorter DNA binding events identified for the MR and GR represent predominantly nonspecific binding to chromatin. Van Royen et al. (2014) examined the dynamics of the AR by SMM and FRAP in a similar design as described in this thesis and reported the same three (putative) DNA-binding events. In these studies an AR point mutation that disrupted specific DNA-binding abolished only the longest binding event, while the shorter DNA-binding events were largely unaltered (van Royen et al., 2014). This finding is reminiscent to observations for other transcription factors showing preservation of a large fraction of DNA-binding events when only specific DNA-binding was inhibited (Elf et al., 2007; Sekiya et al., 2009; Mazza et al., 2012). Transcription factors, including steroid receptors, face the complicated task of finding their few target sites within the bulk of DNA (Hager et al., 2009). It is thought that frequent non-specific binding events aid in this targeting task. Indeed, *in vitro* studies supported by theoretical modeling approaches have suggested that frequent low-affinity interactions with DNA increase the efficiency of transcription factor target finding, because such interactions may keep the transcription factor in close proximity to open DNA (Gowers et al., 2005; Elf et al., 2007; van den Broek et al., 2008; Hager et al., 2009). For this purpose two complementary modes of trafficking may occur. These include both intersegmental jumps with frequent binding and unbinding to the DNA as well as 50–100 bp scanning events where the transcription factor moves over the DNA (Gowers et al., 2005). We present a model that includes the set of DNA-interactions that fit our experimental observations in Figure 7.2a.

In addition, part of the longer-lasting binding events we identified will represent specific binding of the MR and GR to their target sequences. We found that both the ligand-activated MR and the GR spend ∼20 % of their time being bound to the DNA in a more prolonged fashion (approximately 2 to 3 seconds). This fraction of prolonged DNA binding was almost completely lost in DNA-binding deletion mutants. Antagonist-bound MR and GR do still show a fraction of < 1 second bound molecules, albeit at reduced frequency (6–10 %). Moreover, agonist structure affects both the frequency and the duration of the longest DNA-bound state for both the GR and MR. The exact relationship between steroid receptor DNA residence time and transcriptional output is not known. Gene transcription requires many subsequent events. The receptor dimerizes, attracts many co-factors and RNA polymerases and induces gene transcription as well as chromatin remodeling (Datson et al., 2008). It seems reasonable to hypothesize that formation of a more stable co-factor complex will lead to prolonged DNA-binding of a transcription factor, which will then affect local chromatin remodeling.
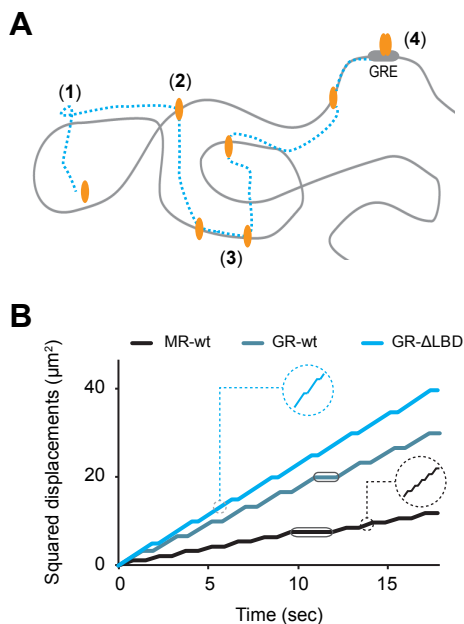
Figure 7.2: Dynamic interactions of the MR and GR at chromatin
(A) A schematic representation of the types of receptor-DNA interactions that are supported by our observation. The receptor shows a combination of (1) free diffusion, (2) ultrashort (< 6 ms) interactions with the DNA, (3) short (~0.5 s) interactions with the DNA that could represent 1D sliding along the DNA strands and least frequent (4) longer (> 2 s) interactions with the DNA that could represent specific binding to target genes. (B) Squared displacements of "perfectly average" MR and GR molecules (i.e. with the use of the average D_{fast}, binding times and fraction distributions as represented in Table 5.1, *Chapter 5* and Table 6.1, *Chapter 6*. This illustrates the difference in intranuclear dynamics of the MR and GR when bound by corticosterone and the GR-ΔLBD mutant. Corticosterone-bound GR has fewer nonspecific interactions (both ultrashort and short) with chromatin resulting in a larger distance traveled before finding a specific binding site (encircled) as compared to corticosterone-bound MR. The specific binding event is also shorter in duration. The GR-ΔLBD mutant lost most capacity for DNA-binding and only preserved a low frequency of ultrashort and short DNA-interactions while prolonged specific binding is lost altogether. Ultrashort DNA-interactions are 'hidden' within the diffusing fraction and result in a lower effective diffusion.

Steroid-receptor interactions determine the affinity for DNA

A main finding from our sets of experiments was that subtle differences in agonist structure have a profound effect on the frequency and duration of DNA-binding events of the MR and GR. For the GR, we identified two steroid side groups (the 17-hydroxyl and the 9-fluor groups) that, when present, induced more frequent and more stable GR-DNA interactions. For MR ligands, the 17-hydroxyl group is without effect, while presence of the 11-hydroxyl group is associated with a higher frequency of MR-DNA binding. We presumed that the more potent agonists make more connections to the amino acids lining the LBP and can therefore induce a stronger conformational shift of the receptor. Indeed, for the GR we found that mutation of a single amino acid in GR's LBP prevented the effect of the 9α-fluoro group (*Chapter 5*). Likely differences in ligand-induced receptors conformational shifts affect dimerization or cofactor binding and ultimately affinity for the DNA. We found that binding of a less potent agonist generally affects both the frequency of nonspecific DNA-interactions and the frequency and duration of binding to specific target sites. We expect that fewer nonspecific binding events could result in a longer search time for target sequence binding. A shorter duration of specific binding likely affects gene transcription and modulation. What the effect of such different chromatin-binding

Chapter 7

dynamics entails on the level of gene regulation by the MR and GR remains to be established. Assessment of the chromatin-binding patterns (e.g. by ChiP studies) after stimulations with a set of different MR and GR agonists would be very valuable and could elucidate the relevance of nonspecific and specific DNA-binding for gene regulation.

When both receptors are bound to a potent agonist, the DNA-binding patterns of the GR and MR are very similar. This is in correspondence to the high sequence homology of their DNA-binding domains, which results in both receptors recognizing the same response elements (GREs). Of note, the longest binding event of agonist-bound MR and GR was much shorter in duration as what was observed for the AR. Van Royen et al. (2014) found a fraction of AR bound for ∼8 seconds, whereas we found ∼3 seconds as longest binding event for the MR and GR. The AR also binds to GREs, however differences known to exist in the groups of cofactors bound and in the conformation of the receptors could underlie the observed prolonged DNA residence times of the AR (Centenera et al., 2008; van de Wijngaart et al., 2012).

Notably, as the natural ligands corticosterone and cortisol have a lower affinity for the GR than for the MR, within physiological conditions the chromatin binding pattern of the two receptors will be very different. In response to its physiological ligand, the MR will be DNA-bound more often and for longer periods than the GR (illustrated in Figure 7.2B). This observation is in in agreement with *in vivo* uptake of tritium labelled corticosterone that shows a much longer retention in the nucleus of MR-expressing than GR-expressing tissues (Reul and de Kloet, 1985). These findings were corroborated with an immunohistochemical study showing also a longer retention of MR than GR in the nucleus (Conway-Campbell et al., 2007) and of dexamethasone-bound GR than corticosterone-bound GR (Stavreva et al., 2009). However, whether such a difference also exists on the level of DNA-binding itself still needs to be established. Interestingly, in one recent study, binding of the GR and MR was assessed for 10 genes (Polman et al., 2013). Here, a lower occupancy rate was found for the MR then for the GR (contrary to our predictions), but this set of genes was initially selected based on GR-binding, thus biased.

Box I Future questions

From the experiments presented in this thesis many new questions came up and some old ones remained partly unanswered. Here, I list a few of the most interesting questions that sprang up from the current studies.

From Chapter 2

1. *Within the scope of neuronal non-genomic effects of corticosteroids, how do these integrate with rapid signaling of other stress hormones; i.e. catecholamines and CRH?*

2. *How are non-genomic and genomic actions of corticosteroids integrated? This question remains to be answered on both the cellular and the organism level.*

From Chapters 2 to 4

3. *What steps are required for membrane translocation of the MR and GR? Is the MR palmitoylated as are other steroid receptors?*

4. *What fraction of both receptors associates with the membrane, and are they located in specific membrane subdomains?*

5. *Is the larger slow diffusing fraction of YFP-MR caused by enrichment for membrane-associated MR in TIRF?*

6. *Is the MR incompatible with cell division? If so, what is the best strategy to create stable MR-expression in vitro?*

From Chapter 5 and 6

7. *What is the result of changes in the frequency of nonspecific DNA interactions of the MR or GR on gene regulation?*

8. *What are the effects of differences in chromatin dwell time on the recruitment of cofactors, the stability of the RNA polymerase cycle and on chromatin modifications?*

9. *How do differences in the binding of agonists to the ligand-binding pocket affect the conformation of the receptor's functional domains?*

10. *With regard to the observed difference in the DNA-binding dynamics of the MR and GR when bound to endogenous corticosteroids. What would be the effect of MR and GR co-expression on their respective DNA-binding dynamics in the presence of endogenous corticosteroids. What is the role of MR-GR heterodimers?*

Chapter 7

References

Acconcia F, Ascenzi P, Bocedi A, Spisni E, Tomasi V, Trentalance A, Visca P, Marino M (2005) *Palmitoylation-dependent estrogen receptor alpha membrane localization: regulation by 17beta-estradiol.* Mol Biol Cell 16:231–237.

Adams JP, Anderson AE, Varga AW, Dineley KT, Cook RG, Pfaffinger PJ, Sweatt JD (2008) *The A-Type Potassium Channel Kv4.2 Is a Substrate for the Mitogen-Activated Protein Kinase ERK.* J Neurochem 75:2277–2287.

Africander D, Louw R, Hapgood JP (2013) *Investigating the anti-mineralocorticoid properties of synthetic progestins used in hormone therapy.* Biochem Biophys Res Commun 433:305–310.

Agarwal AK, Monder C, Eckstein B, White PC (1989) *Cloning and expression of rat cDNA encoding corticosteroid 11 beta-dehydrogenase.* J Biol Chem 264:18939–18943.

Alfarez DN, De Simoni A, Velzing EH, Bracey E, Joëls M, Edwards FA, Krugers HJ (2009) *Corticosterone reduces dendritic complexity in developing hippocampal CA1 neurons.* Hippocampus 19:828–836.

Alfarez DN, Wiegert O, Joëls M, Krugers HJ (2002) *Corticosterone and stress reduce synaptic potentiation in mouse hippocampal slices with mild stimulation.* Neuroscience 115:1119–1126.

Anderson RG (1998) *The caveolae membrane system.* Annu Rev Biochem 67:199–225.

Arnsten AF (2009) *Stress signalling pathways that impair prefrontal cortex structure and function.* Nat Rev Neurosci 10:410–422.

Arriza JL, Weinberger C, Cerelli G, Glaser TM, Handelin BL, Housman DE, Evans RM (1987) *Cloning of human mineralocorticoid receptor complementary DNA: structural and functional kinship with the glucocorticoid receptor.* Science 237:268–275.

Atkinson HC, Wood SA, Castrique ES, Kershaw YM, Wiles CC, Lightman SL (2008) *Corticosteroids mediate fast feedback of the rat hypothalamic-pituitary-adrenal axis via the mineralocorticoid receptor.* Am J Physiol Endocrinol Metab 294:E1011–22.

Auzou G, Fagart J, Souque A, Hellal-Levy C, Wurtz JM, Moras D, Rafestin-Oblin ME (2000) *A single amino acid mutation of ala-773 in the mineralocorticoid receptor confers agonist properties to 11beta-substituted spirolactones.* Mol Pharmacol 58:684–691.

Axelrod D (2001) *Total Internal Reflection Fluorescence Microscopy in Cell Biology: Total Internal Reflection Fluorescence.* Traffic 2:764–774.

Axelrod D (2008) Chapter 7 *Total Internal Reflection Fluorescence Microscopy.* In: Methods in Cell Biology, pp 169–221. Elsevier.

Axelrod D, Thompson N, Burghardt T (1983) *Total internal inflection fluorescent microscopy.* J Microsc 129:19–28.

Barsegyan A, Mackenzie SM, Kurose BD, McGaugh JL, Roozendaal B (2010) *Glucocorticoids in the prefrontal cortex enhance memory consolidation and impair working memory by a common neural mechanism.* Proc Natl Acad Sci U A 107:16655–16660.

Bartel D (2004) *MicroRNAsGenomics, Biogenesis, Mechanism, and Function.* Cell 116:281–297.

Beato M, Sanchez-Pacheco A (1996) *Interaction of steroid hormone receptors with the transcription initiation complex.* Endocr Rev 17:587–609.

Becker M (2002) *Dynamic behavior of transcription factors on a natural promoter in living cells.* EMBO Rep 3:1188–1194.

Bekkers JM, Stevens CF (1989) *NMDA and non-NMDA receptors are co-localized at individual excitatory synapses in cultured rat hippocampus.* Nature 341:230–233.

Berger S, Wolfer DP, Selbach O, Alter H, Erdmann G, Reichardt HM, Chepkova AN, Welzl H, Haas HL, Lipp HP, Schutz G (2006) *Loss of the limbic mineralocorticoid receptor impairs behavioral plasticity.* Proc Natl Acad Sci U A 103:195–200.

Biddie SC, Hager GL (2009) *Glucocorticoid receptor dynamics and gene regulation.* Stress 12:193–205.

Blainey PC, van Oijen AM, Banerjee A, Verdine GL, Xie XS (2006) *A base-excision DNA-repair protein finds intrahelical lesion bases by fast sliding in contact with DNA.* Proc Natl Acad Sci USA 103:5752–5757.

Bledsoe RK, Madauss KP, Holt JA, Apolito CJ, Lambert MH, Pearce KH, Stanley TB, Stewart EL, Trump RP, Willson TM, Williams SP (2005) *A ligand-mediated hydrogen bond network required for the activation of the mineralocorticoid receptor.* J Biol Chem 280:31283–31293.

Bledsoe RK, Montana VG, Stanley TB, Delves CJ, Apolito CJ, McKee DD, Consler TG, Parks DJ, Stewart EL, Willson TM, Lambert MH, Moore JT, Pearce KH, Xu HE (2002) *Crystal structure of the glucocorticoid receptor ligand binding domain reveals a novel mode of receptor dimerization and coactivator recognition.* Cell 110:93–105.

Bledsoe RK, Stewart EL, Pearce KH (2004) *Structure and function of the glucocorticoid receptor ligand binding domain.* Vitam Horm 68:49–91.

Bobroff N (1986) *Position measurement with a resolution and noise-limited instrument.* Rev Sci Instrum 57:1152.

Boldyreff B, Wehling M (2003) *Rapid aldosterone actions: from the membrane to signaling cascades to gene transcription and physiological effects.* J Steroid Biochem Mol Biol 85:375–381.

Bondar G, Kuo J, Hamid N, Micevych P (2009) *Estradiol-induced estrogen receptor-alpha trafficking.* J Neurosci 29:15323–15330.

Boulware MI, Kordasiewicz H, Mermelstein PG (2007) *Caveolin proteins are essential for distinct effects of membrane estrogen receptors in neurons.* J Neurosci 27:9941–9950.

Boulware MI, Weick JP, Becklund BR, Kuo SP, Groth RD, Mermelstein PG (2005) *Estradiol activates group I and II metabotropic glutamate receptor signaling, leading to opposing influences on cAMP response element-binding protein.* J Neurosci 25:5066–5078.

Breuner CW, Orchinik M (2009) *Pharmacological characterization of intracellular, membrane, and plasma binding sites for corticosterone in house sparrows.* Gen Comp Endocrinol 163:214–224.

Brinks V, Berger S, Gass P, de Kloet ER, Oitzl MS (2009) *Mineralocorticoid receptors in control of emotional arousal and fear memory.* Horm Behav 56:232–238.

Buchanan TW, Lovallo WR (2001) *Enhanced memory for emotional material following stress-level cortisol treatment in humans.* Psychoneuroendocrinology 26:307–317.

Buckingham JC, Solito E, John C, Tierney T, Taylor A, Flower R, Christian H, Morris J (2003) *Annexin 1: a paracrine/juxtacrine mediator of glucorticoid action in the neuroendocrine system.* Cell Biochem Funct 21:217–221.

Campolongo P, Roozendaal B, Trezza V, Hauer D, Schelling G, McGaugh JL, Cuomo V (2009) *Endocannabinoids in the rat basolateral amygdala enhance memory consolidation and enable glucocorticoid modulation of memory.* Proc Natl Acad Sci U A 106:4888–4893.

Castillo C, Carreño F, Villegas GM, Villegas R (2001) *Ionic currents in PC12 cells differentiated into neuron-like cells by a cultured-sciatic nerve conditioned medium.* Brain Res 911:181–192.

Catania EH, Pimenta A, Levitt P (2008) *Genetic deletion of Lsamp causes exaggerated behavioral activation in novel environments.* Behav Brain Res 188:380–390.

Centenera MM, Harris JM, Tilley WD, Butler LM (2008) *Minireview: The Contribution of Different Androgen Receptor Domains to Receptor Dimerization and Signaling.* Mol Endocrinol 22:2373–2382.

Chambliss KL, Yuhanna IS, Mineo C, Liu P, German Z, Sherman TS, Mendelsohn ME, Anderson RG, Shaul PW (2000) *Estrogen receptor alpha and endothelial nitric oxide synthase are organized into a functional signaling module in caveolae.* Circ Res 87:E44–52.

Chandy KG, Williams CB, Spencer RH, Aguilar BA, Ghanshani S, Tempel BL, Gutman GA (1990) *A family of three mouse potassium channel genes with intronless coding regions.* Science:973–975.

Chauveau F, Tronche C, Pierard C, Liscia P, Drouet I, Coutan M, Beracochea D (2010) *Rapid stress-induced corticosterone rise in the hippocampus reverses serial memory retrieval pattern.* Hippocampus 20:196–207.

Chen X, Yuan L-L, Zhao C, Birnbaum SG, Frick A, Jung WE, Schwarz TL, Sweatt JD, Johnston D (2006) *Deletion of Kv4.2 Gene Eliminates Dendritic A-Type K+ Current and Enhances Induction of Long-Term Potentiation in Hippocampal CA1 Pyramidal Neurons.* J Neurosci 26:12143–12151.

Chen Y, Muller J, Berland K, Gratton E (1999) *Fluorescence Fluctuation Spectroscopy.* Methods 19:234–252.

Coetzee WA, Amarillo Y, Chiu J, Chow A, Lau D, McCORMACK T, Morena H, Nadal MS, Ozaita A, Pountney D, Saganich M, Miera EV-S, Rudy B (1999) *Molecular Diversity of K+ Channels.* Ann N Y Acad Sci 868:233–255.

Cognet L, Lounis B, Choquet D (2014) *Tracking Receptors Using Individual Fluorescent and Nonfluorescent Nanolabels.* Cold Spring Harb Protoc 2014:pdb.proto80416.

Cohen AW, Hnasko R, Schubert W, Lisanti MP (2004) *Role of caveolae and caveolins in health and disease.* Physiol Rev 84:1341–1379.

Conforti L, Millhorn DE (2000) *Regulation of Shaker-type potassium channels by hypoxia. Oxygen-sensitive K+ channels in PC12 cells.* Adv Exp Med Biol 475:265–274.

Conway-Campbell BL, McKenna MA, Wiles CC, Atkinson HC, de Kloet ER, Lightman SL (2007) *Proteasome-dependent down-regulation of activated nuclear hippocampal glucocorticoid receptors determines dynamic responses to corticosterone.* Endocrinology 148:5470–5477.

Cottrell EC, Seckl JR, Holmes MC, Wyrwoll CS (2014) *Foetal and placental 11β-HSD2: a hub for developmental programming.* Acta Physiol Oxf Engl 210:288–295.

Dallman MF (2005) *Fast glucocorticoid actions on brain: back to the future.* Front Neuroendocr 26:103–108.

Dallman MF, Akana SF, Levin N, Walker CD, Bradbury MJ, Suemaru S, Scribner KS (1994) *Corticosteroids and the control of function in the hypothalamo-pituitary-adrenal (HPA) axis.* Ann N Acad Sci 746:22–31; discussion 31-2, 64–7.

Datson NA, Morsink MC, Meijer OC, de Kloet ER (2008) *Central corticosteroid actions: Search for gene targets.* Eur J Pharmacol 583:272–289.

Datson NA, Polman JA, de Jonge RT, van Boheemen PT, van Maanen EM, Welten J, McEwen BS, Meiland HC, Meijer OC (2011) *Specific regulatory motifs predict glucocorticoid responsiveness of hippocampal gene expression.* Endocrinology 152:3749–3757.

Datson NA, van der Perk J, de Kloet ER, Vreugdenhil E (2001) *Identification of corticosteroid-responsive genes in rat hippocampus using serial analysis of gene expression.* Eur J Neurosci 14:675–689.

De Bosscher K, Haegeman G (2009) *Minireview: Latest Perspectives on Antiinflammatory Actions of Glucocorticoids.* Mol Endocrinol 23:281–291.

De Kloet ER, Fitzsimons CP, Datson NA, Meijer OC, Vreugdenhil E (2009) *Glucocorticoid signaling and stress-related limbic susceptibility pathway: About receptors, transcription machinery and microRNA.* Brain Res 1293:129–141.

De Kloet ER, Joëls M, Holsboer F (2005) *Stress and the brain: from adaptation to disease.* Nat Rev Neurosci 6:463–475.

De Kloet ER, Karst H, Joëls M (2008) *Corticosteroid hormones in the central stress response: quick-and-slow.* Front Neuroendocrinol 29:268–272.

De Kloet ER, Oitzl MS, Joëls M (1999) *Stress and cognition: are corticosteroids good or bad guys?* Trends Neurosci 22:422–426.

De Kloet ER, Reul JM (1987) *Feedback action and tonic influence of corticosteroids on brain function: a concept arising from the heterogeneity of brain receptor systems.* Psychoneuroendocrinology 12:83–105.

De Kloet ER, Vreugdenhil E, Oitzl MS, Joëls M (1998) *Brain corticosteroid receptor balance in health and disease.* Endocr Rev 19:269–301.

De Quervain DJ, Aerni A, Schelling G, Roozendaal B (2009) *Glucocorticoids and the regulation of memory in health and disease.* Front Neuroendocr 30:358–370.

DeRijk RH, de Kloet ER, Zitman FG, van Leeuwen N (2011) *Mineralocorticoid receptor gene variants as determinants of HPA axis regulation and behavior.* Endocr Dev 20:137–148.

Di S, Malcher-Lopes R, Halmos KC, Tasker JG (2003) *Nongenomic glucocorticoid inhibition via endocannabinoid release in the hypothalamus: a fast feedback mechanism.* J Neurosci 23:4850–4857.

Di S, Malcher-Lopes R, Marcheselli VL, Bazan NG, Tasker JG (2005) *Rapid glucocorticoid-mediated endocannabinoid release and opposing regulation of glutamate and gamma-aminobutyric acid inputs to hypothalamic magnocellular neurons.* Endocrinology 146:4292–4301.

Di S, Maxson MM, Franco A, Tasker JG (2009) *Glucocorticoids regulate glutamate and GABA synapse-specific retrograde transmission via divergent nongenomic signaling pathways.* J Neurosci 29:393–401.

Diamond DM, Bennett MC, Fleshner M, Rose GM (1992) *Inverted-U relationship between the level of peripheral corticosterone and the magnitude of hippocampal primed burst potentiation.* Hippocampus 2:421–430.

Dijkmans TF, van Hooijdonk LWA, Schouten TG, Kamphorst JT, Vellinga ACA, Meerman JHN, Fitzsimons CP, de Kloet ER, Vreugdenhil E (2008) *Temporal and functional dynamics of the transcriptome during nerve growth factor-induced differentiation.* J Neurochem 105:2388–2403.

Dooley R, Harvey BJ, Thomas W (2012) *Non-genomic actions of aldosterone: From receptors and signals to membrane targets.* Mol Cell Endocrinol 350:223–234.

Droste SK, de Groote L, Atkinson HC, Lightman SL, Reul JM, Linthorst AC (2008) *Corticosterone levels in the brain show a distinct ultradian rhythm but a delayed response to forced swim stress.* Endocrinology 149:3244–3253.

References

Dundr M, Hoffmann-Rohrer U, Hu Q, Grummt I, Rothblum LI, Phair RD, Misteli T (2002) *A kinetic framework for a mammalian RNA polymerase in vivo.* Science 298:1623–1626.

Duvarci S, Pare D (2007) *Glucocorticoids enhance the excitability of principal basolateral amygdala neurons.* J Neurosci 27:4482–4491.

Edwards CR, Stewart PM, Burt D, Brett L, McIntyre MA, Sutanto WS, de Kloet ER, Monder C (1988) *Localisation of 11 beta-hydroxysteroid dehydrogenase--tissue specific protector of the mineralocorticoid receptor.* Lancet 2:986–989.

Elbi C, Walker DA, Romero G, Sullivan WP, Toft DO, Hager GL, DeFranco DB (2004) *Molecular chaperones function as steroid receptor nuclear mobility factors.* Proc Natl Acad Sci USA 101:2876–2881.

Elf J, Li GW, Xie XS (2007) *Probing transcription factor dynamics at the single-molecule level in a living cell.* Science 316:1191–1194.

Evanson NK, Herman JP, Sakai RR, Krause EG (2010a) *Nongenomic actions of adrenal steroids in the central nervous system.* J Neuroendocr 22:846–861.

Evanson NK, Tasker JG, Hill MN, Hillard CJ, Herman JP (2010b) *Fast feedback inhibition of the HPA axis by glucocorticoids is mediated by endocannabinoid signaling.* Endocrinology 151:4811–4819.

Fagart J, Wurtz JM, Souque A, Hellal-Levy C, Moras D, Rafestin-Oblin ME (1998) *Antagonism in the human mineralocorticoid receptor.* EMBO J 17:3317–3325.

Faresse N, Ruffieux-Daidie D, Salamin M, Gomez-Sanchez CE, Staub O (2010) *Mineralocorticoid receptor degradation is promoted by Hsp90 inhibition and the ubiquitin-protein ligase CHIP.* Am J Physiol - Ren Physiol 299:F1462–F1472.

Faresse N, Vitagliano J-J, Staub O (2012) *Differential ubiquitylation of the mineralocorticoid receptor is regulated by phosphorylation.* FASEB J 26:4373–4382.

Farla P, Hersmus R, Geverts B, Mari PO, Nigg AL, Dubbink HJ, Trapman J, Houtsmuller AB (2004) *The androgen receptor ligand-binding domain stabilizes DNA binding in living cells.* J Struct Biol 147:50–61.

Ffrench-Mullen JM (1995) *Cortisol inhibition of calcium currents in guinea pig hippocampal CA1 neurons via G-protein-coupled activation of protein kinase C.* J Neurosci 15:903–911.

Fuller PJ (1991) *The steroid receptor superfamily: mechanisms of diversity.* FASEB J Off Publ Fed Am Soc Exp Biol 5:3092–3099.

Fuller PJ, Yao Y, Yang J, Young MJ (2012) *Mechanisms of ligand specificity of the mineralocorticoid receptor.* J Endocrinol 213:15–24.

Funder JW (2010) *Minireview: Aldosterone and mineralocorticoid receptors: past, present, and future.* Endocrinology 151:5098–5102.

Funder JW, Pearce PT, Smith R, Smith AI (1988) *Mineralocorticoid action: target tissue specificity is enzyme, not receptor, mediated.* Science 242:583–585.

Fuse H, Kitagawa H, Kato S (2000) *Characterization of Transactivational Property and Coactivator Mediation of Rat Mineralocorticoid Receptor Activation Function-1 (AF-1).* Mol Endocrinol 14:889–899.

Ganguly S, Pucadyil TJ, Chattopadhyay A (2008) *Actin Cytoskeleton-Dependent Dynamics of the Human Serotonin1A Receptor Correlates with Receptor Signaling.* Biophys J 95:451–463.

Gass P, Kretz O, Wolfer DP, Berger S, Tronche F, Reichardt HM, Kellendonk C, Lipp H-P, Schmid W, Schütz G (2000) *Genetic disruption of mineralocorticoid receptor leads to impaired neurogenesis and granule cell degeneration in the hippocampus of adult mice.* EMBO Rep 1:447–451.

Gebhardt JC, Suter DM, Roy R, Zhao ZW, Chapman AR, Basu S, Maniatis T, Xie XS (2013) *Single-molecule imaging of transcription factor binding to DNA in live mammalian cells.* Nat Methods 10:421–426.

Geerling JC, Kawata M, Loewy AD (2006) *Aldosterone-sensitive neurons in the rat central nervous system.* J Comp Neurol 494:515–527.

Gekle M, Freudinger R, Mildenberger S, Schenk K, Marschitz I, Schramek H (2001) *Rapid activation of Na+/H+-exchange in MDCK cells by aldosterone involves MAP-kinase ERK1/2.* Pflugers Arch 441:781–786.

Gilad LA, Schwartz B (2007) *Association of estrogen receptor beta with plasma-membrane caveola components: implication in control of vitamin D receptor.* J Mol Endocrinol 38:603–618.

Gomez-Sanchez CE, de Rodriguez AF, Romero DG, Estess J, Warden MP, Gomez-Sanchez MT, Gomez-Sanchez EP (2006) *Development of a panel of monoclonal antibodies against the mineralocorticoid receptor.* Endocrinology 147:1343–1348.

Gomez-Sanchez CE, Gomez-Sanchez EP (2012) *The Protective Side of the Mineralocorticoid Receptor.* Endocrinology 153:1565–1567.

Gomez-Sanchez CE, Warden M, Gomez-Sanchez MT, Hou X, Gomez-Sanchez EP (2011) *Diverse immunostaining patterns of mineralocorticoid receptor monoclonal antibodies.* Steroids 76:1541–1545.

Gomez-Sanchez EP (2010) *The mammalian mineralocorticoid receptor: tying down a promiscuous receptor.* Exp Physiol 95:13–18.

Gomez-Sanchez EP (2011) *Mineralocorticoid receptors in the brain and cardiovascular regulation: minority rule?* Trends Endocrinol Metab TEM 22:179–187.

Gorosito SV, Lorenzo AG, Cambiasso MJ (2008) *Estrogen receptor alpha is expressed on the cell-surface of embryonic hypothalamic neurons.* Neuroscience 154:1173–1177.

Gorski SA, Dundr M, Misteli T (2006) *The road much traveled: trafficking in the cell nucleus.* Curr Opin Cell Biol 18:284–290.

Gorski SA, Snyder SK, John S, Grummt I, Misteli T (2008) *Modulation of RNA Polymerase Assembly Dynamics in Transcriptional Regulation.* Mol Cell 30:486–497.

Gowers DM, Wilson GG, Halford SE (2005) *Measurement of the contributions of 1D and 3D pathways to the translocation of a protein along DNA.* Proc Natl Acad Sci USA 102:15883–15888.

Groc L, Choquet D, Chaouloff F (2008) *The stress hormone corticosterone conditions AMPAR surface trafficking and synaptic potentiation.* Nat Neurosci 11:868–870.

Groeneweg FL, Karst H, de Kloet ER, Joëls M (2011) *Rapid non-genomic effects of corticosteroids and their role in the central stress response.* J Endocrinol 209:153–167.

Groeneweg FL, Karst H, de Kloet ER, Joëls M (2012) *Mineralocorticoid and glucocorticoid receptors at the neuronal membrane, regulators of nongenomic corticosteroid signalling.* Mol Cell Endocrinol 350:299–309.

Grossmann C, Benesic A, Krug AW, Freudinger R, Mildenberger S, Gassner B, Gekle M (2005) *Human mineralocorticoid receptor expression renders cells responsive for nongenotropic aldosterone actions.* Mol Endocrinol 19:1697–1710.

Grossmann C, Freudinger R, Mildenberger S, Husse B, Gekle M (2008) *EF domains are sufficient for nongenomic mineralocorticoid receptor actions.* J Biol Chem 283:7109–7116.

Grossmann C, Gekle M (2009) *New aspects of rapid aldosterone signaling.* Mol Cell Endocrinol 308:53–62.

Grossmann C, Husse B, Mildenberger S, Schreier B, Schuman K, Gekle M (2010) *Colocalization of mineralocorticoid and EGF receptor at the plasma membrane.* Biochim Biophys Acta 1803:584–590.

Grossmann C, Scholz T, Rochel M, Bumke-Vogt C, Oelkers W, Pfeiffer AF, Diederich S, Bahr V (2004) *Transactivation via the human glucocorticoid and mineralocorticoid receptor by therapeutically used steroids in CV-1 cells: a comparison of their glucocorticoid and mineralocorticoid properties.* Eur J Endocrinol 151:397–406.

Guo Z, Chen YZ, Xu RB, Fu H (1995) *Binding characteristics of glucocorticoid receptor in synaptic plasma membrane from rat brain.* Funct Neurol 10:183–194.

Haam J, Halmos KC, Muglia L, Tasker JG (2010) *Rapid synaptic modulation of hypothalamic neurons by glucocorticoids requires the glucocorticoid receptor.* In, Soc Neurosci Abstract, pp 389.19.

Hafezi-Moghadam A, Simoncini T, Yang Z, Limbourg FP, Plumier JC, Rebsamen MC, Hsieh CM, Chui DS, Thomas KL, Prorock AJ, Laubach VE, Moskowitz MA, French BA, Ley K, Liao JK (2002) *Acute cardiovascular protective effects of corticosteroids are mediated by non-transcriptional activation of endothelial nitric oxide synthase.* Nat Med 8:473–479.

Hager GL, McNally JG, Misteli T (2009) *Transcription dynamics.* Mol Cell 35:741–753.

Haller J, Halasz J, Mikics E, Kruk MR, Makara GB (2000) *Ultradian corticosterone rhythm and the propensity to behave aggressively in male rats.* J Neuroendocr 12:937–940.

Haller J, Mikics E, Makara GB (2008) *The effects of non-genomic glucocorticoid mechanisms on bodily functions and the central neural system. A critical evaluation of findings.* Front Neuroendocr 29:273–291.

Hammar P, Leroy P, Mahmutovic A, Marklund EG, Berg OG, Elf J (2012) *The lac repressor displays facilitated diffusion in living cells.* Science 336:1595–1598.

Hammes SR, Levin ER (2007) *Extranuclear steroid receptors: nature and actions.* Endocr Rev 28:726–741.

Harms GS, Cognet L, Lommerse PH, Blab GA, Schmidt T (2001) *Autofluorescent proteins in single-molecule research: applications to live cell imaging microscopy.* Biophys J 80:2396–2408.

Head BP, Insel PA (2007) *Do caveolins regulate cells by actions outside of caveolae?* Trends Cell Biol 17:51–57.

Heitzer MD, Wolf IM, Sanchez ER, Witchel SF, DeFranco DB (2007) *Glucocorticoid receptor physiology.* Rev Endocr Metab Disord 8:321–330.

Hellal-Levy C, Couette B, Fagart J, Souque A, Gomez-Sanchez C, Rafestin-Oblin M (1999) *Specific hydroxylations determine selective corticosteroid recognition by human glucocorticoid and mineralocorticoid receptors.* FEBS Lett 464:9–13.

Hellal-Levy C, Fagart J, Souque A, Rafestin-Oblin ME (2000) *Mechanistic aspects of mineralocorticoid receptor activation.* Kidney Int 57:1250–1255.

Henckens MJAG, van Wingen GA, Joëls M, Fernández G (2012) *Time-dependent effects of cortisol on selective attention and emotional interference: a functional MRI study.* Front Integr Neurosci 6:eCollection.

Hill MN, Karatsoreos IN, Hillard CJ, McEwen BS (2010) *Rapid elevations in limbic endocannabinoid content by glucocorticoid hormones in vivo.* Psychoneuroendocrinology 35:1333–1338.

Hinz B, Hirschelmann R (2000) *Rapid non-genomic feedback effects of glucocorticoids on CRF-induced ACTH secretion in rats.* Pharm Res 17:1273–1277.

Hirsh JK, Quandt FN (1996) *Down-regulation of Na channel expression by A23187 in NlE-115 neuroblastoma cells.* Brain Res 706:343–346.

Hoffman DA, Magee JC, Colbert CM, Johnston D (1997) *K+ channel regulation of signal propagation in dendrites of hippocampal pyramidal neurons.* Nature 387:869–875.

Holmes A, Wellman CL (2009) *Stress-induced prefrontal reorganization and executive dysfunction in rodents.* Neurosci Biobehav Rev 33:773–783.

Hori K, Nagai T, Izumi Y, Kimura M, Hasuike Y, Nakayama Y, Nanami M, Tokuyama M, Otaki Y, Kuragano T, Kohda Y, Obinata M, Kawahara K, Tanoue A, Tomita K, Nakanishi T, Nonoguchi H (2012) *Vasopressin V1a receptor is required for nucleocytoplasmic transport of mineralocorticoid receptor.* Am J Physiol - Ren Physiol 303:F1080–F1088.

Horwitz KB, Costlow ME, McGuire WL (1975) *MCF-7; a human breast cancer cell line with estrogen, androgen, progesterone, and glucocorticoid receptors.* Steroids 26:785–795.

Hoshi T, Aldrich R (1988) *Voltage-dependent K+ currents and underlying single K+ channels in pheochromocytoma cells.* J Gen Physiol 91:73.

Hu W, Zhang M, Czeh B, Flugge G, Zhang W (2010) *Stress impairs GABAergic network function in the hippocampus by activating nongenomic glucocorticoid receptors and affecting the integrity of the parvalbumin-expressing neuronal network.* Neuropsychopharmacology 35:1693–1707.

Huyet J, Pinon GM, Fay MR, Rafestin-Oblin ME, Fagart J (2012) *Structural determinants of ligand binding to the mineralocorticoid receptor.* Mol Cell Endocrinol 350:187–195.

Jamieson PM, Chapman KE, Edwards CR, Seckl JR (1995) *11 beta-hydroxysteroid dehydrogenase is an exclusive 11 beta- reductase in primary cultures of rat hepatocytes: effect of physicochemical and hormonal manipulations.* Endocrinology 136:4754–4761.

Joëls M (2008) *Functional actions of corticosteroids in the hippocampus.* Eur J Pharmacol 583:312–321.

Joëls M, de Kloet ER (1989) *Effects of glucocorticoids and norepinephrine on the excitability in the hippocampus.* Science 245:1502–1505.

Joëls M, de Kloet ER (1990) *Mineralocorticoid receptor-mediated changes in membrane properties of rat CA1 pyramidal neurons in vitro.* Proc Natl Acad Sci U S A 87:4495–4498.

Joëls M, Hesen W, de Kloet ER (1991) *Mineralocorticoid hormones suppress serotonin-induced hyperpolarization of rat hippocampal CA1 neurons.* J Neurosci 11:2288–2294.

Joëls M, Karst H, DeRijk R, de Kloet ER (2008) *The coming out of the brain mineralocorticoid receptor.* Trends Neurosci 31:1–7.

Joëls M, Pu Z, Wiegert O, Oitzl MS, Krugers HJ (2006) *Learning under stress: how does it work?* Trends Cogn Sci 10:152–158.

Joëls M, Sarabdjitsingh RA, Karst H (2012) *Unraveling the Time Domains of Corticosteroid Hormone Influences on Brain Activity: Rapid, Slow, and Chronic Modes.* Pharmacol Rev 64:901–938.

References

149

John S, Sabo PJ, Thurman RE, Sung MH, Biddie SC, Johnson TA, Hager GL, Stamatoyannopoulos JA (2011) *Chromatin accessibility pre-determines glucocorticoid receptor binding patterns.* Nat Genet 43:264–268.

Johnson LR, Farb C, Morrison JH, McEwen BS, LeDoux JE (2005) *Localization of glucocorticoid receptors at postsynaptic membranes in the lateral amygdala.* Neuroscience 136:289–299.

Johnson TA, Elbi C, Parekh BS, Hager GL, John S (2008) *Chromatin remodeling complexes interact dynamically with a glucocorticoid receptor-regulated promoter.* Mol Biol Cell 19:3308–3322.

Jones MT, Brush FR, Neame RL (1972) *Characteristics of fast feedback control of corticotrophin release by corticosteroids.* J Endocrinol 55:489–497.

Kaffman A, Meaney MJ (2007) *Neurodevelopmental sequelae of postnatal maternal care in rodents: clinical and research implications of molecular insights.* J Child Psychol Psychiatry 48:224–244.

Kaneko M, Hiroshige T (1978) *Fast, rate-sensitive corticosteroids negative feedback during stress.* Am J Physiol 234:R39–45.

Kao J, Salari K, Bocanegra M, Choi Y-L, Girard L, Gandhi J, Kwei KA, Hernandez-Boussard T, Wang P, Gazdar AF, Minna JD, Pollack JR (2009) *Molecular Profiling of Breast Cancer Cell Lines Defines Relevant Tumor Models and Provides a Resource for Cancer Gene Discovery.* PLoS ONE 4:e6146.

Karst H, Berger S, Erdmann G, Schutz G, Joëls M (2010) *Metaplasticity of amygdalar responses to the stress hormone corticosterone.* Proc Natl Acad Sci U A 107:14449–14454.

Karst H, Berger S, Turiault M, Tronche F, Schutz G, Joëls M (2005) *Mineralocorticoid receptors are indispensable for nongenomic modulation of hippocampal glutamate transmission by corticosterone.* Proc Natl Acad Sci 102:19204–19207.

Kasai RS, Suzuki KG, Prossnitz ER, Koyama-Honda I, Nakada C, Fujiwara TK, Kusumi A (2011) *Full characterization of GPCR monomer-dimer dynamic equilibrium by single molecule imaging.* J Cell Biol 192:463–480.

Kassel O, Herrlich P (2007) *Crosstalk between the glucocorticoid receptor and other transcription factors: molecular aspects.* Mol Cell Endocrinol 275:13–29.

Keijzer S de, Sergé A, Hemert F van, Lommerse PHM, Lamers GEM, Spaink HP, Schmidt T, Snaar-Jagalska BE (2008) *A spatially restricted increase in receptor mobility is involved in directional sensing during Dictyostelium discoideum chemotaxis.* J Cell Sci 121:1750–1757.

Keller-Wood M, Dallman MF (1984) *Corticosteroid Inhibition of ACTH Secretion.* Endocr Rev 5:1–24.

Khaksari M, Rashidy-Pour A, Vafaei AA (2007) *Central mineralocorticoid receptors are indispensable for corticosterone-induced impairment of memory retrieval in rats.* Neuroscience 149:729–738.

Kim JB, Ju JY, Kim JH, Kim TY, Yang BH, Lee YS, Son H (2004) *Dexamethasone inhibits proliferation of adult hippocampal neurogenesis in vivo and in vitro.* Brain Res 1027:1–10.

Kim JJ, Diamond DM (2002) *The stressed hippocampus, synaptic plasticity and lost memories.* Nat Rev Neurosci 3:453–462.

Kimura H, Cook PR (2001) *Kinetics of Core Histones in Living Human Cells Little Exchange of H3 and H4 and Some Rapid Exchange of H2b.* J Cell Biol 153:1341–1354.

Kitchener P, Di Blasi F, Borrelli E, Piazza PV (2004) *Differences between brain structures in nuclear translocation and DNA binding of the glucocorticoid receptor during stress and the circadian cycle.* Eur J Neurosci 19:1837–1846.

Klok MD, Giltay EJ, Van der Does AJ, Geleijnse JM, Antypa N, Penninx BW, de Geus EJ, Willemsen G, Boomsma DI, van Leeuwen N, Zitman FG, de Kloet ER, DeRijk RH (2011) *A common and functional mineralocorticoid receptor haplotype enhances optimism and protects against depression in females.* Transl Psychiatry 1:e62.

Komatsuzaki Y, Murakami G, Tsurugizawa T, Mukai H, Tanabe N, Mitsuhashi K, Kawata M, Kimoto T, Ooishi Y, Kawato S (2005) *Rapid spinogenesis of pyramidal neurons induced by activation of glucocorticoid receptors in adult male rat hippocampus.* Biochem Biophys Res Commun 335:1002–1007.

Koopmans WJA, Brehm A, Logie C, Schmidt T, van Noort J (2007) *Single-pair FRET microscopy reveals mononucleosome dynamics.* J Fluoresc 17:785–795.

Krug AW, Schuster C, Gassner B, Freudinger R, Mildenberger S, Troppmair J, Gekle M (2002) *Human epidermal growth factor receptor-1 expression renders Chinese hamster ovary cells sensitive to alternative aldosterone signaling.* J Biol Chem 277:45892–45897.

Krugers HJ, Hoogenraad CC, Groc L (2010) *Stress hormones and AMPA receptor trafficking in synaptic plasticity and memory.* Nat Rev Neurosci 11:675–681.

Kruk MR, Haller J, Meelis W, de Kloet ER (2013) *Mineralocorticoid receptor blockade during a rat's first violent encounter inhibits its subsequent propensity for violence.* Behav Neurosci 127:505–514.

Kumar P, Wu Q, Chambliss KL, Yuhanna IS, Mumby SM, Mineo C, Tall GG, Shaul PW (2007) *Direct Interactions with G alpha i and G betagamma mediate nongenomic signaling by estrogen receptor alpha.* Mol Endocrinol 21:1370–1380.

Kuningas M, DeRijk RH, Westendorp RGJ, Jolles J, Slagboom E, van Heemst D (2007) *Metal Performance in old age dependent on cortisol and genetic variance in the mineralocorticoid and glucocorticoid receptors.* Neuropsychopharmacology:1295–1301.

Lai M, Seckl J, Macleod M (2005) *Overexpression of the mineralocorticoid receptor protects against injury in PC12 cells.* Mol Brain Res 135:276–279.

Lajoie P, Partridge EA, Guay G, Goetz JG, Pawling J, Lagana A, Joshi B, Dennis JW, Nabi IR (2007) *Plasma membrane domain organization regulates EGFR signaling in tumor cells.* J Cell Biol 179:341–356.

Le Menuet D, Munier M, Campostrini G, Lombès M (2012) *Mineralocorticoid receptor and embryonic stem cell models: Molecular insights and pathophysiological relevance.* Mol Cell Endocrinol 350:216–222.

Lee RC, Feinbaum RL, Ambros V (1993) *The C.elegans heterochronic gene lin-4 encodes small RNAs with antisense complementarity to lin-14.* Cell 75:843–854.

Levin ER (2008) *Rapid signaling by steroid receptors.* Am J Physiol Regul Integr Comp Physiol 295:R1425–30.

Levin ER (2009) *Plasma membrane estrogen receptors.* Trends Endocrinol Metab 20:477–482.

Li GW, Elf J (2009) *Single molecule approaches to transcription factor kinetics in living cells.* FEBS Lett 583:3979–3983.

Li GW, Xie XS (2011) *Central dogma at the single-molecule level in living cells.* Nature 475:308–315.

Li Y, Suino K, Daugherty J, Xu HE (2005) *Structural and biochemical mechanisms for the specificity of hormone binding and coactivator assembly by mineralocorticoid receptor.* Mol Cell 19:367–380.

Lightman SL, Conway-Campbell BL (2010) *The crucial role of pulsatile activity of the HPA axis for continuous dynamic equilibration.* Nat Rev Neurosci 11:710–718.

Lightman SL, Wiles CC, Atkinson HC, Henley DE, Russell GM, Leendertz JA, McKenna MA, Spiga F, Wood SA, Conway-Campbell BL (2008) *The significance of glucocorticoid pulsatility.* Eur J Pharmacol 583:255–262.

Lima PA, Vicente MI, Alves FM, Dionísio JC, Costa PF (2008) *Insulin increases excitability via a dose-dependent dual inhibition of voltage-activated K⁺ currents in differentiated N1E-115 neuroblastoma cells.* Eur J Neurosci 27:2019–2032.

Liu L, Wang C, Ni X, Sun J (2007) *A rapid inhibition of NMDA receptor current by corticosterone in cultured hippocampal neurons.* Neurosci Lett 420:245–250.

Liu X, Chen YZ (1995) *Membrane-mediated inhibition of corticosterone on the release of arginine vasopressin from rat hypothalamic slices.* Brain Res 704:19–22.

Liu X, Wang CA, Chen YZ (1995) *Nongenomic effect of glucocorticoid on the release of arginine vasopressin from hypothalamic slices in rats.* Neuroendocrinology 62:628–633.

Liu XH, Zeng JW, Zhao YD, Chen PH, Xiao Z, Ruan HZ (2008) *Rapid inhibition of ATP-induced currents by corticosterone in rat dorsal root ganglion neurons.* Pharmacology 82:164–170.

Lommerse PH, Blab GA, Cognet L, Harms GS, Snaar-Jagalska BE, Spaink HP, Schmidt T (2004) *Single-molecule imaging of the H-ras membrane-anchor reveals domains in the cytoplasmic leaflet of the cell membrane.* Biophys J 86:609–616.

Lommerse PH, Vastenhoud K, Pirinen NJ, Magee AI, Spaink HP, Schmidt T (2006) *Single-molecule diffusion reveals similar mobility for the Lck, H-ras, and K-ras membrane anchors.* Biophys J 91:1090–1097.

Lommerse PHM, Snaar-Jagalska BE, Spaink HP, Schmidt T (2005) *Single-molecule diffusion measurements of H-Ras at the plasma membrane of live cells reveal microdomain localization upon activation.* J Cell Sci 118:1799–1809.

Lord SJ, Lee HL, Moerner WE (2010) *Single-molecule spectroscopy and imaging of biomolecules in living cells.* Anal Chem 82:2192–2203.

Lu ML, Schneider MC, Zheng Y, Zhang X, Richie JP (2001) *Caveolin-1 interacts with androgen receptor. A positive modulator of androgen receptor mediated transactivation.* J Biol Chem 276:13442–13451.

MacLusky N., Chalmers-Redman R, Kay G, Ju W, Nethrapalli I., Tatton W. (2003) *Ovarian steroids reduce apoptosis induced by trophic insufficiency in nerve growth factor-differentiated pc12 cells and axotomized rat facial motoneurons.* Neuroscience 118:741–754.

Maggio N, Segal M (2009) *Differential corticosteroid modulation of inhibitory synaptic currents in the dorsal and ventral hippocampus.* J Neurosci 29:2857–2866.

Maier C, Runzler D, Schindelar J, Grabner G, Waldhausl W, Kohler G, Luger A (2005) *G-protein-coupled glucocorticoid receptors on the pituitary cell membrane.* J Cell Sci 118:3353–3361.

Malcher-Lopes R, Di S, Marcheselli VS, Weng FJ, Stuart CT, Bazan NG, Tasker JG (2006) *Opposing crosstalk between leptin and glucocorticoids rapidly modulates synaptic excitation via endocannabinoid release.* J Neurosci 26:6643–6650.

Martinez F, Mansego ML, Escudero JC, Redon J, Chaves FJ (2009) *Association of a Mineralocorticoid Receptor Gene Polymorphism With Hypertension in a Spanish Population.* Am J Hypertens 22:649–655.

Martin-Fernandez ML, Tynan CJ, Webb SED (2013) *A "pocket guide" to total internal reflection fluorescence.* J Microsc 252:16–22.

Matthews L, Berry A, Ohanian V, Ohanian J, Garside H, Ray D (2008) *Caveolin mediates rapid glucocorticoid effects and couples glucocorticoid action to the antiproliferative program.* Mol Endocrinol 22:1320–1330.

Mazza D, Stasevich TJ, Karpova TS, McNally JG (2012) *Monitoring dynamic binding of chromatin proteins in vivo by fluorescence correlation spectroscopy and temporal image correlation spectroscopy.* Methods Mol Biol 833:177–200.

McCrossan ZA, Lewis A, Panaghie G, Jordan PN, Christini DJ, Lerner DJ, Abbott GW (2003) *MinK-Related Peptide 2 Modulates Kv2.1 and Kv3.1 Potassium Channels in Mammalian Brain.* J Neurosci 23:8077–8091.

McEwen BS (2001) *Plasticity of the hippocampus: adaptation to chronic stress and allostatic load.* Ann N Acad Sci 933:265–277.

McEwen BS (2008) *Central effects of stress hormones in health and disease: Understanding the protective and damaging effects of stress and stress mediators.* Eur J Pharmacol 583:174–185.

McGaugh JL (2013) *Making lasting memories: Remembering the significant.* Proc Natl Acad Sci 110:10402–10407.

McNally JG, Muller WG, Walker D, Wolford R, Hager GL (2000) *The glucocorticoid receptor: rapid exchange with regulatory sites in living cells.* Science 287:1262–1265.

McReynolds JR, Donowho K, Abdi A, McGaugh JL, Roozendaal B, McIntyre CK (2010) *Memory-enhancing corticosterone treatment increases amygdala norepinephrine and Arc protein expression in hippocampal synaptic fractions.* Neurobiol Learn Mem 93:312–321.

Meijsing SH, Elbi C, Luecke HF, Hager GL, Yamamoto KR (2007) *The ligand binding domain controls glucocorticoid receptor dynamics independent of ligand release.* Mol Cell Biol 27:2442–2451.

Meijsing SH, Pufall MA, So AY, Bates DL, Chen L, Yamamoto KR (2009) *DNA binding site sequence directs glucocorticoid receptor structure and activity.* Science 324:407–410.

Métivier R, Penot G, Hübner MR, Reid G, Brand H, Koš M, Gannon F (2003) *Estrogen Receptor-α Directs Ordered, Cyclical, and Combinatorial Recruitment of Cofactors on a Natural Target Promoter.* Cell 115:751–763.

Micevych P, Dominguez R (2009) *Membrane estradiol signaling in the brain.* Front Neuroendocr 30:315–327.

Mihailidou AS, Funder JW (2005) *Nongenomic effects of mineralocorticoid receptor activation in the cardiovascular system.* Steroids 70:347–351.

Mikics E, Barsy B, Barsvari B, Haller J (2005) *Behavioral specificity of non-genomic glucocorticoid effects in rats: effects on risk assessment in the elevated plus-maze and the open-field.* Horm Behav 48:152–162.

Mikics E, Kruk MR, Haller J (2004) *Genomic and non-genomic effects of glucocorticoids on aggressive behavior in male rats.* Psychoneuroendocrinology 29:618–635.

Mirescu C, Gould E (2006) *Stress and adult neurogenesis.* Hippocampus 16:233–238.

Mitra R, Sapolsky RM (2008) *Acute corticosterone treatment is sufficient to induce anxiety and amygdaloid dendritic hypertrophy.* Proc Natl Acad Sci U A 105:5573–5578.

Morsink MC, Joëls M, Sarabdjitsingh RA, Meijer OC, De Kloet ER, Datson NA (2006) *The dynamic pattern of glucocorticoid receptor-mediated transcriptional responses in neuronal PC12 cells.* J Neurochem 99:1282–1298.

Mueller F, Mazza D, Stasevich TJ, McNally JG (2010) *FRAP and kinetic modeling in the analysis of nuclear protein dynamics: what do we really know?* Curr Opin Cell Biol 22:403–411.

Mueller F, Stasevich TJ, Mazza D, McNally JG (2013) *Quantifying transcription factor kinetics: At work or at play?* Crit Rev Biochem Mol Biol 48:492–514.

Mueller F, Wach P, McNally JG (2008) *Evidence for a common mode of transcription factor interaction with chromatin as revealed by improved quantitative fluorescence recovery after photobleaching.* Biophys J 94:3323–3339.

Munck A, Foley R (1976) *Kinetics of glucocorticoid-receptor complexes in rat thymus cells.* J Steroid Biochem 7:1117–1122.

Munier M, Law F, Meduri G, Le Menuet D, Lombès M (2012) *Mineralocorticoid Receptor Overexpression Facilitates Differentiation and Promotes Survival of Embryonic Stem Cell-Derived Neurons.* Endocrinology 153:1330–1340.

Murase K, Fujiwara T, Umemura Y, Suzuki K, Iino R, Yamashita H, Saito M, Murakoshi H, Ritchie K, Kusumi A (2004) *Ultrafine Membrane Compartments for Molecular Diffusion as Revealed by Single Molecule Techniques.* Biophys J 86:4075–4093.

Mutoh A, Isshiki M, Fujita T (2008) *Aldosterone enhances ligand-stimulated nitric oxide production in endothelial cells.* Hypertens Res 31:1811–1820.

Nagaich AK, Walker DA, Wolford R, Hager GL (2004) *Rapid Periodic Binding and Displacement of the Glucocorticoid Receptor during Chromatin Remodeling.* Mol Cell 14:163–174.

Nishi M, Noriko HH, Kawata M (2011) *Intranuclear dynamics of corticosteroid receptors and effects of proteasomal activity in cultured hippocampal neural cells.* Neurosci Lett 494:65–69.

Nishi M, Ogawa H, Ito T, Matsuda KI, Kawata M (2001) *Dynamic changes in subcellular localization of mineralocorticoid receptor in living cells: in comparison with glucocorticoid receptor using dual-color labeling with green fluorescent protein spectral variants.* Mol Endocrinol 15:1077–1092.

Nishi M, Tanaka M, Matsuda K, Sunaguchi M, Kawata M (2004) *Visualization of glucocorticoid receptor and mineralocorticoid receptor interactions in living cells with GFP-based fluorescence resonance energy transfer.* J Neurosci Off J Soc Neurosci 24:4918–4927.

Nixon M, Andrew R, Chapman KE (2013) *It takes two to tango: Dimerisation of glucocorticoid receptor and its anti-inflammatory functions.* Steroids 78:59–68.

Oitzl MS, Champagne DL, van der Veen R, de Kloet ER (2010) *Brain development under stress: hypotheses of glucocorticoid actions revisited.* Neurosci Biobehav Rev 34:853–866.

Oitzl MS, de Kloet ER (1992) *Selective corticosteroid antagonists modulate specific aspects of spatial orientation learning.* Behav Neurosci 106:62–71.

Oitzl MS, Reichardt HM, Joëls M, de Kloet ER (2001) *Point mutation in the mouse glucocorticoid receptor preventing DNA binding impairs spatial memory.* Proc Natl Acad Sci 98:12790–12795.

Olijslagers JE, de Kloet ER, Elgersma Y, van Woerden GM, Joëls M, Karst H (2008) *Rapid changes in hippocampal CA1 pyramidal cell function via pre- as well as postsynaptic membrane mineralocorticoid receptors.* Eur J Neurosci 27:2542–2550.

Orchinik M, Hastings N, Witt D, McEwen BS (1997) *High-affinity binding of corticosterone to mammalian neuronal membranes: possible role of corticosteroid binding globulin.* J Steroid Biochem Mol Biol 60:229–236.

Orchinik M, Matthews L, Gasser PJ (2000) *Distinct specificity for corticosteroid binding sites in amphibian cytosol, neuronal membranes, and plasma.* Gen Comp Endocrinol 118:284–301.

Orchinik M, Murray TF, Franklin PH, Moore FL (1992) *Guanyl nucleotides modulate binding to steroid receptors in neuronal membranes.* Proc Natl Acad Sci U A 89:3830–3834.

Orchinik M, Murray TF, Moore FL (1991) *A corticosteroid receptor in neuronal membranes.* Science 252:1848–1851.

Owen DM, Williamson D, Rentero C, Gaus K (2009) *Quantitative Microscopy: Protein Dynamics and Membrane Organisation.* Traffic 10:962–971.

Pannaccione A, Boscia F, Scorziello A, Adornetto A, Castaldo P, Sirabella R, Taglialatela M, Renzo GFD, Annunziato L (2007) *Up-Regulation and Increased Activity of KV3.4 Channels and Their Accessory Subunit MinK-Related Peptide 2 Induced by Amyloid Peptide Are Involved in Apoptotic Neuronal Death.* Mol Pharmacol 72:665–673.

Pannaccione A, Secondo A, Scorziello A, Calì G, Taglialatela M, Annunziato L (2005) *Nuclear factor-κB activation by reactive oxygen species mediates voltage-gated K+ current enhancement by neurotoxic β-amyloid peptides in nerve growth factor-differentiated PC-12 cells and hippocampal neurones: Nuclear factor-κB and K+ channels in neuronal cell death.* J Neurochem 94:572–586.

Pascual-Le Tallec L, Lombès M (2005) *The Mineralocorticoid Receptor: A Journey Exploring Its Diversity and Specificity of Action.* Mol Endocrinol 19:2211–2221.

Pasricha N, Joëls M, Karst H (2011) *Rapid effects of corticosterone in the mouse dentate gyrus via a nongenomic pathway.* J Neuroendocr 23:143–147.

Pavlides C, Watanabe Y, McEwen BS (1993) *Effects of glucocorticoids on hippocampal long-term potentiation.* Hippocampus 3:183–192.

Pearce D, Yamamoto KR (1993) *Mineralocorticoid and Glucocorticoid Receptor activities distinguished by nonreceptor factors at a composite response element.* Science 259:1161–1165.

Pedram A, Razandi M, Sainson RC, Kim JK, Hughes CC, Levin ER (2007) *A conserved mechanism for steroid receptor translocation to the plasma membrane.* J Biol Chem 282:22278–22288.

Perlmann T, Eriksson P, Wrange O (1990) *Quantitative analysis of the glucocorticoid receptor-DNA interaction at the mouse mammary tumor virus glucocorticoid response element.* J Biol Chem 265:17222–17229.

Persson F, Barkefors I, Elf J (2013) *Single molecule methods with applications in living cells.* Curr Opin Biotechnol 24:737–744.

Picard D (2006) *Chaperoning steroid hormone action.* Trends Endocrinol Metab 17:229–235.

Pippal JB, Fuller PJ (2008) *Structure-function relationships in the mineralocorticoid receptor.* J Mol Endocrinol 41:405–413.

References

155

Pojoga LH, Adamova Z, Kumar A, Stennett AK, Romero JR, Adler GK, Williams GH, Khalil RA (2010a) *Sensitivity of NOS-dependent vascular relaxation pathway to mineralocorticoid receptor blockade in caveolin-1-deficient mice.* Am J Physiol Heart Circ Physiol 298:H1776–88.

Pojoga LH, Romero JR, Yao TM, Loutraris P, Ricchiuti V, Coutinho P, Guo C, Lapointe N, Stone JR, Adler GK, Williams GH (2010b) *Caveolin-1 ablation reduces the adverse cardiovascular effects of N-omega-nitro-L-arginine methyl ester and angiotensin II.* Endocrinology 151:1236–1246.

Polman JA, de Kloet ER, Datson NA (2013) *Two populations of glucocorticoid receptor-binding sites in the male rat hippocampal genome.* Endocrinology 154:1832–1844.

Polman JA, Welten JE, Bosch DS, de Jonge RT, Balog J, van der Maarel SM, de Kloet ER, Datson NA (2012) *A genome-wide signature of glucocorticoid receptor binding in neuronal PC12 cells.* BMC Neurosci 13:118.

Popoli M, Yan Z, McEwen BS, Sanacora G (2011) *The stressed synapse: the impact of stress and glucocorticoids on glutamate transmission.* Nat Rev Neurosci 13:22–37.

Prager EM, Brielmaier J, Bergstrom HC, McGuire J, Johnson LR (2010) *Localization of mineralocorticoid receptors at mammalian synapses.* PLoS One 5:e14344.

Prager EM, Brielmaier J, Johnson LR (2009) *Anatomical evidence for extra nuclear mineralocorticoid receptors.* Poster Annu Soc Neurosci Meet:poster 866.

Prager EM, Johnson LR (2009) *Stress at the synapse: signal transduction mechanisms of adrenal steroids at neuronal membranes.* Sci Signal 2:re5.

Qi AQ, Qiu J, Xiao L, Chen YZ (2005) *Rapid activation of JNK and p38 by glucocorticoids in primary cultured hippocampal cells.* J Neurosci Res 80:510–517.

Qiu J, Wang P, Jing Q, Zhang W, Li X, Zhong Y, Sun G, Pei G, Chen Y (2001) *Rapid activation of ERK1/2 mitogen-activated protein kinase by corticosterone in PC12 cells.* Biochem Biophys Res Commun 287:1017–1024.

Qiu S, Champagne DL, Peters M, Catania EH, Weeber EJ, Levitt P, Pimenta AF (2010) *Loss of limbic system-associated membrane protein leads to reduced hippocampal mineralocorticoid receptor expression, impaired synaptic plasticity, and spatial memory deficit.* Biol Psychiatry 68:197–204.

Quandt FN (1988) *Three kinetically distinct potassium channels in mouse neuroblastoma cells.* J Physiol 395:401–418.

Quinkler M, Meyer B, Bumke-Vogt C, Grossmann C, Gruber U, Oelkers W, Diederich S, Bahr V (2002) *Agonistic and antagonistic properties of progesterone metabolites at the human mineralocorticoid receptor.* Eur J Endocrinol 146:789–799.

Ratman D, Vanden Berghe W, Dejager L, Libert C, Tavernier J, Beck IM, De Bosscher K (2013) *How glucocorticoid receptors modulate the activity of other transcription factors: A scope beyond tethering.* Mol Cell Endocrinol 380:41–54.

Rayasam GV, Elbi C, Walker DA, Wolford R, Fletcher TM, Edwards DP, Hager GL (2005) *Ligand-specific dynamics of the progesterone receptor in living cells and during chromatin remodeling in vitro.* Mol Cell Biol 25:2406–2418.

Razandi M, Alton G, Pedram A, Ghonshani S, Webb P, Levin ER (2003) *Identification of a structural determinant necessary for the localization and function of estrogen receptor alpha at the plasma membrane.* Mol Cell Biol 23:1633–1646.

Razandi M, Oh P, Pedram A, Schnitzer J, Levin ER (2002) *ERs associate with and regulate the production of caveolin: implications for signaling and cellular actions.* Mol Endocrinol 16:100–115.

Razandi M, Pedram A, Levin ER (2010) *Heat shock protein 27 is required for sex steroid receptor trafficking to and functioning at the plasma membrane.* Mol Cell Biol 30:3249–3261.

Reddy TE, Pauli F, Sprouse RO, Neff NF, Newberry KM, Garabedian MJ, Myers RM (2009) *Genomic determination of the glucocorticoid response reveals unexpected mechanisms of gene regulation.* Genome Res 19:2163–2171.

Reichardt HM, Kaestner KH, Tuckermann J, Kretz O, Wessely O, Bock R, Gass P, Schmid W, Herrlich P, Angel P, Schutz G (1998) *DNA binding of the glucocorticoid receptor is not essential for survival.* Cell 93:531–541.

Ren J, Wen L, Gao X, Jin C, Xue Y, Yao X (2008) *CSS-Palm 2.0: an updated software for palmitoylation sites prediction.* Protein Eng Sel 21:639–644.

Rettig J, Heinemann SH, Wunder F, Lorra C, Parcej DN, Oliver Dolly J, Pongs O (1994) *Inactivation properties of voltage-gated K+ channels altered by presence of β-subunit.* Nature 369:289–294.

Reul JM, de Kloet ER (1985) *Two receptor systems for corticosterone in rat brain: microdistribution and differential occupation.* Endocrinology 117:2505–2511.

Reul JM, De Kloet ER, Van Sluijs FJ, Rijnberk A, Rothuizen J (1990) *Binding Characteristics of Mineralocorticoid and Glucocorticoid Receptors in Dog Brain and Pituitary.* Endocrinology 127:907–915.

Reul JM, Gesing A, Droste S, Stec IS, Weber A, Bachmann C, Bilang-Bleuel A, Holsboer F, Linthorst AC (2000) *The brain mineralocorticoid receptor: greedy for ligand, mysterious in function.* Eur J Pharmacol 405:235–249.

Ries J, Schwille P (2012) *Fluorescence correlation spectroscopy.* BioEssays 34:361–368.

Rigaud G, Roux J, Pictet R, Grange T (1991) *In vivo footprinting of rat TAT gene: Dynamic interplay between the glucocorticoid receptor and a liver-specific factor.* Cell 67:977–986.

Ritter JG, Veith R, Veenendaal A, Siebrasse JP, Kubitscheck U (2010) *Light Sheet Microscopy for Single Molecule Tracking in Living Tissue Langowski J, ed.* PLoS ONE 5:e11639.

Roozendaal B, Hernandez A, Cabrera SM, Hagewoud R, Malvaez M, Stefanko DP, Haettig J, Wood MA (2010) *Membrane-associated glucocorticoid activity is necessary for modulation of long-term memory via chromatin modification.* J Neurosci 30:5037–5046.

Roozendaal B, McEwen BS, Chattarji S (2009) *Stress, memory and the amygdala.* Nat Rev Neurosci 10:423–433.

Roozendaal B, Okuda S, Van der Zee EA, McGaugh JL (2006) *Glucocorticoid enhancement of memory requires arousal-induced noradrenergic activation in the basolateral amygdala.* Proc Natl Acad Sci U A 103:6741–6746.

Roozendaal B, Quirarte GL, McGaugh JL (2002) *Glucocorticoids interact with the basolateral amygdala beta-adrenoceptor--cAMP/cAMP/PKA system in influencing memory consolidation.* Eur J Neurosci 15:553–560.

Rupprecht R, Reul JM, van Steensel B, Spengler D, Soder M, Berning B, Holsboer F, Damm K (1993) *Pharmacological and functional characterization of human mineralocorticoid and glucocorticoid receptor ligands.* Eur J Pharmacol 247:145–154.

Sajadi AA, Samaei SA, Rashidy-Pour A (2007) *Blocking effects of intra-hippocampal naltrexone microinjections on glucocorticoid-induced impairment of spatial memory retrieval in rats.* Neuropharmacology 52:347–354.

Sako Y, Minoghchi S, Yanagida T (2000) *Single-molecule imaging of EGFR signalling on the surface of living cells.* Nat Cell Biol 2:168–172.

Salatino M, Beguelin W, Peters MG, Carnevale R, Proietti CJ, Galigniana MD, Vedoy CG, Schillaci R, Charreau EH, Sogayar MC, Elizalde PV (2006) *Progestin-induced caveolin-1 expression mediates breast cancer cell proliferation.* Oncogene 25:7723–7739.

Sanchez AM, Flamini MI, Zullino S, Gopal S, Genazzani AR, Simoncini T (2011) *Estrogen receptor-{alpha} promotes endothelial cell motility through focal adhesion kinase.* Mol Hum Reprod 17:219–226.

Sanderson JM (2012) *Resolving the kinetics of lipid, protein and peptide diffusion in membranes.* Mol Membr Biol 29:118–143.

Sandi C, Rose SP (1994) *Corticosteroid receptor antagonists are amnestic for passive avoidance learning in day-old chicks.* Eur J Neurosci 6:1292–1297.

Sandi C, Venero C, Guaza C (1996a) *Novelty-related rapid locomotor effects of corticosterone in rats.* Eur J Neurosci 8:794–800.

Sandi C, Venero C, Guaza C (1996b) *Nitric oxide synthesis inhibitors prevent rapid behavioral effects of corticosterone in rats.* Neuroendocrinology 63:446–453.

Sarabdjitsingh RA, Conway-Campbell BL, Leggett JD, Waite EJ, Meijer OC, de Kloet ER, Lightman SL (2010) *Stress responsiveness varies over the ultradian glucocorticoid cycle in a brain-region-specific manner.* Endocrinology 151:5369–5379.

Sarabdjitsingh RA, Joëls M, de Kloet ER (2012) *Glucocorticoid pulsatility and rapid corticosteroid actions in the central stress response.* Physiol Behav 106:73–80.

Sarabdjitsingh RA, Meijer OC, Schaaf MJM, de Kloet ER (2009) *Subregion-specific differences in translocation patterns of mineralocorticoid and glucocorticoid receptors in rat hippocampus.* Brain Res 1249:43–53.

Sato A, Funder JW (1996) *High glucose stimulates aldosterone-induced hypertrophy via type I mineralocorticoid receptors in neonatal rat cardiomyocytes.* Endocrinology 137:4145–4153.

Sato S, Osanai H, Monma T, Harada T, Hirano A, Saito M, Kawato S (2004) *Acute effect of corticosterone on N-methyl-D-aspartate receptor-mediated Ca2+ elevation in mouse hippocampal slices.* Biochem Biophys Res Commun 321:510–513.

Schaaf MJ, Cidlowski JA (2003) *Molecular determinants of glucocorticoid receptor mobility in living cells: the importance of ligand affinity.* Mol Cell Biol 23:1922–1934.

Schaaf MJ, Koopmans WJ, Meckel T, van Noort J, Snaar-Jagalska BE, Schmidt TS, Spaink HP (2009) *Single-molecule microscopy reveals membrane microdomain organization of cells in a living vertebrate.* Biophys J 97:1206–1214.

Schaaf MJ, Lewis-Tuffin LJ, Cidlowski JA (2005) *Ligand-selective targeting of the glucocorticoid receptor to nuclear subdomains is associated with decreased receptor mobility.* Mol Endocrinol 19:1501–1515.

Schaaf MJ, Willetts L, Hayes BP, Maschera B, Stylianou E, Farrow SN (2006) *The relationship between intranuclear mobility of the NF-kappaB subunit p65 and its DNA binding affinity.* J Biol Chem 281:22409–22420.

Schmidt KL, Malisch JL, Breuner CW, Soma KK (2010) *Corticosterone and cortisol binding sites in plasma, immune organs and brain of developing zebra finches: intracellular and membrane-associated receptors.* Brain Behav Immun 24:908–918.

Schmidt T, Schutz GJ, Baumgartner W, Gruber HJ, Schindler H (1996) *Imaging of single molecule diffusion.* Proc Natl Acad Sci U A 93:2926–2929.

Schrader LA, Birnbaum SG, Nadin BM, Ren Y, Bui D, Anderson AE, Sweatt JD (2006) *ERK/MAPK regulates the Kv4.2 potassium channel by direct phosphorylation of the pore-forming subunit.* Am J Physiol - Cell Physiol 290:C852–C861.

Schutz GJ, Schindler H, Schmidt T (1997) *Single-molecule microscopy on model membranes reveals anomalous diffusion.* Biophys J 73:1073–1080.

Schwabe L, Schächinger H, de Kloet ER, Oitzl MS (2010) *Corticosteroids Operate as a Switch between Memory Systems.* J Cogn Neurosci 22:1362–1372.

Sekiya T, Muthurajan UM, Luger K, Tulin AV, Zaret KS (2009) *Nucleosome-binding affinity as a primary determinant of the nuclear mobility of the pioneer transcription factor FoxA.* Genes Dev 23:804–809.

Semrau S, Schmidt T (2007) *Particle image correlation spectroscopy (PICS): retrieving nanometer-scale correlations from high-density single-molecule position data.* Biophys J 92:613–621.

Serge A, de Keijzer S, Van Hemert F, Hickman MR, Hereld D, Spaink HP, Schmidt T, Snaar-Jagalska BE (2011) *Quantification of GPCR internalization by single-molecule microscopy in living cells.* Integr Biol 3:675–683.

Silverman MN, Sternberg EM (2012) *Glucocorticoid regulation of inflammation and its functional correlates: from HPA axis to glucocorticoid receptor dysfunction: Glucocorticoid resistance in inflammatory disease.* Ann N Y Acad Sci 1261:55–63.

Simoncini T, Hafezi-Moghadam A, Brazil DP, Ley K, Chin WW, Liao JK (2000) *Interaction of oestrogen receptor with the regulatory subunit of phosphatidylinositol-3-OH kinase.* Nature 407:538–541.

Simons SS, Kumar R (2013) *Variable steroid receptor responses: Intrinsically disordered AF1 is the key.* Mol Cell Endocrinol 376:81–84.

Snaar-Jagalska BE, Cambi A, Schmidt T, de Keijzer S (2013) *Single-molecule imaging technique to study the dynamic regulation of GPCR function at the plasma membrane.* Methods Enzymol 521:47–67.

Sõber S, Laan M, Annilo T (2010) *MicroRNAs miR-124 and miR-135a are potential regulators of the mineralocorticoid receptor gene (NR3C2) expression.* Biochem Biophys Res Commun 391:727–732.

Solito E, Mulla A, Morris JF, Christian HC, Flower RJ, Buckingham JC (2003) *Dexamethasone induces rapid serine-phosphorylation and membrane translocation of annexin 1 in a human folliculostellate cell line via a novel nongenomic mechanism involving the glucocorticoid receptor, protein kinase C, phosphatidylinositol 3-kinase, and mitogen-activated protein kinase.* Endocrinology 144:1164–1174.

Song RX-D, Chen Y, Zhang Z, Bao Y, Yue W, Wang J-P, Fan P, Santen RJ (2010) *Estrogen utilization of IGF-1-R and EGF-R to signal in breast cancer cells.* J Steroid Biochem Mol Biol 118:219–230.

References

Souza RR, Dal Bó S, de Kloet ER, Oitzl MS, Carobrez AP (2014) *Paradoxical mineralocorticoid receptor-mediated effect in fear memory encoding and expression of rats submitted to an olfactory fear conditioning task.* Neuropharmacology 79:201–211.

Spies CM, Schaumann DH, Berki T, Mayer K, Jakstadt M, Huscher D, Wunder C, Burmester GR, Radbruch A, Lauster R, Scheffold A, Buttgereit F (2006) *Membrane glucocorticoid receptors are down regulated by glucocorticoids in patients with systemic lupus erythematosus and use a caveolin-1-independent expression pathway.* Ann Rheum Dis 65:1139–1146.

Stasevich TJ, Mueller F, Brown DT, McNally JG (2010a) *Dissecting the binding mechanism of the linker histone in live cells: an integrated FRAP analysis.* Embo J 29:1225–1234.

Stasevich TJ, Mueller F, Michelman-Ribeiro A, Rosales T, Knutson JR, McNally JG (2010b) *Cross-validating FRAP and FCS to quantify the impact of photobleaching on* in vivo *binding estimates.* Biophys J 99:3093–3101.

Stavreva DA, Muller WG, Hager GL, Smith CL, McNally JG (2004) *Rapid glucocorticoid receptor exchange at a promoter is coupled to transcription and regulated by chaperones and proteasomes.* Mol Cell Biol 24:2682–2697.

Stavreva DA, Wiench M, John S, Conway-Campbell BL, McKenna MA, Pooley JR, Johnson TA, Voss TC, Lightman SL, Hager GL (2009) *Ultradian hormone stimulation induces glucocorticoid receptor-mediated pulses of gene transcription.* Nat Cell Biol 11:1093–1102.

Stenoien DL, Mancini MG, Patel K, Allegretto EA, Smith CL, Mancini MA (2000) *Subnuclear trafficking of estrogen receptor-alpha and steroid receptor coactivator-1.* Mol Endocrinol 14:518–534.

Stenoien DL, Patel K, Mancini MG, Dutertre M, Smith CL, O'Malley BW, Mancini MA (2001) *FRAP reveals that mobility of oestrogen receptor-alpha is ligand- and proteasome-dependent.* Nat Cell Biol 3:15–23.

Strähle U, Klock G, Schütz G (1987) *A DNA sequence of 15 base pairs is sufficient to mediate both glucocorticoid and progesterone induction of gene expression.* Proc Natl Acad Sci 84:7871–7875.

Sud N, Wiseman DA, Black SM (2010) *Caveolin 1 is required for the activation of endothelial nitric oxide synthase in response to 17beta-estradiol.* Mol Endocrinol 24:1637–1649.

Suzuki K, Ritchie K, Kajikawa E, Fujiwara T, Kusumi A (2005) *Rapid hop diffusion of a G-protein-coupled receptor in the plasma membrane as revealed by single-molecule techniques.* Biophys J 88:3659–3680.

Sze PY, Iqbal Z (1994) *Regulation of calmodulin content in synaptic plasma membranes by glucocorticoids.* Neurochem Res 19:1455–1461.

Takahashi T, Kimoto T, Tanabe N, Hattori TA, Yasumatsu N, Kawato S (2002) *Corticosterone acutely prolonged N-methyl-d-aspartate receptor-mediated Ca2+ elevation in cultured rat hippocampal neurons.* J Neurochem 83:1441–1451.

Tanaka M, Nishi M, Morimoto M, Sugimoto T, Kawata M (2003) *Yellow fluorescent protein-tagged and cyan fluorescent protein-tagged imaging analysis of glucocorticoid receptor and importins in single living cells.* Endocrinology 144:4070–4079.

Tasker JG (2006) *Rapid glucocorticoid actions in the hypothalamus as a mechanism of homeostatic integration.* Obes Silver Spring 14 Suppl 5:259S–265S.

Tasker JG, Di S, Malcher-Lopes R (2006) *Minireview: rapid glucocorticoid signaling via membrane-associated receptors.* Endocrinology 147:5549–5556.

Tasker JG, Herman JP (2011) *Mechanisms of rapid glucocorticoid feedback inhibition of the hypothalamic-pituitary-adrenal axis.* Stress 14:398–406.

Tierney T, Christian HC, Morris JF, Solito E, Buckingham JC (2003) *Evidence from studies on co-cultures of TtT/GF and AtT20 cells that Annexin 1 acts as a paracrine or juxtacrine mediator of the early inhibitory effects of glucocorticoids on ACTH release.* J Neuroendocrinol 15:1134–1143.

Tirard M, Almeida OFX, Hutzler P, Melchior F, Michaelidis TM (2007) *Sumoylation and proteasomal activity determine the transactivation properties of the mineralocorticoid receptor.* Mol Cell Endocrinol 268:20–29.

Tokunaga M, Imamoto N, Sakata-Sogawa K (2008) *Highly inclined thin illumination enables clear single-molecule imaging in cells.* Nat Methods 5:159–161.

Toomre D (2012) *Cellular Imaging Using Total Internal Reflection Fluorescence Microscopy: Theory and Instrumentation.* Cold Spring Harb Protoc 2012:pdb.top068650.

Toonen RF, Kochubey O, de Wit H, Gulyas-Kovacs A, Konijnenburg B, Sørensen JB, Klingauf J, Verhage M (2006) *Dissecting docking and tethering of secretory vesicles at the target membrane.* EMBO J 25:3725–3737.

Trapp T, Rupprecht R, Castren M, Reul JM, Holsboer F (1994) *Heterodimerization between mineralocorticoid and glucocorticoid receptor: a new principle of glucocorticoid action in the CNS.* Neuron 13:1457–1462.

Ulrich-Lai YM, Herman JP (2009) *Neural regulation of endocrine and autonomic stress responses.* Nat Rev Neurosci 10:397–409.

Vacher H, Mohapatra DP, Trimmer JS (2008) *Localization and Targeting of Voltage-Dependent Ion Channels in Mammalian Central Neurons.* Physiol Rev 88:1407–1447.

Vale RD, Funatsu T, Pierce DW, Romberg L, Harada Y, Yanagida T (1996) *Direct observation of single kinesin molecules moving along microtubules.* Nature 380:451–453.

Van Ast VA, Cornelisse S, Meeter M, Joëls M, Kindt M (2013) *Time-Dependent Effects of Cortisol on the Contextualization of Emotional Memories.* Biol Psychiatry 74:809–816.

Van de Wijngaart DJ, Dubbink HJ, van Royen ME, Trapman J, Jenster G (2012) *Androgen receptor coregulators: Recruitment via the coactivator binding groove.* Mol Cell Endocrinol 352:57–69.

Van den Broek B, Lomholt MA, Kalisch SM, Metzler R, Wuite GJ (2008) *How DNA coiling enhances target localization by proteins.* Proc Natl Acad Sci USA 105:15738–15742.

Van Leeuwen N, Bellingrath S, de Kloet ER, Zitman FG, DeRijk RH, Kudielka BM, Wust S (2011) *Human mineralocorticoid receptor (MR) gene haplotypes modulate MR expression and transactivation: implication for the stress response.* Psychoneuroendocrinology 36:699–709.

Van Leeuwen N, Caprio M, Blaya C, Fumeron F, Sartorato P, Ronconi V, Giacchetti G, Mantero F, Fernandes-Rosa FL, Simian C, Peyrard S, Zitman FG, Penninx BWJH, de Kloet ER, Azizi M, Jeunemaitre X, DeRijk RH, Zennaro M-C (2010a) *The Functional c.-2G>C Variant of the Mineralocorticoid Receptor Modulates Blood Pressure, Renin, and Aldosterone Levels.* Hypertension 56:995–1002.

Van Leeuwen N, Kumsta R, Entringer S, de Kloet ER, Zitman FG, DeRijk RH, Wüst S (2010b) *Functional mineralocorticoid receptor (MR) gene variation influences the cortisol awakening response after dexamethasone.* Psychoneuroendocrinology 35:339–349.

References

Van Royen ME, Dinant C, Farla P, Trapman J, Houtsmuller AB (2009a) *FRAP and FRET methods to study nuclear receptors in living cells.* Methods Mol Biol 505:69–96.

Van Royen ME, Farla P, Mattern KA, Geverts B, Trapman J, Houtsmuller AB (2009b) *Fluorescence recovery after photobleaching (FRAP) to study nuclear protein dynamics in living cells.* Methods Mol Biol 464:363–385.

Van Royen ME, van Cappellen WA, de Vos C, Houtsmuller AB, Trapman J (2012) *Stepwise androgen receptor dimerization.* J Cell Sci 125:1970–1979.

Van Royen ME, van Cappellen WA, Geverts B, Schmidt T, Houtsmuller AB, Schaaf MJM (2014) *Androgen receptor complexes probe DNA for recognition sequences by short random interactions.* J Cell Sci.

Vasudevan N, Pfaff DW (2007) *Membrane-initiated actions of estrogens in neuroendocrinology: emerging principles.* Endocr Rev 28:1–19.

Venero C, Borrell J (1999) *Rapid glucocorticoid effects on excitatory amino acid levels in the hippocampus: a microdialysis study in freely moving rats.* Eur J Neurosci 11:2465–2473.

Vicente MI, Costa PF, Lima PA (2010) *Galantamine inhibits slowly inactivating K+ currents with a dual dose-response relationship in differentiated N1E-115 cells and in CA1 neurones.* Eur J Pharmacol 634:16–25.

Vinson GP (2011) *The mislabelling of deoxycorticosterone: making sense of corticosteroid structure and function.* J Endocrinol 211:3–16.

Voss TC, Hager GL (2014) *Dynamic regulation of transcriptional states by chromatin and transcription factors.* Nat Rev Genet 15:69–81.

Voss TC, Schiltz RL, Sung MH, Yen PM, Stamatoyannopoulos JA, Biddie SC, Johnson TA, Miranda TB, John S, Hager GL (2011) *Dynamic exchange at regulatory elements during chromatin remodeling underlies assisted loading mechanism.* Cell 146:544–554.

Vreugdenhil E, Kolk SM, Boekhoorn K, Fitzsimons CP, Schaaf M, Schouten T, Sarabdjitsingh A, Sibug R, Lucassen PJ (2007) *Doublecortin-like, a microtubule-associated protein expressed in radial glia, is crucial for neuronal precursor division and radial process stability.* Eur J Neurosci 25:635–648.

Walker D, Htun H, Hager GL (1999) *Using inducible vectors to study intracellular trafficking of GFP-tagged steroid/nuclear receptors in living cells.* Methods 19:386–393.

Wang CC, Wang SJ (2009) *Modulation of presynaptic glucocorticoid receptors on glutamate release from rat hippocampal nerve terminals.* Synapse 63:745–751.

Widmaier EP, Dallman MF (1984) *The effects of corticotropin-releasing factor on adrenocorticotropin secretion from perifused pituitaries in vitro: rapid inhibition by glucocorticoids.* Endocrinology 115:2368–2374.

Wiegert O, Joëls M, Krugers H (2006) *Timing is essential for rapid effects of corticosterone on synaptic potentiation in the mouse hippocampus.* Learn Mem 13:110–113.

Wilson P, Morgan J, Funder JW, Fuller PJ, Young MJ (2009) *Mediators of mineralocorticoid receptor-induced profibrotic inflammatory responses in the heart.* Clin Sci 116:731–739.

Windle RJ, Wood SA, Shanks N, Lightman SL, Ingram CD (1998) *Ultradian rhythm of basal corticosterone release in the female rat: dynamic interaction with the response to acute stress.* Endocrinology 139:443–450.

Wyrwoll CS, Holmes MC, Seckl JR (2011) *11β-hydroxysteroid dehydrogenases and the brain: from zero to hero, a decade of progress.* Front Neuroendocrinol 32:265–286.

Xiao L, Feng C, Chen Y (2010) *Glucocorticoid rapidly enhances NMDA-evoked neurotoxicity by attenuating the NR2A-containing NMDA receptor-mediated ERK1/2 activation.* Mol Endocrinol 24:497–510.

Xiao L, Qi A, Chen Y (2005) *Cultured embryonic hippocampal neurons deficient in glucocorticoid (GC) receptor: a novel model for studying nongenomic effects of GC in the neural system.* Endocrinology 146:4036–4041.

Yang J, Fuller PJ (2012) *Interactions of the mineralocorticoid receptor — Within and without.* Mol Cell Endocrinol 350:196–205.

Yang J, Young MJ (2009) *The mineralocorticoid receptor and its coregulators.* J Mol Endocrinol 43:53–64.

Yang W, Gelles J, Musser SM (2004) *Imaging of single-molecule translocation through nuclear pore complexes.* Proc Natl Acad Sci USA 101:12887–12892.

Yang W, Musser SM (2006) *Visualizing single molecules interacting with nuclear pore complexes by narrow-field epifluorescence microscopy.* Methods 39:316–328.

Yehuda R (2009) *Status of glucocorticoid alterations in post-traumatic stress disorder.* Ann N Acad Sci 1179:56–69.

Young EA, Abelson J, Lightman SL (2004) *Cortisol pulsatility and its role in stress regulation and health.* Front Neuroendocr 25:69–76.

Young EA, Haskett RF, Murphy-Weinberg V, Watson SJ, Akil H (1991) *Loss of glucocorticoid fast feedback in depression.* Arch Gen Psychiatry 48:693–699.

Yu CY, Mayba O, Lee JV, Tran J, Harris C, Speed TP, Wang JC (2010) *Genome-wide analysis of glucocorticoid receptor binding regions in adipocytes reveal gene network involved in triglyceride homeostasis.* PLoS One 5:e15188.

Yuan LL, Adams JP, Swank M, Sweatt JD, Johnston D (2002) *Protein kinase modulation of dendritic K+ channels in hippocampus involves a mitogen-activated protein kinase pathway.* J Neurosci 22:4860–4868.

Yuan L-L, Chen X, Kunjilwar K, Pfaffinger P, Johnston D (2006) *Acceleration of K+ channel inactivation by MEK inhibitor U0126.* Am J Physiol - Cell Physiol 290:C165–C171.

Yuen EY, Liu W, Karatsoreos IN, Feng J, McEwen BS, Yan Z (2009) *Acute stress enhances glutamatergic transmission in prefrontal cortex and facilitates working memory.* Proc Natl Acad Sci U A 106:14075–14079.

Yuen EY, Liu W, Karatsoreos IN, Ren Y, Feng J, McEwen BS, Yan Z (2010) *Mechanisms for acute stress-induced enhancement of glutamatergic transmission and working memory.* Mol Psychiatry 16:156–170.

Zalachoras I, Houtman R, Meijer OC (2013) *Understanding stress-effects in the brain via transcriptional signal transduction pathways.* Neuroscience 242:97–109.

Zhou M, Bakker EHM, Velzing EH, Berger S, Oitzl M, Joëls M, Krugers HJ (2010) *Both mineralocorticoid and glucocorticoid receptors regulate emotional memory in mice.* Neurobiol Learn Mem 94:530–537.

Zhou M, Kindt M, Joëls M, Krugers HJ (2011) *Blocking Mineralocorticoid Receptors prior to Retrieval Reduces Contextual Fear Memory in Mice Bartolomucci A, ed.* PLoS ONE 6:e26220.

Zhu BG, Zhu DH, Chen YZ (1998) *Rapid enhancement of high affinity glutamate uptake by glucocorticoids in rat cerebral cortex synaptosomes and human neuroblastoma clone SK-N-SH: possible involvement of G-protein.* Biochem Biophys Res Commun 247:261–265.

Addendum

English summary

Stress has many faces. A balanced activation and suppression of our stress system enables a highly adaptive response to disturbances in homeostasis. But when this balance is disrupted, for example when stress responses are not terminated properly, stress acts as an important risk factor for a large number of diseases. These diseases range from obesity, heart and cardiovascular problems to psychiatric disorders including major depression and posttraumatic stress disorder. Key to understanding the cause of the shift from adaptive towards detrimental effects is a comprehensive understanding of the different players and phases involved in the stress response and their interactions.

In this thesis, I focus on the actions of the corticosteroid hormones: corticosterone and cortisol. Of note, I use the term corticosteroids throughout this thesis only in referral to corticosterone, cortisol and their synthetic analogues (the term officially also includes mineralocorticoids). Corticosteroids are one of the main hormones released from the adrenals during stress. They exert their cellular actions through binding to two receptor types: the glucocorticoid receptor (GR) and the mineralocorticoid receptor (MR). The receptors have two distinct modes of action. They translocate to the nucleus upon activation, where they act as transcription factors and bind directly and indirectly to the DNA, regulating overlapping sets of stress-responsive genes (i.e. genomic actions). Recently, a small subpopulation of each receptor has been postulated to be present at the plasma membrane. This subpopulation is essential for rapid corticosteroid actions (i.e. non-genomic actions). In this thesis I aimed to explore further finesses in the cellular dynamics of the MR and GR in both their membrane-associated and their nuclear subpopulations. I specified three specific aims which are addressed in *Chapters 2 till 6*.

Aim I "To investigate the multitude of non-genomic effects of corticosteroids in different brain areas and to explore how these fit within the onset of the stress response"

In *Chapter 2* we evaluated the current state of knowledge on the non-genomic actions of corticosteroids through membrane-associated receptors and their relevance for brain functioning. Many non-genomic actions have been described in the hypothalamus and limbic brain areas. Interestingly, like the genomic steroid actions, the vast majority of these effects are conditional; i.e. they increase or decrease the threshold for neuronal activation. This implies that only in those brain areas that are also activated by the context of the stressor, the non-genomic actions will affect neuronal activity. The non-genomic actions of corticosteroids are followed up by genomic actions at a later time point: this results in diverse temporal patterns of enhanced or decreased excitability between brain areas. These temporal patterns correlate well with rapid corticosteroid modulation of neuro-endocrine output and behavior. Finally, we addressed the current state of knowledge regarding underlying signaling cascades of these corticosteroid effects and listed the main caveats in the current knowledge. For example, the regulation of MR and GR translocation to the membrane is still elusive, as is the proportion of the membrane population involved.

Aim II "To set up *in vitro* models to show the presence and function of a distinct membrane-associated population of the MR"

Corticosteroids rapidly affect the excitability status of neurons in multiple brain areas. These actions arise from a membrane-localized receptor, but only bits and pieces of the signaling cascades are known. In this regard, it would be very valuable to establish a functional *in vitro* model that enables manipulations of the system and thereby investigations of the downstream and upstream molecular pathways. In *Chapter 3* we mimicked a functional non-genomic corticosteroid effect in a neuronal-like cell line. Potassium A-type currents have previously been shown to be inhibited by corticosterone in a non-genomic, membrane-initiated and MR-dependent manner within the hippocampus. We studied this same effect in the neuronal-like cell line: NS-1 cells. NS-1 cells show large potassium currents, including A-type currents. Only after MR-transfection, corticosterone induced a > 25 % reduction in A-type current amplitudes, while no effect was seen in control-transfected cells. We could replicate this effect with a membrane-impermeable corticosterone-BSA conjugate. In contrast, the slowly-inactivated potassium currents in N1E-115 cells were not affected by corticosterone in the presence of the MR. The MR is thus sufficient for a rapid inhibition of A-type potassium channels by corticosterone and this effect is specific for certain subtypes of potassium channels.

With EM microscopy a subfraction of the MR has been shown at the plasma membrane where it functions as non-genomic corticosteroid receptor. However,

this fraction of membrane-associated MR is very small compared to the bulk of cytoplasmically localized MR and conventional imaging methods fail to show the existence of this fraction. In *Chapter 4* we imaged the putative membrane-associated fraction of the MR using TIRF microscopy. In TIRF microscopy a thin wavefield is created that excites fluorophores in a $60–100$ nm sheet from the coverglass. This includes all membrane-associated molecules, but excludes the majority of cytoplasmic proteins. We imaged YFP-tagged MR using conventional wide-field (only cytoplasm) and TIRF microscopy (highly enriched for membrane-associated molecules) and assessed protein dynamics in both imaging modes using single-molecule microscopy (SMM). We observed a > 1.5 fold larger fraction of slowly diffusing YFP-MR molecules in TIRF. This fits with the notion of an enrichment of membrane-associated molecules as these are known to diffuse very slowly. This effect was also replicated in a second cell line. We next applied hormones. Ligand activation has been shown to change the dynamics of most (membrane-associated) receptors. However, we did not observe any effect of short-term corticosterone treatment on YFP-MR's dynamics at the membrane. In conclusion, the combination of TIRF and SMM provides a strong suggestion for the existence of a membrane-associated MR fraction. Future studies and further manipulations will show whether this imaging approach is a valid method to distinguish between membrane-associated and cytoplasmic subpopulations of proteins.

Aim III "To characterize the chromatin binding dynamics of the MR and GR and to explore the effect of mutations within the receptors and different ligands on their nuclear dynamics"

The GR and MR bind to the DNA and regulate gene transcription. This process is highly dynamic: the receptors do not stay bound to the DNA, but show only transient interactions. Quantification of these rapid processes has remained difficult and small errors in modelling presumptions have resulted in a large variability in outcomes between studies. New approaches such as SMM enable more precise quantifications of protein dynamics with a high temporal and spatial resolution. In *Chapter 5*, we assessed the intranuclear dynamics of the GR using both SMM and FRAP. Importantly, we found that this combination of approaches gave a very consistent quantification of the DNA-binding dynamics of the GR. We found that agonist-bound GR is diffusing throughout the nucleus for $\sim$50 % of the time, interspersed with transient DNA-binding events of $\sim$0.5 seconds ($\sim$30 %) and 2–3 seconds ($\sim$20 %). GR deletion mutants devoid of DNA-binding showed predictably a stark reduction of these DNA-binding events. Similarly, when bound to an antagonist, the GR also showed a reduced frequency of DNA-binding events. In both cases, the receptor also showed faster diffusion, therefore, we presume that a third type of very short DNA-interactions were included in the diffusion coefficient. The GR thus shows (i) ultrashort (< 6 ms), short ($\sim$0.5 seconds) and long (2–3 seconds)

binding to the DNA. We presume that most of these DNA-interactions are nonspecific binding to the chromatin and only part of the longer binding events represent specific binding to GR-regulated genes. A final observation from these experiments was that subtle differences in agonist structure have a profound effect on the frequency and duration of DNA-binding events of the GR. The most potent agonists make more connections to the amino acids lining the ligand-binding pocket. This affects the conformational shift of the receptor and ultimately affects its affinity for DNA.

The MR and GR share very high sequence homology. They share part of their DNA binding sequences and part of their ligands, but there are also differences. For example, the MR binds both mineralocorticoids and corticosteroids and has ~10-fold higher affinity for the endogenous corticosteroids as the GR. In *Chapter 6*, we utilized the same combination of SMM and quantitative FRAP to assess the intranuclear dynamics of the MR. First, as for the GR we found that the combinational approach gave a highly consistent analysis of MR's DNA-binding dynamics. Also the MR, when bound to a potent agonist, spends approximately 50 % of its time diffusing, and the remainder being transiently bound to the DNA. In correspondence to the GR, MR binds the DNA with ultrashort, short and long binding events. Also for the MR, small differences in agonist structure affected the MR's DNA-binding affinity. But, this effect was seen for different steroid side-groups, suggesting that different ligand-receptor interactions affect the conformational shift of the MR. Finally, when bound to the natural corticosteroids (cortisol or corticosterone) the MR shows more frequent and longer DNA-binding than the GR.

Conclusion

In conclusion, in this thesis I explored further finesses in the cellular action of corticosteroids. Membrane-initiated and non-genomic actions of corticosteroids are shown throughout the brain and play an important role in the early phases of the stress response. With use of TIRF and SMM microscopy we found a strong indication that the MR is present in a detectable amount at the plasma membrane. Within the nucleus, we focused on the highly dynamic behavior of the GR and MR and we could quantify multiple nonspecific and specific DNA-binding events for both receptors. The finding that these DNA binding patterns are highly affected by specific ligand attributes is intriguing and calls out for further research.

Nederlandse samenvatting

"ziekteverzuim neemt fors toe door stress"
"stress verdubbelt kans op onvruchtbaarheid"
"link tussen stress en verslaving"
"6 jaar ouder door stress"

Zomaar wat koppen uit de krant. Stress wordt vaak gezien als iets negatiefs, iets ongezonds en als risicofactor voor allerlei ziektes en aandoeningen. En dat is waar: mensen die veelvuldig blootgesteld zijn aan stress of zelfs eenmalig aan zeer ernstige stress hebben een hoger risico op verschillende ziektes zoals hart- en vaat-aandoeningen en vele psychiatrische aandoeningen (bijvoorbeeld depressie of post-traumatisch stress syndroom). Maar dit is slechts één kant van de medaille. Ons stress-systeem is in de basis een systeem dat er voor zorgt dat wij heel snel en correct kunnen reageren als er een plotselinge dreiging wordt waargenomen. Pas wanneer de stress niet meer gehanteerd kan worden wordt de gezondheid bedreigd.

De HPA-as

De allereerste reacties na stress komen van het sympatisch zenuwstelsel en de afgifte van adrenaline. De hartslag wordt verhoogd en energie wordt gemobiliseerd voor onmiddellijke actie: vechten of vluchten. Adrenaline verhoogt ook de algehele alertheid: de oren zijn gespitst.

Een tweede belangrijk systeem dat wordt geactiveerd tijdens stress is de HPA-as (*hypothalamic-pituitary-adrenal axis*). Deze as wordt zo genoemd omdat de activatie ervan loopt vanaf de hypothalamus in de hersenen, via de hypofyseklier naar de bijnierschors. Activatie van de bijnier leidt tot productie van het stresshormoon cortisol bij de mens en het nauw verwante corticosteron bij de muis en de rat. Deze hormonen worden afgegeven aan het bloed waardoor ze alle organen en weefsels van ons lichaam bereiken.

De effecten van cortisol en corticosteron zijn veelzijdig. Al binnen enkele minuten zorgt cortisol voor een snelle reactie op de stressvolle gebeurtenis. Via activatie van verschillende hersengebieden zorgt cortisol bijvoorbeeld voor een verhoogde alertheid en een juiste inschatting van de situatie: moet ik vluchten, vechten of is er niets aan de hand? Deze onmiddellijke reactie is essentieel, maar wordt zelf schadelijk indien deze niet beteugeld wordt. Cortisol zorgt zelf voor deze beteugeling, dit gebeurt via activatie van nieuwe genen en deze effecten komen met een vertraging van een half uur tot zelfs enkele uren tot stand. Cortisol stimuleert ook het geheugen. Zo komt het dat we stressvolle gebeurtenissen veel beter onthouden dan de alledaagse routine. Cortisol is onderdeel van de familie der corticosteroïden. In de experimenten beschreven in dit proefschrift heb ik verschillende corticosteroïden gebruikt en ik zal vanaf hier steeds spreken over corticosteroïden als algemene term voor deze hormonen.

Een balans in het stress systeem; vanaf de cel tot het organisme

Bij milde en niet te langdurige stress werkt het stress-systeem heel adaptief: het zorgt ervoor dat alle systemen die nodig zijn voor een snelle reactie 'aan' worden gezet terwijl alle systemen die niet direct nodig zijn even op een laag pitje staan. Maar in geval van langdurige of heel heftige stress kan de balans zoek raken. Dan wordt de stressreactie niet meer goed aangezet of (wat vaker voor komt) gaat hij niet meer goed uit als dit nodig is. Al decennia lang proberen onderzoekers erachter te komen hoe deze balans bijgestuurd kan worden.

In dit proefschrift draag ik een (klein) steentje bij aan dit onderzoek. Ik heb onderzoek gedaan naar de werking van corticosteroïden en enkele synthetische analogen. Hierbij heb ik mij met name gericht op de processen die zich afspelen in de cel. De effecten van corticosteroïden op celniveau bepalen uiteindelijk ook wat het effect zal zijn op het weefsel, orgaan en het hele organisme.

Corticosteroïden in de cel

Corticosteroïden kunnen binden aan twee verschillende receptoreiwitten: de Mineralocorticoïd Receptor (MR) en de Glucocorticoïd Receptor (GR). Bijna alle cellen in ons lichaam bezitten de GR, terwijl de MR alleen in specifieke weefsels voorkomt.

De twee receptoren hebben ook twee verschillende werkingsmechanismes in de cel (geïllustreerd in Figuur 1). De meeste receptoren bevinden zich in het cytoplasma van de cel en zodra het hormoon bindt, verplaatst de geactiveerde receptor zich naar de kern. In de kern kunnen de receptoren direct binden aan het DNA. Binding van de receptoren zorgt ervoor dat nieuwe genen worden afgeschreven. Hierdoor worden nieuwe eiwitten geproduceerd, die uiteindelijk zorgen voor verdere effecten. Deze route geeft de **genomische effecten**. Deze effecten zijn pas met een vertraging zichtbaar, maar houden wel erg lang aan.

Een kleiner gedeelte van de receptoren bevindt zich op het membraan. Ook deze membraangebonden MR en GR worden geactiveerd door binding van corticosteroïden, wanneer ze geactiveerd zijn kunnen ze al bestaande eiwitten activeren. Dit geeft de **niet-genomische effecten**. Niet-genomische effecten zijn al binnen enkele minuten zichtbaar, maar houden korter aan.

Doel van dit proefschrift

In dit proefschrift heb ik zowel de genomische als de niet-genomische effecten van corticosteroïden onderzocht, ik had hierbij 3 specifieke doelen.

I Het evalueren van de verschillende niet-genomische effecten van corticosteroïden in de hersenen. Tevens om te beschrijven hoe deze passen binnen de stress reactie.

II Het opzetten van *in vitro* modellen die gebruikt kunnen worden om de membraangebonden fractie van de MR te laten zien en te karakteriseren.

III Het onderzoeken van de dynamiek van DNA-binding door zowel de GR als de MR. Tevens om te bepalen hoe deze dynamiek wordt beïnvloed door mutaties in de receptoren en door binding van verschillende liganden.

Deze specifieke doelen heb ik verder uitgewerkt in hoofdstukken 2 tot en met 6. In hoofdstuk 7 heb ik de belangrijkste bevindingen verder bediscussieerd.

Fluorescentie-microscopie en single-molecule microscopie

Voordat ik de belangrijkste bevindingen uit dit proefschrift beschrijf eerst een korte uitweiding over de gebruikte technieken. In mijn onderzoek heb ik gebruik gemaakt van verschillende moleculaire technieken, maar voor het belangrijkste deel heb ik gebruik gemaakt van geavanceerde fluorescentie-microscopie. Hieronder leg ik een aantal basisprincipes van fluorescentie-microscopie en de gebruikte variaties hierop uit.

niet-genomische effecten

membraan

cytoplasma

transport naar kern

specifieke binding

aspecifieke binding

kern

DNA

aspecifieke binding

genomische effecten

MR / GR

cofactoren / bindingspartners etc.

corticosteroïde

molecuul beweging
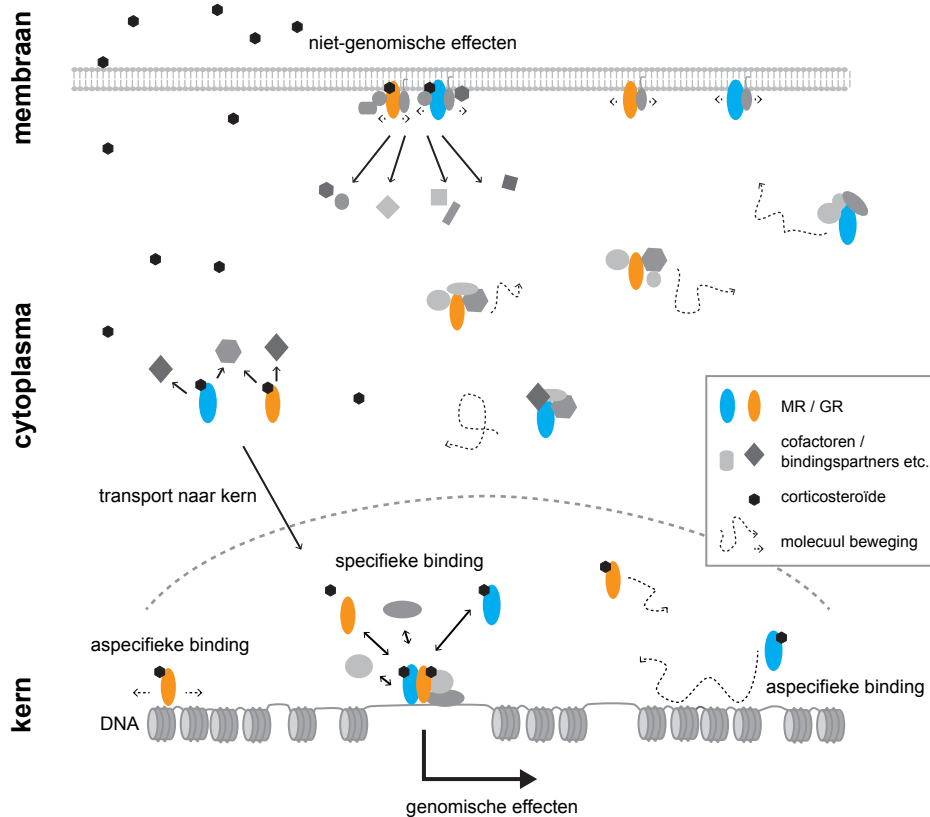
Figuur 1: De dynamiek van corticosteroïd receptoren in de cel
In dit proefschrift heb ik de functie en de dynamiek van de twee corticosteroïd receptortypen, de MR en de GR, onderzocht. De beweging, of dynamiek, van de MR en GR hangt samen met hun verschillende functies binnen de cel. Een aantal belangrijke bevindingen van mijn proefschrift zijn hier geïllustreerd. In afwezigheid van hormoon bevinden de meeste MR en GR moleculen zich in het cytoplasma van de cel. Ze zijn hier gebonden door hulpeiwitten (cofactoren) en ze bewegen grotendeels vrijelijk. Binding van het hormoon, bijvoorbeeld cortisol, leidt ertoe dat de receptoren zich naar de kern verplaatsen. In de kern bewegen de receptoren ook vrijelijk, maar gaan ze tevens korte bindingen aan met het DNA. DNA binding leidt tot immobilisatie van de eiwitten. In hoofdstukken 5 en 6 laten wij zien dat deze binding altijd kortdurend is, maar wel in verschillende vormen kan voorkomen. Aspecifieke bindingen met het DNA zijn zeer kort (milliseconds tot een halve seconde) terwijl langere bindingen (meerdere secondes) waarschijnlijk wijzen op specifieke binding van de receptor. Specifieke binding leidt tot gentranscriptie en tot de genomische effecten van corticosteroïden. Een kleiner gedeelte van de receptorpopulatie bevindt zich aan het celmembraan. Cofactoren helpen met de membraanbinding. In hoofdstuk 4 laten wij zien dat de membraangebonden MR langzamer beweegt dan in het cytoplasma of de kern. Cortisol binding aan de membraangebonden receptoren leidt tot snelle modificaties van eiwitten en tot de niet-genomische effecten van corticosteroïden. Welke verder staan beschreven in hoofdstukken 2 en 3.

Fluorescentie-microscopie gaat uit van fluorescerende moleculen. Dit zijn moleculen die de energie van een lichtbron (bijvoorbeeld een laser of een lamp van een specifieke golflengte) kunnen absorberen en als reactie zelf ook licht gaan uitstralen. Het bekendste fluorescerende eiwit is GFP (*green fluorescent protein*), dit eiwit

absorbeert blauw licht en straalt hierop zelf groen licht uit. Er zijn vele varianten op GFP ontwikkeld met andere kleuren. In dit proefschrift maak ik voornamelijk gebruik van YFP (*yellow fluorescent protein*) een eiwit dat geel licht uitzendt. Om de functie van de twee corticosteroïd receptoren —de MR en GR— te onderzoeken heb ik deze receptoren gefuseerd aan YFP. Het resulterende eiwit —YFP-MR of YFP-GR— gedraagt zich als de MR of GR, maar dan zit er een fluorescerend deel aan vast.

Voor de experimenten in dit proefschrift heb ik veelvuldig gebruik gemaakt van een variatie op fluorescentie-microscopie: *single-molecule* microscopie. Hierbij worden individuele fluorescerende moleculen gevolgd over de tijd waardoor de beweging (dynamiek) van moleculen bestudeerd kan worden (geïllustreerd in Figuur 2a). Wij gebruikten hiervoor cellen die YFP-MR of YFP-GR bezitten. In elke cel zitten dan vele duizenden YFP-MR of YFP-GR moleculen. Om individuele moleculen van elkaar te onderscheiden moet eerst het overgrote gedeelte van de moleculen worden uitgedoofd. Dit wordt gedaan door de cel langdurig met de lichtbron te beschijnen. De meeste YFP moleculen doven dan uit. Zodra de dichtheid van de nog fluorescerende moleculen laag genoeg is kan met een zeer gevoelige camera de fluorescentie van deze individuele moleculen zichtbaar worden gemaakt. Wij maakten hiervan filmpjes met om elke 6 milliseconds een nieuwe foto. Een individueel molecuul kan dan op opeenvolgende foto's worden gevolgd en als het tijdens deze periode beweegt zien we het steeds op een andere plek terug. Met een pakket aan analysesoftware kunnen we de bewegingen van vele individuele moleculen samen analyseren en dit geeft ons een beeld van hoe deze moleculen bewegen.

Een tweede methode om de dynamiek van fluorescerende moleculen te onderzoeken is FRAP (*fluorescence recovery after photobleaching*). Hierbij wordt een sterke laser gebruikt die fluorescerende moleculen uitdooft (*photobleaching*). Deze laser wordt maar op een deel van de cel gezet, dus alleen in dit stukje cel wordt de fluorescentie gedoofd en dit stukje wordt dan een tijdlang gevolgd. Omdat eiwitten bewegen zullen fluorescerende eiwitten uit andere delen van de cel zich verplaatsen naar het uitgedoofde gebied en zal er dus langzaam herstel van de fluorescentie gezien worden. Hoe sneller een eiwit beweegt, des te sneller zal het gebied weer opnieuw opgevuld worden met fluorescentie (zie Figuur 2b).

Een laatste variatie op fluorescentie-microscopie die wij hebben gebruikt is TIRF (*total internal reflection fluorescence*) microscopie. Bij TIRF-microscopie wordt de activatie laser in een scherpe hoek geplaatst waardoor het licht op het glas wordt gereflecteerd. Als reactie hierop wordt een dun energieveld gevormd. Dit energieveld reikt maar tot maximaal 100 nanometer diep en activeert dus alleen fluorescerende moleculen die zich in dit dunne veld bevinden. Wij hebben TIRF-microscopie gebruikt op cellen die bovenop het glas waren geplaatst. Cellen zijn meerdere micrometers dik en met TIRF-microscopie wordt dus alleen het onderste laagje van de cel belicht. Aangezien het membraan het laagste deel van de cel is worden met TIRF-microscopie alle fluorescerende moleculen in het (onderste) membraan be-
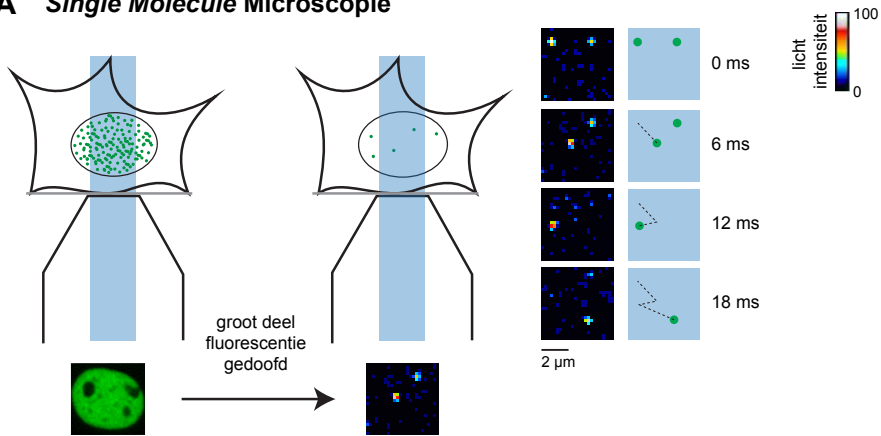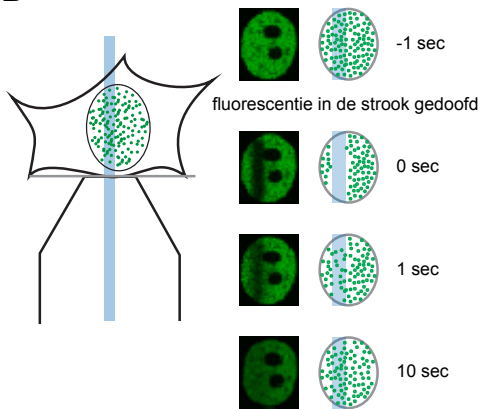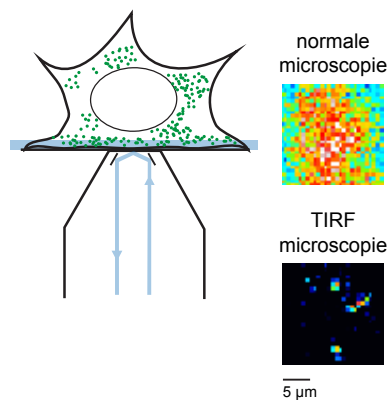
Figuur 2: Geavanceerde fluorescentie microscopie

(A) *Single molecule* microscopie. Een fluorescerend eiwit (bijvoorbeeld YFP-GR) bevindt zich in de kern van een cel. Het fluorescentiesignaal van vele moleculen samen geeft een beeld van een volledige cel-kern (meest links). Voor *single molecule* microscopie wordt de cel eerst langdurig met een laser bestraald zodat de meeste fluorescentie uitdooft: slechts enkele nog fluorescerende moleculen blijven over. Met een zeer gevoelige camera wordt de fluorescentie van deze individuele moleculen zichtbaar gemaakt en gevolgd (figuur midden). Meest rechts zijn twee individuele YFP-GR moleculen afgebeeld: één zit gedurende 6 millisecondes op 1 plaats (en is daarna niet meer zichtbaar), de andere beweegt geduren-de 18 millisecondes door de kern heen. (B) FRAP. Bij FRAP wordt een klein gedeelte van de celkern met een sterke laser beschenen zodat alle fluorescerende moleculen hier uitdoven. Daarna vindt vermenging plaats van nog fluorescerende moleculen uit andere gedeelten van de kern en de uitgedoofde moleculen waardoor er nieuwe fluorescentie in het bestraalde gebied terugkeert. Hoe sneller een eiwit beweegt, hoe sneller dit herstel zal zijn. Rechts staat een voorbeeld van FRAP op YFP-GR. (C) TIRF-microscopie. TIRF-microscopie is een techniek om fluorescerende eiwitten bij het membraan te bekijken. Bij TIRF-microscopie komt de laser met een sterke hoek binnen, waardoor vrijwel alle energie van de laser terug-kaatst het objectief in. Een klein deel van de energie komt aan het oppervlak vrij, slechts een tiende van een micrometer diep. Rechts ziet u voorbeelden van de fluorescentie van een membraangebonden eiwit eerst bekeken met 'normale' fluorescentie microscopie waarbij veel en diffuse fluorescentie te zien is en daarna is hetzelfde gebied met TIRF microscopie waarbij individuele moleculen te zien zijn en de hoge achtergrondfluorescentie is verdwenen.

licht samen met een klein stukje van het bovenliggende cytoplasma. Hierdoor krijgen we met TIRF-microscopie een grote verrijking van fluorescerende moleculen in het membraan ten opzichte van het cytoplasma (zie Figuur 2c).

Belangrijkste bevindingen van dit proefschrift

Gedurende de laatste 20 jaar is er veel nieuw onderzoek gedaan naar de niet-genomische effecten van corticosteroïden. Voor het eerst werd gevonden dat deze snelle effecten ook via de MR en GR lopen en dat deze receptoren aan het membraan voor komen. In **hoofdstuk 2** evalueer ik de huidige kennis over de niet-genomische corticosteroïd effecten in de hersenen. Voorts beschrijf ik de relevantie van deze effecten voor de stressreactie. Een belangrijke bevinding hierbij is dat deze niet-genomische effecten conditioneel zijn en werken als een neuromodulator. Dat wil zeggen dat ze zelf geen neurale activiteit veroorzaken maar wel de afgifte van een transmitter kunnen beïnvloeden of de gevoeligheid van neuronen voor activatie veranderen.

Het mechanisme dat ten grondslag ligt aan de niet-genomische werking van corticosteroïden is slechts in beperkte mate onderzocht. In **hoofdstuk 3** hebben wij een niet-genomisch effect nagebootst in een *in vitro* cellijn. In hippocampale neuronen geeft een korte behandeling met corticosteron een inhibitie van één specifiek type kaliumkanaal: het A-type. Wij hebben laten zien dat ook de NS-1 cellijn een A-type kaliumstroom bevat. Na transfectie met de MR, leidt kortstondige behandeling met corticosteron tot een inhibitie van deze A-type kanalen in NS-1 cellen. In NS-1 cellen zonder MR heeft corticosteron geen effect. Bovendien vonden we dat corticosteron ook geen effect gaf op een ander type kaliumkanaal (langzaam inactiverend). Samengevat vonden we dat aanwezigheid van de MR voldoende is voor een niet-genomisch effect van corticosteron en dat dit effect specifiek is voor A-type kanalen.

In **hoofdstuk 4** beschrijf ik verder onderzoek naar de membraangebonden MR. Het is bekend dat een kleine fractie van alle MR moleculen aan het membraan geankerd zit, maar het is heel moeilijk om deze kleine fractie te onderscheiden van de veel grotere populatie MR moleculen die zich in het cytoplasma bevindt. In dit hoofdstuk vergeleken wij de dynamiek van YFP-MR moleculen tussen conventionele-microscopie (voornamelijk cytoplasma) en TIRF-microscopie (grote verrijking van membraan fractie). De dynamiek van YFP-MR werd gemeten met *single-molecule* microscopie. Met TIRF-microscopie werd een anderhalf maal grotere fractie aan zeer langzaam bewegende YFP-MR moleculen gevonden dan met conventionele-microscopie. Membraangebonden moleculen bewegen zeer langzaam, dus deze bevinding wijst erop dat er inderdaad een kleine membraangebonden fractie van YFP-MR bestaat (geïllustreerd in Figuur 1).

Zowel de GR en de MR kunnen direct aan het DNA binden. Deze bindingen zijn niet statisch: de receptoren binden het DNA steeds kort en laten dan weer los om kort erop weer opnieuw te binden. Het kwantificeren van deze bindingsdynamiek

is zeer lastig. In **hoofdstuk 5** gebruikten wij een combinatie van *single-molecule* microscopie en FRAP om de bindingsdynamiek van de GR aan het DNA te kwantificeren. Ten eerste vonden wij dat beide onafhankelijke technieken een zeer vergelijkbare kwantificatie van de DNA-bindingen van de GR gaven. In zijn geactiveerde vorm was op elk moment 50 % van de GR moleculen aan het DNA gebonden terwijl de resterende 50 % vrij bewoog. Met FRAP konden wij tevens de duur van de DNA bindingen kwantificeren en vonden bindingstijden rond de halve seconde (30 %) en tussen de 2 en 3 secondes (20 %). Niet-geactiveerde GR liet minder frequente en kortere DNA-binding zien en tevens een snellere diffusie. Deze laatste bevinding suggereert dat er in de bewegende fractie nog een derde zeer korte DNA-binding verstopt zit: bindingen van minder dan 6 millisecondes. Alles samen genomen kunnen we concluderen dat de GR binnen de kern veel korte —aspecifieke— bindingen met het DNA laat zien en slechts sporadisch voor langere tijd aan zijn specifieke bindingsplaatsen zit gebonden (geïllustreerd in Figuur 1).

In **hoofdstuk 6** hebben wij dezelfde combinatie van *single-molecule* microscopie en FRAP gebruikt om de bindingsdynamiek van de MR aan het DNA te bestuderen. Ook voor de MR vonden wij dat de geactiveerde receptor voor 50 % van de tijd aan het DNA gebonden zat. De frequentie en duur van deze DNA-bindingen was veel lager als de receptor met een antagonist was gebonden. De natuurlijke corticosteroïden —cortisol en corticosteron— hebben een hogere affiniteit voor de MR dan voor de GR. Dit leidt tot een verschil in bindingsdynamiek tussen de MR en de GR. Wanneer beide gebonden zijn door hun natuurlijke ligand laat de MR meer en langere DNA-binding zien dan de GR.

Conclusie

In dit proefschrift heb ik onderzoek naar de cellulaire effecten van corticosteroïden beschreven. Ik heb hiervoor verschillende geavanceerde fluorescentie microscopie methodes gebruikt. Met TIRF en *single-molecule* microscopie heb ik sterke indicaties gevonden voor het bestaan van een membraangebonden fractie van de MR. De combinatie van FRAP en *single-molecule* microscopie gaf een zeer precieze kwantificatie van de bindingsdynamiek van zowel de GR als de MR aan het DNA. Hierbij kon ik onderscheid maken tussen frequente aspecifieke bindingen en minder frequente specifieke bindingen. Ook de bevinding dat verschillende hormonen een heel ander DNA-bindingsdynamiek van de MR en de GR aan het DNA laten zien is zeer interessant en kan de basis vormen voor verder onderzoek.

Curriculum Vitae

Femke Lokke Groeneweg was born on the 21st of August, 1982 in Leiden, The Netherlands. She attended secondary school at the Leonardo Da Vinci College in Leiden and graduated in 2000. In the same year she started her Bachelor of Biology at the University of Utrecht. After graduating from her Bachelor in 2004 she enrolled in the Master's programme Neuroscience and Cognition, track of Experimental and Clinical Neuroscience at the Graduate School of Life Sciences at Utrecht University. This programme included two internships. In 2005 she performed a 9-month internship at the Rudolf Magnus Institute under supervision of Dr. Susanne la Fleur on the effects of a high fat, high-sugar diet on physiology and hypothalamic neuropeptide expression in rats. In 2006 she performed a 6-month internship at Columbia University Medical School in New York City, USA under supervision of Dr. Lu Cao and Prof. Joseph Gogos. The topic was the effect of between-cell competition on axonal arborization in olfactory neurons. During the same period Femke also enrolled in the excellence track "Xtrack" which she concluded with winning the first price for her research proposition. She obtained her Master's diploma with honors (*cum laude*) in 2007.

After graduation, Femke moved her studies back to Leiden and started working as a PhD student at the Department of Medical Pharmacology of the Leiden/Amsterdam Center for Drug Research at Leiden University and the LUMC. She studied the genomic and non-genomic cellular actions of corticosteroids through the glucocorticoid and mineralocorticoid receptors under supervision of Prof. Ron de Kloet and Dr. Marcel Schaaf (of the Department of Molecular Cell Biology at Leiden University). The results of her PhD research are reported in this thesis.

Since 2012 Femke works as postdoctoral researcher in the workgroup of Synapse and Network Development at the Institute of Neuroscience in Amsterdam, under supervision of Dr. Christian Lohmann. Femke is married and lives in Duivendrecht with her husband and daughter.

Publication list

Groeneweg F.L., Sierksma M., de Kloet E.R., van Noort J., Schmidt T.S., Schaaf M.J.M.
A combination of wide-field and TIRF single-molecule microscopy as method to visualize the membrane-associated population of the mineralocorticoid receptor. Manuscript in preparation

Groeneweg F.L., van Royen M.E., Fenz S., Keizer V.I., Geverts B., Prins J., de Kloet E.R., Houtsmuller A.B., Schmidt T.S., Schaaf M.J.M.
Quantitation of glucocorticoid receptor DNA-binding dynamics by single-molecule microscopy and FRAP. PLoS One (2014) 9 (3): e90532

Groeneweg F.L., Karst H., de Kloet E.R., Joëls M.
Mineralocorticoid and glucocorticoid receptors at the neuronal membrane, regulators of nongenomic corticosteroid signaling. Molecular and Cellular Endocrinology (2012) 350 (2): 299-309

Groeneweg F.L., Karst H., de Kloet E.R., Joëls M.
Rapid non-genomic effects of corticosteroids and their role in the central stress response. Journal of Endocrinology (2011) 209 (2): 153-167

Joëls M., **Groeneweg F.L.**, Karst H.
Nongenomic cellular actions of corticosteroids in the brain. Chapter in "The handbook of stress: neuropsychological effects on the brain". Blackwell publishing (2011) doi: 10.1111/b.9781444330236.2011.00008.x

La Fleur S.E., van Rozen A.J., Luijendijk M.C., **Groeneweg F.L.**, Adan R.A.
A free-choice high-fat high-sugar diet induces changes in arcuate neuropeptide expression that support hyperphagia. International Journal of Obesity (2010) 34 (3): 537-546